Universidad de Valladolid

FACULTAD DE CIENCIAS

DEPARTAMENTO DE FÍSICA DE LA MATERIA CONDENSADA, CRISTALOGRAFÍA Y MINERALOGÍA

TESIS DOCTORAL:

UNDERSTANDING THE FOAMABILITY OF COMPLEX POLYMERIC SYSTEMS BY USING EXTENSIONAL RHEOLOGY

Presentada por Ester Laguna Gutiérrez para optar al grado de doctora por la Universidad de Valladolid

Dirigida por:
Miguel Ángel Rodríguez Pérez

FINANCIACIÓN

He de agradecer la financiación para llevar a cabo esta investigación que he recibido de diversas instituciones. En primer lugar agradecer a la Junta de Castilla y León por la financiación y al Fondo Social Europeo por la cofinanciación del contrato PIRTU (EDU/289/2011). Además quiero agradecer la financiación recibida por el grupo CellMat, proveniente de los siguientes proyectos de investigación:

- Desarrollo de plásticos sub-microcelulares y nanocelulares: fabricación, estructura, propiedades y potenciales aplicaciones (MAT2012-34901). Financiado por el Programa Nacional de Materiales (MICIN).
- Desarrollo de una nueva generación de aislantes térmicos avanzados basados en la obtención de estructuras porosas nanocelulares (VA035U13). Financiado por la Junta de Castilla y León.
- Nuevos desarrollos en el campo de los materiales poliméricos microcelulares: fabricación, estructura, propiedades, modelización y aplicaciones (MAT 2009-14001). Financiado por el Programa Nacional de Materiales (MICIN).
- Nancore: Microcellular nanocomposite for substitution of Balsa wood and PVC core material (FP7. 214148). Fiananciado por VII Framework Program (Comisión Europea).

FUNDING

Financial support from PIRTU contract by Junta of Castilla y León and co-financed by the European Social Fund is gratefully acknowledged.

Financial assistance provided by the following research projects is also acknowledged:

- Desarrollo de plásticos sub-microcelulares y nanocelulares: fabricación, estructura, propiedades y potenciales aplicaciones (MAT2012-34901). Funded by Programa Nacional de Materiales (MICIN).
- Desarrollo de una nueva generación de aislantes térmicos avanzados basados en la obtención de estructuras porosas nanocelulares (VA035U13). Funded by Junta de Castilla y León.
- Nuevos desarrollos en el campo de los materiales poliméricos microcelulares: fabricación, estructura, propiedades, modelización y aplicaciones (MAT 2009-14001). Funded by Programa Nacional de Materiales (MICIN).
- Nancore: Microcellular nanocomposite for substitution of Balsa wood and PVC core material (FP7. 214148). Funded by VII Framework Program (European Commission).

LIST OF SYMBOLS AND ABBREVIATIONS

A	surface area
	empirical constant
	cross-section of the sample
	micrograph area
AR	anisotropy ratio
A_0	cross-section of the initial sample
a_T	shift factor
B	empirical constant
B_n	branching degree
C	empirical constant
C_c	crosslinking agent content
cf	correction factor
CR	coalescence ratio
C_0	concentration of gas molecules
C_1	concentration of nucleation sites
D	aperture pinhole geometry
d	interlayer spacing between the stacks
D_d	drum diameter
D_e	Deborah number
D_s	sorption diffusivity coefficient
E	Young's modulus (elastic modulus)
E_a	activation energy
E_{cm}	elastic (compression) modulus cellular material
E_m	activation energy of the melt strength
ER	expansion ratio
E_s	elastic (tensile) modulus solid materials
F	force
f_0	frequency factor of the gas molecules (homogeneous nucleation)
f_1	frequency factor of the gas molecules (heterogeneous nucleation)
G	relaxation modulus
G'	storage modulus
G''	loss modulus
G^*	complex modulus
GC	gel content
h	gap between two plates
h_F	final height of the sample after being foamed by improved compression molding
h_0	initial height of the sample prior to be foamed by improved compression molding
k	Boltzman's constant
K_1	material-specific factor
L	distance between the neutron aperture and the detector
l	length of the sample
	final length of the sample
	sample thickness
l_0	initial length of the sample
M	torque

	magnification factor
M_c	critical value of molecular weight
MFR	melt flow rate
MS	melt strength
M_s	sorption amount at a certain time
MVR	melt volume rate
M_W	molecular weight
M_∞	sorption amount at a certain time
n	particles density
	power law exponent
	number of counted cells
N_{HET}	heterogeneous nucleation rate
N_{HOM}	homogeneous nucleation rate
n_{per}	percolation threshold density
N_V	number of cells per unit volume of the solid material (cell nucleation density, cell density)
$N_{V\text{-}cm}$	number of cells per unit volume of the cellular material
OC	open cell content
P	pressure
p	sample porosity
P_a	atmospheric pressure
P_{cm}	any property of a cellular material
P_F	pressure inside the mold after a certain time in improved compression molding
P_i	pressure inside the bubble
P_m	applied pressure during foam stabilization in improved compression molding
P_o	external pressure to the bubble
P_s	saturation pressure during the gas dissolution process
	any property of a solid material
P_0	initial pressure applied to the system in (improved) compression molding
R	radius
	gas constant
	rheological function
S, SHC	strain hardening coefficient
SDC	standard deviation coefficient
T	temperature
t, t'	time
T_a	room temperature
$tan\delta$	loss tangent (loss factor, damping factor)
T_c	crystallization temperature
t_c	crosslinking time
T_F	foaming temperature
t_F	foaming time
T_g	glass transition temperature
T_m	melting temperature
t_s	saturation time during the gas dissolution process

v	velocity
V_p	volume of an individual particle
V_{pyc}	volume measured by the gas pycnometer
V_{sample}	geometrical volume of the sample
v_x, v_y, v_z	velocity field
W	absorbed energy per unit volume in a compression test
w_f	weight of the specimen after being immersed in xylene
W_p	weight fraction of the blowing agent particles
w_0	weight of the original specimen before being immersed in xylene
X_c	polymer crystallinity
α	angle between the cone and the plate
γ	strain
	shear strain
$\dot{\gamma}$	strain rate
	shear strain rate
γ_d	dashpot strain
γ_{P-B}	surface tension in the polymer-bubble interface
γ_s	spring strain
γ_0	shear strain amplitude
δ	phase shift angle (loss angle)
δ_{CW}	thickness of the cell walls
$\Delta G'_{HET}$	activation energy of the heterogeneous nucleation
$\Delta G'_{HOM}$	activation energy of the homogeneous nucleation
ΔP	pressure drop
ΔT	difference between the melting temperature and the crystallization temperature
ε	strain
$\dot{\varepsilon}$	extensional strain rate
ε_F	final strain
ε_H	Hencky strain
$\dot{\varepsilon_H}$	Hencky strain rate
η	viscosity
	shear viscosity
η'	real part of complex viscosity
η''	imaginary part of complex viscosity
η^*	complex viscosity (dynamic shear viscosity)
η_e	extensional viscosity
η_e^+	transient extensional viscosity
η_{e0}^+	transient extensional viscosity in the linear viscoelastic regime
$\eta^0(t)$	time-dependent linear shear viscosity
η_0	zero-shear viscosity
η_0^B	zero-shear viscosity of a branched polymer
η_0^L	zero-shear viscosity of a linear polymer
η_∞	infinite-shear viscosity

θ	contact angle at the polymer-nucleating agent interface
2θ	diffraction angle
λ	stretching ratio
	wavelength
ρ	density
ρ_c	density of the polymeric composite
ρ_{cm}	density of the cellular material
ρ_M	melt density of a polymer
ρ_p	density of the particles
ρ_R	relative density
ρ_S	density of the solid polymeric matrix
σ	stress
	shear stress
σ_c	collapse stress
σ_d	stress applied on the dashpot
σ_e	extensional stress
σ_{P-B}	surface free energy of the polymer-bubble interface
σ_s	stress applied on the spring
σ_0	shear stress amplitude
τ	relaxation time
τ_R	stretch relaxation time (longest Rouse relaxation time)
Φ	average cell size
Φ_{FFT}	cell size determined by fast Fourier transform
$\varphi_{HMS\ PP}$	content in volume percent of high melt strength polypropylene
Φ^i	cell size of the cell i
Φ_x^i	chord length of the cell i in the x direction
Φ_y^i	chord length of the cell i in the y direction
Φ_p	particle volume fraction
Φ_{per}	percolation threshold volume fraction
Ω	drive shaft rotation rate
ω	angular frequency
	oscillation frequency
ω_x, G_x	cross-over point

ADC	azodicarbonamide
CBA	chemical blowing agent
CFCs	chlorofluorocarbons
CSR	controlled shear rate
CSS	controlled shear stress
DCP	dicumyl peroxide
DSC	differential scanning calorimetry
EVA	ethylene vinyl acetate
EVF	extensional viscosity fixture
FFT	fast Fourier transform

HC	hydrocarbons
HCFCs	hydrochlorofluorocarbons
HDPE	high density polyethylene
HMS PP	high melt strength polypropylene
ICM	improved compression molding
LCB	long chain branch
LDPE	low density polyethylene
LLDPE	linear low density polyethylene
LVR	linear viscoelastic regime
MMT	montmorillonite
m-PE	metallocene polyethylene
MWD	molecular weight distribution
PBA	physical blowing agent
PC	polycarbonate
PE	polyethylene
PMMA	poly(methyl methacrylate)
PO	polyolefin
PP	polypropylene
PP-MA	maleic anhydride modified polypropylene
PS	polystyrene
PU	polyurethane
PVC	polyvinyl chloride
SAOS	small amplitude oscillatory shear
SCB	short chain branch
SEM	scanning electron microscopy
TEM	transmission electron microscopy
TGA	thermogravimetric analysis
TTS	time-temperature superposition
x-HDPE	crosslinked high density polyethylene
x-LLDPE	crosslinked linear low density polyethylene
XRD	X-ray diffraction

CONTENTS

Resumen en Español

CHAPTER 1. Introduction

CHAPTER 2. Background and State of the Art

CHAPTER 3. Materials, Production Processes and Characterization Techniques

RESUMEN EN ESPAÑOL

INDEX

0.1 Introducción

Se puede definir un **material celular** (también conocido como espuma) como una estructura de dos fases en la cual una fase gaseosa se ha dispersado a lo largo de una fase sólida. Este tipo de materiales se pueden encontrar en la naturaleza. Algunos ejemplos de **materiales celulares naturales** son: el corcho, la madera de balsa, las esponjas, los huesos trabeculares, el coral, la jibia de la sepia, la hoja de Iris, los tallos de las plantas, etc. [1] (Figura 0.1).

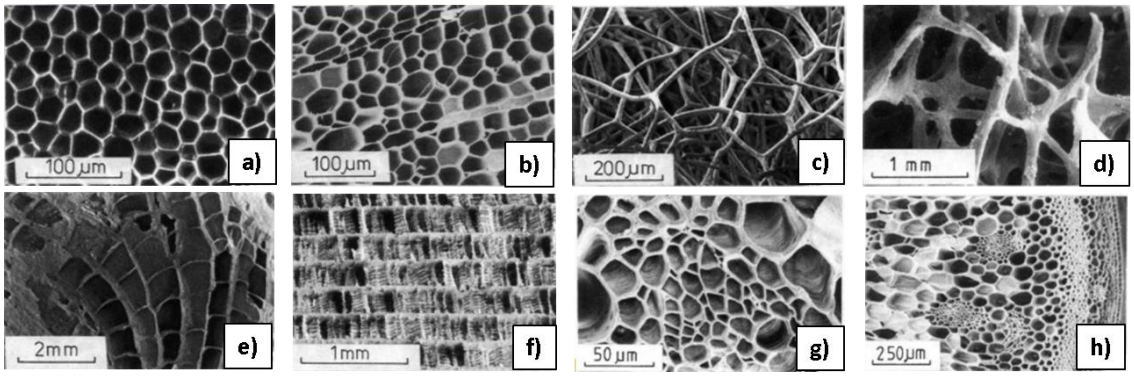

Figura 0.1. Ejemplos de materiales celulares naturales. a) Caucho. b) Madera de balsa. c) Esponja, d) Hueso trabecular. e) Coral. f) Jibia de sepia. g) Hoja de Iris. h) Tallo de planta.

Debido a las excelentes propiedades que presentan estos materiales celulares naturales, hoy en día se han creado multitud de materiales artificiales que tratan de imitar estas estructuras naturales. Estos materiales artificiales pueden producirse a partir de polímeros, metales, cerámicas e incluso a partir de vidrios [1].

Cuando a un cierto material se le dota de una estructura celular, se pueden alcanzar mejoras en diferentes aspectos [2,3]:

- Reducciones de peso.
- Reducción de la cantidad de materia prima utilizada, con los consiguientes beneficios económicos y medioambientales.
- Propiedades mecánicas adaptables en función de la densidad.
- Mayor capacidad como aislantes térmicos.
- Mayor absorción de energía en impactos.
- Posibilidad de absorción acústica en el caso de configurar el producto con celdas interconectadas.

Los materiales celulares tienen un gran presente y un futuro muy prometedor en diversos sectores tecnológicos importantes, debido a sus excelentes propiedades y en especial debido a la posibilidad que existe de diseñar y producir estos materiales para que cumplan con los requisitos establecidos por los usuarios finales (materiales diseñados a la carta).

En particular, los materiales celulares que se producen utilizando una **matriz polimérica** (**materiales celulares poliméricos**) se utilizan hoy en día en aplicaciones como embalaje, deportes y ocio, juguetes, aislamiento térmico, automoción, aeronáutica, aplicaciones

militares, aviones, flotabilidad, amortiguación, etc. [4]. En la Figura 0.2 se muestran diferentes ejemplos de algunas de las principales aplicaciones de los materiales celulares poliméricos.

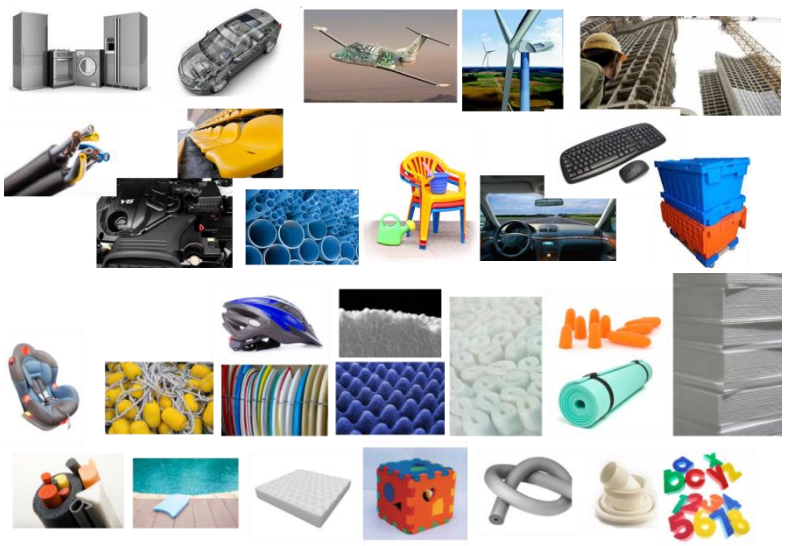

Figura 0.2. Ejemplos de algunas de las principales aplicaciones de los materiales celulares poliméricos.

Para poder tener una idea acerca de la importancia del sector de los materiales celulares poliméricos en la sociedad actual, a continuación, se proporcionan algunas cifras numéricas correspondientes al **mercado global de espumas poliméricas**. Este mercado ha experimentado un crecimiento constante en demanda en los últimos años, aumentando un promedio anual del 4.4 % entre los años 2009 y 2014. En particular, en el año 2013 el mercado global de espumas poliméricas alcanzó un total de 19.1 millones de toneladas lo que representa aproximadamente 86.9 billones de dólares. En los próximos años (desde el 2014 hasta el 2019) se espera que esta tasa de crecimiento se acelere ligeramente y pase a alcanzar un valor promedio de crecimiento anual del 4.8 %. Se espera que para el año 2019 se produzca un consumo por parte del mercado de las espumas poliméricas de 25.3 millones de toneladas [5]. Todas estas cifras se resumen en la Figura 0.3.

Figura 0.3. Crecimiento del mercado de las espumas poliméricas en el periodo 2009-2019.

De entre todas las matrices poliméricas disponibles, las más utilizadas para producir materiales celulares son las que se basan en poliuretano (PU), poliestireno (PS), policloruro de vinilo (PVC) y poliolefinas (PO), debido a su elevado número de potenciales aplicaciones. Para tener una idea de la importancia de cada una de estas resinas poliméricas, en la Figura 0.4 se muestra el mercado de espumas, para cada tipo de familia polimérica, de los Estados Unidos, en el periodo comprendido entre los años 2009 y 2015 [6]. Los porcentajes que aparecen en la

figura se han calculado teniendo en cuenta los millones de toneladas totales consumidos en el periodo mencionado.

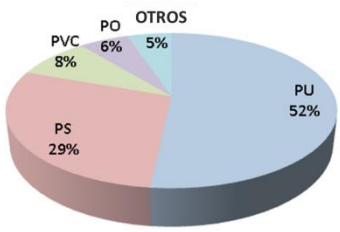

Figura 0.4. Mercado de espumas poliméricas, para cada tipo de familia polimérica, de EEUU, en el periodo 2009-2015.

Las espumas de PU se utilizan principalmente como aislantes térmicos en edificios y en electrodomésticos (frigoríficos). Éstas también se utilizan como rellenos de asientos, sillas y cojines, en colchones, etc. [7]. Las espumas de PS se emplean principalmente en embalaje y protección, en construcción para aislamiento de paredes suelos y techos, en el campo de la ingeniería como rellenos ligeros en la construcción de carreteras y railes, en los cascos para las bicicletas, en las tablas de surf, etc. [8,9,10]. En cuanto a las espumas de PVC, existen tres principales mercados para estas espumas: perfiles, láminas y tubos [10]. Las aplicaciones de las espumas de PVC son muy diversas: revestimientos, productos para techos, ventanas y marcos de puertas, zócalos, paneles publicitarios, paneles de construcción, barcos y tanques, tuberías de drenaje, tuberías de alcantarillado, conductos de ventilación, etc. Finalmente, las espumas de PO se utilizan en electrodomésticos como juntas y almohadillas anti-vibración, en el sector de la automoción como juntas y sellos, barreras contra el agua, aislantes acústicos, almohadillas anti-vibración, protectores contra impactos, componentes ligeros, etc. En el sector de la construcción las espumas de PO se utilizan como aislantes acústicos y aislantes de tuberías, en el sector de embalaje y protección se utilizan como almohadillas para esquinas, envases, colchones, etc. Estas espumas son además utilizadas en otros muchos sectores como el aeroespacial, medico, marina, etc. [10].

Esta tesis se ha centrado en estudiar y entender la capacidad de espumar de **diferentes poliolefinas** y las propiedades de las espumas producidas con este tipo de polímeros. En esta tesis se han seleccionado matrices poliméricas pertenecientes al grupo de las poliolefinas debido al elevado número de posibilidades que ofrece este tipo de polímeros al presentar una gran variedad de estructuras moleculares. Sin embargo, se espera que la metodología desarrollada en esta tesis se pueda aplicar a otros tipos de matrices poliméricas.

El proceso de espumado es un proceso que comprende varios pasos importantes: nucleación, crecimiento de las celdas, degeneración de las celdas y estabilización (ver, para más detalles, capítulo 2, sección 2.4.2.2) [11]. Se utiliza el término nucleación para denotar cualquier proceso que conduce a la formación de las celdas en la matriz polimérica. Posteriormente, estas celdas crecen debido a que se produce una difusión del gas desde la matriz polimérica hasta las celdas nucleadas. Este crecimiento de las celdas continúa hasta que se estabiliza la estructura celular mediante el enfriamiento de la espuma. Durante el crecimiento de las celdas, el polímero es sometido a flujos extensionales [12]. A medida que las celdas crecen la extensión que sufre el polímero (contenido en las paredes de las celdas) también aumenta y

como consecuencia el espesor de las paredes de las celdas (δ_{CW}) se reduce. Si no se utiliza el polímero apropiado, las paredes de las celdas no pueden resistir la deformación a la que están sometidas y finalmente se rompen (Figura 0.5). Además, cuando las paredes se rompen, la espuma no es capaz de retener el gas durante el proceso de expansión y la estructura celular colapsa [11,12]. Por lo tanto, se puede concluir que no todas las poliolefinas son adecuadas para producir materiales celulares, especialmente cuando se quieren producir espumas de media y baja densidad en las que el polímero se somete a elevadas elongaciones.

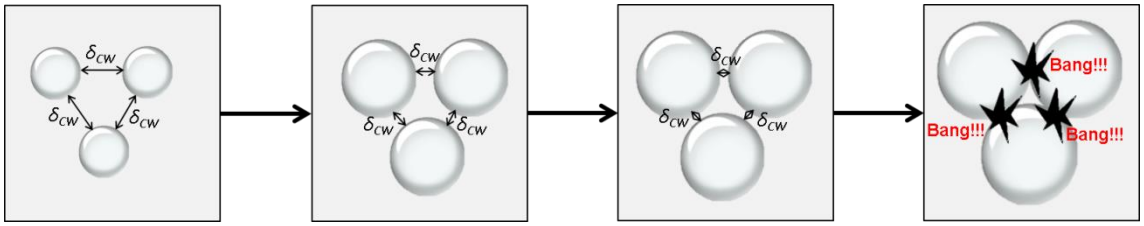

Figura 0.5. Crecimiento de las celdas durante el proceso de espumado de un polímero que no es adecuado para este tipo de aplicación.

Varios trabajos han demostrado que el tipo de **comportamiento reológico extensional** que muestran los polímeros, es decir, la manera en la que la viscosidad extensional de los polímeros depende de la extensión a la que éstos son sometidos, es un aspecto clave a la hora de producir espumas de media y baja densidad [13,14,15]. Los polímeros apropiados para aplicaciones de espumado son aquellos cuya viscosidad extensional aumenta bruscamente a medida que la extensión aumenta, en otras palabras, son adecuados los polímeros que presentan **endurecimiento por deformación (*strain hardening*)**. En estos trabajos se demuestra que dos de los principales pasos que componen el proceso de espumado: crecimiento de las celdas y degeneración de las celdas, están muy influenciados por el comportamiento reológico extensional de la matriz polimérica. Por ejemplo, se obtienen mayores grados de expansión (y por lo tanto menores densidades) y estructuras celulares más homogéneas con los polímeros que muestran endurecimiento por deformación (ver capítulo 2, sección 2.5.2).

A partir de los conocimientos previos sobre las relaciones entre el comportamiento reológico extensional de una cierta matriz polimérica y su comportamiento a la hora de espumar, es decir, a partir de los conocimientos previos sobre la manera en la que tanto el crecimiento como la degeneración de las celdas están condicionados por el comportamiento reológico extensional de la matriz polimérica, surgió la idea de usar la reología extensional como una **herramienta para predecir la capacidad de espumar** de sistemas poliméricos complejos. De esta manera, estaría disponible una herramienta muy interesante que permite seleccionar las matrices poliméricas más apropiadas para aplicaciones de espumado.

Teniendo en mente estas ideas, en la siguiente sección (sección 0.2) se presentan los objetivos de esta tesis.

0.2 Objetivos

Se podría decir que esta tesis tiene dos objetivos principales. El **primer objetivo** consiste en:

Analizar y entender en que situaciones la reología extensional se puede utilizar como una herramienta para predecir la capacidad de espumar de diferentes matrices poliméricas complejas.

La clave para poder cumplir el primer objetivo consiste en realizar un **estudio sistemático** en el cual se analice, bajo diferentes condiciones, el efecto que el comportamiento reológico extensional de una matriz polimérica tiene sobre el comportamiento de espumado.

En esta tesis se han seguido dos caminos diferentes para analizar el efecto que tiene el comportamiento reológico extensional de una matriz polimérica sobre su capacidad de espumar:

- Analizar las relaciones que existen entre las propiedades reológicas extensionales de una matriz polimérica y el máximo grado de expansión alcanzado por los materiales espumados.
- Analizar las relaciones que existen entre reología extensional y estructura celular, cuando los materiales espumados tienen la misma densidad.

Para poder desarrollar este estudio sistemático se han definido una serie de objetivos parciales:

- Realizar el análisis utilizando **diferentes matrices poliméricas complejas**, entre las que se incluyen: mezclas de polímeros, micro/nano compuestos poliméricos y matrices poliméricas entrecruzadas.
- Fabricar los materiales espumados utilizando **diferentes procesos**, con el objetivo de determinar si la relación: reología extensional/comportamiento de espumado se ve afectada, de alguna manera, por el tipo de proceso de fabricación empleado.
- Realizar una **caracterización in-situ** de la expansión de la matriz polimérica que permita por un lado, visualizar la evolución de la estructura interna de la espuma polimérica durante su formación y por otro lado, analizar la estabilidad de la espuma en función de diferentes variables como por ejemplo, el comportamiento reológico extensional del polímero.
- Analizar los efectos que se producen sobre la capacidad de espumar por el hecho de cambiar algunos **parámetros del proceso de espumado** como el tiempo de espumado y la temperatura de espumado. Este estudio se realizará en materiales con comportamientos reológicos extensionales muy diferentes. De esta manera, será posible analizar si el comportamiento reológico de la matriz polimérica determina la manera en la que la estructura celular se ve afectada por los parámetros de espumado.

Después de realizar este estudio sistemático, debería ser posible conocer en que situaciones la reología extensional puede ser utilizada como una **herramienta predictiva**. Además, el conocimiento adquirido se utilizará para poder cumplir el **segundo objetivo** general de esta tesis:

Desarrollar una metodología que permita realizar las medidas de reología extensional y analizar los resultados obtenidos en condiciones que sean útiles para posteriormente poder comprender el proceso de espumado; se tendrá en cuenta una posible aplicación de esta metodología como una herramienta que permite seleccionar las formulaciones más adecuadas para espumar sin la necesidad de producir las espumas.

Esta metodología tiene como objetivo establecer una serie de directrices relacionadas tanto con el desarrollo de las medidas de reología extensional como con su interpretación. Para poder cumplir este segundo objetivo, se han definido una serie de objetivos parciales:

- Analizar la importancia de realizar las medidas de reología extensional en un polímero sometido a la misma **historia termo-mecánica** que la empleada con el polímero utilizado para producir las espumas.
- Analizar la importancia de realizar las medidas de reología extensional a la misma **temperatura** que la utilizada para producir las espumas (temperatura de espumado).
- Determinar si es posible establecer una relación entre parámetros característicos del ensayo de reología extensional y parámetros característicos del proceso de espumado, como por ejemplo:
  - **Velocidad de deformación real** o *Hencky strain rate* (ensayo de reología extensional) y **velocidad de crecimiento de las celdas/espuma** (proceso de espumado).
  - **Relación de estiramiento** o *stretching ratio* (ensayo de reología extensional) y **grado de expansión** (proceso de espumado).

Hasta ahora, para evaluar si una matriz polimérica era apropiada (o no) para ser utilizada en procesos de espumado era necesario producir y caracterizar las espumas. Gracias a los conocimientos adquiridos en esta tesis, podría ser posible seleccionar las formulaciones más adecuadas para este proceso sin la necesidad de producir la espuma, siendo solamente necesario un estudio adecuado del comportamiento reológico extensional de las correspondientes formulaciones. A la hora de producir espumas a escala industrial, esto implicaría una gran reducción de costes relacionados con la optimización de las distintas formulaciones.

Con el objetivo de ejemplificar que implica, en términos de reducción de costes, el hecho de aplicar los conocimientos adquiridos en esta tesis en una planta industrial de fabricación de espumas, a continuación se realiza un simple cálculo numérico. Para ello, se considera una compañía especializada en producir espumas poliméricas por extrusión. Esta compañía dispone de una extrusora cuya tasa de producción es de 500 kg/h. Cada prueba de espumado, requerida para determinar si una cierta matriz polimérica es apropiada (o no) para esta aplicación, tiene una duración de al menos cuatro horas incluyendo: el tiempo necesario para purgar la extrusora, el tiempo de estabilización de línea y el tiempo de producción del producto final. Esto significa que se utilizan al menos 2000 kg de polímero en cada prueba de espumado. Considerando un precio de la matriz polimérica de 1.3 €/kg, los costes de materia prima ascienden a 2600 €. Este valor debería incrementarse aproximadamente un 25 % para poder considerar los costes asociados a la producción (consumo de la máquina, costes de personal, etc.). En conclusión, el coste de cada prueba de espumado es de 3250 €. Este valor

no incluye ni los costes asociados a la caracterización de los materiales celulares ni los costes asociados a la gestión de residuos. Si en vez de producir el material, la compañía realiza un estudio reológico extensional de la matriz polimérica (con un coste de aproximadamente 200 €) los costes se reducirían más de 15 veces.

0.3 Marco de la tesis

Este trabajo es parte de la investigación realizada en el **laboratorio de Materiales Celulares (CellMat)** del Departamento de Física de la Materia Condensada de la Universidad de Valladolid, el cual es dirigido por el Prof. Dr. Miguel Ángel Rodríguez Pérez, supervisor también de esta tesis doctoral [16].

CellMat se fundó en el año 1999 en la Universidad de Valladolid por el Prof. Dr. José Antonio de Saja y por el Prof. Dr. Miguel Ángel Rodríguez Pérez. El principal objetivo de este laboratorio consiste en realizar investigaciones sobre materiales celulares, entre los que cabe destacar los siguientes tipos: materiales microcelulares [17,18,19], compuestos celulares [2,20,21], materiales celulares basados en bioplásticos [22,23,24], materiales nanocelulares [25,26,27] y materiales celulares basados en aluminio [28,29,30]. Todos ellos tienen un futuro muy prometedor.

Durante los primeros años, las investigaciones realizadas en CellMat se centraban principalmente en la **caracterización de los materiales celulares** [31,32,33,34,35,36,37]. En estas tesis se analizaba tanto la estructura celular (caracterización microscópica) como las propiedades físicas (caracterización macroscópica) de diferentes tipos de materiales celulares poliméricos comerciales. Gracias a estos trabajos CellMat adquirió un elevado grado de comprensión de las **relaciones existentes entre estructura y propiedades** en materiales celulares poliméricos. Además de las tesis doctorales mencionadas anteriormente, se publicaron más de 30 artículos científicos relacionados con este tema.

Durante este periodo inicial, y continuando con la caracterización de espumas poliméricas comerciales, se realizaron algunos trabajos científicos con el objetivo de analizar como la estructura celular y las propiedades físicas de los materiales espumados se veían afectadas tanto por la composición química de la matriz polimérica como por las condiciones de procesamiento usadas para producir las espumas [38,39,40,41].

No fue hasta el año 2005 cuando el laboratorio CellMat adquirió los equipos necesarios para producir, por sí mismos, materiales espumados. En el año 2012, C. Saiz-Arroyo [2] presentó la primera tesis doctoral que analiza las **relaciones entre composición química, procesado, estructura celular y propiedades físicas** en materiales espumados basados en poliolefinas producidos en CellMat.

Además de todos los trabajos mencionados en los párrafos previos, las investigaciones realizadas en este laboratorio cubren un amplio rango de temas, que han hecho que el laboratorio CellMat sea una referencia internacional en el campo de los materiales celulares. Por ejemplo, CellMat está especializado en analizar los mecanismos que tienen lugar durante el proceso de espumado (**mecanismos de espumado**) [3,42]. Además, las investigaciones de CellMat también se han centrado en optimizar los sistemas actuales de producción de

materiales celulares así como en desarrollar nuevos procesos de producción [2,43,44,45,46,47].

Todas las investigaciones desarrolladas en CellMat se realizan siempre teniendo en cuenta la **aplicación final** de los materiales espumados, ya que uno de los principales principios de este laboratorio es la **transferencia de conocimiento y tecnología** entre la Universidad y la empresa, como un factor clave para el desarrollo industrial. En la Figura 0.6 se resumen los principales temas tratados en CellMat.

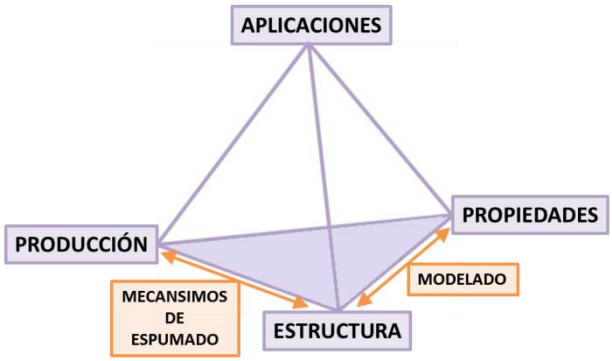

Figura 0.6. Resumen de los temas tratados en CellMat (Tetraedro de los Materiales).

El trabajo de investigación presentado en esta tesis pretende continuar con una de las líneas de investigación "clásicas" desarrolladas en CellMat: establecer una relación entre composición química, producción, estructura y propiedades.

Hasta ahora (Figura 0.7), para obtener esta relación, en un primer paso se seleccionaban las formulaciones, se producían los materiales celulares y posteriormente se caracterizaba su estructura celular y sus propiedades físicas. En un segundo paso se establecían las relaciones entre formulación y estructura celular así como, las relaciones entre proceso de producción y estructura celular. Finalmente, en un tercer paso, se establecía una relación entre estructura celular y propiedades físicas.

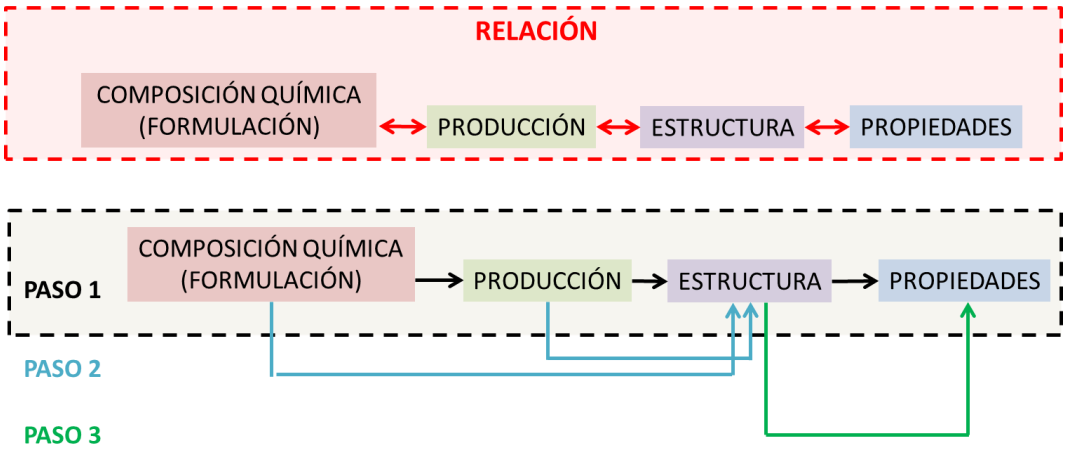

Figura 0.7. Pasos "clásicos" seguidos para poder obtener una relación entre composición química, procesado, estructura y propiedades.

Sin embargo, esta tesis pretende ir un paso más allá. Como ya se ha indicado en la sección previa (sección 0.2), en esta tesis se pretende poner a punto la técnica de reología extensional de manera que esta técnica pueda ser utilizada como una herramienta para predecir la capacidad de espumar de diferentes sistemas poliméricos complejos, sin la necesidad de producir ni caracterizar los materiales celulares (ver Figura 0.8). Además, gracias a los conocimientos previos adquiridos por el grupo, se podrá establecer una relación entre estructura celular y propiedades físicas lo cual permite, finalmente, relacionar los siguientes parámetros: reología extensional, estructura celular y propiedades físicas. Finalmente, para cumplir los objetivos de esta tesis y por lo tanto, poner a punto la técnica de reología extensional, se tendrá en cuenta en todo momento el tipo de proceso seleccionado para producir los materiales celulares.

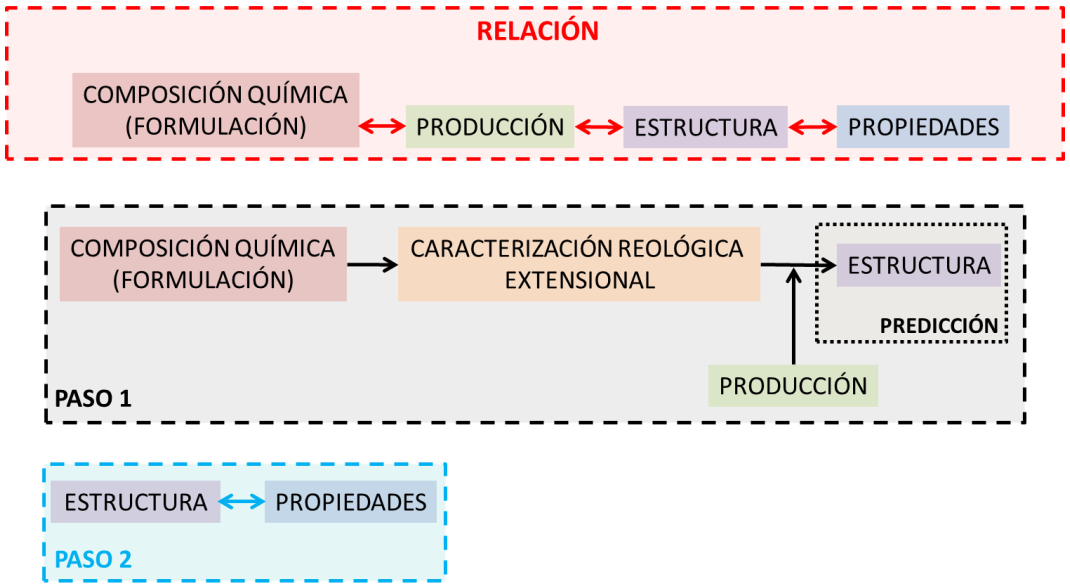

Figura 0.8. Metodología propuesta en esta tesis para obtener la relación entre composición química, procesado, estructura y propiedades, sin la necesidad de producir ni caracterizar los materiales celulares.

Para poder realizar la caracterización reológica extensional, requerida en esta tesis, el laboratorio CellMat adquirió en el año 2010 un reómetro de esfuerzo controlado AR 2000 EX de TA Instruments junto con el accesorio SER 2 de Xpansion Instruments para poder medir la viscosidad extensional de diferentes matrices poliméricas. Por lo tanto, hay que destacar que hasta el comienzo de esta tesis (principios del 2011) nunca antes en CellMat se había realizado una caracterización reológica de las matrices poliméricas que se emplean para producir los materiales celulares.

También es importante mencionar que todas las medidas de reología de cizalla y parte de la caracterización reológica extensional, incluidas en esta tesis, se realizaron en el grupo **SMaRT (Soft Matter, Rheology and Technology**) perteneciente al Departamento de Ingeniería Química de la Universidad de Lovaina (KU Leuven) en Bélgica, bajo la supervisión de la Prof. Dr. Paula Moldenaers (directora de SMaRT) [48]. En este grupo se realizó una estancia de investigación de tres meses que tenía dos objetivos principales:

- Mejorar nuestros conocimientos sobre las técnicas de caracterización reológicas utilizadas para caracterizar matrices poliméricas así como, mejorar nuestros conocimientos sobre la interpretación de los resultados obtenidos con los equipos de reología.
- Realizar una caracterización reológica de las matrices poliméricas seleccionadas, empleando para ello equipos que no estaban disponibles en CellMat.

SMaRT es un grupo con una reputación internacional en el campo de la reología. Probablemente este grupo sea el más potente en este campo en Europa. Su laboratorio dispone de equipos de última generación apropiados para realizar la investigación propuesta en esta tesis.

El conocimiento desarrollado a lo largo de esta tesis se está usando en **proyectos de investigación** con empresas privadas (*Artículos 83)* lo cual, es un indicador de la gran importancia que esta investigación tiene para el sector industrial. Como ya se mencionó anteriormente el desarrollo de la metodología propuesta en esta tesis permitiría seleccionar la formulación más apropiada para aplicaciones de espumado sin la necesidad de producir ni caracterizar los materiales celulares, lo que implicaría una gran reducción de costes.

Estos proyectos han permitido aplicar el trabajo realizado en esta tesis así como, extender este estudio a nuevos materiales y procesos de producción. A continuación (en Tabla 0.1) se recopilan algunos de los proyectos en los que se han utilizado los conocimientos adquiridos a lo largo de esta tesis.

Tabla 0.1. Proyectos de investigación que han surgido a partir de la investigación desarrollada en esta tesis.

Título del Proyecto	Development of microcellular foams
Compañía Financiadora	EPOLI S.A. (PORTUGAL)
Duración	Desde: Enero 2010 hasta: Diciembre 2011
Investigador Principal	M.A. Rodriguez Perez
Presupuesto	140000 €

Título del Proyecto	Utilización de nanopartículas en base sepiolitas para optimizar la estructura y propiedades de espumas con base poliuretano y poliestireno
Compañía Financiadora	TOLSA S.A. (Madrid)
Duración	Desde: Enero 2012 hasta: Enero 2013
Investigador Principal	M.A. Rodriguez Perez
Presupuesto	50000 €

Título del Proyecto	Desarrollo de espumas poliméricas con grados de Repsol
Compañía Financiadora	REPSOL YPF. (Madrid)
Duración	Desde: Enero 2012 hasta: Noviembre 2012
Investigador Principal	M.A. Rodriguez Perez
Presupuesto	48000 €

Título del Proyecto	Development of halogen free flame retardant cellular plastics for the jackets of cables
Compañía Financiadora	NEXANS FR (France)
Duración	Desde: Marzo 2012 hasta: Marzo 2013
Investigador Principal	M.A. Rodriguez Perez
Presupuesto	42000 €

Título del Proyecto	Desarrollo de espumas poliméricas de media-baja densidad
Compañía Financiadora	REPSOL YPF. (Madrid)
Duración	Desde: Enero 2013 hasta: Diciembre 2013
Investigador Principal	M.A. Rodriguez Perez
Presupuesto	58165,9 €

Título del Proyecto	Desarrollo de bandejas de espuma de poliestireno extruido con baja densidad y propiedades mejoradas (XPSLIFE)
Compañía Financiadora	LINPAC PACKAGING (Asturias)
Duración	Desde: Julio 2014 hasta: Diciembre 2015
Investigador Principal	M.A. Rodriguez Perez
Presupuesto	68888,47 €

La investigación desarrollada en esta tesis y el consiguiente dominio de la técnica de reología extensional aplicada al campo de los materiales espumados han permitido al laboratorio (CellMat) mejorar de manera significativa la calidad de sus investigaciones. De hecho, el conocimiento desarrollado en esta tesis también se ha aplicado en diferentes proyectos con financiación pública como los que se muestran en la Tabla 0.2.

Tabla 0.2. Proyectos de investigación, con financiación pública, en los que CellMat ha aplicado los conocimientos adquiridos en esta tesis.

Título del Proyecto	Nancore: Microcellular nanocomposite for substitution of Balsa wood and PVC core material. FP7. 214148
Entidad Financiadora	VII Programa Marco, Comisión Europea
Duración	Desde: Noviembre 2008 hasta: Noviembre 2012
Investigador Principal	M.A. Rodriguez Perez
Presupuesto	407800 €

Título del Proyecto	Nuevos desarrollos en el campo de los materiales poliméricos microcelulares: fabricación, estructura, propiedades, modelización y aplicaciones. MAT 2009-14001
Entidad Financiadora	Programa Nacional de Materiales, MICINN
Duración	Desde: Diciembre 2009 hasta: Diciembre 2012
Investigador Principal	M.A. Rodriguez Perez
Presupuesto	150000 €

Título del Proyecto	Nanocompuestos celulares en base polipropileno diseñados a medida: fabricación, caracterización y aplicaciones. VA174A12-2
Entidad Financiadora	Junta de Castilla y León
Duración	Desde: Enero 2012 hasta: Diciembre 2013
Investigador Principal	M.A. Rodriguez Perez
Presupuesto	30000 €

Título del Proyecto	EVOLUTION: The Electric Vehicle rEVOLUTION enabled by advanced materials highly hybridized into lightweight components for easy integration and dismantling providing a reduced life cycle cost. FP7. 314744
Entidad Financiadora	VII Programa Marco, Comisión Europea
Duración	Desde: Diciembre 2012 hasta: Octubre 2016
Investigador Principal	M.A. Rodriguez Perez
Presupuesto	230000 €

Título del Proyecto	Desarrollo de una nueva generación de aislantes térmicos avanzados basados en la obtención de estructuras porosas nanocelulares. VA035U13
Entidad Financiadora	Junta de Castilla y León
Duración	Desde: Enero 2013 hasta: Diciembre 2014
Investigador Principal	M.A. Rodriguez Perez
Presupuesto	30000 €

Título del Proyecto	Desarrollo de plásticos sub-microcelulares y nanocelulares: fabricación, estructura, propiedades y potenciales aplicaciones. MAT2012-34901
Entidad Financiadora	Programa Nacional de Materiales, MICINN
Duración	Desde: Enero 2013 hasta: Diciembre 2015
Investigador Principal	M.A. Rodriguez Perez
Presupuesto	130000 €

0.4 Principales novedades

Merece la pena señalar que la novedad principal de este trabajo sobre la literatura científica actual es:

El desarrollo de una metodología de trabajo para realizar los ensayos de reología extensional y para interpretar los resultados obtenidos de manera que está técnica pueda ser utilizada como una herramienta para determinar la capacidad de espumar de diferentes sistemas poliméricos.

Además de esta novedad principal (o general), otras novedades más específicas también han surgido de la investigación llevada a cabo en esta tesis. Estas novedades se citan a continuación:

- Caracterización in-situ, mediante radiografías de neutrones con resolución temporal, de la evolución de la estructura interna de espumas basadas en poliolefinas durante su producción dentro de moldes metálicos (ver capítulo 4).
- Análisis de los efectos que el comportamiento reológico extensional de matrices poliméricas basadas en mezclas de polipropileno tiene sobre la estructura celular y sobre las propiedades mecánicas de materiales celulares producidos con la misma densidad (ver capítulo 4).
- Análisis, a través de medios reológicos, de cómo la estructura de las partículas dentro del compuesto polimérico (grado de exfoliación/intercalación y distribución de las partículas) se ve afectada por el tipo de partículas utilizadas (arcillas naturales u organomodificadas), en compuestos basados en polipropileno de alta resistencia en fundido (HMS PP) (ver capítulo 5).
- Análisis, a través de medios reológicos, del efecto del proceso de extrusión sobre la estructura de las partículas en compuestos basados en HMS PP (ver capítulo 5).
- Análisis del efecto del proceso de espumado sobre la estructura de las partículas en compuestos basados en HMS PP (ver capítulo 5).
- Análisis de cómo el proceso de extrusión afecta a las propiedades reológicas (cizalla y extensional) de un HMS PP (ver capítulo 5).
- Análisis de los efectos del comportamiento reológico extensional de compuestos de HMS PP y montmorillonitas sobre la estructura celular y sobre las propiedades mecánicas de materiales celulares producidos con la misma densidad (ver capítulo 5).

- Producción de espumas microcelulares de polietileno de alta densidad entrecruzado (x-HDPE) utilizando un proceso por lotes, como es el proceso de espumado en estado sólido (ver capítulo 6).
- Análisis de los efectos del comportamiento reológico extensional de diferentes x-HDPEs sobre la estructura y densidad de los materiales espumados (ver capítulo 6).
- Análisis de como los parámetros asociados al proceso de producción afectan a la estructura celular de espumas de polietileno de alta densidad, reticulado y sin reticular, producidas por espumado en estado sólido (ver capítulo 6).

0.5 Estructura de la tesis

Esta tesis está escrita por **compendio de publicaciones**. Los resultados experimentales están incluidos en cinco artículos científicos. Tres de ellos ya se encuentran publicados y los otros dos se encuentran pendientes de publicación (ver Tabla 0.3). Estos artículos se incluyen en los capítulos 4, 5 y 6. Además, esta tesis cumple con los requerimientos necesarios para ser acreditada con la **Mención Internacional**.

El manuscrito se divide en **ocho capítulos** que contienen la siguiente información:

Capítulo 1. Introducción. En este capítulo se presenta el marco de esta tesis. También se incluyen los objetivos, contenidos y principales novedades de la tesis. Además, en este capítulo se incluye una lista de todos los artículos científicos, conferencias y proyectos derivados de la investigación realizada en esta tesis. Este capítulo también muestra las ventajas, desde un punto de vista industrial, de poner a punto una técnica como la reología extensional con la finalidad de utilizarla para predecir el comportamiento de espumado de diferentes matrices poliméricas complejas.

Capítulo 2. Antecedentes y estado del arte. Este capítulo aborda una revisión de los principales conceptos relacionados con la reología de polímeros fundidos. Se tienen en cuenta tanto las propiedades reológicas en cizalla (ensayos rotacionales y ensayos oscilatorios de baja amplitud) como las propiedades reológicas extensionales uniaxiales. Además, este capítulo incluye una breve descripción de las características y propiedades de las diferentes matrices poliméricas con las que se ha trabajado en esta tesis. Este capítulo también aborda una revisión de los principales conceptos relacionados con los materiales celulares poliméricos, como los derivados de los principios de formación de espumas poliméricas, técnicas de producción, relaciones entre estructura celular y propiedades mecánicas, etc. Para finalizar, se presenta una descripción de los trabajos científicos existentes que preceden a los realizados en esta tesis como, por ejemplo, los trabajos que analizan el papel que tiene la reología en el espumado de las matrices poliméricas utilizadas en esta tesis: mezclas de polímeros, compuestos poliméricos, y polímeros entrecruzados. Estos estudios más específicos también se pueden encontrar en cada una de las publicaciones científicas incluidas en esta tesis.

Capítulo 3. Materiales, procesos de producción y técnicas de caracterización. En este capítulo se incluye una descripción de toda la colección de materiales empleados en esta tesis, entre otros: polímeros, nanopartículas (arcillas), agentes espumantes, antioxidantes, etc. También se describen los procesos de producción empleados para fabricar los materiales celulares: moldeo por compresión mejorado (ICM), espumado en estado sólido y espumado a presión

atmosférica en molde. Finalmente, en este capítulo se proporciona una breve descripción de las técnicas de caracterización empleadas a lo largo de esta tesis. A pesar de que se puede encontrar una descripción más detallada de todas estas técnicas en los artículos científicos donde son utilizadas, se ha decidido incluir en este capítulo un análisis exhaustivo de dos de estas técnicas: reología y radiografías de neutrones con resolución temporal, debido a su novedad y a su importancia dentro de esta tesis.

Capítulo 4. Espumas de polipropileno: efecto de la reología extensional sobre el comportamiento de espumado. En este capítulo se presenta la investigación desarrollada con matrices poliméricas basadas en polipropileno (PP) puro (sin cargas). Este capítulo se divide en dos partes cada una de las cuales incluye un artículo científico. Los dos artículos tienen una característica en común ya que ambos analizan el efecto del comportamiento reológico extensional sobre el comportamiento de espumado de diferentes materiales: un polipropileno lineal, un polipropileno de alta resistencia en fundido y mezclas, a diferentes contenidos, de los dos polipropilenos anteriores. Sin embargo, el proceso seleccionado para producir los materiales celulares no es el mismo. En el primer artículo el proceso empleado es *espumado a presión atmosférica en molde* y en el segundo artículo las espumas se producen mediante *moldeo por compresión mejorado*. Otra diferencia entre ambos artículos es el tipo de sistema de caracterización empleado. Mientras que en el primer artículo el proceso de espumado es caracterizado in-situ mediante radiografías de neutrones con resolución temporal, en el segundo artículo se realiza una caracterización ex-situ de los materiales.

Capítulo 5. Espumas de nanocompuestos de polipropileno: efecto de la reología extensional sobre el comportamiento de espumado. En este capítulo la investigación se realiza en dos diferentes tipos de compuestos que contienen polipropileno de alta resistencia en fundido y montmorillonitas. Uno de ellos contiene solamente arcillas naturales y el otro contiene arcillas organomodificadas y un agente compatibilizante. El objetivo de este capítulo consiste en analizar las relaciones entre el comportamiento reológico extensional de estos compuestos y la estructura y propiedades de los materiales espumados a partir de ellos, para poder determinar, finalmente, si en este tipo de sistemas poliméricos complejos se puede utilizar la reología extensional como una herramienta predictiva. El proceso seleccionado para producir las espumas ha sido moldeo por compresión mejorado. Sin embargo, antes de presentar este estudio, se muestra un artículo complementario en el que se analiza en detalle la estructura de estos compuestos, es decir, el grado de exfoliación/intercalación y la distribución de las partículas dentro de la matriz polimérica. Este artículo se incluye debido a la importancia que tiene el control de la estructura de las partículas a la hora de obtener las propiedades deseadas.

Capítulo 6. Espumas microcelulares en base polietileno de alta densidad. La última matriz polimérica utilizada en esta tesis es un polietileno de alta densidad (HDPE). Este capítulo contiene un artículo científico. En esta artículo se usan diferentes polietilenos entrecruzados, en los que se ha variado el grado de reticulación, para producir espumas microcelulares mediante un proceso de espumado físico conocido como *espumado en estado sólido*. Las propiedades reológicas extensionales de los diferentes polietilenos entrecruzados se miden para analizar su efecto sobre la estructura y densidad de los materiales espumados. Además, también se analizan los efectos que se producen en los materiales con el mayor y el menor

grado de reticulación, por el hecho de variar parámetros del proceso de espumado como el tiempo de espumado y la temperatura de espumado.

Capítulo 7. Desarrollo de una metodología para usar la reología extensional como una herramienta para predecir la capacidad de espumar de matrices poliméricas complejas. En este capítulo, y teniendo en cuenta los resultados experimentales obtenidos en los capítulos previos (capítulos 4, 5 y 6), se propone y se desarrolla una metodología de trabajo. El objetivo de esta metodología consiste en establecer una serie de directrices para realizar e interpretar las medidas de reología extensional de manera que estas medidas puedan ser relacionadas con la capacidad de espumar de una cierta matriz polimérica. El seguimiento de estas directrices permitirá usar la reología extensional como una herramienta predictiva que permite seleccionar las formulaciones más apropiadas para aplicaciones de espumado sin la necesidad de producir ni caracterizar los materiales celulares.

Capítulo 8. Conclusiones y trabajo futuro. En este capítulo se presentan las conclusiones más destacables obtenidas después de completar todo el trabajo de investigación. También se evalúa el grado de cumplimiento de los objetivos propuestos. Para finalizar, en este capítulo se proponen nuevas líneas de investigación, relacionadas con los temas tratados en esta tesis, con el objetivo de poder ampliar los conocimientos y resultados adquiridos durante esta investigación.

En la Figura 0.9 se resumen los capítulos y publicaciones científicas que contribuyen a esta investigación.

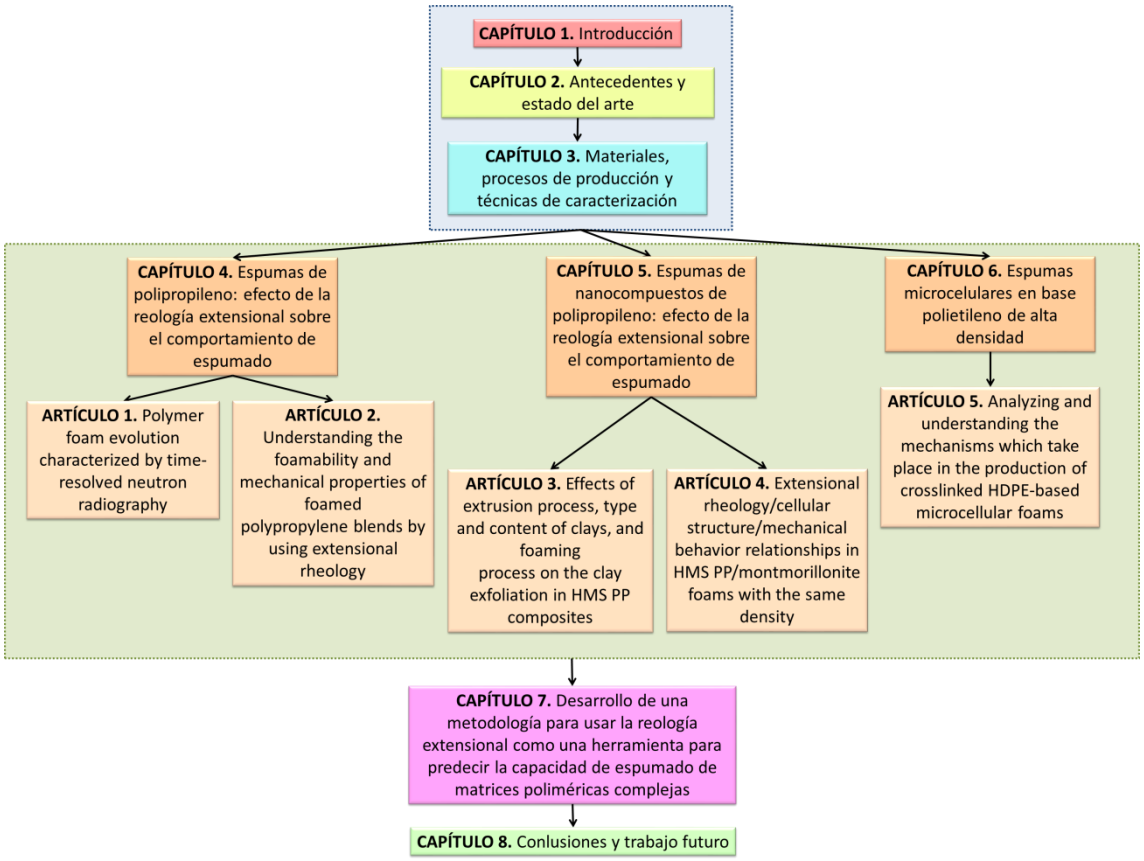

Figura 0.9. Resumen de los capítulos y publicaciones científicas que contribuyen a esta investigación.

0.6 Publicaciones, conferencias y cursos

El trabajo desarrollado durante esta tesis ha dado como resultado la redacción de varios artículos científicos, algunos de los cuales ya se encuentran publicados en revistas internacionales y otros están enviados. Todos ellos se incluyen en la Tabla 0.3. Además, en esta tabla también se especifican los capítulos en los que se incluyen estos artículos.

Tabla 0.3. Artículos científicos que contribuyen a esta tesis.

Nº	Referencia del Artículo	Capítulo
1	E. Solorzano, E. Laguna-Gutierrez, S. Perez-Tamarit, A. Kaestner, M. A. Rodriguez-Perez POLYMER FOAM EVOLUTION CHARACTERIZED BY TIME-RESOLVED NEUTRON RADIOGRAPHY Colloids and Surfaces A: Physicochemical and Engineering Aspects, 473, 46-54, 2015	4
2	E. Laguna-Gutierrez, R. Van Hooghten, P. Moldenaers, M. A. Rodriguez-Perez UNDERSTANDING THE FOAMABILITY AND MECHANICAL PROPERTIES OF FOAMED POLYPROPYLENE BLENDS BY USING EXTENSIONAL RHEOLOGY Journal of Applied Polymer Science, In Press, DOI: 10.1002/app.42430, 2015	4
3	E. Laguna-Gutierrez, R. Van Hooghten, P. Moldenaers, M. A. Rodriguez-Perez EFFECTS OF EXTRUSION PROCESS, TYPE AND CONTENT OF CLAYS AND FOAMING PROCESS ON THE CLAY EXFOLIATION IN HMS PP COMPOSITES Journal of Applied Polymer Science, In Press, DOI: 10.1002/app.42828, 2015	5
4	E. Laguna-Gutierrez, A. Lopez-Gil, C. Saiz-Arroyo, R. Van Hooghten, P. Moldenaers, M. A. Rodriguez-Perez EXTENSIONAL RHEOLOGY/CELLULAR STRUCTURE/MECHANICAL BEHAVIOR RELATIONSHIPS IN HMS PP/MONTMORILLONITE FOAMS WITH THE SAME DENSITY Artículo enviado	5
5	E. Laguna-Gutierrez, J. Pinto, V. Kumar, M. A. Rodriguez-Perez ANALYZING AND UNDERSTANDING THE MECHANISMS WHICH TAKE PLACE IN THE PRODUCTION OF CROSSLINKED HDPE-BASED MICROCELLULAR FOAMS Artículo enviado	6

Además estos trabajos se han presentado en conferencias internacionales y nacionales (ver Tabla 0.4).

Tabla 0.4. Comunicaciones orales, posters y contribuciones a conferencias internacionales y nacionales.

1	E. Laguna-Gutierrez, J. Escudero, M. A. Rodriguez-Perez **CHARACTERIZATION OF POLYMERIC NANOCOMPOSITES BY USING EXTENSIONAL RHEOLOGY** XII ESCUELA NACIONAL DE MATERIALES MOLECULARES, Febrero 2011, Benicàssim, Castellón, España. Presentación oral
2	E. Laguna-Gutierrez, J. Escudero, A. Lopez-Gil and M. A. Rodriguez-Perez **UNDERSTANDING THE FOAMABILITY OF POLYPROPYLENE BLENDS AND POLYPROPYLENE NANOCOMPOSITES BY USING EXTENSIONAL RHEOLOGY** 8th ANNUAL EUROPEAN RHEOLOGY CONFERENCE (AERC), Abril 2013, Lovaina, Bélgica. Presentación oral
3	A. Lopez-Gil, J. Escudero, E. Laguna-Gutierrez, C. Saiz-Arroyo, M.A. Rodriguez-Perez **ANICELL. LOW DENSITY AND NON-CROSSLINKED POLYPROPYLENE FOAMS AS A PROMISING OPTION TO PRODUCE STRUCTURAL PANELS** EUROTEC 2013, Julio 2013, Lyon, Francia. Presentación oral
4	E. Solórzano, E. Laguna-Gutierrez, S. Pérez-Tamarit, A. Kaestner, J. Pinto, M.A. Rodríguez-Pérez **POLYMER FOAM EVOLUTION CHARACTERIZED BY TIME-RESOLVED NEUTRON RADIOGRAPHY** EUFOAM 2014, 10th EUROPEAN CONFERENCE ON FOAMS AND APPLICATIONS, Julio 2014, Tesalónica, Grecia. Presentación oral

5	E. Laguna-Gutierrez, A. Lopez-Gil, C. Saiz- Arroyo, M.A. Rodriguez-Perez **EXTENSIONAL RHEOLOGY: A TOOL TO PREDICT THE FOAMABILITY OF COMPLEX SYSTEMS SUCH AS POLYMER BLENDS AND RECYCLED POLYMERS** FOAMS 2014, 12th INTERNTIONAL CONFERENCE ON FOAMS MATERIALS & TECHNOLOGY, Septiembre 2014, Iselin, NJ, EEUU. Presentación oral
6	E. Laguna-Gutierrez, P. Moldenaers, M.A. Rodriguez-Perez **UNDERSTANDING THE CELLULAR STRUCTURE AND MECHANICAL PROPERTIES OF CELLULAR NANOCOMPOSITES BASED ON POLYPROPYLENE AND LAYERED SILICATES BY USING EXTENSIONAL VISCOSITY MEASUREMENTS** FOAMS 2014, 12th INTERNTIONAL CONFERENCE ON FOAMS MATERIALS & TECHNOLOGY, Septiembre 2014, Iselin, NJ, EEUU. Poster *Poster Premiado*
7	A. Kaestner, E. Solórzano, E. Laguna-Gutierrez, S. Pérez-Tamarit, J. Pinto, M.A. Rodríguez-Pérez **POLYMER FOAM EVOLUTION CHARACTERIZED BY TIME-RESOLVED NEUTRON RADIOGRAPHY** WCNR-10. 10th WORLD CONFERENCE ON NEUTRON RADIOGRAPHY, Octubre 2014, Grindelwald, Suiza. Poster
8	C. Saiz-Arroyo, E. Laguna-Gutiérrez, M. A. Rodríguez-Pérez **EXTENSIONAL RHEOLOGY AS A TOOL TO PREDICT THE FOAMING BEHAVIOUR OF POLYMERIC FORMULATIONS. CASE STUDIES** POLYMER FOAM 2014, Noviembre 2014, Colonia, Alemania. Presentación oral
9	E. Laguna-Gutierrez, R. Van Hooghten, M. A. Rodriguez-Perez, P. Moldenaers **UNDERSTANDING THE FOAMABILITY AND MECHANICAL PROPERTIES OF FOAMED POLYPROPYLENE BLENDS BY USING EXTENSIONAL RHEOLOGY** PPS-31, 31st INTERNATIONAL CONFERENCE OF THE POLYMER PROCESSING SOCIETY, Junio 2015, Isla de Jeju, Corea. Presentación oral

Además durante esta tesis se han realizado varios cursos con el objetivo de adquirir nuevos conocimientos en el área de reología. Estos cursos se incluyen en la Tabla 0.5.

Tabla 0.5. Cursos que se han realizado durante esta tesis.

1	TA INSTRUMENTS: SEMINARIOS Y CURSOS DE USUARIO DE REOLOGÍA Madrid, España, Junio 2011
2	CURSO TEÓRICO/PRÁCTICO DE REOLOGÍA: COMPORTAMIENTO MECÁNICO/REOLÓGICO DE MATERIALES Ferrol, España, Junio 2011
3	14th EUROPEAN SCHOOL ON RHEOLOGY Lovaina, Bélgica, Septiembre 2013

Para finalizar, en la Tabla 0.6 se muestran las actividades adicionales que se han desarrollado durante esta tesis y que no contribuyen directamente a los resultados presentados en el manuscrito.

Tabla 0.6. Actividades adicionales.

PUBLICACIONES CIENTÍFICAS	
1	J. Lazaro, E. Laguna-Gutiérrez, E. Solorzano, M.A. Rodríguez-Pérez EFFECT OF MICROSTRUCTURAL ANISOTROPY OF PM PRECURSORS ON THE CHARACTERISTIC EXPANSION OF ALUMINUM FOAMS Metallurgical and Materials Transactions B, 984-991, 44B, 2013

2	S. Pardo-Alonso, E. Solorzano, J. Vicente, L. Brabant, M. Dierick, I. Manke, A. Hilger, E. Laguna-Gutierrez, M. A. Rodriguez-Perez µCT-BASED ANALYSIS OF THE SOLID PHASE IN FOAMS: CELL WALL CORRUGATION AND OTHER PRACTICAL MICROSCOPIC FEATURES Microscopy and Microanalysis, In Press, DOI:10.1017/S1431927615014890, 2015
3	J. Escudero, A. Lopez-Gil, E. Laguna-Gutierrez, M.A. Rodriguez-Perez LOW DENSITY NON-CROSSLINKED CLOSED/OPEN CELL POLYPROPYLENE FOAMS WITH HIGH MECHANICAL PROPERTIES Cellular Polymers, In Press
CONFERENCIAS	
1	J. Escudero, E. Laguna Gutierrez, M.A. Rodriguez-Perez, V. Kumar, A. Galeski **GAS DIFFUSION AND FOAMING IN LOW DENSITY POLYETHYLENE/CLAYS NANOCOMPOSITES** FOAMS 2011, 9th INTERNTIONAL CONFERENCE ON FOAMS MATERIALS & TECHNOLOGY, Septiembre 2011, Iselin, NJ, EEUU. Presentación oral
2	E. Laguna-Gutierrez, E. Solórzano, S. Pardo-Alonso and M. A. Rodríguez-Pérez **MODELLING THE COMPRESSION BEHAVIOUR OF LOW-DENSITY FLEXIBLE FOAMS WITH A PARTIALLY INTER-CONNECTED CELLULAR STRUCTURE** FOAMS 2012, 10th INTERNTIONAL CONFERENCE ON FOAMS MATERIALS & TECHNOLOGY, Septiembre 2012, Barcelona, España. Poster
3	E. Laguna-Gutierrez, B. Notario, J. Pinto, M. A. Rodriguez-Perez **PREPARING STUDENTS OF SCIENTIFIC AND TECHNICAL DEGREES FOR THEIR FUTURE PROFESSIONAL CAREERS** EDULEARN 2015, 7th INTERNATIONAL CONFERENCE ON EDUCATION AND NEW LEARNING TECHNOLOGIES, Julio 2015, Barcelona, España. Presentación virtual
4	B. Notario, E. Laguna-Gutierrez, J. Pinto, M. A. Rodriguez-Perez **FINAL YEAR PROJECT IN PHYSICS´S DEGREE: A NEW CHALLENGE FOR THE SCIENTIFIC AND TECHNICAL TRAINING OF STUDENTS IN THEIR LAST YEAR OF THE PHYSIC´S DEGREE** EDULEARN 2015, 7th INTERNATIONAL CONFERENCE ON EDUCATION AND NEW LEARNING TECHNOLOGIES, Julio 2015, Barcelona, España. Presentación virtual

0.7 Metodología de trabajo empleada en la tesis

En esta sección se describe la metodología de trabajo que se ha seguido a lo largo de esta tesis para desarrollar el trabajo experimental que permite cumplir los objetivos establecidos en la sección 0.2.

1. **Selección de las materias primas.** En primer lugar se han seleccionado las materias primas que se van a emplear para desarrollar el trabajo experimental presentado en esta tesis. Esta selección incluye diferentes tipos de materiales: polímeros (polipropileno lineal, polipropileno de alta resistencia en fundido, polietileno de alta densidad), nanopartículas (arcillas naturales y arcillas organomodificadas), polímeros compatibilizantes, agentes espumantes (químicos y físicos), agentes reticulantes y antioxidantes. Los nombres comerciales así como las principales características de estos materiales se pueden encontrar en el capítulo 3 (sección 3.2).

2. **Producción de las formulaciones sólidas**. Una vez seleccionadas las materias primas, el siguiente paso consiste en producir las formulaciones sólidas. Estas formulaciones se han fabricado con dos principales finalidades. En primer lugar, para caracterizar sus propiedades (térmicas, reológicas, mecánicas, etc.), las cuales posteriormente serán relacionadas con las de los materiales espumados y en segundo lugar, para ser espumadas. Cuando las formulaciones fabricadas van a ser espumadas mediante el uso de agentes

espumantes químicos, para poder caracterizar las mismas, es necesario producir nuevas formulaciones que no contengan el agente espumante. En esta tesis se han utilizado tres sistemas distintos para producir las formulaciones sólidas (Tabla 0.7). Más detalles acerca del proceso en sí mismo, así como de los pasos seguidos en cada proceso para finalmente producir las diferentes formulaciones sólidas pueden ser encontrados en el capítulo 3, sección 3.3.1.

Tabla 0.7. Procesos de producción empleados para fabricar las formulaciones sólidas.

PRODUCCÍON DE LAS FORMULACIONES SÓLIDAS	
Proceso de Producción	**Capítulos**
Extrusión	4, 5, 6
Moldeo por Compresión	4, 5, 6
Entrecruzamiento	6

3. **Caracterización de las materias primas y de las formulaciones sólidas.** Diferentes técnicas de caracterización se han empleado a lo largo de esta tesis para caracterizar tanto las materias primas como las formulaciones sólidas producidas a partir de ellas (Tabla 0.8). Estás técnicas se describen brevemente en el capítulo 3, sección 3.4. Además, un análisis más detallado de cada una de ellas puede encontrarse en los artículos científicos donde estás técnicas son utilizadas.

Tabla 0.8. Resumen de las técnicas empleadas para caracterizar los materiales sólidos.

CARACTERIZACIÓN DE LOS MATERIALES SÓLIDOS	
Técnica de Caracterización	**Capítulos**
Calorimetría Diferencial de Barrido (DSC) (DSC822e de Mettler)	4, 6
Análisis Termogravimétrico (TGA) (TGA/SDTA 861 de Mettler)	4, 5, 6
Reología de Cizalla (AR 2000 EX de TA Instruments)	4, 5
Reología Extensional (AR 2000 EX/SER 2 de TA Instruments/Xpansion Instruments)	4, 6
Reología Extensional (ARES ARES-2K/EVF de TA Instruments)	4, 5
Determinación de la Densidad (Picnometría de gases) (Accupyc II 1340 de Micromeritics)	4, 5, 6
Difracción de Rayos X (D8 Discover A25 de Bruker)	5
Microscopía Electrónica de Barrido (SEM) (Quanta 200 F de FEI)	5
Ensayos de Tracción (Máquina Universal de Ensayos 5.500R6025 de Instron)	5
Determinación del Contenido de Gel (Inmersión en Xileno en Ebullición)	6

4. **Producción de los materiales celulares.** Una vez que se han seleccionado las materias primas, se han producido las formulaciones sólidas y ambas se han caracterizado en detalle, el siguiente paso ha consistido en producir los materiales celulares. Para fabricar

las espumas se han utilizado tres procesos diferentes (Tabla 0.9), los cuales son descritos en detalle en el capítulo 3, sección 3.3.2.

Tabla 0.9. Procesos de producción empleados para fabricar los materiales celulares.

PRODUCCIÓN DE LOS MATERIALES CELULARES	
Proceso de Producción	**Capítulos**
Moldeo por Compresión Mejorado	4, 5
Espumado en Estado Sólido	6
Espumado en Molde a Presión Atmosférica	4

5. **Caracterización de los materiales celulares.** Diferentes técnicas han sido utilizadas para caracterizar los materiales celulares fabricados. Esta caracterización ha permitido analizar cualitativamente la estructura celular de estos materiales así como, cuantificar parámetros estructurales como el tamaño de celda, el contenido de celdas abiertas, la anisotropía de las celdas, la homogeneidad de la estructura celular, etc. Además, a través de esta caracterización se ha podido determinar la densidad de estos materiales y sus propiedades mecánicas (Tabla 0.10). Una vez más, en el capítulo 3 (sección 3.4) se puede encontrar una descripción más detallada de estas técnicas.

Tabla 0.10. Resumen de las técnicas empleadas para caracterizar los materiales celulares.

CARACTERIZACIÓN DE LOS MATERIALES CELULARES	
Técnica de Caracterización	**Capítulos**
Radiografías de Neutrones con Resolución Temporal (Fuente de Espalación de Neutrones de Suiza, SINQ)	4
Microscopía Electrónica de Barrido (SEM) (JSM-820 de Jeol)	4, 5, 6
Microscopía Electrónica de Barrido (SEM) (Quanta 200 F de FEI)	5
Determinación de la Densidad (Método Geométrico) (Balanza de Precisión AT 261 de Mettler)	4, 5
Determinación de la Densidad (Método de Arquímedes) (Balanza de Precisión AT 261 de Mettler)	6
Determinación del Contenido de Celdas Abiertas (Picnometría de Gases) (Accupyc II 1340 de Micromeritics)	4, 5
Ensayos de Compresión (Máquina Universal de Ensayos 5.500R6025 de Instron)	4, 5
Difracción de Rayos X (D8 Discover A25 de Bruker)	5

6. **Análisis e interpretación de los resultados obtenidos**. Los resultados obtenidos tras la producción y caracterización de los distintos tipos de materiales (formulaciones sólidas y materiales celulares) han sido analizados y relacionados entre sí con el objetivo principal de determinar en qué situaciones (es decir, para qué materiales poliméricos y para que procesos de producción de espumas) la reología extensional es la herramienta clave a la hora de entender la capacidad de espumar de los materiales poliméricos. Tanto estos resultados como el análisis e interpretación de los mismos se encuentran en los artículos científicos incluidos en los capítulos 4, 5 y 6 de esta tesis.

7. **Desarrollo de una metodología de trabajo**. Los conocimientos adquiridos tras el análisis e interpretación de los resultados incluidos en los capítulos 4, 5 y 6 se han utilizado para crear una metodología de trabajo que permita realizar los ensayos de reología extensional e interpretar los resultados obtenidos tras el ensayo, de manera que estos puedan ser utilizados para seleccionar las formulaciones más apropiadas para aplicaciones de espumado sin la necesidad de producir las espumas (ver capítulo 7).

0.8 Principales resultados y conclusiones

Para concluir, en esta sección se muestran los principales resultados y conclusiones obtenidos en esta tesis.

Para cumplir el **primer objetivo** de esta tesis (ver sección 0.2) se ha realizado un estudio sistemático en el que se analiza, bajo diferentes condiciones, los efectos que tiene el comportamiento reológico extensional de diferentes matrices poliméricas sobre su comportamiento a la hora de espumar.

1. En este estudio sistemático, por un lado, se ha analizado como las propiedades reológicas extensionales de **diferentes tipos de matrices poliméricas** afectan a la estructura celular de los materiales espumados, producidos con el **mismo proceso de producción**. Después de este estudio, se han obtenido las siguientes conclusiones:

- Se han medido y analizado las propiedades reológicas extensionales de tres tipos diferentes de matrices poliméricas (polipropilenos puros, mezclas de polipropilenos miscibles y compuestos basados en polipropileno).
- Se ha realizado un análisis detallado de la estructura de los compuestos en base polipropileno que ha permitido cuantificar el nivel de dispersión de las partículas y su grado de exfoliación/intercalación.
- Se han analizado los efectos que el proceso de extrusión, el tipo y contenido de partículas y el proceso de espumado tienen sobre la estructura de los diferentes compuestos poliméricos.
- Todas estas matrices poliméricas han sido espumadas con **densidades similares**, mediante moldeo por compresión mejorado, y se han caracterizado sus estructuras y propiedades mecánicas.
- Cuando se trabaja o bien, con polipropilenos puros (sin cargas) o bien, con mezclas de polipropilenos miscibles se ha demostrado que mediante el análisis de las propiedades reológicas extensionales de las matrices poliméricas es posible entender la estructura de los materiales espumados. En estos sistemas se puede establecer una relación entre reología extensional, estructura celular y propiedades mecánicas.
- Cuando se trabaja con compuestos basados en polipropileno, no siempre es posible establecer una relación entre reología extensional y estructura celular. La obtención de esta relación está condicionada por el nivel de dispersión y por el tamaño de las partículas en la matriz polimérica.
- Si las partículas que forman el compuesto están aglomeradas y el tamaño de esos aglomerados es mayor que el espesor de las paredes de las celdas, entonces la reología

extensional no es la técnica más apropiada para entender la estructura celular de los materiales espumados.
- Cuando las partículas no están aglomeradas, es decir, se encuentran bien dispersas en la matriz polimérica, es posible establecer una relación entre reología extensional, estructura celular y propiedades mecánicas.

2. Por otro lado, se ha analizado la influencia que tiene el **proceso seleccionado** para producir los materiales celulares, en el establecimiento de una relación entre reología extensional y estructura celular. Con este fin, las **mismas matrices poliméricas** se han espumado empleando diferentes procesos. A continuación se muestran las principales conclusiones obtenidas:

- Se han analizado las propiedades reológicas de dos tipos de matrices poliméricas (polipropilenos puros y mezclas de polipropilenos miscibles).
- Estos dos tipos de matrices poliméricas se han espumado empleando dos procesos diferentes: moldeo por compresión mejorado (ICM) y espumado en molde a presión atmosférica. Los dos procesos permiten controlar la densidad final de las espumas.
- Mientras que la estructura celular de los materiales producidos por ICM se ha caracterizado mediante un análisis ex-situ, la evolución de la estructura celular durante el proceso de espumado se ha analizado in-situ, en las espumas producidas mediante espumado en molde a presión atmosférica.
- Gracias a este análisis in-situ ha sido posible visualizar y cuantificar el efecto que tienen las propiedades reológicas de los polímeros sobre el crecimiento y degeneración de la estructura celular.
- Hay un acuerdo entre los resultados obtenidos tras los dos tipos de caracterizaciones (in-situ y ex-situ): la manera en la que la espuma envejece, que a su vez determina la estructura final del material celular, está condicionada por las propiedades reológicas extensionales de la matriz polimérica.
- El análisis in-situ, demuestra que la estabilidad de la espuma depende, además de las propiedades reológicas, de la densidad final de los materiales celulares y de la cantidad de agente espumante utilizado.
- Si el endurecimiento por deformación (*strain hardening*) de los polímeros que están siendo comparados, depende de la misma manera de la velocidad de deformación real (*Hencky strain rate*), es posible establecer una relación entre reología extensional y estructura celular, independientemente del proceso de espumado empleado.

3. Para finalizar, en este estudio sistemático, se ha analizado la manera en la que tanto las **propiedades reológicas** de las matrices poliméricas como los **parámetros de espumado** (temperatura y tiempo de espumado) afectan a la capacidad de dichos polímeros de alcanzar **altos grados de expansión**, y por lo tanto bajas densidades. Las conclusiones obtenidas son:

- Se han medido las propiedades reológicas de diferentes tipos de matrices poliméricas, las cuales se han obtenido a partir de un polietileno de alta densidad (HDPE) que ha sido entrecruzado empleando diferentes cantidades de un agente de entrecruzamiento.
- Los diferentes HDPEs entrecruzados (x-HDPE) se espumaron mediante el proceso conocido como espumado en estado sólido. Con este proceso es muy difícil controlar la densidad de

las espumas. Se han empleado diferentes tiempos y temperaturas para producir las espumas.

- Cuando el contenido de agente entrecruzante aumenta por un lado, aumenta la cantidad de gas disponible para espumar y por otro lado, las propiedades reológicas extensionales mejoran. Como consecuencia, se obtienen materiales celulares con mayores grados de expansión, menores tamaños de celdas y mayores densidades celulares.
- Después de analizar el efecto del tiempo de espumado, se puede concluir que la estructura celular del material con el mayor grado de entrecruzamiento es la más estable con el tiempo, debido al elevado endurecimiento por deformación de este material.
- La coalescencia celular ocurre a mayores temperaturas en el HDPE con el mayor grado de entrecruzamiento que en el HDPE no entrecruzado, debido a las mejores propiedades reológicas extensionales del polietileno entrecruzado.

Por lo tanto, a partir de este estudio sistemático se puede obtener la siguiente conclusión general:

En los siguientes tipos de matrices poliméricas: polímeros puros, mezclas de polímeros miscibles y polímeros entrecruzados, la reología extensional es la herramienta que permite entender por un lado, la estructura celular de las espumas producidas con la misma densidad y por otro lado, la estructura celular y la capacidad de los materiales poliméricos de alcanzar altos grados de expansión, cuando el proceso seleccionado para producir las espumas no permite controlar la densidad de los materiales celulares. Por lo tanto, en estos sistemas poliméricos se puede utilizar la reología extensional como una herramienta para predecir la capacidad de espumar de las matrices poliméricas sin la necesidad de producir ni caracterizar las espumas.

Además, la relación entre reología extensional y estructura celular se puede establecer independientemente del proceso seleccionado para producir los materiales celulares siempre que el endurecimiento por deformación de los materiales estudiados dependa de la misma manera de la velocidad de deformación real.

Para cumplir el **segundo objetivo** de esta tesis (ver sección 0.2) se han realizado diferentes estudios que permiten determinar por un lado, la manera más apropiada de realizar las medidas de reología extensional y por otro lado, la manera más apropiada de representar e interpretar los resultados reológicos, de manera que la reología extensional pueda utilizarse para determinar cuáles son las matrices poliméricas más apropiadas para aplicaciones de espumado. De estos trabajos se han obtenido las siguientes conclusiones:

- Para poder establecer una relación entre reología extensional y comportamiento de espumado, es necesario realizar las medidas de reología extensional en un polímero con la misma historia termo-mecánica que la del polímero que va a ser espumado, ya que el comportamiento reológico extensional de un polímero está muy influenciado por su historia termo-mecánica.
- El comportamiento reológico extensional de una cierta matriz polimérica está muy influenciado por la temperatura de medida. Por lo tanto se recomienda realizar la caracterización reológica a la misma temperatura que la empleada en el proceso de espumado.

- Se ha diseñado una nueva manera de representar los resultados de reología extensional, que consiste en representar el endurecimiento por deformación como una función de la relación de estiramiento para diferentes velocidades de deformación real.
- Esta nueva manera de representar los resultados de reología extensional permite analizar la dependencia del endurecimiento por deformación con la velocidad de deformación real para los diferentes polímeros bajo estudio. Se ha demostrado que el tipo de dependencia seguida por las diferentes matrices poliméricas es fundamental para determinar si la reología extensional puede emplearse como una herramienta predictiva, sin tener en cuenta el tipo de proceso seleccionado para producir los materiales celulares.
- Gracias a esta manera de representar los datos ha sido posible demostrar que a bajas relaciones de estiramiento, todos los materiales muestran el mismo valor del endurecimiento por deformación, lo que significa que a la hora de producir espumas de alta densidad no importa el tipo de matriz polimérica que se utilice.
- Para mayores valores de la relación de estiramiento, se ha observado que en general, si un polímero presenta un endurecimiento por deformación mayor que otro cualquiera, esta tendencia se va a satisfacer en todo el rango de relaciones de estiramiento analizado. Esto significa que el valor de la relación de estiramiento seleccionada para determinar el coeficiente de endurecimiento por deformación (*strain hardening coefficient*) no depende de la expansión final del material celular.
- No es posible establecer una relación matemática ni entre la velocidad de deformación real y la velocidad de crecimiento de la espuma (o proceso de espumado) ni entre la relación de estiramiento y el grado de expansión de la espuma (o densidad de la espuma). Esto es debido a que las medidas de reología extensional someten a la muestra a una extensión uniaxial y por el contrario, el tipo de extensión experimentada por el polímero contenido en las paredes celulares cuando las celdas crecen, es una extensión biaxial.

A partir de estos estudios ha sido posible establecer una metodología de trabajo mediante el establecimiento de una serie de directrices que deben ser seguidas para poder usar la reología extensional como una herramienta para determinar que matrices poliméricas son las más apropiadas para aplicaciones de espumado.

La metodología desarrollada en esta tesis es una herramienta muy potente desde un punto de vista industrial. Mediante el seguimiento de las directrices establecidas se pueden comparar un elevado número de matrices poliméricas para poder seleccionar la más apropiada para aplicaciones de espumado sin la necesidad de producir ni caracterizar los materiales celulares, lo cual lleva asociado una significante reducción de costes.

0.9 Referencias

[1] L. J. Gibson, M. F. Ashby. Cellular Solids: Structure and Properties (2nd Edition). Cambridge University Press, Cambridge, 1997.
[2] C. Saiz-Arroyo. Fabricación de Materiales Celulares Mejorados Basados en Poliolefinas. Relación procesado-composición-estructura-propiedades. Phd Thesis, University of Valladolid, 2012. I
[3] S. Pardo. X-Ray Imaging Applied to the Characterization of Polymer Foams' Cellular Structure and its Evolution. PhD Thesis, University of Valladolid, 2014.
[4] M. A. Rodriguez-Perez, J. I. Velasco, D. Arencon, O. Almanza, J. A. de Saja. Journal of Applied Polymer Science, 75, 156-166, 2000.
[5] The Future of Polymer Foams to 2019. Market Report, Smithers Rapra, 2014.
[6] http://www.plastemart.com/
[7] http://www.recticel.com/index.php/company/what-is-polyurethane
[8] http://www.eps.co.uk/applications/index.html
[9] http://building.dow.com/eu/gbr/en/products/styrofoam/index.htm
[10] D. Eaves. Handbook of Polymer Foams. Rapra Technology Limited, Shawbury, 2004.
[11] H. E. Naguib, C. B. Park, U. Panzer, N. Reichelt. Polymer Engineering and Science, 42, 1481-1492, 2002.
[12] S. T. Lee. Foam Extrusion: Principles and Practice, CRC Press, Boca Raton, 2000.
[13] R. Liao, W. Yu, C. Zhou. Polymer, 51, 568-580, 2010.
[14] R. Liao, W. Yu, C. Zhou. Polymer, 51, 6334-6345, 2010.
[15] R. Gendron. Thermoplastic Foam Processing. Principles and Development. CRC Press, Boca Raton, 2005.
[16] www.cellmat.es
[17] J. Lobos. Improving the Stiffness and Strenght of Porous Materials by Enhancement of the Matrix Microstructure and Cellular Morphology. PhD Thesis, University of Valladolid, 2012.
[18] M. Dumon, J. A. Reglero-Ruiz, J. Pinto, M. A. Rodriguez-Perez, J. M. Tallon, M. Pedros, E. Cloutet, P. Viot. Cellular Polymers, 31, 207-212, 2012.
[19] J. A. Reglero, C. Saiz-Arroyo, M. Dumon, M. A. Rodriguez-Perez, J. A. de Saja, L. Gonzalez. Polymer International, 60, 146-152, 2011.
[20] S. Roman-Lorza. Fabricación y Caracterización de Materiales Celulares Retardantes de Llama Libres de Halógenos Basados en Poliolefinas. PhD Thesis, University of Valladolid, 2010.
[21] S. Estravis. Cellular Nanocomposites Based on Rigid Polyurethane and Nanoclays: Fabrication, Characterization and Modeling of the Mechanical and Thermal Properties. PhD Thesis, University of Valladolid, 2014.
[22] A. Lopez-Gil, F. Silva-Bellucci, D. Velasco, M. Ardanuy, M. A. Rodriguez-Perez.Industrial Crops and Products, 66, 194-205, 2015.
[23] M. A. Rodriguez-Perez, R. D. Simoes, S. Roman-Lorza, M. Alvarez-Lainez, C. Montoya-Mesa, C. J. L. Constantino, J. A. de Saja. Polymer Engineering and Science, 52, 62-70, 2012.
[24] M. A. Rodriguez-Perez, R. D. Simoes, C. J. L. Constantino, J. A. De Saja. Journal of Applied Polymer Science, 121, 2324-2330, 2011.
[25] J. Pinto. Fabrication and characterization of nanocellular polymeric materials from nanostructured polymers. PhD Thesis, University of Valladolid, 2014.
[26] B. Notario, J. Pinto, M. A. Rodriguez-Perez. Polymer, 63, 116-126, 2015.
[27] B. Notario, J. Pinto, E. Solorzano, J. A. de Saja, M. Dumon, M. A. Rodríguez-Pérez. Polymer, 15, 57-67, 2015.
[28] J. A. Reglero-Ruiz. Fabricación y Caracterización de Espumas de Aluminio: Aplicaciones en el Sector Aeronáutico. PhD Thesis, University of Valladolid, 2007.
[29] E. Solorzano. Espumas de Aluminio: Proceso de Espumado, Estructura Celular y Propiedades. PhD Thesis, University of Valladolid, 2008.

[30] J. Lazaro. Optimización de la Estructura Cellular en Espumas de Aluminio. PhD Thesis, University of Valladolid, 2014.
[31] M. A. Rodriguez-Perez. Propiedades térmicas y mecánicas de espumas de poliolefinas. PhD Thesis, University of Valladolid, 1998.
[32] O. Almanza. Caracterización y Modelización de las Propiedades Térmicas y Mecánicas de Espumas con Base Polietileno. PhD Thesis, University of Valladolid, 2000.
[33] L. O. Arcos y Rabago. Propiedades Térmicas y Mecánicas en Espumas de Poliolefinas Fabricadas en un Proceso de Moldeo por Compresión. PhD Thesis, University of Valladolid, 2002.
[34] J. L. Ruiz-Herrero. Impacto y Fluencia en Espumas con Base Polietileno. PhD Thesis, University of Valladolid, 2004.
[35] J. I. Gonzalez-Peña. Efecto de Tratamientos Térmicos en Bloques de Espumas de Polietileno de Baja Densidad Fabricados mediante Moldeo por Compresión. PhD Thesis, University of Valladolid, 2006.
[36] M. Alvarez-Lainez. Propiedades térmicas, mecánicas y acústicas de espumas de poliolefina de celda abierta. PhD Thesis, University of Valladolid, 2007.
[37] R. A. Campo-Arnaiz. Aplicación de Técnicas Espectroscópicas al Estudio de la Morfología Polimérica, Propiedades Térmicas y de Emisión de Espumas de Baja Densidad con Base Poliolefina. PhD Thesis, University of Valladolid, 2011.
[38] M. A. Rodriguez-Perez, A. Duijsens, J. A. De Saja. Journal of Applied Polymer Science, 68, 1237-1244, 1998.
[39] M. A. Rodriguez-Perez, J. A. de Saja. The Effect of Blending on the Physical Properties of Crosslinked Closed Cell Polyethylene Foams. Cellular Polymers, 18, 1-20, 1999.
[40] M. A. Rodriguez-Perez. The Effect of Chemical Composition, Density and Cellular Structure on the Dynamic Mechanical Response of Foams. Cellular polymers, 21, 117-136, 2002.
[41] F. Hidalgo. Design and Optimization of Process Parameters in the Manufacture of Crosslinked Polyolefin Foams by Compression Molding. PhD Thesis, University of Valladolid, 2008.
[42] L. O. Salmazo. Cineticas de Espumacion y control de la Estructura Celular en Materiales Basados en caucho Natural y poliolefinas. Phd Thesis, University of Valladolid, 2015.
[43] C. Saiz-Arroyo, J. A. de Saja, J. I. Velasco, M. A. Rodriguez-Perez. Journal of Materials Science, 47, 5680-5692, 2012.
[44] C. Saiz-Arroyo, M. A. Rodriguez-Perez, J. I. Velasco, J. A. de Saja. Composites: Part B, 48, 40-50, 2013.
[45] C. Saiz-Arroyo, M. A. Rodriguez-Perez, J. Tirado, A. Lopez-Gil, J. A. de Saja. Polymer International, 62, 1324-1333, 2013.
[46] M. A. Rodriguez-Perez, J. A. de Saja, J. Escudero, A. Lopez-Gil. Procedimiento de Fabricación de Materiales Celulares de Matriz Termoplástica. Patent, WO 2014009579 A1, 2013.
[47] M. A. Rodriguez-Perez, J. A. de Saja, J. Escudero, J. A. Vazquez. Sistema y Procedimiento de Moldeo de Piezas con Moldes Autoportantes. Patent, ES 2364263 A1, 2012.
[48] https://cit.kuleuven.be/smart

CHAPTER 1

INTRODUCTION

INDEX

1.1 Introduction

Cellular materials (also known as foams) are two-phase materials in which a gaseous phase has been dispersed in a solid phase. These materials, showing an internal cellular structure, can be found in nature. Examples of **natural cellular materials** are: cork, balsa wood, sponge, trabecular bone, coral, cuttlefish bone, Iris leaf, plant stalk, etc. [1] (Figure 1.1).

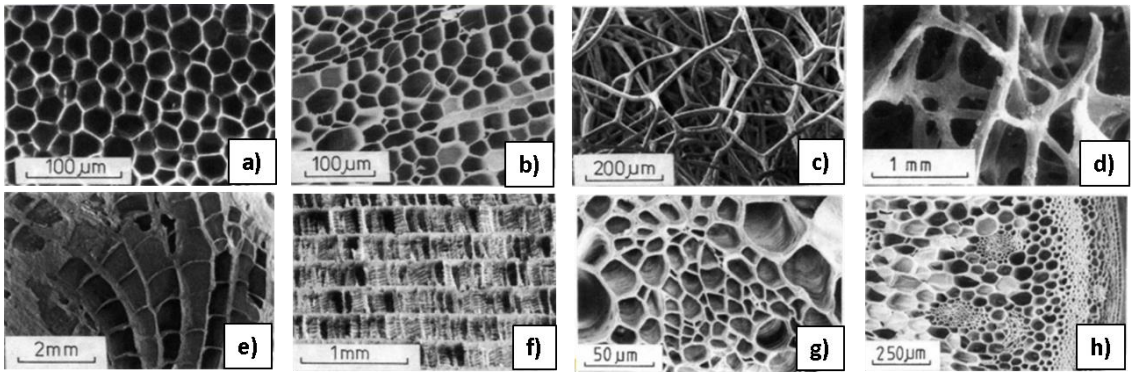

Figure 1.1. Examples of natural cellular materials. a) Cork. b) Balsa wood. c) Sponge. d) Trabecular bone. e) Coral. f) Cuttlefish bone. g) Iris leaf. h) Plant stalk.

Due to the excellent properties that these natural cellular materials show, nowadays different manufactured (man-made) cellular materials have been created imitating these natural structures. These man-made cellular materials can be made from polymers, metals, ceramics, and even glasses [1].

By incorporating a cellular structure into a given material, improvements in different aspects can be achieved [2,3]:

- Reductions of weight.
- Reduction of the amount of raw materials employed with the consequent environmental and economic benefits.
- Adaptable mechanical properties in terms of density.
- Increased ability as thermal insulators.
- Greater absorption of impact energy.
- Sound absorption ability if a cellular structure with interconnected cells is obtained.

Cellular materials have a great present and a promising future in important technological sectors on the one hand, due to their excellent properties and on the other hand, due to the possibility of designing and producing cellular materials that allow fulfilling the requirements demanded by the end-users of these particular materials (tailor-made design).

In particular, the cellular materials produced with a **polymeric matrix** (**polymeric cellular materials**) are, nowadays, used in applications such as packaging, sports and leisure, toys, thermal insulation, automotive, aeronautics, military, aircraft, buoyancy, cushioning, etc. [4]. Figure 1.2 shows examples of some of the main applications of polymeric cellular materials.

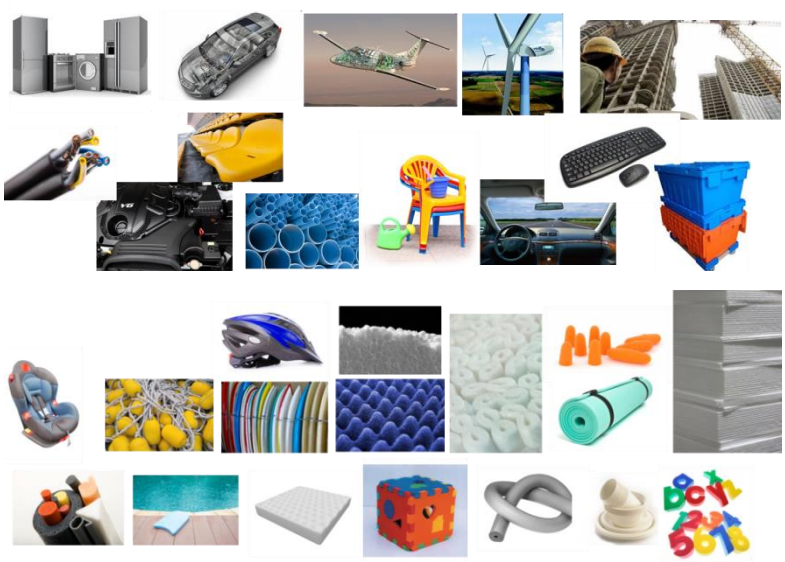

Figure 1.2. Examples of some of the main applications of polymeric cellular materials.

To have an idea of the importance of the polymeric cellular materials sector in today's society, some numerical figures corresponding to the **global market of polymer foams** are provided. The polymer foam market has seen steady growth in demand in the last years, increasing an annual average of 4.4 % between 2009 and 2014. In 2013, the global market for polymer foams totaled 19.1 million tons, representing approximately 86.9 billion dollars. Moreover, growth is expected to slightly accelerate in coming years, seeing an average annual growth of 4.8 % from 2014 until 2019. The polymer foams market expected to consume 25.3 million tons by 2019 [5]. All these figures are summarized in Figure 1.3.

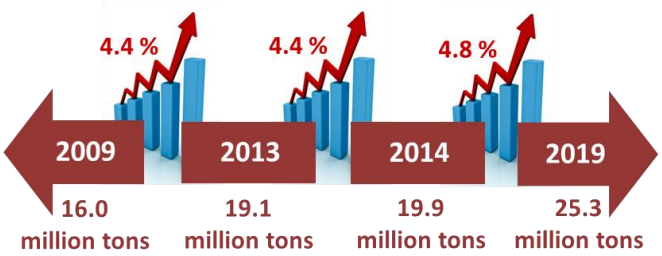

Figure 1.3. Growth of the polymer foam market in the period 2009-2019.

Between all the available polymeric matrices, those based on polyurethane (PU), polystyrene (PS), polyvinyl chloride (PVC) and polyolefins (PO) are the most used to produce cellular materials due to their large number of applications. To have an idea of the importance of each polymeric resin, Figure 1.4 shows the polymeric foam market of the United States in the period 2009-2015 by resin family [6]. The percentages have been calculated according to the millions of tons consumed in this period.

PU foams are mainly used as thermal insulators in buildings and appliances (refrigerators) and also as fillers for seats, chairs and seat cushions, mattress centers, etc. [7]. PS foams are mainly employed in packaging and protections, in construction for the insulation of walls, floors and roofs, in the engineering field as lightweight fillers in road and rail construction, in cycle helmets and surf boards, etc. [8,9,10]. There are three major markets for PVC foam: profiles,

sheets and pipes [10]. The applications of PVC foams are very diverse: cladding, roofing products, windowsills and door frames, skirting boards, advertising boards, building panels, boats and tanks, drain pipes, sewer pipes, ventilation ducts, etc. Finally, PO foams are employed in appliances as gaskets and vibration pads, in the automotive sector as gaskets and seals, water barriers, sound insulators, vibration pads, impact protectors or as lightweight components, in the building and construction sector, they are used as sound absorbers and pipe insulators, in the packaging and protection sector as corner pads, cushion packaging, etc. and in many other sectors such as aerospace, marine, medical and health care, etc. [10].

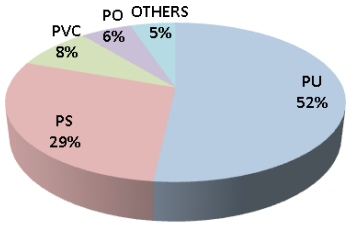

Figure 1.4. Polymeric foam U. S. market by resin family, 2009-2015.

This thesis has been focused on studying and understanding the **foamability and properties** of different **polyolefins**. The reason for selecting polymeric matrices belonging to the group of polyolefins is the large number of possibilities offered by this type of polymers as they present a wide variety of molecular structures. Nevertheless, it is expected that the methodology developed in this thesis can be applied to other types of polymeric matrices.

The foaming process is a process that comprises several major steps: nucleation, cell growth, cell degeneration and stabilization [11] (see chapter 2, section 2.4.2.2 for further details). Cell nucleation is used to denote any process that leads to the formation of bubbles in the polymeric matrix. Then these bubbles grow because the gas diffuses from the gas-polymer matrix into the nucleated cells. Cell growth continues until it stops due to the stabilization of the cellular structure by cooling. During this growth the polymer is subjected to **extensional flows** [12]. As the cells grow the extension to which the polymer (contained in the cell walls) is subjected increases and in addition the thickness of the cell walls (δ_{CW}) is reduced. Therefore, if the appropriate polymer is not employed, the cell walls cannot withstand the deformation to which they are subjected and they break (Figure 1.5). Moreover, if the cell walls break, the foam is unable to retain the gas during the expansion process and consequently, the cellular structure collapses [11,12]. Therefore, it can be concluded that not all the polyolefins are suitable for foam production, especially for the production of medium-density, low-density foams in which the polymer is subjected to high elongations.

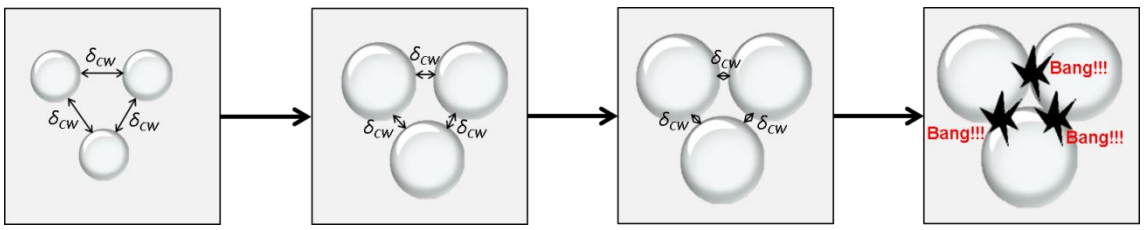

Figure 1.5. Cell growth during the foaming process of a non-suitable polymer for foaming applications.

Several works have demonstrated that the type of **extensional rheological behavior** showed by the polymer, i.e. the way in which the extensional viscosity of the polymer depends on the extension, is a key aspect when producing low/medium density foamed materials [13,14,15]. The suitable polymers for foaming applications are those whose extensional viscosity increases abruptly as the extension increases, that is, those presenting a **strain hardening behavior**. These works demonstrate that two of the main steps comprised by the foaming process: cell growth and cell degeneration are highly influenced by the extensional rheological behavior of the polymeric matrix. For instance, higher expansion ratios (and hence lower densities) and more homogeneous cellular structures are obtained with the polymers presenting strain hardening (see chapter 2, section 2.5.2).

From the previous knowledge about the relationships between the extensional rheological behavior of a given polymeric resin and the foaming behavior, that is, from the previous knowledge about the way in which both, the cell growth and the cell degeneration are conditioned by the extensional rheological behavior of the polymeric matrix, the idea of using the extensional rheology as a **tool to predict the foamability** of more complex polymeric systems was born. Thus, a very powerful tool to select the most appropriate polymeric matrices for foaming applications would be available.

Taking these ideas into account, the objectives of this thesis are presented in the following section (section 1.2).

1.2 Objectives

It could be said that this thesis has two main objectives. The **first objective** is:

To analyze and understand in which situations extensional the rheology can be used as a tool to predict the foamability of complex polymeric systems.

The key to fulfill this first objective consists on performing a **systematic study** which analyzes the effect that the extensional rheological behavior of a polymeric matrix has on the foaming behavior under different conditions.

In this thesis two different ways have been followed in order to analyze the effect of the extensional rheological behavior on the foamability of the polymeric matrix:

- To analyze the relationships between the extensional rheological properties of the polymeric matrix and the maximum expansion ratio achieved by the foamed materials.
- To analyze the relationships between extensional rheology and cellular structure in foamed materials with the same density.

In order to develop this systematic study, a set of partial objectives have been defined:

- To perform the analysis employing different **complex polymeric matrices**, including: polymer blends, polymeric micro/nanocomposites and crosslinked polymeric matrices.
- To produce the foamed materials employing **different foaming processes**, with the aim of determining if the relationship: extensional rheology/foaming behavior is affected, in some way, by the foaming process employed.

- To perform an **in-situ characterization** of the polymer expansion that allows on the one hand, visualizing the evolution of the internal structure of the polymeric foam during its production and on the other hand, analyzing the foam stability as a function of different variables such as the extensional rheological behavior, among others.
- To analyze the effects on the foamability obtained by changing **foaming parameters** like the foaming time and the foaming temperature. This study will be performed in materials with a very different extensional rheological behavior. Thereby, it will be possible to analyze if the rheological behavior of the polymeric matrix determines the way in which the cellular structure is affected by the foaming parameters.

After performing this systematic study, one should be able to know in which situations the extensional rheology can be used as a **predictive tool**. Moreover, the acquired knowledge can be also used to fulfill the **second overall objective** of this thesis.

To develop a methodology to perform the extensional rheological measurements and to analyze the obtained results in conditions which are useful to understand the foaming tests; a possible application of this methodology to the selection of the appropriate formulations without the need to produce the foams will be taken into account.

This methodology aims at giving a set of guidelines related to both, the development of the extensional rheological measurements and their interpretation. To fulfil this second objective, a set of partial objectives have been defined:

- To analyze the importance of performing the extensional rheological measurements in a polymer with the same **thermo-mechanical** history as that of the polymer used for the production of the foam.
- To analyze the importance of performing the extensional rheological measurements at the same **temperature** as that employed to produce the foams (foaming temperature).
- To determine if it is possible to relate characteristic parameters of the extensional rheological test with characteristic parameters of the foaming test, such as:
  - **Hencky strain rate** (extensional rheological test) with **cell growth rate** or **foam growth rate** (foaming test).
  - **Stretching ratio** (extensional rheological test) with **expansion ratio** (foaming test).

Up to now, to evaluate whether a certain (complex) polymeric matrix was suitable (or not) to be used in foaming processes, it was necessary to produce and characterize the foam. With the knowledge acquired in this thesis, it could be possible to select the appropriate formulations without the need to manufacture the foam, being only needed a proper study of the rheological behavior of these formulations. This involves, when it comes to produce foams at **industrial scale**, a huge reduction of costs related to the testing and optimization of the different formulations.

In order to exemplify which implies, in costs reduction, the fact of applying the knowledge acquired in this thesis in an industrial plant of foam production, a simple numerical calculus is performed. For this purpose, a company specialized in producing polymeric foamed materials by extrusion is considered. This company has an extruder with a production rate of 500 kg/h.

Each foaming test, required to determine whether a polymer is appropriate (or not) for foaming, lasts at least four hours, including: the purge of the extruder, the stabilization of the extrusion line and the production of the final product. That means that 2000 kg of polymer are employed in each foaming test. Considering a price of the polymeric matrix of 1.3 €/kg, the raw material costs amounted to 2600 €. This value should be incremented about a 25 % to consider the costs associated with the production (machine consumption, personal costs, etc.). In conclusion, the cost of each foaming test is 3250 €. This cost does not include neither the characterization of the cellular materials produced nor the costs associated to the waste management. If instead of producing the material, the company conducts an extensional rheological study of the polymeric matrix (with a cost of approximately 200 €) the costs would be reduced more than 15 times.

1.3 Framework of this thesis

This investigation is part of the research developed in the **laboratory of Cellular Materials (CellMat**) in the Condensed Matter Physics Department of the University of Valladolid, which is led by Prof. Dr. Miguel Ángel Rodríguez Pérez, supervisor of this PhD thesis [16].

CellMat was founded in 1999 at University of Valladolid by Prof. Dr. José Antonio de Saja and by Prof. Dr. Miguel Angel Rodríguez Pérez, with the main objective of performing investigations on cellular materials, among which it should be highlighted cellular materials such as: microcellular materials [17,18,19], cellular composites [2,20,21], bioplastic based cellular materials [22,23,24], nanocellular materials [25,26,27] and aluminum based cellular materials [28,29,30]. All these materials have a very promising future.

During the first years, the research performed at CellMat was mainly focused on the **characterization of foamed materials** [31,32,33,34,35,36,37]. In these PhD theses both, the cellular structure (microscopic characterization) and the physical properties (macroscopic characterization) of different types of commercial polymeric cellular materials were analyzed. After this initial research CellMat acquired a high degree of compression of the **relationships between structure and properties** in polymeric cellular materials. Besides the aforementioned PhD thesis, more than 30 scientific articles, related to this topic, were also published.

During this initial period, and continuing with the characterization of commercial polymeric foams, some scientific works were also performed with the aim of analyzing how the chemical composition of the polymeric matrix and the foam processing conditions affected the structure and physical properties of the foamed materials [38,39,40,41].

It was in 2005 when the laboratory CellMat acquired the equipment necessary to produce, by themselves, cellular materials. C. Saiz-Arroyo [2] presented in the year 2012, the first PhD thesis which analyzes the **relationships between chemical composition, processing, cellular structure and physical properties** in polyolefin based foamed materials produced in CellMat.

Besides all the works mentioned in the previous paragraphs, the investigations carried out in this lab cover a wide range of topics, which have made the laboratory CellMat an international reference in the field of cellular materials. For instance, CellMat is specialized in analyzing the mechanisms that take place during the foaming process (**foaming mechanisms**) [3,42].

Furthermore, the investigations of CellMat have also been focused on optimizing the current production systems of foamed materials as well as, on developing new foaming processes [2,43,44,45,46,47].

All the investigations developed in CellMat are always performed taking into account the **final application** of the foamed materials, as one of the main principles of this laboratory is the **transfer of knowledge and technology** between the University and the industry, as a key factor to the industrial development. Figure 1.6 summarizes the topics covered by CellMat.

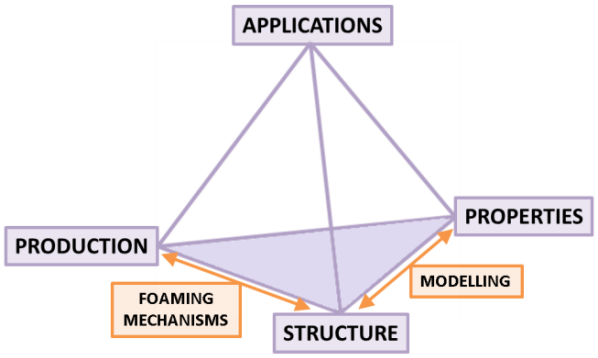

Figure 1.6. Summary of the topics covered by CellMat (Materials Tetrahedron).

The research work presented in this thesis intends to continue with one of the "classical" lines of investigation developed in CellMat: establishing a relationship between chemical composition, production, structure and properties.

Up to now (Figure 1.7), to obtain this relationship, in a first step the formulations were selected, the cellular materials were produced and then the cellular structure and the physical properties were characterized. In a second step the relationships between the formulation and the cellular structure as well as, the relationships between the production process and the cellular structure were established. Finally, in a third step, the cellular structure and the physical properties were related.

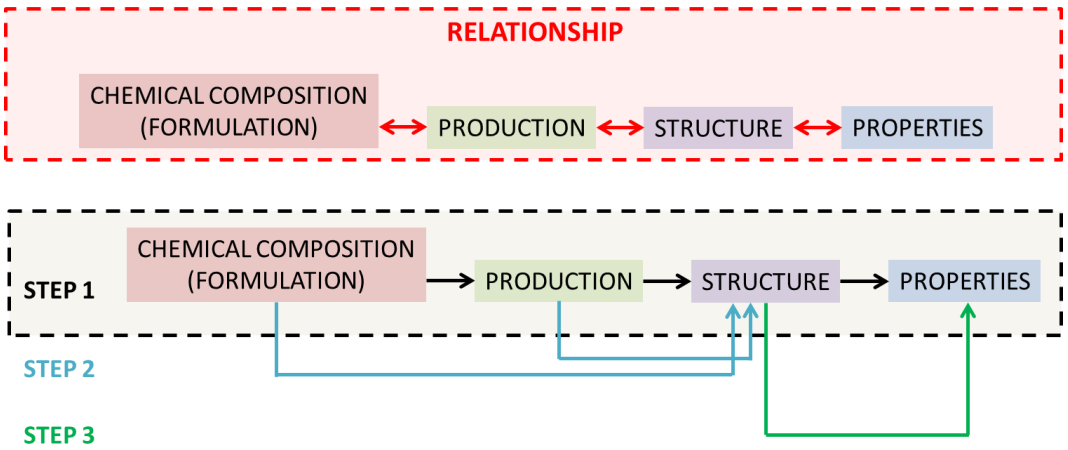

Figure 1.7. "Classical" steps followed to obtain the chemical composition/processing/structure/properties relationship.

However, this thesis intends to go one step further. As was already indicated in the previous section the objective of this thesis consists on tuning up the extensional rheology technique (section 1.2), so that this technique can be used as a tool to predict the foamability of different complex polymeric systems, without the necessity of producing and characterizing the cellular materials (see Figure 1.8). Moreover, thanks to the previous knowledge acquired by the group, the cellular structure and the physical properties may be related with the aim of establishing a relationship between extensional rheology, cellular structure and physical properties. Finally, to fulfill the main objective of this thesis and hence, to tune up the extensional rheology technique, the processes used to produce the foamed materials should be also considered.

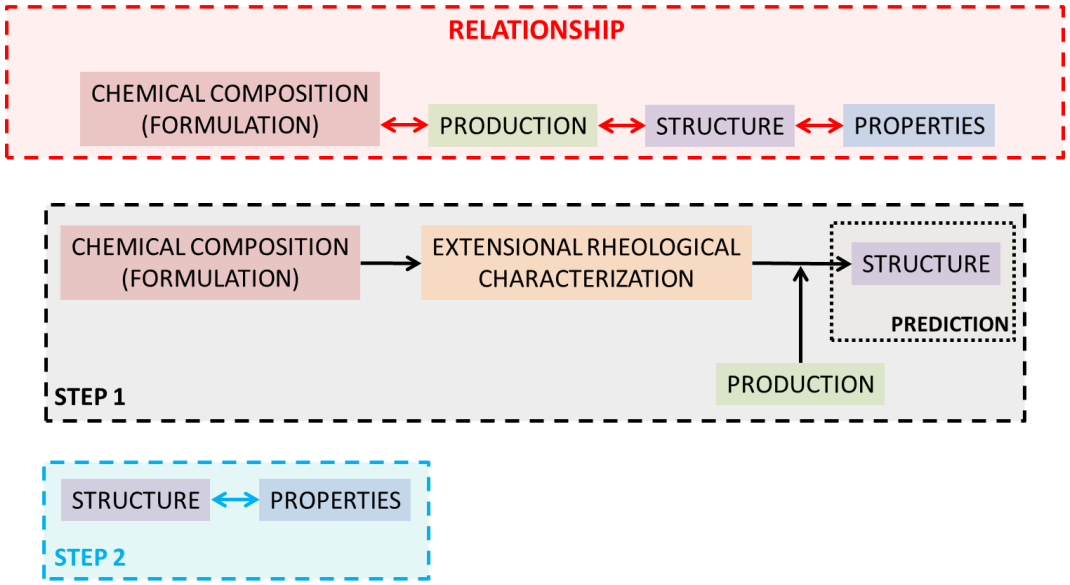

Figure 1.8. Methodology proposed in this thesis to obtain the chemical composition/processing/structure/properties relationship, without the need of producing and characterizing the foamed materials.

To perform the extensional rheological characterization, required in this thesis, a stress controlled rheometer AR 2000 EX, from TA Instruments and the accessory SER 2, from Xpansion Instruments, to measure the extensional viscosity, were acquired by CellMat, in the year 2010. Hence, it must be stressed that until the beginning of this thesis (early 2011), a rheological characterization of the polymeric matrices used for foaming had never been carried out in CellMat.

It is also important to mention that all the shear rheological measurements and part of the extensional rheological characterization, included in this thesis, were performed in the **SMaRT (Soft Matter, Rheology and Technology**) group belonging to the Department of Chemical Engineering at the University of Leuven (KU Leuven) in Belgium, under the supervision of Prof. Dr. Paula Moldenaers (chair of SMaRT) [48]. A stay of three months was carried out in SMaRT with two main objectives.

- To improve our knowledge about both, the rheological characterization techniques employed with polymers and the interpretation of the results obtained with the rheology equipment.

- To perform a rheological characterization of the selected polymeric matrices using some devices which were not available in CellMat.

SMaRT is a group with an international reputation in the field of rheology and it is probably the most powerful group in this field, in Europe. Its laboratory is equipped with the latest equipment, appropriate for the research performed in this thesis.

A large number of **research projects** with private companies (*Artículos 83*) have used the knowledge developed in this thesis, which indicates the great importance of this investigation for the industrial sector. As it was already mentioned the development of the methodology proposed in this thesis would allow selecting the appropriate formulations for foaming without the need of producing and characterizing the cellular materials, which would involve a large cost reduction.

These projects have allowed implementing the work made in this thesis as well as, extending this study to new materials and production process. Some of the projects in which the knowledge developed in this thesis has been used are collected in Table 1.1.

Table 1.1. Research projects that have emerged from the investigation performed in this thesis.

Project Title	Development of microcellular foams
Financial Company	EPOLI S.A. (PORTUGAL)
Duration	From: January 2010 to: December 2011
Principal Investigator	M.A. Rodriguez Perez
Budget	140000 €

Project Title	Use of nanoparticles based on sepiolites to optimize the structure and properties of polyurethane and polystyrene based foams
Financial Company	TOLSA S.A. (Madrid)
Duration	From: January 2012 to: January 2013
Principal Investigator	M.A. Rodriguez Perez
Budget	50000 €

Project Title	Development of polymeric foams with grades of Repsol
Financial Company	REPSOL YPF. (Madrid)
Duration	From: January 2012 to: November 2012
Principal Investigator	M.A. Rodriguez Perez
Budget	48000 €

Project Title	Development of halogen free flame retardant cellular plastics for the jackets of cables
Financial Company	NEXANS FR (France)
Duration	From: March 2012 to: March 2013
Principal Investigator	M.A. Rodriguez Perez
Budget	42000 €

Project Title	Development of low/medium density polymeric foams
Financial Company	REPSOL YPF. (Madrid)
Duration	From: January 2013 to: December 2013
Principal Investigator	M.A. Rodriguez Perez
Budget	58165,9 €

Project Title	Development of extruded polystyrene foamed trays with low density and improved properties (XPSLIFE)
Financial Company	LINPAC PACKAGING (Asturias)
Duration	From: July 2014 to: December 2015
Principal Investigator	M.A. Rodriguez Perez
Budget	68888,47 €

The research developed in this thesis and the consequently mastery of the extensional rheology technique in the field of the foamed materials have allowed the laboratory (CellMat) to improve in a significant way the quality of its investigations. In fact, the knowledge developed in this thesis has also been applied in different research projects with public funding such as those showed in Table 1.2.

Table 1.2. Research projects with public funding in which CellMat has applied the knowledge developed in this thesis.

Project Title	Nancore: Microcellular nanocomposite for substitution of balsa wood and PVC core material. FP7. 214148
Funding Body	VII Framework Programme, European Commission
Duration	From: November 2008 to: November 2012
Principal Investigator	M.A. Rodriguez Perez
Budget	407800 €

Project Title	New developments in the field of microcellular polymeric materials: manufacture, structure, properties, modeling and applications. MAT 2009-14001
Funding Body	National Materials Program, MICINN
Duration	From: December 2009 to: December 2012
Principal Investigator	M.A. Rodriguez Perez
Budget	150000 €

Project Title	Cellular nanocomposites based on polypropylene: production, characterization and applications. VA174A12-2
Funding Body	Junta of Castile and Leon
Duration	From: January 2012 to: December 2013
Principal Investigator	M.A. Rodriguez Perez
Budget	30000 €

Project Title	EVOLUTION: The electric vehicle rEVOLUTION enabled by advanced materials highly hybridized into lightweight components for easy integration and dismantling providing a reduced life cycle cost. FP7. 314744
Funding Body	VII Framework Programme, European Commission
Duration	From: December 2012 to: October 2016
Principal Investigator	M.A. Rodriguez Perez
Budget	230000 €

Project Title	Development of a new generation of advanced thermal insulators based on the obtaining of nanocellular porous structures. VA035U13
Funding Body	Junta of Castile and Leon
Duration	From: January 2013 to: December 2014
Principal Investigator	M.A. Rodriguez Perez
Budget	30000 €

Project Title	Development of sub-microcellular and nanocellular plastics: production, structure, properties and potential applications. MAT2012-34901
Funding Body	National Materials Program, MICINN
Duration	From: January 2013 to: December 2015
Principal Investigator	M.A. Rodriguez Perez
Budget	130000 €

1.4 Main novelties

It is worth pointing out that the main novelty of this work over current scientific literature is:

The development of a methodology of wok to perform the extensional rheological tests, as well as, to interpret the results obtained with them so that, the extensional rheology can be used as a tool to determine the foamability of different complex polymeric systems.

Besides this main (or general) novelty, other more specific novelties have also emerged from the investigation carried out in this thesis. They are listed below:

- In-situ characterization by means of time-resolved neutron radiography of the evolution of the internal structure of polyolefin based foams inside metallic molds during its production (see chapter 4).
- Analysis of the effects of the extensional rheological behavior of polymeric matrices based on polypropylene blends on the cellular structure and mechanical properties of foamed materials produced with the same density (see chapter 4).
- Analysis, by rheological means, of the effects on the clay structure (degree of exfoliation and clay distribution) produced by using different types of particles (natural and organomodified clays), in high melt strength polypropylene (HMS PP) based composites (see chapter 5).
- Analysis, by rheological means, of the effect of the extrusion process on the clay structure in HMS PP based composites (see chapter 5).
- Analysis of the effect of the foaming process, by itself, on the clay structure of HMS PP based composites (see chapter 5).
- Analysis of the effect of the extrusion process on the rheological properties (shear and extensional) of a HMS PP (see chapter 5).
- Analysis of the effect of the extensional rheological behavior of HMS PP/montmorillonite composites on the cellular structure and mechanical properties of foams produced with the same density (see chapter 5).
- Microcellular foaming of crosslinked high density polyethylene (x-HDPE) using a batch process like solid state foaming (see chapter 6).
- Analysis of the effect of the extensional rheological behavior of x-HDPEs on the cellular structure and density of the foamed materials (see chapter 6).
- Analysis of the effect of the production process parameters on the cellular structure of non-crosslinked and crosslinked HDPEs produced by solid state foaming (see chapter 6).

1.5 Structure of the thesis

This thesis is written as a **compendium of publications**. The experimental results are supported by five scientific papers. Three of them have already been published and the other

two are pending of publication (see Table 1.3). These papers are included in the chapters 4, 5 and 6. Moreover, this thesis fulfills the necessary requirements to be accredited with the **International Mention**.

The manuscript is divided into **eight chapters** containing the following information:

Chapter 1. Introduction. The framework of this thesis is presented in this chapter. Also the objectives, contents and main novelties of this thesis are included here. Moreover, in this chapter the scientific articles, conferences and projects derived from this thesis are also listed. In addition, this chapter shows the advantages, from an industrial point of view, of tuning up a technique like extensional rheology to be used as a tool to predict the foamability of different complex polymeric matrices.

Chapter 2. Background and state of the art. This chapter deals with a revision of the main concepts related to the rheology of molten polymers. Both, the rheological properties in shear (rotational tests and small amplitude oscillatory tests) and in uniaxial extension are considered. Moreover, this chapter also includes a brief description of the characteristics and properties of the different polymeric matrices included in this thesis. The main concepts related to polymeric cellular materials, such as those derived from the principles of foaming formation, production techniques, cellular structure/mechanical properties relationships, etc. are also included in this chapter. Finally, a description of the works leading up to those performed in this thesis is also presented here, such as those which analyze the role of extensional rheology in the foaming of the polymeric matrices employed in this thesis: polymer blends, polymeric composites and crosslinked polymers. These specific studies can also be found in each of the scientific publications included in this thesis.

Chapter 3. Materials, production processes and characterization techniques. The whole collection of materials employed in this thesis, such as: polymers, nanofillers (clays), blowing agents, crosslinking agents, antioxidants, etc. are described in this chapter. The production processes employed to produce the foamed materials: improved compression molding (ICM), solid state foaming and foaming at atmospheric pressure in a mold are also described in detail. Finally, in this chapter a brief description of the characterization techniques used throughout this thesis is given. Although a detailed description of these techniques can be found in the scientific papers in which they are used, it was decided to include in this chapter a comprehensive analysis of two of these characterization techniques: rheology and time-resolved neutron radiography, due to their importance and novelty.

Chapter 4. Polypropylene foams: effect of extensional rheology on the foaming behavior. In this chapter the research carried out with pure (unfilled) polypropylene (PP) based polymeric matrices is described. This chapter is divided into two parts including, each of them, a scientific paper. Both papers have a common characteristic as they analyze the effect of the extensional rheological behavior on the foaming behavior of a linear polypropylene (linear PP), a HMS PP and different blends of the linear and the HMS PP. However, the processes employed to produce the cellular materials are not the same. In the first paper, the process used has been *foaming at atmospheric pressure in a mold*, and in the second paper the *improved compression molding* route has been used. Another difference is the characterization system employed. While in the first paper and in-situ characterization of the foaming process is carried out by

using time-resolved neutron radiography, an ex-situ characterization (traditional characterization) is performed in the second paper.

Chapter 5. Polypropylene nanocomposite foams: effect of extensional rheology on the foaming behavior. In this chapter the research is conducted in two different types of HMS PP/montmorillonite composites, one of them containing only natural clays and the other one containing organomofified montmorillonites and a compatibilizer agent. The aim of this chapter is to analyze the relationships between the extensional rheological behavior of these composites and the structure and properties of the foamed materials produced with them, to finally determine if in these types of complex polymeric systems the extensional rheology can be used as a predictive tool. Improved compression molding has been the process selected to produce the foams. However, before presenting this study, a complementary scientific paper which analyzes the structure of these composites, that is, the degree of exfoliation and the clay distribution in the polymeric matrix, is also included in this chapter, due to the importance of controlling the particles structure to finally obtain the desired properties.

Chapter 6. Microcellular foams based on high density polyethylene. The last polymeric matrix employed in this thesis is a high density polyethylene (HDPE). This chapter contains a scientific paper. In this paper different x-HDPEs, in which the crosslinking degree has been varied, are used to produce microcellular materials by a physical foaming method called *solid state foaming*. The extensional rheological properties of the different x-HDPEs are analyzed to determine its effect on the cellular structure and density of the foamed materials. Moreover, the effects on the materials with the highest and the lowest crosslinking degrees produced by varying foaming parameters like the foaming time and the foaming temperature are also analyzed.

Chapter 7. Development of a methodology to use the extensional rheology as a tool to predict the foamability of complex polymeric systems. Taking into account the experimental results obtained previously (chapters 4, 5 and 6); in this chapter a methodology of work is proposed. The objective of this methodology is to establish a set of guidelines for conducting and interpreting the extensional rheological measurements so that these measurements can be related to the foamability of a given polymeric resin. By following these guidelines, the extensional rheology may be used as a predictive tool which allows selecting the appropriate formulations for foaming without the need of producing and characterizing the cellular materials.

Chapter 8. Conclusions and future work. In this chapter the most remarkable conclusions obtained after the completion of all the research work are presented. Moreover, the degree of fulfillment of the proposed objectives is also assessed. Finally, in this chapter new research lines, related to the topic of this thesis, are proposed with the aim of expanding the knowledge and results acquired during this investigation.

Figure 1.9 summarizes the chapters and scientific publications contributing to this investigation.

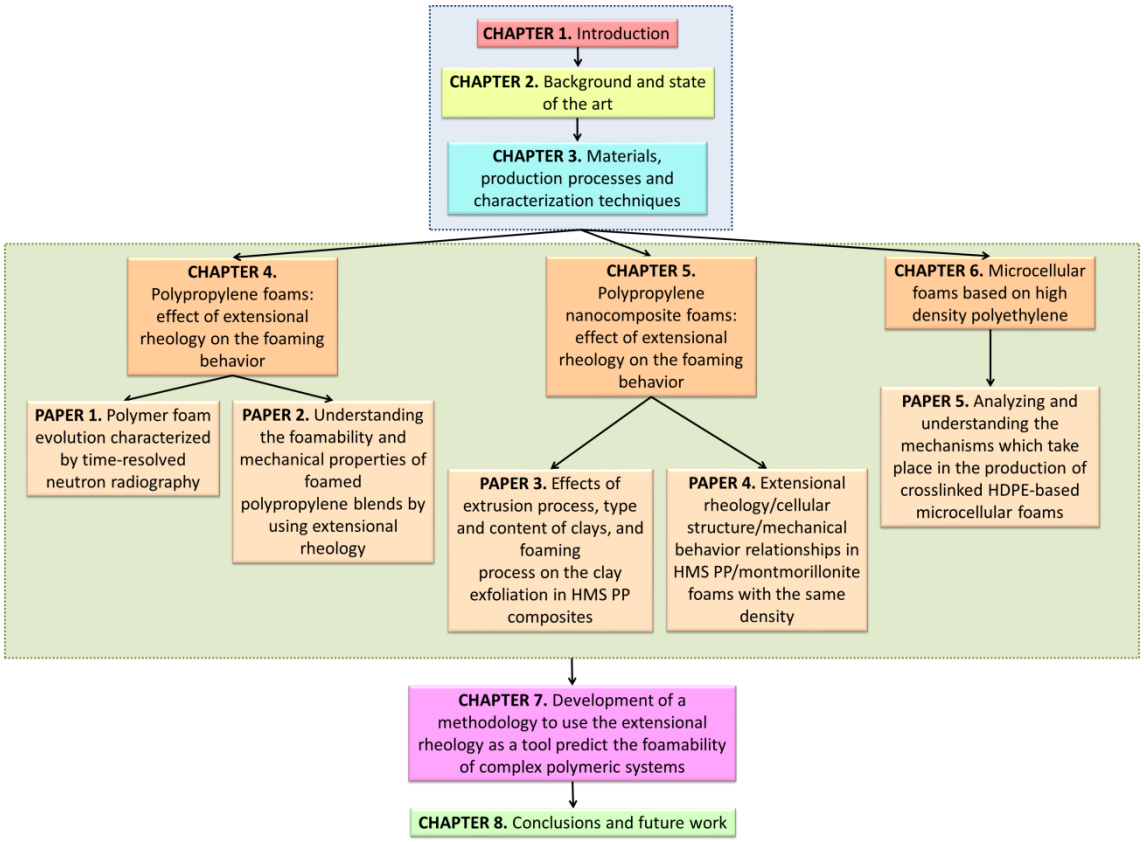

Figure 1.9. Summary of the chapters and scientific publications contributing to this investigation.

1.6 Publications, conferences and courses

The work developed during this thesis resulted in the production of several scientific articles, some of them already published in international journals and others submitted. They are listed in Table 1.3. Moreover, the chapter in which the different articles are included is also specified.

Table 1.3. Scientific articles with results contributing to this thesis.

No.	Article reference	Chapter
1	E. Solorzano, E. Laguna-Gutierrez, S. Perez-Tamarit, A. Kaestner, M. A. Rodriguez-Perez POLYMER FOAM EVOLUTION CHARACTERIZED BY TIME-RESOLVED NEUTRON RADIOGRAPHY Colloids and Surfaces A: Physicochemical and Engineering Aspects, 473, 46-54, 2015	4
2	E. Laguna-Gutierrez, R. Van Hooghten, P. Moldenaers, M. A. Rodriguez-Perez UNDERSTANDING THE FOAMABILITY AND MECHANICAL PROPERTIES OF FOAMED POLYPROPYLENE BLENDS BY USING EXTENSIONAL RHEOLOGY Journal of Applied Polymer Science, In Press, DOI: 10.1002/app.42430, 2015	4
3	E. Laguna-Gutierrez, R. Van Hooghten, P. Moldenaers, M. A. Rodriguez-Perez EFFECTS OF EXTRUSION PROCESS, TYPE AND CONTENT OF CLAYS AND FOAMING PROCESS ON THE CLAY EXFOLIATION IN HMS PP COMPOSITES Journal of Applied Polymer Science, In Press, DOI: 10.1002/app.42828, 2015	5
4	E. Laguna-Gutierrez, A. Lopez-Gil, C. Saiz-Arroyo, R. Van Hooghten, P. Moldenaers, M. A. Rodriguez-Perez EXTENSIONAL RHEOLOGY/CELLULAR STRUCTURE/MECHANICAL BEHAVIOR RELATIONSHIPS IN HMS PP/MONTMORILLONITE FOAMS WITH THE SAME DENSITY Article submitted	5

5	E. Laguna-Gutierrez, J. Pinto, V. Kumar, M. A. Rodriguez-Perez ANALYZING AND UNDERSTANDING THE MECHANISMS WHICH TAKE PLACE IN THE PRODUCTION OF CROSSLINKED HDPE-BASED MICROCELLULAR FOAMS Article submitted	6

In addition, this work was presented in national and international conferences (see Table 1.4).

Table 1.4. Oral communications, posters and contributions to international and national conferences.

1	E. Laguna-Gutierrez, J. Escudero, M. A. Rodriguez-Perez **CHARACTERIZATION OF POLYMERIC NANOCOMPOSITES BY USING EXTENSIONAL RHEOLOGY** XII ESCUELA NACIONAL DE MATERIALES MOLECULARES, February 2011, Benicàssim, Castellón, Spain. Talk
2	E. Laguna-Gutierrez, J. Escudero, A. Lopez-Gil and M. A. Rodriguez-Perez **UNDERSTANDING THE FOAMABILITY OF POLYPROPYLENE BLENDS AND POLYPROPYLENE NANOCOMPOSITES BY USING EXTENSIONAL RHEOLOGY** 8TH ANNUAL EUROPEAN RHEOLOGY CONFERENCE (AERC), April 2013, Leuven, Belgium. Talk
3	A. Lopez-Gil, J. Escudero, E. Laguna-Gutierrez, C. Saiz-Arroyo, M.A. Rodriguez-Perez **ANICELL. LOW DENSITY AND NON-CROSSLINKED POLYPROPYLENE FOAMS AS A PROMISING OPTION TO PRODUCE STRUCTURAL PANELS** EUROTEC 2013, July 2013, Lyon, France. Talk
4	E. Solórzano, E. Laguna-Gutierrez, S. Pérez-Tamarit, A. Kaestner, J. Pinto, M.A. Rodríguez-Pérez **POLYMER FOAM EVOLUTION CHARACTERIZED BY TIME-RESOLVED NEUTRON RADIOGRAPHY** EUFOAM 2014, 10th EUROPEAN CONFERENCE ON FOAMS AND APPLICATIONS, July 2014, Thessaloniki, Greece. Talk
5	E. Laguna-Gutierrez, A. Lopez-Gil, C. Saiz- Arroyo, M.A. Rodriguez-Perez **EXTENSIONAL RHEOLOGY: A TOOL TO PREDICT THE FOAMABILITY OF COMPLEX SYSTEMS SUCH AS POLYMER BLENDS AND RECYCLED POLYMERS** FOAMS 2014, 12th INTERNTIONAL CONFERENCE ON FOAMS MATERIALS & TECHNOLOGY, September 2014, Iselin, NJ, USA. Talk
6	E. Laguna-Gutierrez, P. Moldenaers, M.A. Rodriguez-Perez **UNDERSTANDING THE CELLULAR STRUCTURE AND MECHANICAL PROPERTIES OF CELLULAR NANOCOMPOSITES BASED ON POLYPROPYLENE AND LAYERED SILICATES BY USING EXTENSIONAL VISCOSITY MEASUREMENTS** FOAMS 2014, 12th INTERNTIONAL CONFERENCE ON FOAMS MATERIALS & TECHNOLOGY, September 2014, Iselin, NJ, USA. Poster *Awarded Poster*
7	A. Kaestner, E. Solórzano, E. Laguna-Gutierrez, S. Pérez-Tamarit, J. Pinto, M.A. Rodríguez-Pérez **POLYMER FOAM EVOLUTION CHARACTERIZED BY TIME-RESOLVED NEUTRON RADIOGRAPHY** WCNR-10. 10th WORLD CONFERENCE ON NEUTRON RADIOGRAPHY, October 2014, Grindelwald, Switzerland. Poster
8	C. Saiz-Arroyo, E. Laguna-Gutiérrez, M. A. Rodríguez-Pérez **EXTENSIONAL RHEOLOGY AS A TOOL TO PREDICT THE FOAMING BEHAVIOUR OF POLYMERIC FORMULATIONS. CASE STUDIES** POLYMER FOAM 2014, November 2014, Cologne, Germany. Talk
9	E. Laguna-Gutierrez, R. Van Hooghten, M. A. Rodriguez-Perez, P. Moldenaers **UNDERSTANDING THE FOAMABILITY AND MECHANICAL PROPERTIES OF FOAMED POLYPROPYLENE BLENDS BY USING EXTENSIONAL RHEOLOGY** PPS-31, 31st INTERNATIONAL CONFERENCE OF THE POLYMER PROCESSING SOCIETY, June 2015, Jeju Island, Korea. Talk

Moreover, during this thesis several courses have been conducted with the aim of acquiring new knowledge in the area of rheology. These courses are summarized in Table 1.5.

Table 1.5. Attended courses during this thesis.

1	TA INSTRUMENTS: SEMINARIOS Y CURSOS DE USUARIO DE REOLOGÍA Madrid, Spain, June 2011
2	CURSO TEÓRICO/PRÁCTICO DE REOLOGÍA: COMPORTAMIENTO MECÁNICO/REOLÓGICO DE MATERIALES Ferrol, Spain, June 2011
3	14th EUROPEAN SCHOOL ON RHEOLOGY Leuven, Belgium, September 2013

Finally, Table 1.6 shows additional activities developed during this thesis which are not directly contributing to the results presented in this manuscript.

Table 1.6. Additional activities.

SCIENTIFIC PUBLICATIONS	
1	J. Lazaro, E. Laguna-Gutiérrez, E. Solorzano, M.A. Rodríguez-Pérez EFFECT OF MICROSTRUCTURAL ANISOTROPY OF PM PRECURSORS ON THE CHARACTERISTIC EXPANSION OF ALUMINUM FOAMS Metallurgical and Materials Transactions B, 984-991, 44B, 2013
2	S. Pardo-Alonso, E. Solorzano, J. Vicente, L. Brabant, M. Dierick, I. Manke, A. Hilger, E. Laguna-Gutierrez, M. A. Rodriguez-Perez µCT-BASED ANALYSIS OF THE SOLID PHASE IN FOAMS: CELL WALL CORRUGATION AND OTHER PRACTICAL MICROSCOPIC FEATURES Microscopy and Microanalysis, In Press, DOI:10.1017/S1431927615014890, 2015
3	J. Escudero, A. Lopez-Gil, E. Laguna-Gutierrez, M.A. Rodriguez-Perez LOW DENSITY NON-CROSSLINKED CLOSED/OPEN CELL POLYPROPYLENE FOAMS WITH HIGH MECHANICAL PROPERTIES Cellular Polymers, In Press
CONFERENCES	
1	J. Escudero, E. Laguna Gutierrez, M.A. Rodriguez-Perez, V. Kumar, A. Galeski **GAS DIFFUSION AND FOAMING IN LOW DENSITY POLYETHYLENE/CLAYS NANOCOMPOSITES** FOAMS 2011, 9th INTERNTIONAL CONFERENCE ON FOAMS MATERIALS & TECHNOLOGY, September 2011, Iselin, NJ, USA. Talk
2	E. Laguna-Gutierrez, E. Solórzano, S. Pardo-Alonso and M. A. Rodríguez-Pérez **MODELLING THE COMPRESSION BEHAVIOUR OF LOW-DENSITY FLEXIBLE FOAMS WITH A PARTIALLY INTER-CONNECTED CELLULAR STRUCTURE** FOAMS 2012, 10th INTERNTIONAL CONFERENCE ON FOAMS MATERIALS & TECHNOLOGY, September 2012, Barcelona, Spain. Poster
3	E. Laguna-Gutierrez, B. Notario, J. Pinto, M. A. Rodriguez-Perez **PREPARING STUDENTS OF SCIENTIFIC AND TECHNICAL DEGREES FOR THEIR FUTURE PROFESSIONAL CAREERS** EDULEARN 2015, 7th INTERNATIONAL CONFERENCE ON EDUCATION AND NEW LEARNING TECHNOLOGIES, July 2015, Barcelona, Spain. Virtual Presentation
4	B. Notario, E. Laguna-Gutierrez, J. Pinto, M. A. Rodriguez-Perez **FINAL YEAR PROJECT IN PHYSICS´S DEGREE: A NEW CHALLENGE FOR THE SCIENTIFIC AND TECHNICAL TRAINING OF STUDENTS IN THEIR LAST YEAR OF THE PHYSIC´S DEGREE** EDULEARN 2015, 7th INTERNATIONAL CONFERENCE ON EDUCATION AND NEW LEARNING TECHNOLOGIES, July 2015, Barcelona, Spain. Virtual Presentation

1.7 References

[1] L. J. Gibson, M. F. Ashby. Cellular Solids: Structure and Properties (2nd Edition). Cambridge University Press, Cambridge, 1997.
[2] C. Saiz-Arroyo. Fabricación de Materiales Celulares Mejorados Basados en Poliolefinas. Relación procesado-composición-estructura-propiedades. Phd Thesis, University of Valladolid, 2012.
[3] S. Pardo. X-Ray Imaging Applied to the Characterization of Polymer Foams' Cellular Structure and its Evolution. PhD Thesis, University of Valladolid, 2014.
[4] M. A. Rodriguez-Perez, J. I. Velasco, D. Arencon, O. Almanza, J. A. de Saja. Journal of Applied Polymer Science, 75, 156-166, 2000.
[5] The Future of Polymer Foams to 2019. Market Report, Smithers Rapra, 2014.
[6] http://www.plastemart.com/
[7] http://www.recticel.com/index.php/company/what-is-polyurethane
[8] http://www.eps.co.uk/applications/index.html
[9] http://building.dow.com/eu/gbr/en/products/styrofoam/index.htm
[10] D. Eaves. Handbook of Polymer Foams. Rapra Technology Limited, Shawbury, 2004.
[11] H. E. Naguib, C. B. Park, U. Panzer, N. Reichelt. Polymer Engineering and Science, 42, 1481-1492, 2002.
[12] S. T. Lee. Foam Extrusion: Principles and Practice, CRC Press, Boca Raton, 2000.
[13] R. Liao, W. Yu, C. Zhou. Polymer, 51, 568-580, 2010.
[14] R. Liao, W. Yu, C. Zhou. Polymer, 51, 6334-6345, 2010.
[15] R. Gendron. Thermoplastic Foam Processing. Principles and Development. CRC Press, Boca Raton, 2005.
[16] www.cellmat.es
[17] J. Lobos. Improving the Stiffness and Strenght of Porous Materials by Enhancement of the Matrix Microstructure and Cellular Morphology. PhD Thesis, University of Valladolid, 2012.
[18] M. Dumon, J. A. Reglero-Ruiz, J. Pinto, M. A. Rodriguez-Perez, J. M. Tallon, M. Pedros, E. Cloutet, P. Viot. Cellular Polymers, 31, 207-212, 2012.
[19] J. A. Reglero, C. Saiz-Arroyo, M. Dumon, M. A. Rodriguez-Perez, J. A. de Saja, L. Gonzalez. Polymer International, 60, 146-152, 2011.
[20] S. Roman-Lorza. Fabricación y Caracterización de Materiales Celulares Retardantes de Llama Libres de Halógenos Basados en Poliolefinas. PhD Thesis, University of Valladolid, 2010.
[21] S. Estravis. Cellular Nanocomposites Based on Rigid Polyurethane and Nanoclays: Fabrication, Characterization and Modeling of the Mechanical and Thermal Properties. PhD Thesis, University of Valladolid, 2014.
[22] A. Lopez-Gil, F. Silva-Bellucci, D. Velasco, M. Ardanuy, M. A. Rodriguez-Perez.Industrial Crops and Products, 66, 194-205, 2015.
[23] M. A. Rodriguez-Perez, R. D. Simoes, S. Roman-Lorza, M. Alvarez-Lainez, C. Montoya-Mesa, C. J. L. Constantino, J. A. de Saja. Polymer Engineering and Science, 52, 62-70, 2012.
[24] M. A. Rodriguez-Perez, R. D. Simoes, C. J. L. Constantino, J. A. De Saja. Journal of Applied Polymer Science, 121, 2324-2330, 2011.
[25] J. Pinto. Fabrication and characterization of nanocellular polymeric materials from nanostructured polymers. PhD Thesis, University of Valladolid, 2014.
[26] B. Notario, J. Pinto, M. A. Rodriguez-Perez. Polymer, 63, 116-126, 2015.
[27] B. Notario, J. Pinto, E. Solorzano, J. A. de Saja, M. Dumon, M. A. Rodríguez-Pérez. Polymer, 15, 57-67, 2015.
[28] J. A. Reglero-Ruiz. Fabricación y Caracterización de Espumas de Aluminio: Aplicaciones en el Sector Aeronáutico. PhD Thesis, University of Valladolid, 2007.
[29] E. Solorzano. Espumas de Aluminio: Proceso de Espumado, Estructura Celular y Propiedades. PhD Thesis, University of Valladolid, 2008.

[30] J. Lazaro. Optimización de la Estructura Cellular en Espumas de Aluminio. PhD Thesis, University of Valladolid, 2014.
[31] M. A. Rodriguez-Perez. Propiedades térmicas y mecánicas de espumas de poliolefinas. PhD Thesis, University of Valladolid, 1998.
[32] O. Almanza. Caracterización y Modelización de las Propiedades Térmicas y Mecánicas de Espumas con Base Polietileno. PhD Thesis, University of Valladolid, 2000.
[33] L. O. Arcos y Rabago. Propiedades Térmicas y Mecánicas en Espumas de Poliolefinas Fabricadas en un Proceso de Moldeo por Compresión. PhD Thesis, University of Valladolid, 2002.
[34] J. L. Ruiz-Herrero. Impacto y Fluencia en Espumas con Base Polietileno. PhD Thesis, University of Valladolid, 2004.
[35] J. I. Gonzalez-Peña. Efecto de Tratamientos Térmicos en Bloques de Espumas de Polietileno de Baja Densidad Fabricados mediante Moldeo por Compresión. PhD Thesis, University of Valladolid, 2006.
[36] M. Alvarez-Lainez. Propiedades térmicas, mecánicas y acústicas de espumas de poliolefina de celda abierta. PhD Thesis, University of Valladolid, 2007.
[37] R. A. Campo-Arnaiz. Aplicación de Técnicas Espectroscópicas al Estudio de la Morfología Polimérica, Propiedades Térmicas y de Emisión de Espumas de Baja Densidad con Base Poliolefina. PhD Thesis, University of Valladolid, 2011.
[38] M. A. Rodriguez-Perez, A. Duijsens, J. A. De Saja. Journal of Applied Polymer Science, 68, 1237-1244, 1998.
[39] M. A. Rodriguez-Perez, J. A. de Saja. The Effect of Blending on the Physical Properties of Crosslinked Closed Cell Polyethylene Foams. Cellular Polymers, 18, 1-20, 1999.
[40] M. A. Rodriguez-Perez. The Effect of Chemical Composition, Density and Cellular Structure on the Dynamic Mechanical Response of Foams. Cellular polymers, 21, 117-136, 2002.
[41] F. Hidalgo. Design and Optimization of Process Parameters in the Manufacture of Crosslinked Polyolefin Foams by Compression Molding. PhD Thesis, University of Valladolid, 2008.
[42] L. O. Salmazo. Cineticas de Espumacion y control de la Estructura Celular en Materiales Basados en caucho Natural y poliolefinas. Phd Thesis, University of Valladolid, 2015.
[43] C. Saiz-Arroyo, J. A. de Saja, J. I. Velasco, M. A. Rodriguez-Perez. Journal of Materials Science, 47, 5680-5692, 2012.
[44] C. Saiz-Arroyo, M. A. Rodriguez-Perez, J. I. Velasco, J. A. de Saja. Composites: Part B, 48, 40-50, 2013.
[45] C. Saiz-Arroyo, M. A. Rodriguez-Perez, J. Tirado, A. Lopez-Gil, J. A. de Saja. Polymer International, 62, 1324-1333, 2013.
[46] M. A. Rodriguez-Perez, J. A. de Saja, J. Escudero, A. Lopez-Gil. Procedimiento de Fabricación de Materiales Celulares de Matriz Termoplástica. Patent, WO 2014009579 A1, 2013.
[47] M. A. Rodriguez-Perez, J. A. de Saja, J. Escudero, J. A. Vazquez. Sistema y Procedimiento de Moldeo de Piezas con Moldes Autoportantes. Patent, ES 2364263 A1, 2012.
[48] https://cit.kuleuven.be/smart

CHAPTER 2

BACKGROUND AND STATE OF THE ART

INDEX

2.1 Introduction

In this chapter the state of the art related to the topics analyzed in this work is reviewed. Therefore, it deals with the revision of the main concepts associated to the rheological behavior of molten polymers. Both, the rheological properties in shear and in uniaxial extension are considered. Furthermore, several aspects and general concepts concerning to polyolefin based cellular materials are also included in this chapter, as well as, a brief description of all the materials usde in this work belonging to this group of polymers.

Taking into account the main objective of this work (see section 1.2), an entire section of this chapter is dedicated to review the previous works focused on understanding the role that the extensional rheological behavior of a polymeric matrix plays during the foaming process.

Finally, an exhaustive revision of the works found in the literature dealing with the concepts covered in the chapters 4, 5 and 6 is also included along this chapter.

2.2 Rheology of molten polymers

2.2.1 Introduction and definition of terms

Rheology is the science of deformation and flow. This definition was accepted when the American Society of Rheology was founded in 1929. The term "rheology" originates from the Greek "rheos" meaning "the river", "flowing", "streaming". Thus, rheology is literally "flow science" [1,2].

From an historical perspective, the properties of the materials were represented by both the Hooke and the Newton-Stokes laws [1,3]. The behavior of the **ideal elastic solids** (Hookean solids) is described by the **Hooke's law** which states that in deformation of solids, *stress* (σ) is proportional to *strain* (γ), being the coefficient of proportionality the elastic or *Young's modulus* (*E*) (Equation 2.1) [1,3].

$$\sigma = E\gamma \tag{2.1}$$

On the other hand, a general law known as the **Newton-Stokes law** is used to describe the behavior of the **ideal viscous liquids** (Newtonian liquids). This law establishes that the *strain rate* ($\dot{\gamma}$) is proportional to the stress, being the *viscosity* (η) the coefficient of proportionality (Equation 2.2) [1,3].

$$\sigma = \eta\dot{\gamma} \tag{2.2}$$

Both models represent properties of many materials and work well in describing their behavior with a considerably degree of accuracy. However, these commonly used concepts were insufficient to describe the properties of many other materials. Rheology emerged from the need to understand the properties of the "real" materials, who can display either the two behaviors described previously or a combination of both simultaneously.

Which property dominates (ideal elastic solid or ideal viscous liquid) depends on the stress and on the duration of the application of this *stress* [1,3]. The scaling of time in rheology is

achieved by means of the ***Deborah number*** (D_e) which was defined by Professor Marcus Reiner (Equation 2.3) [1,4].

$$D_e = \frac{\tau}{t} \tag{2.3}$$

Where τ is the *relaxation time* (a characteristic time of each material) and t is the *observation time*. In his paper, Prof. Reiner [4] introduces the Deborah number as follows: "*This seems ridiculous, but there is some relation between rheology and theology… In her famous song after the victory over the Philistines, Deborah sang: The Mountains flowed before the Lord… Deborah knew two things: first that the mountains flow, as everything flows, and secondly that they flowed before the Lord, and not before man, for the simple reason that man in his short lifetime cannot see them flowing, while the time of observation of God is infinite*". As a consequence, the difference between solids and liquids can be defined by the magnitude of D_e. If the observation time is larger than the relaxation time, one can see the material flowing. On the other hand, if the relaxation time is larger than the observation time, the material behaves as a solid [5]. If a wide range of stresses is applied over a wide spectrum of time, or frequency, using rheological equipment, it is possible to see liquid-like properties in solids and solid-like properties in liquids.

The technology used to determine the rheological data is known as **rheometry**. In rheometry materials are investigated in simple flows (rotational tests), oscillatory shear flows (oscillatory tests) and extensional flows (extensional tests). Each of these types of tests, as well as the results obtained with them, are described in detail in sections 2.2.3, 2.2.4 and 2.2.5, respectively.

2.2.2 Viscoelasticity

The properties of **polymers** lie somewhere between those of the Hookean (elastic) and Newtonian (viscous) materials, thus they are known as **viscoelastic materials**. For instance, the response of a typical viscoelastic material to a creep-recovery test is shown in Figure 2.1.b. This test involves loading the material at a constant stress, keeping this stress for a period of time and then removing the load (Figure 2.1.a). This figure also shows the response of a Hookean solid (Figure 2.1.c) and a Newtonian liquid (Figure 2.1.d).

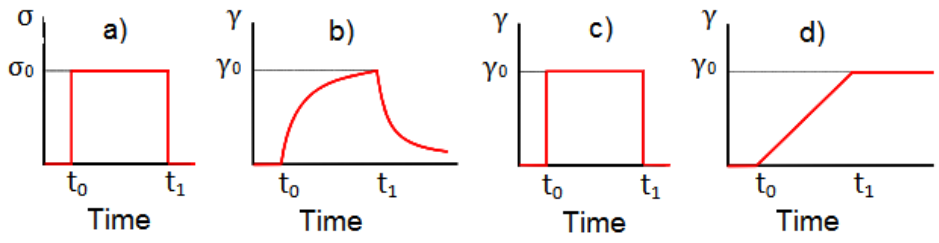

Figure 2.1. Response of different materials to a creep-recovery test. a) Definition of the test. b) Viscoelastic materials response. c) Hookean solids response. d) Newtonian liquids response.

When the stress is applied in a Hookean solid, the solid deforms until the load is removed and then the deformation recovers its initial value. If the material loaded is a Newtonian material, the material deforms but the deformation does not recover its initial value when the load is removed. In the case of a viscoelastic material its response is something in between of that of

the solid and the viscous materials. When the load is applied the material has a progressive deformation with time, and when the load is removed, the viscoelastic material recovers only a part of the applied deformation [6].

The Deborah number of these viscoelastic materials is close to 1, which means that the time of observation and the time of relaxation are comparable [7]. Summarizing, the materials can be classified according to their Deborah number as follows: viscous materials are those with a low D_e, elastic materials are those with a high D_e and finally viscoelastic materials show a D_e of approximately 1.

2.2.2.1 Linear and non-linear viscoelasticity

Polymers consist of long molecules that entangle with each other, forming several flexible, reversible, "joints" [8]. This enables different types of motions: micro and macro-Brownian motions. On the one hand, several chain segments can move as a unit within a macromolecule (**micro-Brownian motion**). On the other hand, **macro Brownian-motions**, the whole macromolecule can also move relative to others (reptation). Far below the *glass transition temperature* (T_g) the macro-Brownian motions and most of the micro-Brownian motions are completely frozen. Near the T_g the micro-Brownian motions begin to occur and they become stronger as the temperature increases. Finally, upon further rise of *temperature* (T), the macro-Brownian motions set in as well, and the polymer can be easily deformed by applying an external force [9]. The behavior of the viscoelastic materials depend on both, the strain and the strain rate applied. At **low strains** there is a linear relationship between the stress and the strain. This is the domain of **linear viscoelasticity**. However, at **higher strains** this relation is not linear and the zone of **non-linear viscoelasticity** is reached [1]. If a molten polymer is subjected to a very small strain, the molecules of the polymeric material are disturbed from their equilibrium configuration to a negligible extent. Moreover, in molten polymers this linear behavior is also observed when a deformation occurs very slowly. This is because the relaxation processes due to the Brownian motions tend to return the molecules towards their equilibrium state. If the strain applied is tending to take them away from this state only very slowly, these relaxation mechanisms have plenty of time to continue with their process and therefore no significant deviations from the equilibrium occur [10]. To characterize the inherent material properties in rheological experiments, it is essential to carry out the measurements in the linear viscoelastic range as in this regime the response of the material is strongly influenced by its structure. However, in polymer melt processing the extent of deformation is not small nor slow and hence, it occurs in the non-linear region. Therefore, the rheological measurements in the non-linear region are important to obtain information related to the melt behavior in processing flows.

According to the Boltzmann superposition principle, in the linear viscoelastic region, one can assume that each loading step makes an independent contribution to the total loading history and the final deformation is the sum of the response to each step. Therefore, the relationship between the stress, the strain and the strain rate is given by the rheological equation of state (Equation 2.4) [11].

$$\sigma(t) = \int_{-\infty}^{t} G(t-t')\dot{\gamma}\,(t')dt' \tag{2.4}$$

Where *G* is the *relaxation modulus*, *t* is the *current time* and *t'* is *any previous instant* of the process.

As the rheological behavior of the viscoelastic materials is difficult to visualize, **mechanical models** provide a popular method of describing the linear viscoelastic behavior. These one-dimensional models consist of springs and dashpots so arranged (in parallel or in series) that the overall system behaves analogously to a real material [1]. In the **Maxwell model** (Figure 2.2.a) a spring is connected in series with a dashpot. In this case, the stress applied to the entire system is applied equally on the spring and on the dashpot ($\sigma_s = \sigma_d = \sigma$) and the resulting strain is the sum of the strains in the spring and in the dashpot ($\gamma = \gamma_s + \gamma_d$). A force applied will cause both, the spring and the dashpot to deform. However, while the deformation of the spring is finite, the dashpot deforms as long as the force is maintained. Therefore, the overall behavior of the Maxwell model is more like a liquid than a solid and due to this, it is known to be a viscoelastic fluid model [12]. This model describes very well the concept of stress relaxation: decay of stress at a constant strain [13]. Another model is the **Kelvin-Voigt model** (Figure 2.2.b). In this system the spring and the dashpot are connected in parallel. The total stress applied is shared by the spring and the dashpot ($\sigma = \sigma_s + \sigma_d$). Due to this parallel arrangement, the spring and the dashpot deform by an equally amount ($\gamma_s = \gamma_d = \gamma$). In this system, the dashpot cannot undergo continuous deformations and therefore this model represents a viscoelastic solid behavior [12]. This model describes the creep behavior: a constant load causes a time dependent deformation of the material [13]. However, these systems, alone, are not able to describe the rheological behavior of molten polymers. With the **generalized Maxwell model** (Figure 2.2.c) in which several Maxwell elements are connected in parallel, it is possible to describe the relaxation time spectrum of a polymer. Each of the individual Maxwell elements represents an individual polymer fraction having a specific molar mass and molecular structure and also having a specific relaxation time [2].

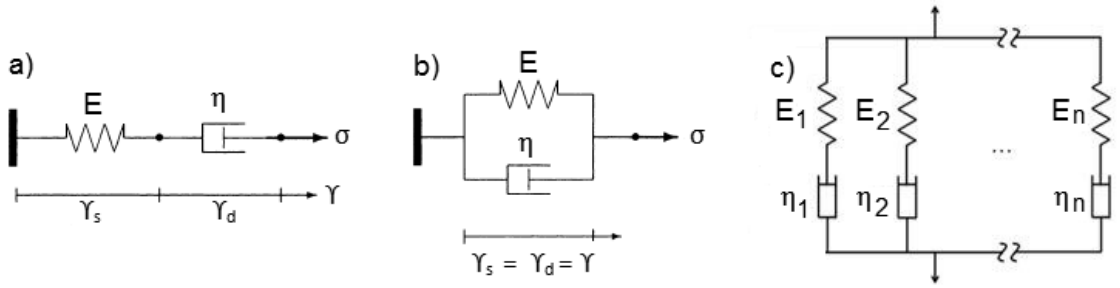

Figure 2.2. Mechanical models to analyze the viscoelastic behavior of materials. a) Maxwell model. b) Kelvin-Voigt model. c) Maxwell generalized model.

2.2.3 Rotational tests

2.2.3.1 Basics of rotational tests

Rotational rheometers are the most commonly used devices to measure the **viscous** properties of materials. These rheometers apply a rotation to achieve a simple shear flow. They are classified into two types, depending on how the flow is induced [2]:

- **Controlled shear rate (CSR) rheometers**: In these tests the shear rate (or the strain) is set and controlled and the stress is measured.
- **Controlled shear stress (CSS) rheometers**: In these tests the shear stress or torque is set and controlled.

The use of one or another rheometer depends on the type of measurement and on the sample characteristics.

The **simple shear flow** is defined as the flow between two parallel plates; one of them is stationary and the other moves in a straight line with a *velocity v*, as Figure 2.3 indicates [14].

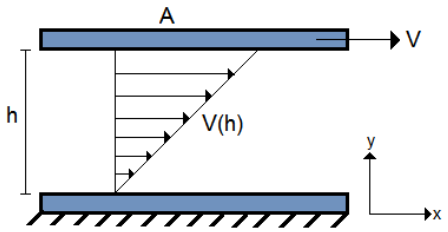

Figure 2.3. Representation of velocity fields in the simple shear flow.

The strain rate (or shear rate) at each point in the fluid is given by Equation 2.5 [14].

$$\dot{\gamma} = \frac{v}{h} \tag{2.5}$$

Where *h* is the *gap* between the two plates. Therefore, the shear rate is uniform throughout the fluid. If *V* does not change with time, the shear flow is a *steady shear flow*. Moreover, if *F* is the *total force* required to move the upper plate and *A* is the *surface area* of this plate, then the stress (or shear stress) is given by Equation 2.6 [14].

$$\sigma = \frac{F}{A} \tag{2.6}$$

As it was previously indicated, (see section 2.2.1), the viscosity is defined as the ratio between the stress and the strain rate. However, while for Newtonian fluids the viscosity is a constant, for molten polymers the viscosity is a function of time, shear rate [15], temperature [15] and *pressure* (*P*) [16]. Moreover, the viscosity of molten polymers also depends on their morphology and structure, that is, the viscosity also depends on the polymer molecular weight, molecular weight distribution and chain branching, among others [17,18].

The two main applications of the rotational rheometer, within the polymers field, are the following:

- Obtaining the steady state flow curves (dependence of viscosity with shear rate).
- Analysis of the time-dependent flow behavior (dependence of viscosity with time).

In addition, with this rheometer it is also possible to analyze the temperature-dependence of the shear viscosity as well as the effects that the polymer parameters, especially those related to the polymer structure, have on the shear rate. However, to analyze the effect of pressure on shear viscosity other devices should be used (capillary rheometers).

A scheme of a typical rotational rheometer is depicted in Figure 2.4. This measuring system consists of two parts: one part is a fixed plate and the other part (the geometry) is attached to the driving motor spindle and therefore, it constitutes the moving member of the system. These geometries can be cones or plates. Figure 2.4.a shows a schematic representation of the **cone-plate system** and Figure 2.4.b shows the one corresponding to a **parallel plates system**.

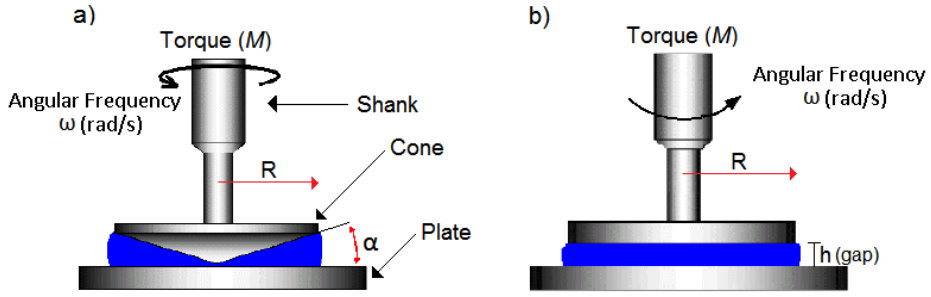

Figure 2.4. Rotational rheometer systems. a) Cone-plate system. b) Parallel plates system.

In the **cone-plate system** the shear rate and the shear stress are given by the Equations 2.7 and 2.8, respectively.

$$\dot{\gamma} = \frac{\omega}{\alpha} \tag{2.7}$$

$$\sigma = \frac{3M}{2\pi R^3} \tag{2.8}$$

Where ω is the *angular frequency*, α is the *angle between the cone and the plate*, M is the *torque* and R is the *cone radius* [19]. As Figure 2.4.a shows, the cone is truncated and therefore there is no physical contact between the cone and the plate. Furthermore, the angle between the cone and the plate is very small (between 0.5˚ and 4˚). The sample is located in the space between the cone and the plate. The main advantage of the cone-plate rheometer is that the shear rate, the shear strain and the shear stress are homogeneous throughout of the sample. However, this system also has some disadvantages. Measurements cannot be performed at high shear rates because when the shear rate increases secondary flows are normally developed in the polymer and in addition, the polymer tends to crawl out of the instrument due to the influence of centrifugal forces and elastic instabilities. The *gap* (h), separation between the cone and the plate, is fixed and as a consequence difficulties may arise, for instance, to characterize filled polymers in which the size of the particles is comparable to the gap [20].

On the other hand, the **parallel plate system** is normally used with materials containing large particles as in this system the gap is variable. Moreover, the shear rate limits can be modified by changing the gap or the plate radius. However, the main disadvantage of this system is that the shear strain and the shear rate vary with radial position, complicating the process of data analysis [20]. Nevertheless, the current software programs are able to compensate this fact. In this system the shear rate and the shear stress (at R) are given by the Equations 2.9 and 2.10, respectively [19,21].

$$\dot{\gamma} = \frac{\omega R}{h} \tag{2.9}$$

$$\sigma = \frac{M}{2\pi R^3}\left(3 + \frac{d\ln M}{d\ln \omega}\right) \tag{2.10}$$

2.2.3.2 Influence of measuring parameters and polymer characteristics on the viscosity

In the following sub-sections the effects of the measuring parameters (time, shear rate and temperature) on the shear viscosity of molten polymers are analyzed. In the same way, the effects of parameters related to the polymer morphology (molecular weight, molecular weight distribution and chain branching) are also described.

2.2.3.2.1 Dependence of shear viscosity of molten polymers with time

When a constant shear strain is applied, the **viscosity** of a molten polymer changes with **time** as Figure 2.5 indicates [22].

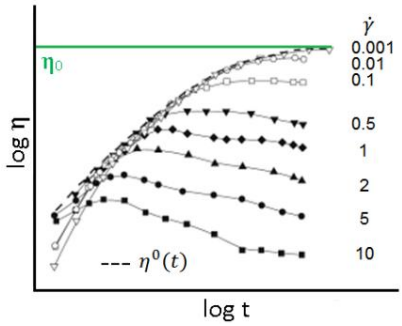

Figure 2.5. Shear viscosities as function of time at various constant shear rates.

It is possible to observe a clear difference between the behavior of the curves measured at high shear rates and that of the curves obtained at low shear rates. While the curves measured at high shear rates show a maximum, the curves obtained at low shear rates do not. Furthermore, they reach a stationary state which becomes independent on the shear rate if it is low enough. This rate-independent curve represents the *time-dependent linear shear viscosity* ($\eta^0(t)$) which is an important parameter to verify the reliability of the extensional viscosity measurements (see section 2.2.5.4.1). The steady state of this curve is known as *zero-shear viscosity* (η_0) [22].

2.2.3.2.2 Dependence of steady shear viscosity of molten polymers with shear rate

To obtain the **steady shear viscosity** curve, a steady shear flow is imposed on a material for a suitable period of time until the shear stress reaches a steady state, i.e. it becomes independent on time. The ratio between the measured steady state stress and the applied shear rate is known as **steady shear viscosity**. The uncrosslinked molten polymers are characterized by their shear-thinning behavior as their steady shear viscosity decreases when the applied shear rate increases. The typical logarithmic **flow curves (steady shear viscosity versus shear rate)** of molten polymers can be observed in Figure 2.6, where it is possible to distinguish three different ranges [2,23]:

- At low shear rates the **first Newtonian range** is reached with the plateau value of the *zero-shear viscosity* (η_0).
- Over several decades of intermediate shear rates a **shear-thinning** behavior is detected. In this region the viscosity depends on the shear rate ($\eta = f(\dot{\gamma})$).
- At high shear rates the **second Newtonian range** is reached with the plateau value of the *infinite-shear viscosity* (η_∞).

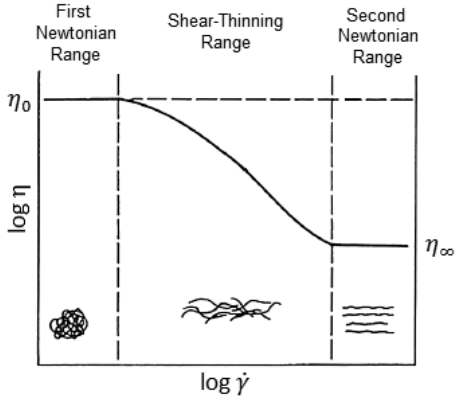

Figure 2.6. Flow properties of molten polymers: steady shear viscosity as a function of shear rate.

At rest, each macromolecule is found in the state of the lowest level of energy consumption showing the shape of a three dimensional coil (Figure 2.7.a). Moreover, each coil is highly entangled with the neighboring macromolecules [2]. As the relaxation processes, due to the Brownian motions, tend to return the macromolecules towards their equilibrium state, if the shear rate applied is very low these thermal motions overcomes the molecular alignments in the shear fields. In this state, the macromolecules have the highest resistance to flow and therefore the viscosity remains constant [23]. When the shear rate increases, some macromolecules are oriented in the shear field. As a consequence, the molecules disentangle to a certain extent and their resistance to flow is reduced. In this case, the relaxation processes do not have time to return the macromolecules towards their equilibrium state and the viscosity decreases [2,23]. Finally, when the shear rate is very high all macromolecules are almost fully oriented and disentangled (Figure 2.7.b). The flow resistance is reduced to a minimum and cannot further decrease because it is only caused by the friction between the single molecules gliding off each other. Consequently, again the viscosity remains constant [2].

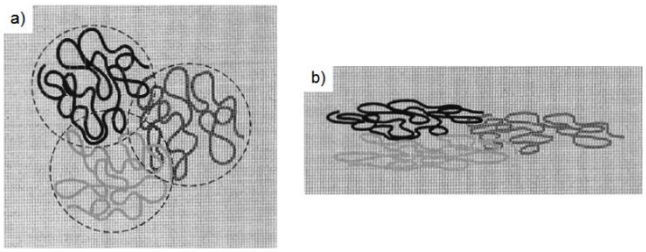

Figure 2.7. Scheme of the shape of the molten polymer macromolecules. a) Macromolecules at rest, showing coiled and entangled chains. b) Macromolecules under high shear rates, showing oriented and disentangled chains.

2.2.3.2.3 Dependence of shear viscosity of molten polymers with temperature

Figure 2.8 shows the typical logarithmic curves of the **shear viscosity** as a function of the shear rate for different **temperatures** [24].

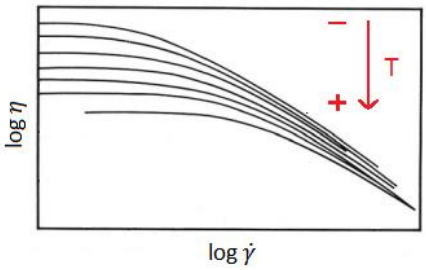

Figure 2.8. Effect of temperature on the shear viscosity.

At temperatures well above the melting point (T_m) the polymer is a viscoelastic liquid with a measurable shear-thinning viscosity. When the melt temperature is reduced the elastic behavior becomes more evident and therefore a rapid increase in the viscosity is produced [1]. An Arrhenius-type equation is normally used to relate viscosity with temperature in ranges well above T_g (Equation 2.11).

$$\eta = Ae^{E_a/RT} \tag{2.11}$$

Where A is an *empirical constant*, E_a is the *activation energy* and R is the *gas constant*. E_a is a measure of the sensitivity of the shear viscosity towards temperature change. A high value of E_a indicates a high sensitivity towards temperature change [25]. To estimate these constants, it is necessary to measure the viscosity at least at two different temperatures.

2.2.3.2.4 Dependence of shear viscosity of molten polymers with molecular weight

Molecular weight of a polymer (M_W) is another important factor affecting rheology, being the zero shear viscosity a sensitive measurement of this parameter. Figure 2.9 shows the effect of the molecular weight on the shear viscosity.

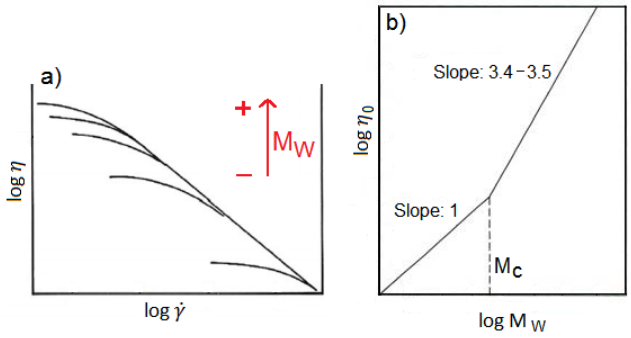

Figure 2.9. Effect of molecular weight on the shear viscosity. a) Viscosity as a function of shear rate for molten polymers with different molecular weight. b) Dependence of zero-shear viscosity on molecular weight.

For most molten polymers the zero-shear viscosity is approximately proportional to the average molecular weight below a *critical value* (M_c) and depends on M_W to a power of

approximately 3.4-3.5 at molecular weights above M_c, as Figure 2.9.b indicates [17]. Therefore, for $M_W < M_c$:

$$\eta_0 = K_1 M_W \tag{2.12}$$

where, K_1 is a *material-specific factor*. Polymers with small molecules (low molecular weight), which do not show effective entanglements between the single molecule chains, display ideal viscous flow behaviors (their viscosity does not change with the shear rate). In this case, η_0 is directly proportional to the molar weight, according to Equation 2.12 [2]. On the other hand, for $M_W > M_c$:

$$\eta_0 = K_1 {M_W}^{3.5} \tag{2.13}$$

Polymers with large molecules, which show effective entanglements between the single molecule chains, display the zero-shear viscosity value in a lower shear range than polymers with small molecules. In this case, η_0 increases abruptly with the molecular weight, as Equation 2.13 also indicates [2].

The relations above permit determining the average molecular weight from the results obtained in shear viscosity measurements.

2.2.3.2.5 Dependence of shear viscosity of molten polymers with molecular weight distribution

Molecular weight distribution (MWD) also influences the shear viscosity behavior. To determine, quantitatively, the effect of MWD on the shear viscosity a method of data reduction is required in which η/η_0 is represented as a function of $\eta_0\dot{\gamma}$ (Figure 2.10) [26].

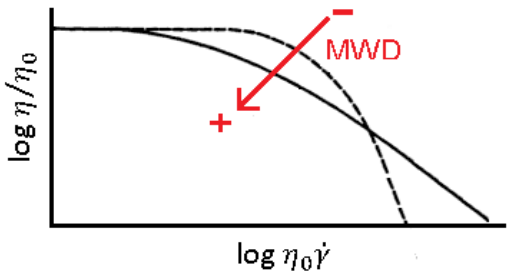

Figure 2.10. Effect of molecular weight distribution on the shear viscosity.

The polymer with the broader MWD (solid line) shows a non-Newtonian flow at a lower shear rate than the polymer with the narrower MWD (dash line). Moreover, the shear-thinning is more pronounced in the polymer presenting the narrowest MWD. This effect has important practical applications. Polymers with a very narrow MWD appear to have a higher viscosity than the same polymer with a broader MWD. As a consequence, polymers with a broad MWD are easier to extrude than polymers with a narrow MWD (that is, lower energy is required to extrude polymers with a broad MWD) [20].

2.2.3.2.6 Dependence of shear viscosity of molten polymers with chain branching

The rheology of a molten polymer is also affected by **chain branching,** in fact, rheology has proved to be a reliable method for the verification of the existence of long chain branches on

the polymeric chains. The effect of branching on the shear viscosity also depends on the branching structure: length of branches, *branching degree* (B_n), distance between branched points, etc. [24]. These chain branches can be long or short. **Short chain branches** (SCBs) generally do not have a significant effect on the linear viscoelastic flow behavior of the melt. The viscosity is not influenced by the amount of SCBs [27,28]. On the other hand, the presence of **long chain branches** (LCB), even at quite low levels, has an important effect on the zero-shear viscosity and on the shape of the viscosity curve [24]. Branches that are long but are still shorter than those required to have effective entanglements induce a decrease in the zero-shear viscosity when compared to a linear polymer with the same molecular weight [29]. This is a result of the smaller coil radius of branched polymers which results in fewer entanglements and lower viscosity [10]. Nevertheless, when the branches are long enough to participate in entanglements, the zero-shear viscosity of a branched polymer is much higher than that of a linear one with the same molecular weight (Figure 2.11) [29]. As polymers relax by motion along their backbones, long chain branching hinders relaxation, that is, the relaxation spectrum is extended to longer relaxation times and therefore, the viscosity continues to increase at low shear rates [10,19].

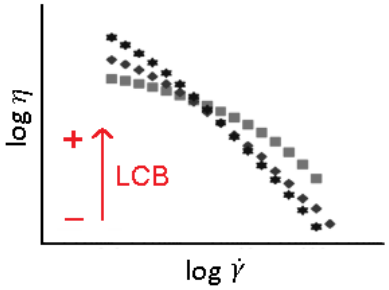

Figure 2.11. Effect of the degree of LCBs on the shear viscosity of long chain branched polymers with moderate to low branching degrees. The square symbols belong to a linear polymer.

Shear thinning becomes stronger in the long chain branched polymers as Figure 2.11 also indicates, making the viscosity of branched polymers, at high shear rates, to be even lower than that of linear polymers [30,31]. At high shear rates, branched molecules have a more compact molecular profile than linear ones. Consequently, they have fewer entanglements to impede flow and hence lower viscosities [19,32]. However, not only the length of the branched chains influences the rheological behavior; this is also affected by **the branching degree (B_n)**. Figure 2.12 shows the ratio between the *zero-shear viscosity of a branched polymer* (η_0^B) and the zero-shear viscosity of a linear polymer (η_0^L) as a function of B_n, in polymers with the same M_W.

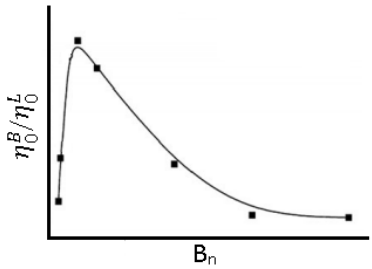

Figure 2.12. Effect of the degree of LCBs on the zero shear viscosity.

At low chain branching levels the viscosity increases, reaching a maximum, and then decreases (at high chain branching degrees). At low degrees of chain branching, the viscosity enhancement, caused by entanglement, predominates. However, when the degree of long chain branches increases a reduction in the coil radius occurs and the zero-shear viscosity decreases [33].

2.2.4 Small amplitude oscillatory shear (SAOS)

2.2.4.1 Basics of SAOS tests

This technique allows analyzing the linear viscoelastic properties of molten polymers. During the test, the sample is deformed in an oscillatory shear flow when placed in a cone-plate or parallel plate geometry such as those presented in Figure 2.4. In this test the bottom plate is stationary and the upper plate is oscillating with a certain *oscillation frequency* (ω). In a similar way that in rotational tests both, a controlled shear rate rheometer and a controlled shear stress rheometer can be employed to perform these measurements, although the same results are obtained with the two devices [34]. For instance, the controlled strain experiment can be represented mathematically by Equations 2.14 and 2.15 [1,2]:

$$\gamma = \gamma_0 \sin(\omega t) \tag{2.14}$$

$$\sigma = \sigma_0 \sin(\omega t + \delta) \tag{2.15}$$

where γ is the *shear strain*, σ is the *shear stress*, γ_0 is the *shear strain amplitude*, σ_0 is the *shear stress amplitude* and δ is the *phase shift angle* between the shear strain and shear stress curves, also known as ***loss angle*** (Figure 2.13) [2]. Furthermore, as the shear rate is defined as $\dot{\gamma} = d\gamma/dt$, the time derivate of the sinusoidal strain results in a cosinusoidal shear rate (Equation 2.16),

$$\dot{\gamma}(t) = \gamma_0 \omega \cos(\omega t) \tag{2.16}$$

To determine the linear viscoelastic properties, γ_0 should be low enough so that the material is not perturbed by the deformation. The shear stress produced by a small amplitude deformation is proportional to the amplitude of the applied strain and it varies sinusoidally with time [35].

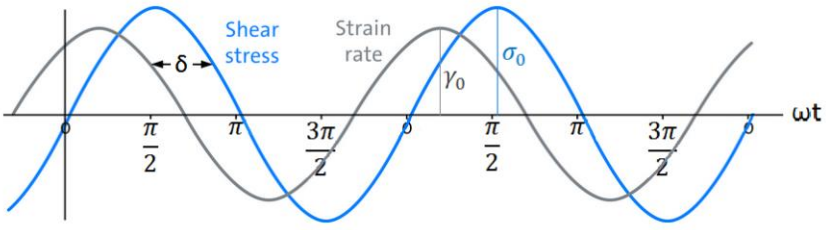

Figure 2.13. Sinusoidal forms of stress and strain for a viscoelastic material.

While the loss angle of an ideal elastic solid is $\delta = 0°$, the loss angle of an ideal viscous liquid is $\delta = 90°$. However, in viscoelastic materials the loss angle $0° < \delta < 90°$, that is, the resultant stress shows a certain delay period compared to the pre-set strain curve. In rheology, this

delay is not expressed in terms of a time but of an angle (δ). This is due to the use of "complex numbers", which are required to analyze the obtained results [2].

In general, the stress can also be represented as (Equation 2.17) [35]:

$$\sigma = \gamma_0[G'(\omega)\sin(\omega t) + G''(\omega)\cos(\omega t)] \tag{2.17}$$

where the term containing *G'(ω)* (*storage modulus*) is in-phase with the strain and the term containing *G''(ω)* (*loss modulus*) is in-phase with the shear rate. The **storage modulus** is a measure of the amount of energy stored in the material during the shear process. When the load is removed this stored energy is completely available and it acts as the driving force for the re-formation process to compensate the previous deformation of the structure. The ideal elastic solids store the whole deformation energy and hence they show a completely reversible deformation behavior when the applied load is removed. Therefore, *G'(ω)* represents the elastic behavior of the tested material. On the other hand, the **loss modulus** is a measure of the amount of energy dissipated during the shear process. That is the energy used by the sample during the process. For instance, part of this energy is spent in changing the structure of the tested materials when the material is flowing and another part of this energy is spent in heating up the material. The ideal viscous liquids loss completely all the deformation energy and thus they show an irreversible deformation behavior when the applied load is removed. It can be said that *G''(ω)* represents the viscous behavior of the tested material [2,35,36]. The following expressions (Equations 2.18, 2.19 and 2.20), which define the viscoelastic behavior, can be derived from Equations 2.15 and 2.17:

$$G' = \frac{\sigma_0}{\gamma_0} cos\delta \tag{2.18}$$

$$G'' = \frac{\sigma_0}{\gamma_0} sin\delta \tag{2.19}$$

$$tan\delta = \frac{G''}{G'} \tag{2.20}$$

where *tanδ* is the *loss tangent* (also known as *loss factor* or *damping factor*). The **loss tangent** reveals the ratio between the viscous and the elastic portion of the viscoelastic deformation behavior. Taking this into account, the ideal elastic behavior is represented in terms of $tan\delta = 0$, the ideal viscous behavior is expressed as $tan\delta = \infty$ and the viscoelastic behavior holds $0 < tan\delta < \infty$ [2].

When the harmonic functions are expressed in their complex form, the Equation 2.21 can be obtained [37]:

$$G^* = G' + iG'' \tag{2.21}$$

where *G** is known as *complex modulus*. The modulus of *G** ($|G^*|$) is given by Equation 2.22 [35]:

$$|G^*| = \sqrt{G'^2 + G''^2} = \frac{\sigma_0}{\gamma_0} \tag{2.22}$$

On the other hand, the so-called *complex viscosity* (η^*) is defined by Equation 2.23 [35].

$$\eta^* = \eta' - i\eta'' = \frac{G^*}{i\omega} \tag{2.23}$$

where η' is the *real part of the complex viscosity* and η'' is the *imaginary part of the complex viscosity*.

The real part (Equation 2.24) accounts for the viscous behavior and the imaginary part (Equation 2.25) accounts for the elastic behavior [2].

$$\eta' = \frac{G''}{\omega} = \frac{\sigma_0}{\omega\gamma_0} sin\delta \tag{2.24}$$

$$\eta'' = \frac{G'}{\omega} = \frac{\sigma_0}{\omega\gamma_0} cos\delta \tag{2.25}$$

The modulus of η^* ($|\eta^*|$) is given by Equation 2.26 [35,36]:

$$|\eta^*| = \sqrt{\eta'^2 + \eta''^2} = \frac{|G^*|}{\omega} \tag{2.26}$$

2.2.4.2 Cox-Merz Rule

The so-called **Cox-Merz rule** is an empirical equation which establishes a relationship between the steady shear viscosity versus the shear rate and the complex viscosity versus the frequency (Equation 2.27) [38]:

$$\eta(\dot{\gamma}) = |\eta^*(\omega)| \tag{2.27}$$

To apply this rule the appropriate values of $\eta(\dot{\gamma})$ and $|\eta^*(\omega)|$ should be used. For instance, a steady viscosity is required, that is, no transient effects should occur during the process [39]. It has been found that this rule holds for almost all molten polymers. However, it does not apply to crosslinked systems [39].

The main advantage of employing the Cox-Merz rule is that the number of experiments required to characterize the sample can be reduced as it is possible to determine the linear viscoelastic behavior and the non-linear flow properties in the same experiment [36]. The continuum mechanics establishes that at low frequencies and low shear rates, when the Newtonian plateau is reached, the following relationship is always fulfilled (Equation 2.28) [39]:

$$\lim_{\omega\to 0} \eta'(\omega) = \lim_{\dot{\gamma}\to 0} \eta(\dot{\gamma}) \tag{2.28}$$

Therefore, the zero-shear viscosity can be also obtained by using Equation 2.29 [40]:

$$\eta_0 = \lim_{\omega\to 0} \eta'(\omega) = \lim_{\omega\to 0} \frac{G''(\omega)}{\omega} \tag{2.29}$$

As the elastic contribution to $\eta'(\omega)$ disappears in the low frequency limit, because *G'* decreases with frequency much faster than *G''*, the Equation 2.28 can be rewritten as:

$$\lim_{\omega \to 0} |\eta^*(\omega)| = \lim_{\dot{\gamma} \to 0} \eta(\dot{\gamma}) \tag{2.30}$$

This limit is known as the **viscoelastic limiting behavior**. For higher frequencies (or shear rates) this relation often still holds (Cox-Merz rule) but, it is no longer a requirement.

2.2.4.3 Time-Temperature Superposition Principle

Before going into details with the **time-temperature superposition (TTS) principle** it is worthy to analyze the meaning of the **relaxation time**. It can be defined as the time required by a substance to reorganize its structure and achieve a new equilibrium after its initial state has been disturbed by an external stress [37]. When the temperature of the melt is increased the Brownian motions of the polymeric chains increase and consequently the corresponding relaxation times decrease [36,37]. Therefore, the material can achieve the same relaxation state using either high temperatures and short times or low temperatures and high times, that is, there is an equivalence between time and temperature. The TTS principle was derived from these ideas. This principle establishes that if the viscoelastic functions of a polymer measured at different temperatures can be shifted to a selected temperature of reference enabling the formation of a master curve with a good superposition, the material is *thermo-rheologically simple*, meaning that all the polymer relaxation times depend on temperature in the same way. Mathematically, the TTS principle can be expressed as follows:

$$R(T_1, t) = R\left(T_2, \frac{t}{a_T}\right) \tag{2.31}$$

where R is a *rheological function* (for instance, $|\eta^*|$, G', G'', etc.), T_1 and T_2 are temperatures ($T_2 > T_1$) and a_T is a constant quantity for each temperature which is known as *shift factor*. It is obtained from the experimental curve by measuring the amount of shift along the *log t* scale necessary to match the curve obtained at different temperatures. At the reference temperature this parameter is chosen as unity. Furthermore, the shift parameter decreases as the temperature increases [17]. The TTS principle can be also expressed in terms of frequency (frequency-temperature superposition principle) according to Equation 2.32 [41]:

$$R(T_1, \omega) = R(T_2, \omega a_T) \tag{2.32}$$

In other words, a measure at low temperatures might be equivalent to a measure at high frequencies and on the other hand, a measure at high temperatures might be equivalent to a measure at low frequencies.

2.2.4.4 Description of the typical SAOS test of molten polymers

The typical behavior of a polymer as a function of both **temperature** (Figure 2.14.a) and **frequency** (Figure 2.14.b) is presented in Figure 2.14 [42].

At very low temperatures (below T_g), or at very high frequencies, the elastic modulus (storage modulus) is higher than the viscous one (loss modulus). This region is known as the **glassy state** (or **glassy region**). Then, when the temperature increases (above T_g), or the frequency decreases, the mobility of the polymeric chains also increases and therefore a transition takes place until reaching the so-called **rubbery plateau**, where the elastic behavior is still the

predominant one. Between the glassy state and the rubbery plateau there is a transition region (T_g region) in which the loss modulus shows a maximum. This behavior is produced as a result of the contribution of the energy required to induce an increase in the mobility of the polymeric chains. Finally, when the temperature raises again (above the **melting temperature**, T_m) the material starts flowing and the **terminal flow region** is achieved. In this region, the viscous modulus is higher than the elastic one. In addition, in the terminal region the viscosity remains constant and the slopes of the storage modulus and the loss modulus, versus frequency, are, in general, 2 and 1, respectively (Figure 2.14.b) [37].

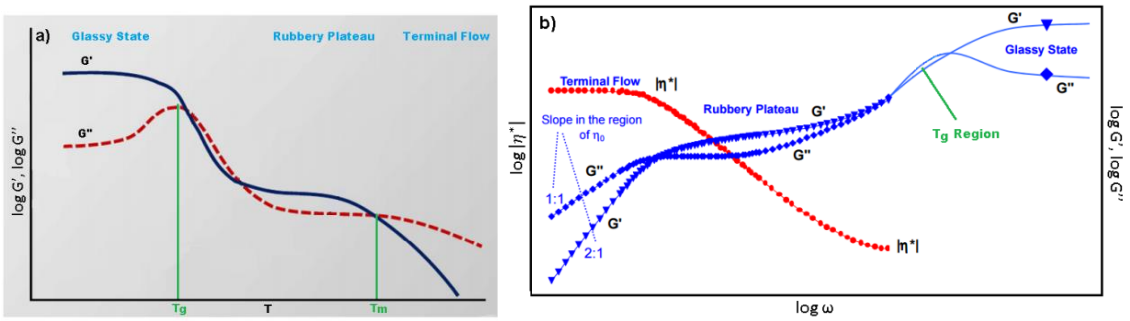

Figure 2.14. Typical SAOS test of polymers. a) Rheological functions versus temperature at a constant frequency. b) Rheological functions versus angular frequency at a constant temperature.

Typically, the behavior of a **molten polymer** is not analyzed in a frequency range as wide as that showed in Figure 2.14.b and only the terminal region and the rubbery plateau are evaluated. In these regions, the obtained **cross-over point** of the curves (where *G'=G''*) can be related to M_W, *MWD* and long chain branching.

The presence of a pronounced rubbery plateau is associated with high M_W polymers. Figure 2.15 shows the dependence of the storage modulus with the **molecular weight**. As M_W increases, the plateau becomes more pronounced and can cover many orders of magnitude in the applied frequency [43].

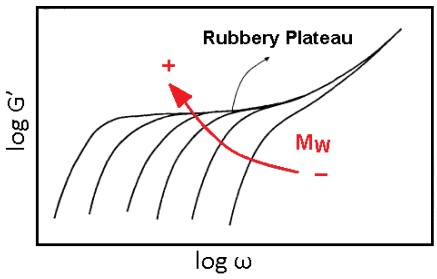

Figure 2.15. Dependence of the storage modulus as a function of frequency with the average molecular weight.

In an ideal elastic solid with permanent entanglements, *G'(ω)* is constant, with no frequency dependence, which reflects the absence of relaxation mechanisms. On the other hand, the ideal viscous liquid does not show storage modulus as it relaxes instantaneously. The behavior of the storage modulus of viscoelastic materials, such as molten polymers, is as follows: at low frequencies the polymer can quickly relax (as both micro and macro-Brownian motions occur much faster than the experimental time) and as a consequence it becomes like a viscous liquid

being the storage modulus small. When the frequency increases, as the motion of the large-range polymer chains (macro-Brownian motion) slows down, the relaxation times do not have enough time to respond and the material behaves increasingly elastic. With a further increase in the frequency, the storage modulus of the polymers presenting a high M_W shows a plateau. The polymers with long molecules show effective entanglements thus, the macro-Brownian motions are highly restricted. Besides this, in this range the micro-Brownian motions still occur much faster than the experimental time. Consequently, at sufficiently high frequencies, none of the entanglements have enough time to relax acting as effective crosslinks (see section 2.2.4.5) and as a consequence, a plateau in the elastic modulus is detected. Finally, when the frequency is once again further increased, the elastic modulus increases with frequency as the motion of the short-range polymer chains (micro-Brownian motion) is also slower than the experimental time and as a result, the relaxation times do not have enough time to respond [43,44].

As it was previously indicated, the cross-over point (ω_x and G_x) can also be related to M_W, as well as MWD and long chain branching. Figure 2.16 schematizes the effect of both M_W and MWD on the cross-over point [36,45].

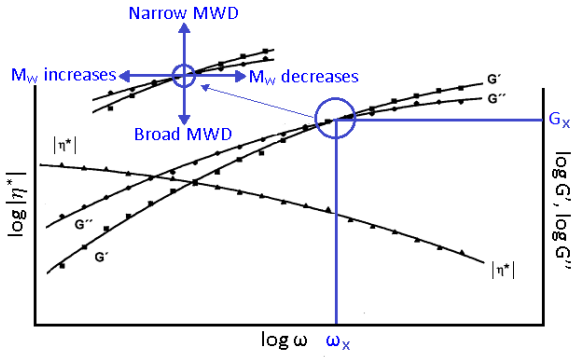

Figure 2.16. Effect of M_W and *MWD* on the cross-over point.

Taking into account the facts summarized in this section together with those included in section 2.2.3.2.4, it is possible to conclude that when M_W increases, the zero-shear viscosity increases and the ω_x is shifted to lower frequencies. Furthermore, for polymers with high molecular weight, determining the zero-shear viscosity is not always possible as very low frequencies might be reached to finally achieve the terminal region. On the contrary, for these polymers the cross-over point could be readily determined. In connection with MWD, changes in this parameter could also be detected with rheological measurements. When MWD becomes broader the cross-over modulus (G_x=G'(ω_x)=G''(ω_x)) decreases [45,46].

To conclude this section, the effect of having **long chain branches** is also considered. As it was indicated in section 2.2.3.2.6, when the branches are long enough to participate in entanglements, the zero-shear viscosity of a branched polymer is much higher than that of a linear one with the same M_W and MWD. However, the effect of long chain branching can also be detected in other viscoelastic properties such as the storage and loss moduli as well as in the loss angle. The storage modulus, at low frequencies, increases with the number of branches per molecule. Despite this, at high frequencies these differences become smaller (Figure 2.17.a) [27,47,48] because at high frequencies, dynamic response reflects only the

molecular dynamics of small segments [47]. On the contrary, the loss modulus is less affected by the branching degree. In connection with the cross-over point, this parameter shifts to lower values as the branching degree increases [36,47].

At low frequencies, in the terminal region where only the longest relaxation times contribute to the viscoelastic behavior, it is well known that the storage modulus is proportional to the square of the frequency, $G' \propto \omega^2$ (Figure 2.14.b). Nevertheless, the presence of LCBs adds additional longer relaxations modes and thus, the slope of the storage modulus, in the terminal region, is reduced [30]. The loss angle is even a more precise indicator of the presence of LCBs (Figure 2.17.b). Figure 2.17.b shows that the behavior of the branched polymers is different to that of a linear polymer (filled squares). The curve (loss angle versus frequency) of the long chain branched polymers shows an inflection with a tendency towards a plateau at high frequencies. The magnitude and breadth of this plateau depend on the degree of LCBs [27].

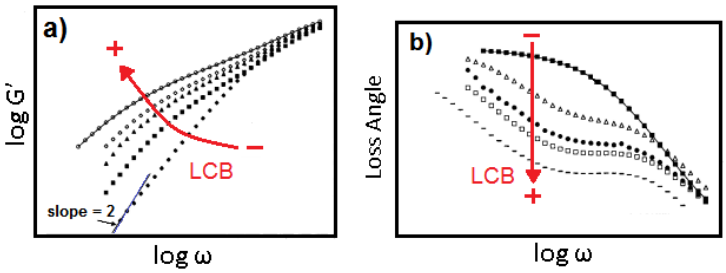

Figure 2.17. Effect of long-chain branching on the viscoelastic properties. a) Effect on the storage modulus. b) Effect on the loss-angle.

2.2.4.5 Description of the SAOS tests of crosslinked polymers

Up to now the typical rheological behavior of uncrosslinked polymers has been considered. This section aims at analyzing, in very general terms, the rheological properties of **crosslinked polymers**. The main difference between crosslinked and non-crosslinked polymers lies in the kind of interaction between the macromolecules. While in the uncrosslinked polymers the nature of these interactions (known as entanglements) is not very clear, the macromolecules of the crosslinked polymers are joined by chemical bonds [44]. The behavior of both types of polymers, as a function of temperature, is compared in Figure 2.18.

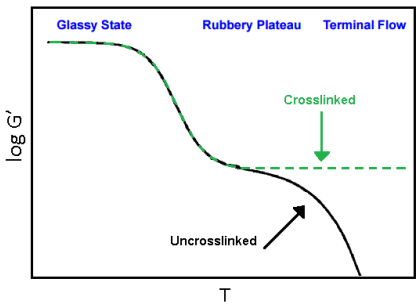

Figure 2.18. Storage modulus as a function of temperature for both, uncrosslinked and crosslinked polymers.

The viscoelastic response of both types of polymers is identical until the rubbery plateau region is reached. However, as the temperature is further increased, the differences between the two polymers become more evident. The macromolecules of crosslinked polymers can undergo micro-Brownian but not macro-Brownian motions and as a result neither melting nor flow are observed as the temperature increases. Thus, the changes in the storage modulus in the rubbery plateau region are small compared to those observed during the glass transition. In a first approximation it can be concluded that the syorage modulus remains constant up to temperatures in which chemical degradation occurs [9,44].

Many polymers are not completely crosslinked and they only contain crosslinked portions. These crosslinked portions consist on small polymer particles whose macromolecules are chemically linked. The mass portion of these particles (also known as gel portion) can represent only a small percentage of the total mass of the polymer. This percentage is also known as gel content (or crosslinking degree). Several authors have studied the effect of the *gel content* (*GC*) on the viscoelastic properties [49,50,51,52]. The main results obtained in these works are summarized in Figure 2.19.

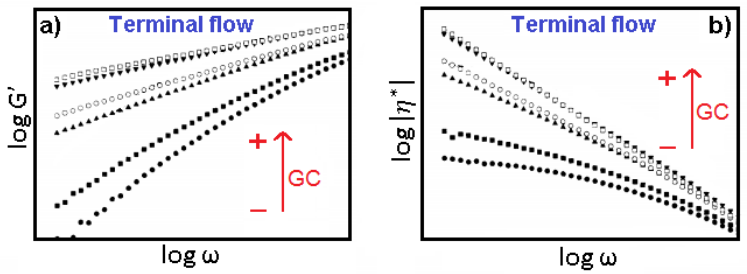

Figure 2.19. Effect of the gel content on the viscoelastic properties. a) Storage modulus. b) Complex viscosity.

The figure above illustrates the changes produced in the storage modulus by modifying the gel content. When the *GC* is very low, the shape of this curve is similar to that of an uncrosslinked material. On the other hand, as the *GC* increases the low frequency storage modulus also increases and it tends towards a plateau, indicating an increased elastic response for these types of polymers. On the other hand, the changes produced in the complex viscosity are shown in Figure 2.19.b. The curves with the lowest levels of gel content show a plateau at low frequencies. As the gel content increases the dynamic viscosity continues to increase linearly as the frequency decreases, with no signs of levelling off (at least in the frequency range tested).

2.2.5 Extensional Rheology

2.2.5.1 Introduction

Although most of the rheological studies are carried out in simple shear flows, melts can also experience extensional (or elongational) flow during processing. To recap, in extensional flow the elements of a fluid are stretched out rather than sheared. However, in general, the information obtained in shear cannot be used to predict the response of a molten polymer to an extensional flow. The simplest extensional flow type is **uniaxial extension**: stretching of the

material in one direction causes compression in the other two directions (Figure 2.20.a). The *velocity field* (v_x, v_y, v_z), for this type of extensional flow, is expressed as follows [1]:

$$\left.\begin{aligned} v_x &= \dot{\varepsilon}x \\ v_y &= -\frac{1}{2}\dot{\varepsilon}y \\ v_z &= -\frac{1}{2}\dot{\varepsilon}z \end{aligned}\right\} \tag{2.33}$$

where $\dot{\varepsilon}$ is a constant *extensional strain rate* and the stretching is carried out in the x direction.

Another type of extensional deformation is the so-called **biaxial extension** (Figure 2.20.b). In this case, the velocity field is given by [1]:

$$\left.\begin{aligned} v_x &= \dot{\varepsilon}x \\ v_y &= \dot{\varepsilon}y \\ v_z &= -2\dot{\varepsilon}z \end{aligned}\right\} \tag{2.34}$$

where the biaxial extension is performed in the xy plane.

Finally, the **planar extensional flow** (Figure 2.20.c) is given by [1]:

$$\left.\begin{aligned} v_x &= \dot{\varepsilon}x \\ v_y &= 0 \\ v_z &= -\dot{\varepsilon}z \end{aligned}\right\} \tag{2.35}$$

where the extension is produced in the x direction and there is no deformation in the y direction.

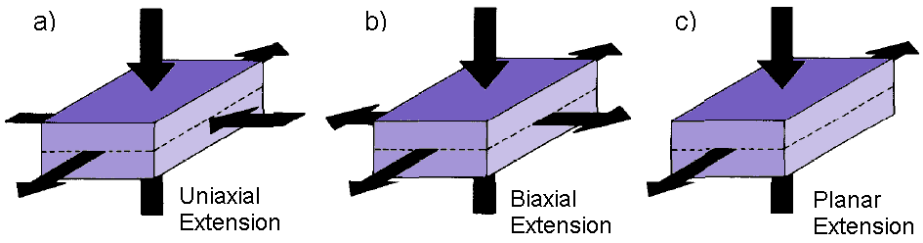

Figure 2.20. Types of extensional flow fields. a) Uniaxial extension. b) Biaxial extension. c) Planar extension.

Biaxial and planar extensional experiments are less frequently found in the literature than the uniaxial ones due to several factors [22]:

- The demanding experimental conditions.
- The small number of experimental equipment available to perform planar and biaxial tests.
- The range of total elongation and elongational rates which can be experimentally achieved are not so broad compared to those achieved in uniaxial elongation.

In fact, the experimental device used in this thesis to perform the extensional viscosity measurements subject the material to a uniaxial extension (section 2.2.5.3) and hence, from now the revision of concepts is focused on this kind of deformation.

2.2.5.2 Basics of uniaxial extension

In the same way as there was a stress (σ) and a strain rate ($\dot{\gamma}$) in shear flow, in extensional flow there is also an *extensional stress* (σ_e) and an *extensional rate* ($\dot{\varepsilon}_H$) also known as ***Hencky strain rate*** or ***natural strain rate***. The ***extensional viscosity*** (η_e) is defined as the ratio between both parameters (Equation 2.36) [53]:

$$\eta_e(t) = \frac{\sigma_e(t)}{\dot{\varepsilon}_H(t)} \tag{2.36}$$

The extensional stress is given by:

$$\sigma_e(t) = \frac{F(t)}{A(t)} \tag{2.37}$$

with *F* being the *tensile force* acting on the actual *cross-section* (*A*) of the sample which changes according to [22]:

$$A(t) = \frac{A_0 l_0}{l(t)} \tag{2.38}$$

A_0 and l_0 are the *cross-section* and *length*, respectively, of the *initial sample* and l is the a*ctual length* of the sample. The dimensions of the samples are measured at room temperature. However, when the samples are heated to perform the extensional test a volumetric expansion of the sample occurs. In order to account for this dimensional expansion the following expression is employed [54]:

$$A(t) = A_0 \left(\frac{\rho_S}{\rho_M}\right)^{2/3} \frac{l_0}{l(t)} \tag{2.39}$$

where ρ_S is the *solid state density* and ρ_M is the *melt density* of the polymer. This melt density is tabulated for a high amount of polymers [55]. Nevertheless, this value can also be experimentally determined as the ratio between the *melt flow rate* (*MFR*) which is reported as the mass per unit time (g/10 min) and the *melt volume rate* (*MVR*) which is reported as the volume per unit time (cm^3/10 min) [56]:

$$\rho_M = \frac{MFR}{MVR} \tag{2.40}$$

The differential extensional strain is defined by relating the change in length to the actual length (and not to the initial length) as Equation 2.41 indicates [22]:

$$d\varepsilon_H = \frac{dl}{l} \tag{2.41}$$

where, ε_H is the *extensional strain* also known as **Hencky strain** or **natural strain**. This Hencky/natural strain is preferably used in applications in which large deformations are employed. Integrating:

$$\varepsilon_H = \int_{l_0}^{l} d\varepsilon_H = \int_{l_0}^{l} \frac{dl}{l} = \ln\left(\frac{l}{l_0}\right) = \ln(\lambda) \tag{2.42}$$

where $\lambda = l/l_0$ is known as *stretching ratio*.

The Hencky strain rate and the Hencky strain are related as follows [22]:

$$\dot{\varepsilon_H} = \frac{d\varepsilon_H}{dt} \rightarrow \varepsilon_H = \dot{\varepsilon_H} t \tag{2.43}$$

2.2.5.3 Experimental devices for uniaxial extension

In this thesis two different experimental devices for uniaxial extension have been used. The first one is known as **SER (or SER 2) Universal Testing Platform** (from now called SER 2). This device is designed for a controlled shear stress rheometer. The second one is known as **Extensional Viscosity Fixture** (from now called EVF) and it is designed for a controlled shear strain rheometer. However, both devices are based on the same operational principle as they are based on the Meissner concept of elongating the sample within a confined space by expelling the sample with rotary clamps. In these devices, instead of the rotary clamps two cylinders are used to wind up the sample as the schemes showed in Figure 2.21 indicate [57,58].

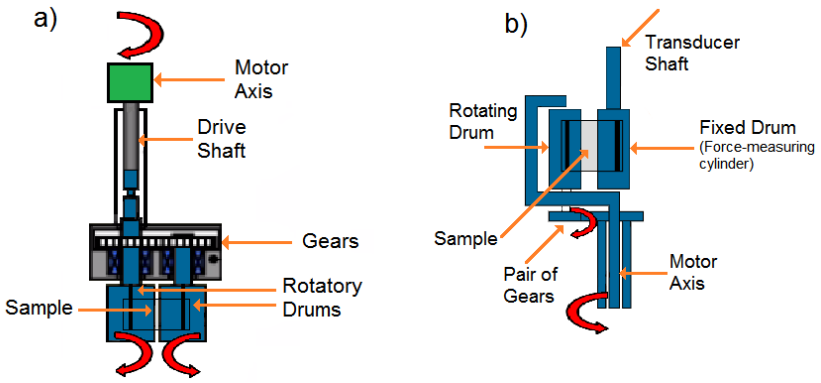

Figure 2.21. Schemes of two experimental devices for uniaxial extension. a) SER 2 universal testing platform. b) Extensional viscosity fixture.

In the SER 2 (Figure 2.21.a) the sample is clamped to two cylinders (rotatory drums) which are rotating in opposite directions to finally stretch the sample. In this device the tensile force and the Hencky strain rate are expressed as follows [57]:

$$F(t) = \frac{M(t)}{D_d} \tag{2.44}$$

$$\dot{\varepsilon_H}(t) = \frac{\Omega(t) D_d}{l_0} \tag{2.45}$$

where *M(t)* is the *torque*, D_d is the *drum diameter* and *Ω(t)* is the *drive shaft rotation rate*.

In the EVF (Figure 2.21.b) the sample is also clamped to two cylinders. However, in this device one of these cylinders is fixed and the other one rotates. The rotating cylinder moves on a circular orbit around the fixed cylinder (which is in turn the force measuring cylinder) while rotating around its own axis at the same time. The Hencky strain rate is the same as the one

defined in Equation 2.45. However, the expression of the tensile force is different to the one defined in Equation 2.44, as Equation 2.46 indicates [58].

$$F(t) = \frac{M(t)}{D_d/2} \tag{2.46}$$

2.2.5.4 Uniaxial extensional behavior of molten polymers

The typical uniaxial extensional behavior of molten polymers is summarized in Figure 2.22. In this figure the extensional viscosity is represented as a function of time in a double logarithmic scale. Moreover, Figure 2.22 also shows the *steady elongational viscosity* as a function of the Hencky strain rate. The steady state is achieved when $\eta_e(t) =$ constant. Normally, the time-dependent extensional viscosity is called ***transient extensional viscosity*** ($\eta_e^+(t)$), to differentiate this viscosity from the steady one.

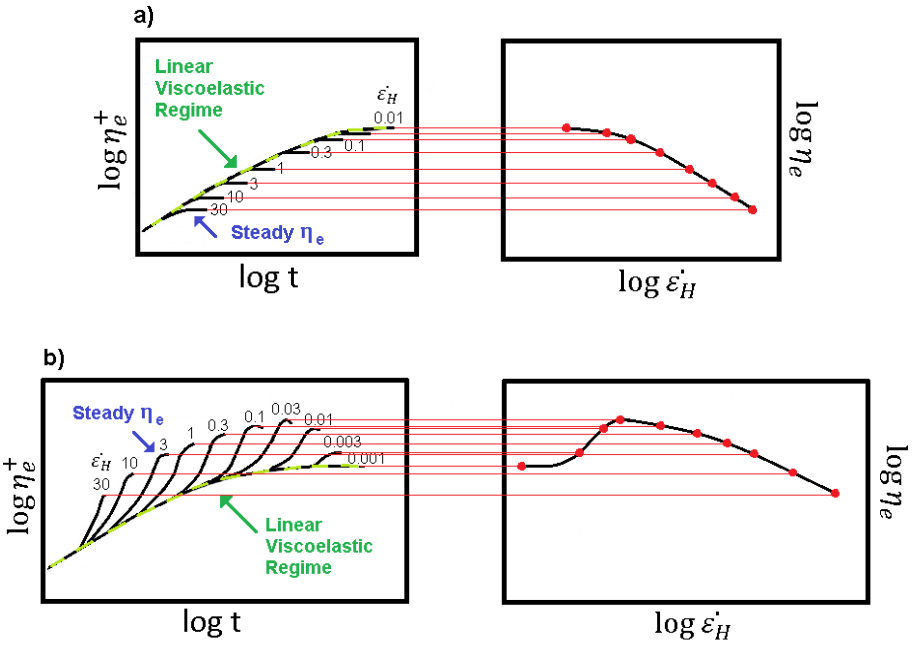

Figure 2.22 Typical uniaxial extensional behaviors of molten polymers. a) Strain-softening polymers. b) Strain-hardening polymers.

Non-linearity manifests itself as a deviation from the **linear viscoelastic regime (LVR)**. For **strain-softening materials**, the non-linearity appears as a steady-state level below LVR. This behavior is represented in Figure 2.22.a and it is the typical behavior of linear polymers [24]. On the other hand, in the **strain-hardening materials** the curves start to rise abruptly before levelling off to a steady-state, as Figure 2.22.b indicates. Both, branched polymers and linear polymers with a small amount of very high M_W fractions are strain-hardening polymers, that is, strain hardening polymers are those presenting a well-entangled structure regardless of their chain architecture [24]. Traditionally, the strain hardening has been quantified by using the ***strain hardening coefficient*** (*S*), which is defined as follows (for a particular value of time and Hencky strain rate):

$$S = \frac{\eta_e^+(t_0, \dot{\varepsilon}_{H0})}{\eta_{e0}^+(t_0)} \tag{2.47}$$

where the numerator is the value of the transient extensional viscosity obtained for a certain time (t_0) and a certain Hencky strain rate ($\dot{\varepsilon}_{H0}$) and the denominator is the value of the transient extensional viscosity in the linear viscoelastic regime obtained for the same time [24]. Several authors have used this coefficient to compare the extensional rheological behavior of different polymers [27,59,60].

2.2.5.4.1 Relationship between shear and uniaxial extensional behaviors

From Figure 2.22, it can be derived that at low Hencky strain all the curves come to lie on the linear viscoelastic regime ($\eta_{e0}^{+}(t)$). In this linear range of deformation, the uniaxial time-dependent elongational viscosity is three times the time-dependent linear shear viscosity ($\eta^0(t)$). This relationship was first found by Trouton and therefore it is named **Trouton's ratio** (Equation 2.48) [22].

$$\frac{\eta_{e0}^{+}(t)}{\eta^0(t)} = 3 \tag{2.48}$$

Figure 2.23 shows a comparison of the time dependence of elongational and shear viscosities.

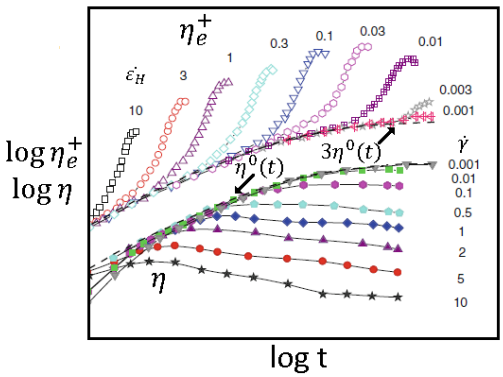

Figure 2.23. Comparison of the time dependence of elongational and shear viscosities of strain-hardening polymers.

From both, Figure 2.23 and Equation 2.48 it is possible to conclude that the transient extensional viscosity in the linear viscoelastic regime can be determined in two different but equivalent ways: as three times the shear viscosity curve obtained at very low shear rates or by extrapolating the superimposed portion of the curves for different extensional rates [59,60].

The origin of this strain hardening is not very clear. Several authors have tried to find an explanation for this behavior. McLeish and Larson [61] analyzed the behavior of long chain branched polymers. In these polymers, the most important aspect is the presence of multiple branch points on the same molecule. Because of the multiple branch points, there are molecular strands that lie between two branch points and hence they have no free ends (backbones). Moreover, these branch points are entangled with other macromolecules forming a network and acting as anchors which prevent the backbone to retract (relaxation mechanism) after a strain step. Consequently, the backbone can readily be stretched in an extensional flow, producing strain hardening. In shear, however, the backbone stretches only temporarily and it eventually collapses as the molecules are aligned, producing strain softening. On the other hand, the backbones of linear polymers have free ends. Under flow

these free ends allow the chain polymer to retract very quickly and hence large stresses cannot readily build up. Consequently, these polymers do not show strain hardening. In the work of Micic and Bhattacharya [62] it is explained the reason of the existence of a critical strain (or time) from which the strain hardening occurs. While the critical time depends on the strain rate, the critical strain is independent on this parameter. They relate this change in the rheological behavior to a structural change in the macromolecular network. From the critical strain an increase in the number of entanglements or in the efficiency of the entanglement coupling is produced. The critical strain may represent the required stretching for the parts of macromolecular chains to be able to overlap more efficiently to form new entanglements. These stretched macromolecules should occupy much less free volume than in the undisturbed state. Therefore, they share space with other macromolecules and larger contact surface and more effective overlapping occur in this state. The theory presented by these two authors does not differ much from that of McLeish and Larson [61] although there is a slight variation. The new theory allows the branches to stretch and to form entanglements once the critical strain is achieved therefore, they produce strain hardening by themselves in addition to the strain hardening produced by the chain backbone.

In both, Figure 2.22.b and Figure 2.23, it is also possible to see that, in these particular polymers, at low Hencky strain rates strain hardening does not occur. Strain hardening only takes place when the rate of the elongation flow (Hencky strain rate) exceeds the inverse of the *stretch relaxation time*, τ_R, (also known as *longest Rouse relaxation time*) of the long molecules that are stretched by the flow [24,63]. However, not all the polymers follow this behavior as it is indicated in section 2.2.5.4.2.

Up to now, the works mentioned in this thesis have been focused on explaining the extensional behavior of long chain branched polymers. Nevertheless, many experimental studies have shown that linear polymers with a bimodal MWD also show strain hardening (see section 2.2.5.4.2). In their work, Liu et al. [64] studied the origin of strain hardening as well as the differences between extensional and shear flow. Their theoretical analysis shows that molten polymers, regardless on their chain architecture, always exhibit strain hardening at high enough Hencky strain rates, because the entanglement network can be effectively strengthened during extension. That means that the Hencky strain rates normally employed to perform the extensional tests do not allow observing strain hardening in linear polymers. They concluded that molten polymers tend to display strain hardening due to two main reasons: on the one hand, the removal of chain entanglement appears to be difficult at high rates in extension and on the other hand, the corresponding cross-sectional area shrinkage (also known as geometric condensation), which makes the system to be strengthen. They explain the differences between elongational and shear flow considering the kinematic difference between both processes. Despite the fact that the same kind of chain disentanglement observed in shear also takes place during uniaxial extension, the effect of the geometric condensation cause the appearance of strain hardening.

Another way to analyze the differences between shear and extensional flows consists on representing together the steady shear viscosity as a function of the shear rate and the steady extensional viscosity as a function of the Hencky strain rate (Figure 2.24), which is obtained as

indicated in Figure 2.22. Figure 2.24 shows the typical behaviors of both strain-softening polymers (Figure 2.24.a) and strain-hardening polymers (Figure 2.24.b).

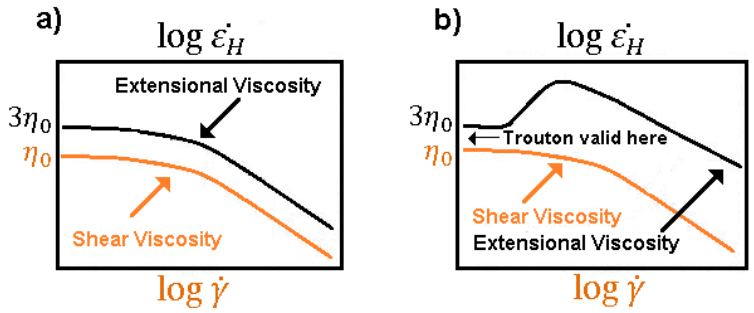

Figure 2.24. Comparison of the strain rate dependence of elongational and shear viscosities. a) Strain-softening polymers. b) Strain-hardening polymers.

The obvious difference between the two kinds of viscosities is most marked in strain-hardening polymers in which the extensional viscosity increases as the Hencky strain rate increases (extensional thickening) and then, at much higher extensional rates, this viscosity decreases (extensional thinning) although, it is still much higher than the shear viscosity [53]. In strain-softening polymers the two curves are parallel in the whole measurement range.

2.2.5.4.2 Influence of molecular weight, molecular weight distribution and long chain branching on the strain hardening behavior

The effect of $\boldsymbol{M_W}$ on the extensional rheology is shown in Figure 2.25. In the same way as the shear viscosity increased with M_W (Figure 2.9) the extensional viscosity is also enhanced [53].

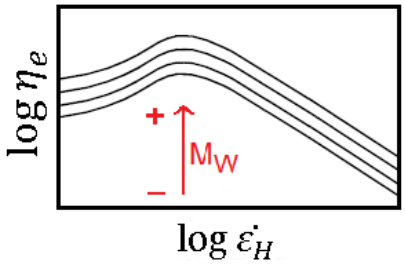

Figure 2.25. Effect of molecular weight on uniaxial extensional viscosity.

In polyolefins, strain hardening is not highly influenced by M_W, in the sense that, in general, strain hardening is not induced by changing this parameter, at least at accessible Hencky strain rates. Nevertheless, it has been proved that one might be able to generate strain hardening in linear monodisperse polystyrenes, in a practical experiment, by increasing M_W. However, these samples are not typical commercial resins [65.66]

Nevertheless, the strain hardening is strongly influenced by other parameters such as **MWD** and long chain branching. Several authors have proved that linear polymers, which are strain-softening, can be made strongly strain-hardening by the introduction of a small amount of a relatively high molecular weight material, that is, linear polymers with a **bimodal MWD** can also show strain hardening. This fact has been tested in different types of polymers: polystyrene [67, 68], polypropylene [69] and polyethylene [70].

Chain branching is another parameter affecting strain hardening. However, a great variety of branched structures are possible. Neither star-shaped polymers nor polymers containing short chain branches exhibit strain hardening [24,30]. Nevertheless, several works have proved that strain hardening in extensional flow can be caused by **long chain branches** [47,59,71,72]. In fact, strain hardening in extension is the most prominent indicator of long chain branches in a polymer [24].

Gabriel and Münstedt [71] were able to separate the effects of LCBs and a bimodal MWD distribution by performing the elongational experiments on two metallocene polyethylenes (m-PEs) with a very similar molecular weight distribution. They concluded that small amounts of LCBs can cause significant strain hardening in elongational flow. They also investigated the rheological behavior of a linear high density polyethylene (HDPE) and that of a long chain branched low density polyethylene (LDPE). The two materials showed a different dependence of the strain hardening with the Hencky strain rate. Auhl et al. [72] studied the changes produced in the rheological properties of a linear polypropylene (PP) modified by electron beam irradiation. They detected an increase in the number of long chain branches by increasing the irradiation dose. They obtained a clear relationship between strain hardening and long chain branching as the strain hardening also increased with the irradiation dose. Moreover, they found that a change in the dependence of the strain hardening with the Hencky strain rate occurred when the irradiation dose was modified. Gotsis et al. [47] added branches to a linear PP, in different amounts, by using reactive modification with peroxydicarbonates. Similar results to that obtained in the work of Auhl et al. [72] were also found here. Stange et al. [59] investigated the changes produced in a linear PP after being blended with different amounts of a commercial long chain branched PP. For a constant Hencky strain rate, an increase in the strain hardening was obtained by increasing the amount of long chain branched PP. Moreover, they found that very low amounts of long chain branched PP led to a pronounced strain hardening. Again, they observed that the behavior of the strain hardening versus the Hencky strain rate was not the same in all the blends.

In the previous works it was found that, for a same range of Hencky strain rates, the dependence of the strain hardening coefficient (determined for a fixed Hencky strain) with the strain rate was not always the same. On the one hand, there are materials in which the strain hardening coefficient (*S*) increases as the elongational rate increases (Figure 2.26) and on the other hand, there are materials in which the strain hardening coefficient decreases as the elongational rate increases (Figure 2.27).

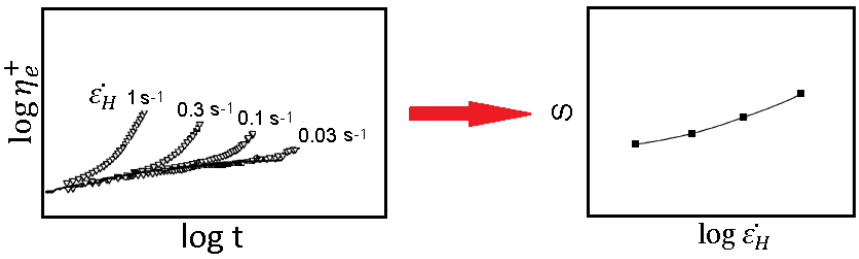

Figure 2.26. Behavior of materials in which the strain hardening coefficient (*S*) increases by increasing Hencky strain rate.

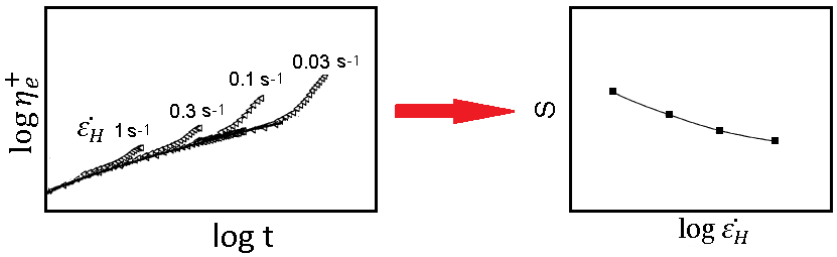

Figure 2.27. Behavior of materials in which the strain hardening coefficient (*S*) decreases as the Hencky strain rate increases.

While the behavior represented in Figure 2.26 is characteristic of branched polymers containing high amounts of long chain branches, the behavior showed in Figure 2.27 corresponds to branched polymers with a low amount of long chain branches.

2.2.5.4.3 Dependence of uniaxial extensional viscosity with temperature

While it is well known that the transient extensional viscosity in the linear viscoelastic regime decreases as the temperature increases in the same way as shear viscosity did (see section 2.2.3.2.3) as far as the author knowledge, the effect of the temperature on the strain hardening coefficient is not so clear.

As it was previously indicated, strain hardening polymers show a gradually increase in viscosity with time followed by a rapid increase in viscosity (strain hardening) after a certain time. Takahashi et al. [73] investigated the elongational behavior of a LDPE and of a LDPE graft-copolymerized with polystyrene (LDPE-g-PS). While the behavior of the LDPE was found to be almost independent on temperature, the behavior of the LDPE-g-PS is highly influenced by this parameter. At 140 ºC the material does not show strain hardening but when the temperature is raised to 200 ºC a rapid increase in viscosity occurs. Micic et al. [74] measured the transient extensional viscosity of blends of a LDPE and a linear low density polyethylene (LLDPE). They found that both, the pure LLDPE and the blends rich in LLDPE showed a faster rise in the elongational viscosity in the strain hardening region of deformation (that is, stronger strain hardening) when the temperature was increased. However, the pure LDPE and the blend rich in LDPE showed an opposite behavior as an increase in the strain hardening was detected when the temperature decreased.

2.2.5.4.4 Uniaxial extensional behavior of crosslinked polymers

This section aims at analyzing the effect of the crosslinking degree on the uniaxial extensional behavior. For this purpose the main results founded in different works are summarized.

Yamaguchi et al. [75] studied the effect on the uniaxial extensional behavior of blending a crosslinked linear low density polyethylene (x-LLDPE) with a LLDPE. They obtained a significantly increase in the strain hardening when the LLDPE was blended just with a small amount of x-LLDPE. Moreover, they found that the strain hardening also increased as the content of x-LLDPE increased. The same authors, Yamaguchi et al. [76], performed a similar study blending, in this occasion, a HDPE with a crosslinked HDPE (x-HDPE). Similar results to those obtained with the LLDPE were also found in this work. Chen [77] analyzed the

extensional rheological properties of different crosslinked ethylene vinyl acetates (EVAs). The crosslinked was performed by using a dicumyl peroxide (DCP). It was found an enhanced strain hardening as the crosslinking degree increased.

2.2.5.4.5 Strain hardening and melt strength

The ***melt strength*** (*MS*) of a polymer is a measure of the tenacity of the melt. The experimental set-up to determine the melt strength consists on a single-screw extruder equipped with a capillary die and a Rheotens melt strength tester (Figure 2.28).

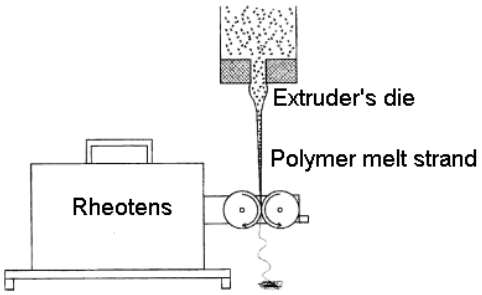

Figure 2.28. Experimental set-up for determining the melt strength.

With this set-up the molten polymer is stretched in uniaxial extension. The polymer melt strand is extruded continuously. After a certain spinline length the polymer is taken up by the wheels of the **Rheotens**. These wheels turn with a slowly increasing *velocity* (*v*) and draw down the polymer strand. The resistance of the material against this drawdown is then measured by a force balance in the arm onto which the wheels are fixed. This results in an extension diagram: force (*F*) as a function of the drawdown velocity, as Figure 2.29 indicates [78,79]. The resulting force is measured until the rupture of the strand.

The melt strength is defined as the maximum (drawdown) force by which a molten strand can be drawn, under standard conditions, before it breaks [30]. The maximum velocity achieved before the molten breaks is called **drawability** of the melt [78].

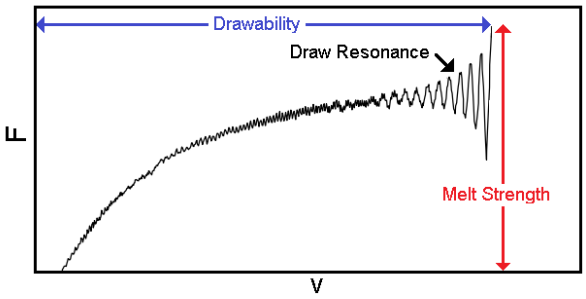

Figure 2.29. Rheotens test: force as a function of the drawdown velocity.

High melt strength is usually accompanied by strain hardening, that is, polymers with strain hardening in elongational viscosity are known to exhibit a high melt strength [80]. For example, the melt strength of long chain branched LDPE samples has been found to be twice or even five times higher than the melt strength of linear HDPE samples and linear low density polyethylene (LLDPE) samples with the same melt flow rate (*MFR*) [81,82]. It has also been

found that a branched PP may have a melt strength ten times higher than a linear PP, with the same *MFR* [82].

The melt strength is highly influenced by both the *MFR* and the temperature. Figure 2.30 shows the effect of *MFR* and temperature on the *MS* of PP [79].

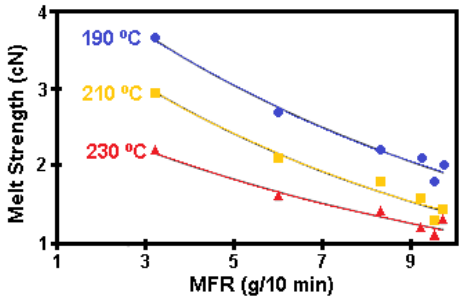

Figure 2.30. Effect of MFR and temperature on the melt strength.

The melt strength decreases as the melt flow rate increases. For polypropylenes and polyethylenes a linear relationship between the *MS* and the *MFR* has been found (Equation 2.49) [79,83]:

$$MS = A - Blog(MFR) \tag{2.49}$$

where *A* and *B* are constants. Therefore, it can be concluded that for a constant temperature it is not possible to compare the melt strength of polymers with different *MFR*. To solve this problem the **relative melt strength** is normally considered. This is the value of the *MS* multiplied by the *MFR* [81].

Figure 2.30 also shows how the melt strength depends on temperature. The melt strength increases as the temperature decreases. Therefore, to compare materials it is convenient to measure the *MS* at the same temperature. Muke et al. [79] found an Arrhenius temperature dependence of melt strength for polypropylene (Equation 2.50):

$$\log(MS) = \frac{E_m}{RT} + \log(C) \tag{2.50}$$

where E_m is known as the *activation energy of the melt strength*, *R* is the universal molar gas constant and *C* is a constant.

2.3 Polymeric matrices

In this section a brief description of the polymeric matrices employed in this thesis is given with the aim of understanding why these polymers have been selected to perform the experimental work.

2.3.1 Polypropylene

Polypropylene (PP) has been selected due to two main reasons. First, its excellent properties: high melting temperature, stiffness, capability of static load bearing, good temperature stability and high chemical resistance [84]. The second reason of selecting this polymer is

because in the market two different types of polypropylenes, with completely different extensional rheological properties are available: linear PPs and high melt strength PPs (HMS PPs). Due to this second reason, it has been possible to obtain polymeric matrices with different extensional behavior (by blending the linear PP and the HMS PP) in order to fulfill with the objectives of the thesis (see chapter 1, section 1.2).

2.3.1.1 High melt strength polypropylene

Linear PP is the common PP. It is a polymer which does not show any indication of strain hardening and hence, it is a polymer with a weak melt strength [68]. In certain applications, such as foaming, blowing molding, fiber spinning, etc., (see section 2.5) it is necessary to work with polymers presenting high melt strength. For this reason, long chain branches have been incorporated to the common linear PPs to finally create HMS PPs. Different methods have been used to modify PP with LCBs. Some of them produce long chain branched PP by in-situ polymerization using metallocene catalyst [85,86,87,88,89]. Other methods include post-reactor treatments such as electron beam irradiation [72,90,91], reactive extrusion [80,92,93] and grafting [94,95].

2.3.2 Polypropylene/montmorillonite nanocomposites

Different **HMS polypropylene/montmorillonite nanocomposites** have also been employed in this thesis. One of the reasons why this system has been selected is to have a new polymeric system with a new rheological behavior to fulfill the objectives proposed in this thesis, as it is well known that the polymer morphology and hence the polymer rheological properties are greatly affected by nanoparticles (see section 2.3.2.1). Moreover, the complexity of this new system has also made possible to understand and analyze in which situations (that is, with which types of polymeric matrices) it is possible to use the extensional rheology as predictive tool. Moreover, the number of studies in which a HMS PP is blended with layered clays is scarce. In fact, only two papers have been found [96,97]. This fact is other of the reasons that motivated the selection of this particular composite for being analyzed in this thesis.

The nanocomposites studied in this thesis have been produced by blending the HMS PP with two different types of **montmorillonites (MMTs)**: natural MMTs (also called, in this thesis, natural clays) and organomodified MMTs (or organomodified clays). Among all the potential nanoparticles, those based on layered (clay) silicates, like montmorillonites, have been selected due to several reasons: they have been widely investigated, they are easily available and they can be processed by employing common processing routes [98]. MMTs belong to the structural family known as the 2:1 phyllosilicates. Their crystal lattice consists of two-dimensional layers where a central octahedral sheet is fused to two external silica tetrahedrons by the tip, so that the oxygen ions of the octahedral sheet also belong to the tetrahedral sheets. The layer thickness is around 1 nm and the lateral dimensions of these layers may vary from 300 Å up to several microns and even larger depending on the particular silicate. These layers organize themselves to form **stacks** with a regular Van der Walls gap between them called the **interlayer** or the gallery, that is, layered silicates are made up of several hundred thin platelets stacked in orderly particles or tactoids (Figure 2.31). Isomorphic substitution within the layers (for example, Al^{3+} replaced by Mg^{2+} or by Fe^{2+}, or Mg^{2+} replaced by Li^{+}) generates negative charges that are counterbalanced by earth cations situated in the

interlayer. As the forces that hold the stacks together are relatively weak, the intercalation of small molecules between the layers is possible.

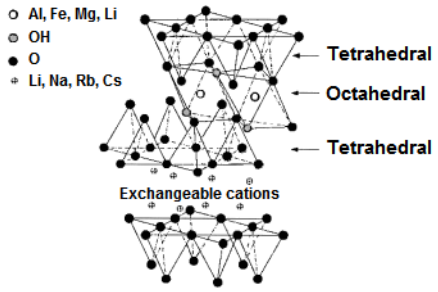

Figure 2.31. Structure of 2:1 phyllosilicates.

2.3.2.1 Properties of polypropylene/montmorillonite nanocomposites

When nanoparticles are added to the polymeric matrix, many properties can be improved. Several works have analyzed the effect of the MMTs content on the **tensile properties**. The characteristic behavior of polymer/layered clays nanocomposites is as follows. In general, an increase in the Young's modulus is observed for very small clay loadings (MMTs content < 3 %). Then, for higher clay contents a much slower increase is detected. The yield stress does not change markedly compared to the neat polymer and there is only a small decrease in the maximum strain at break [99,100]. Similar improvements in mechanical properties can be obtained with other layered fillers; however, much higher filler contents are normally required [99]. Another property that is strongly affected by these inorganic fillers is the **scratch resistance**. A sharp increase of this parameter is observed for very moderate clay loadings [99]. The incorporation of clays into the polymeric matrix was found to enhance **thermal stability** as an increase in the decomposition temperature was observed by increasing the clay content. This increase of the decomposition temperature can be ascribed to the hindered diffusion of volatile decomposition products caused by the clay particles [101,102]. Improvements in the **flame retardant properties** are also achieved when layered clays are added to a polymeric matrix. Heat transfer from an external source promotes thermal decomposition of both, the clay and the polymer which results in the formation of a thermal insulating and low permeability char on the outer surface of the nanocomposite. The carbonaceous char produced acts as an excellent physical barrier which protects the substrate from heat and oxygen and slows down the scape of flammable volatiles generated during polymer degradation [102,103].

However, not only improvements in the physical properties of the polymeric nanocomposites are obtained, the polymer morphology is also affected by nanoparticles as the changes observed in the polymer crystallinity and in the rheological behavior indicate. It is well known that nanometer size clay platelets are effective nucleating agents for the **crystallization** of a polymeric matrix [102]. Regarding the **rheological properties**, it is generally established that when nanocomposites are formed, the viscosity, at low shear rates, increases with filler concentration. Very often a solid-like behavior, which is attributed to the physical percolation of the randomly distributed layers, is observed. As the rheological behavior of particle-filled materials is very sensitive to their structure, rheology offers a means to assess the state of

dispersion in nanocomposites, directly in the molten state (see section 2.3.2.2) [102]. The **extensional rheological** properties of a polymeric matrix are also highly influenced by the fact of adding layered clays. The extensional rheological behavior of composites based on MMT and linear polypropylene has been widely investigated. Okamoto et al. [104] observed a strong induced strain hardening behavior under uniaxial extensional flow that, according to their arguments, originates from the alignment of the silicate layers perpendicular to the flow direction. Park et al. [105] observed strain hardening in the polymeric systems in which the clays were completely exfoliated. They also observed a preferred orientation of the silicate layers in the extensional flow direction, that is, a parallel alignment of the silicate layers to the stretching direction. They attributed both, the strain hardening and the morphological change under the uniaxial extensional flow (clay orientation) to the fact of having a good compatibility between the clays and the polymeric matrix. Koo et al. [106] observed an increase in the melt strength and a decrease in the drawability when the clay concentration increased. Lee et al. [107] founded an enhanced strain hardening in the samples presenting a good compatibilization between the clays and the polymeric matrix. They attributed the strain hardening to both, an increase in the possibility of entanglements in the melt and a reduction in the rate of disentanglement, caused by the generated three-dimensional network structure during the melt compounding. Summing up, when a good compatibilization between the clays and the linear PP based polymeric matrix occurs, an enhanced strain hardening is obtained although, there is still no agreement on the origin of this phenomenon. However, while the effect of these nanoparticles on the rheological behavior of common linear PPs has been widely investigated, only two papers have analyzed this effect in a HMS PP. Bhattacharya et al. [96] showed that all the polymers (pure polymer and nanocomposites) displayed strain hardening although, it is more pronounced in the polymeric nanocomposites. Su et al. [97] determined the melt strength and the apparent elongational viscosity from the Rheotens data. They obtained that the melt strength of nanocomposites was lower than that of the unfilled polymer. In general they found a decrease in the melt strength by increasing the clay content. Moreover, the same behavior was followed by the apparent elongational viscosity. The results obtained in these two papers are contradictory which indicates that a more thorough study of the rheological behavior of HMS PP/clays nanocomposites should be performed. As it was previously indicated, this is another reason why this material has been selected in this thesis.

2.3.2.2 Analysis of the dispersion and compatibilization of montmorillonites

The improvements obtained in all the properties mentioned above are greatly affected by the degree of filler exfoliation and dispersion achieved during the mixing process as well as by the compatibilization degree between the clays and the polymer [108]. A fully dispersed and stable state will lead to optimal properties whereas the presence of particle agglomerates or a low compatibility between the particles and the polymeric matrix lead to a poor material performance, which can be even lower than that of the virgin polymeric matrix [109].

Clay particles can be presented in three different configurations, when they are incorporated into the polymeric matrix (Figure 2.32) [103]:

- **Phase separated composite**. If the polymer is unable to intercalate into the galleries, a phase separated composite is formed, and its properties are similar to that of traditional microcomposites.

- **Intercalated nanocomposite**. An intercalated nanocomposite is obtained when the polymer macromolecules diffuse between unchanged clay sheets, leading to a well ordered multilayer structure of alternating polymer and inorganic layers with a repeating distance of few nanometers between them.
- **Exfoliated nanocomposite**. In these composites clay layers are separated and uniformly dispersed, maximizing thus the polymer-clay interactions. The most significant changes in physical properties are observed in these nanocomposites.

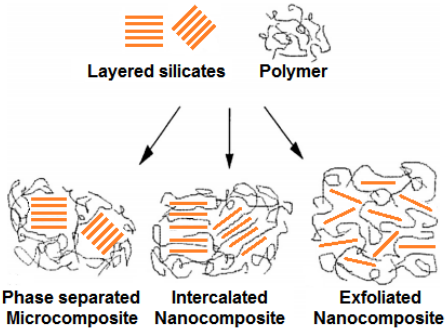

Figure 2.32. Possible polymer/layered silicate structures.

Nevertheless, as the clays are naturally hydrophilic materials it is very difficult to exfoliate them in a polymeric matrix with low polarity such as PP. Major efforts were dedicated to obtain an intercalated or exfoliated structure either by changing the interlayer structure of montmorillonites (organomodified montmorillonites), by introducing a polar group (compatibilizer agent) in the polymeric matrix or by combining both strategies.

As it was previously indicated, the structure of montmorillonites is made of several stacked layers which organize themselves to form stacks with a regular gap between them, called gallery or interlayer. With the aim of render these phyllosilicates more organophilic, the cations in the gallery can be exchanged by cationic modifiers (for example, quaternary ammonium salts). The surface energy of the **organomodified** clay is lowered and consequently this organophilic clay is more compatible with organic polymers [108,110]. Moreover, this modification also leads to expand the space between the silicate layers due to the presence of alkyl chains intercalated in the interlayer, which facilitates the clay exfoliation when they are blended with the polymeric matrix [111,112]. However, in general, the use of organomodified clays is not enough to achieve an intercalated/exfoliated structure in PP due to its low polarity. With PP it is necessary to use **compatibilizer agents** to promote strong interactions between the polymer and the clays, which helps to obtain the desired structure (exfoliated structure) during melt compounding. These compatibilizers must fulfill two requirements to finally achieve clay exfoliation: (1) the compatibilizer should be miscible with the polymeric matrix and (2) the compatibilizer should include a certain amount of polar functional groups in the molecule. Maleic anhydride modified polypropylene (PP-MA) is one of the most used compatibilizer agents as it fulfills the requirements described previously [113,114].

The dispersion and exfoliation degrees have been traditionally characterized by **X-ray diffraction** (XRD) and **transmission electron microscopy** (TEM). XRD allows measuring the ***interlayer spacing between the stacks*** (*d*) as the clays show a characteristic diffraction peak

corresponding to the (001) plane. From this peak the interlayer spacing (*d*) was calculated using the Bragg's equation:

$$\lambda = 2dsin(\theta) \tag{2.51}$$

where λ is the *wavelength* and 2θ is the *diffraction angle*.

Once the clays are blended with the polymeric matrix, XRD can be used to describe the nanoscale exfoliation level of the clays in the polymer. In a phase separated composite no changes in *d* are obtained, meaning that no polymer has entered the gallery and that the spacing between the clay layers is unchanged. Intercalated nanocomposites have an increased *d*, indicating that the polymer has entered the gallery, expanding the layers. Finally, exfoliated nanocomposites do not show the peak corresponding to the (001) plane, suggesting that a great amount of polymer has entered the gallery space, expanding the clay layers so far apart that no ordered structure is found and as a consequence diffraction cannot be observed [115].

As one of the keys to achieve the desired properties is the control of the structure of the nanocomposites, that is, the degree of exfoliation and the clay distribution in the polymeric matrix, there are several works in which these traditional techniques have been employed to analyze the structure of the particles in composites produced with polypropylene and montmorillonites. In these works, the effects of using non organomodified and organomodified clays have been analyzed. It was concluded that a better intercalation between the clays and the polymer is obtained by using organomodified montmorillonites [116]. Also the effects of the amount and kind of compatibilizer have been investigated, concluding that the use of a compatibilizer improves the intercalation between the montmorillonites and the PP and that an increase in the interlayer spacing is produced by increasing the amount of compatibilizer agent [107,112,117,118]. The effect of the initial interlayer spacing of the clays and the effect of the clay content were also studied. There seems to be an optimum range of initial interlayer distance for obtaining an effective intercalation [112]. Moreover, when the clay content increases an aggregation of small portions of layers is produced and the level of intercalation is reduced [96,106,119]. Finally, the production parameters have also been modified in order to analyze the effect of the production process on the structure of the nanocomposites. It has been proved that the structure of the nanocomposites is highly affected by the processing route, that is, by the way in which the different raw materials are blended [120].The processing temperature is also very important. When a low processing temperature is used the shear stress is higher and therefore, the clay exfoliation is promoted [112,118,121]. With the exception of the works of Bhattacharya et al. [96] and Su et al. [97] in which the structure of the nanocomposites is analyzed in nanocomposites produced with a HMS PP, the rest of authors work with nanocomposites based on common linear polypropylenes.

Nevertheless, the techniques normally used to characterize the structure of the nanocomposites, XRD and TEM, are limited in the sense that they only prove a small volume of the sample and therefore, they must be combined with other techniques such as melt rheology. Both, linear and non-linear rheological properties are very sensitive to changes in the nanoscale and mesoscale structure and therefore, rheology can be used as a powerful tool to evaluate the dispersion of the particles in the melt state. Moreover, one of the main

advantages of rheology is that samples of macroscopic dimensions are used and hence, rheology offers an integrated picture of the composite material. Research on the influence of the clay presence on the shear rheology of filled polymers is relatively common because the rheological characteristics can be directly related to the structure and properties of the nanocomposites [97,107,117,118,120,122,123,124]. The results obtained in these papers are summarized in the Figure 2.33.

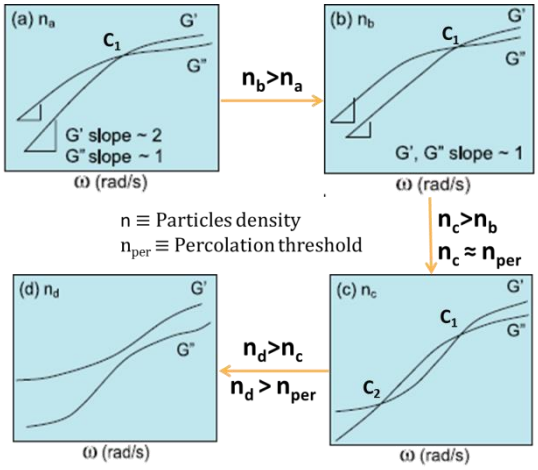

Figure 2.33. Schematic representation of the rheological response to the increase in the number of particles per unit volume.

Pure polymeric matrices and polymeric matrices with a very low level of agglomerated clay particles give the typical relaxation behavior where, $G' \sim \omega^2$ and $G'' \sim \omega$, in the terminal region (Figure 2.33.a). Then, when the number of particles per unit volume increases a change of the spectrum in the terminal region occurs as $G', G'' \sim \omega$ (Figure 2.33.b). An increase in the particles density can occur either by increasing the amount of particles or by increasing the exfoliation degree. As the particles density increases, G' and G'' show a more solid-like behavior especially at low frequencies as, $G' > G''$ (Figure 2.33.c). At this point, nanocomposites show two cross-over frequencies and the particles density is close to the percolation threshold. Further increase in the particles density can produce a response where $G' > G''$ in all the frequency range (Figure 2.33.d). This solid-like response indicates a percolated organization of the platelets in a network-like structure. The percolation threshold, that is, the clay volume fraction from which a percolated structure is obtained in a determined system can be quantified by using Equation 2.52,

$$G' = C\left(\Phi_p - \Phi_{per}\right)^n \tag{2.52}$$

where *C* is a constant, n is a power law exponent, Φ_p is the clay volume fraction, Φ_{per} is the percolation threshold volume fraction and G' is the value of the storage modulus at low frequencies. Φ_{per} is obtained by fitting to a linear regression the curve $\log G'$ (where G' is measured at low frequencies) versus $\log\left(\Phi - \Phi_{per}\right)$. This is done for different values of Φ_{per}. The value of Φ_{per} for which the best fit is obtained is the percolation threshold of the composite.

2.3.3 High density polyethylene

High density polyethylene (HDPE) is another polymeric matrix selected to perform the experimental work of this thesis. This polymer has been selected for several reasons. On the one hand, to analyze how the rheological properties affect the cellular structure (main objective of this thesis) in a polymeric matrix different to the other materials proposed (PP and PP composites). Another reason of selecting this polymer is because of its great properties. HDPE is tough, stiff, chemical and abrasion resistant and present a low absorption and permeability to water and moisture. Moreover, HDPE can withstand higher temperatures than other polymers such as LDPE or EVA, which is an essential requirement for some applications [125,126]. In addition, this polymer can be easily crosslinked by using peroxides, which allows strongly modifying its rheological properties.

2.3.3.1 Crosslinked high density polyethylene

As PP, HDPE is also a linear polymer and hence this polymer does not show strain hardening and its melt strength is very low, which hinders the use of this polymer for foaming applications. From the foaming applications point of view, another disadvantage that HDPE shows is its high crystallinity which difficults the gas dissolution in the polymeric matrix (see section 2.4.2.1.2). The solution proposed in this thesis to increase the strain hardening has been to crosslink the polymeric matrix (see section 2.2.5.4.4) by a thermochemical method (using an organic peroxide). Moreover, it is well known that chemical crosslinking has a direct effect on the crystallization process; in general, an increase in the crosslinking degree is related to a decrease in the polymer crystallinity [127,128,129]. Crosslinking is a process in which carbon atoms, of either the same or different polyethylene chains, are joined together to form a three-dimensional network structure. The crosslinking process essentially forms bonds between the polymer chains, which can be directly between carbon to carbon or a chemical bridge linking two or more carbon atoms [130]. Different ways can be followed to crosslink HDPE. One of the most employed methods consists on using organic peroxides to produce a thermochemical crosslinking. Organic peroxides are widely used because of their controlled decomposition rate, minimal side products and economical process [131]. Among others, HDPE has been crosslinked with dicumyl peroxide [131,132], benzoyl peroxides [133], t-butyl perbenzoate [131,133], etc. The thermochemical crosslink of the polymeric matrix is randomly produced in the molten state where the polymer has only amorphous structure. As the crosslink junctions are formed in the molten state, a modification in the reorganization and chain folding during the crystallization process occurs. The crosslinks act as defect centers, hindering both, the crystal growth as well as the formation of crystals. As a result imperfect crystallite with smaller sizes and also less in content are formed, that is, a reduction in the polymer crystallinity is obtained [127,128,129]. Electron beam irradiation has also been used to crosslink HDPE [130,134,135]. One of the most important differences between this method and the thermochemical crosslinking method is that the crosslink junctions are now formed in a solid state and hence, no changes in the crystalline structure of the irradiated samples occur [134].

2.4 Polymeric cellular materials

2.4.1 General concepts

A **polymeric cellular material** consists of a two-phase structure, in which a gaseous phase has been dispersed in a solid polymeric matrix [136]. The most usual way to produce this type of materials is based on the use of blowing agents. Blowing agents include gases that expand when pressure is released, liquids that develop cells when they change to gases, and chemical agents that decompose or react under the influence of heat/catalyst to form a gas [137]. Therefore, the most used route to produce polymeric cellular material consists on generating a gas that expands within a polymeric matrix and forms a structure of cells, resulting in a porous body. These types of cellular materials are also known as **foamed materials** or **foams**.

The fact of introducing a gaseous phase allows reducing the material weight and hence the amount of raw material required to produce the cellular material, which it is translated into a cost reduction. Moreover, the fact of introducing a gaseous phase leads to a class of materials with different properties, which allows broadening the range of applications of the common solid materials. Due to the combination of both, cost reduction and widening of the solid properties, these materials are highly demanded by today's society for applications such as: packaging, sports and leisure, toys, thermal insulation, automotive, aeronautics, military, aircraft, buoyancy, cushioning, renewable energy, construction, biotechnology, etc. [138,139].

Different criteria have been followed to classify polymeric cellular materials. The first one takes into account an important property of cellular materials, the **density** [136,137,140]. In cellular materials it is more common to work with the **relative density** than with the foam density. The *relative density* (ρ_R) is defined as the ratio between the *density of the cellular material* (ρ_{cm}) and that of the *solid polymeric matrix* (ρ_s) as Equation 2.53 indicates.

$$\rho_R = \frac{\rho_{cm}}{\rho_s} \tag{2.53}$$

Another parameter normally employed when dealing with cellular materials is the ***expansion ratio*** (*ER*), which is in turn the inverse of the relative density (Equation 2.54).

$$ER = \frac{1}{\rho_R} = \frac{\rho_s}{\rho_{cm}} \tag{2.54}$$

According to its relative density, there are three types of cellular materials: **low density** ($\rho_R < 0.2$), **medium density** ($0.2 \leq \rho_R < 0.7$) and **high density** cellular materials ($\rho_R \geq 0.7$).

Taking into account the cellular structure two different classifications can be done. The first one considers the disposition of the polymeric matrix in the cellular structure and the second one considers the size of the cells. If the polymeric matrix is only contained in the cell edges the foam is said to be **open cell** (Figure 2.34.a). On the other hand, if the polymeric matrix is contained in both, the walls and the edges the foam is said to be **closed cell** (Figure 2.34.b). Finally, there are foams whose cells are partially opened and partially closed. These cellular materials are said to be **partially open cell** (Figure 2.34.c).

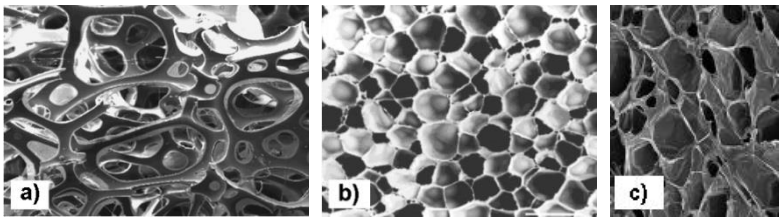

Figure 2.34. a) Open-cell cellular structure. b) Closed-cell cellular structure. c) Partially open-cell cellular structure.

When the **cell size** is the parameter considered to perform the classification, four different types of materials can be considered: **nanocellular foams** are those with a cell size lower than 0.2 μm, **ultramicrocellular foams** are those with a cell size in the range 0.2-1 μm, **microcellular foams** are those with a cell size in the range of 1-10 μm and finally, **macrocellular foams** are those with a cell size higher than 10 μm [141]. Figure 2.35 shows an example of nanocellular (Figure 2.35.a) and microcellular foams (Figure 2.35.b).

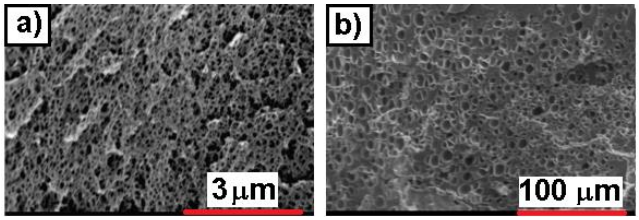

Figure 2.35. Classification of the cellular materials according to their cell size. a) Nanocellular foams. b) Microcellular foams.

Finally, polymeric cellular materials can also be classified as flexible or rigid. **Flexible foams** are those involving an elastomeric or soft plastic such as: low-density polyethylene (LDPE), ethylene vinyl acetate (EVA), natural rubber, flexible polyurethane (PU), etc. **Rigid foams** are those involving rigid matrices such as: polystyrene (PS), polypropylene (PP), polycarbonate (PC), Poly(methyl methacrylate) (PMMA), etc. The type of polymer matrix, thermoplastic or thermoset can also form the basis for a classification scheme [142].

2.4.2 Polyolefin based cellular materials

All the polymeric matrices that have been employed in this work (PPs and HDPE) belong to the group of **polyolefins**. For this reason, a detailed analysis of polyolefin based cellular materials is performed in this section The cellular materials produced with this kind of polymers keep some of the properties of polyolefins such as toughness, flexibility and resistance to chemicals and abrasion [140,143].

2.4.2.1 Blowing agents

The substance that produces the cellular structure in a polymer mass is defined as **blowing agent**, that is, the gaseous phase to produce the foamed material derives from the blowing agent used in the manufacturing process. The blowing agent plays an important role not only in the manufacturing of the polymeric foam but also in its performance. For instance, in thermal insulation applications closed-cell foams are required and hence, the gas derived from the blowing agent is retained in the cellular structure, to reduce the thermal conductivity, at

least until it diffuses out, which in some cases can be decades. Therefore, in this application the blowing agent plays an important role in the overall performance of the cellular material. In other applications, like packaging and cushioning, open-cell foams are required. In the cellular materials with open cells, the gas escapes from the foam almost immediately and hence, the impact of the blowing agent on the foam performance is not so significant [137].

In the case of polyolefins, the blowing agent modifies the melt viscosity and the thermal history of the polymer and thus, the rheology of the polymer during the formation of the foam [137]. Unfortunately, the rheology of the blend blowing agent-polymer cannot be measured in standard rheology equipment because a closed pressurizer rheometer is necessary to prevent degassing and material expansion. Due to this, most of the studies (including this thesis) only analyze the rheological behavior of the polymer, without the blowing agent. Despite the technical difficulties, different systems have been created to measure the viscosity of polymers containing blowing agents [144]. They can be in-line systems (mounted directly on the foaming device) [145,146], on-line systems (the sample is deviated from the process flow line and transferred to the measuring apparatus) [147,148] and off-line systems (the rheometer has been modified to accommodate the pressure requirements) [149,150]. Although the literature is scarce, the key element of the viscosity response is that the dissolved gas induces plasticization of the polymer which can be translated in a reduction of the shear viscosity, which decreases as the blowing agent content increases.

There are two general types of blowing agents: chemical blowing agents and physical blowing agents. In general, chemical blowing agents are used to produce high-density foams and physical blowing agents are the primary source for low-density foams [151].

2.4.2.1.1 Chemical blowing agents

It is well known that some chemicals release gases via chemical reactions or thermal decomposition. When this effect takes place within the molten polymeric matrix, the decomposing chemical acts as a blowing agent. These kinds of substances are known as **chemical blowing agents** (CBAs) [137,152]. Therefore, the decomposition of CBAs depends on the processing thermal profile. However, it also depends on the residence time under a certain temperature [152]. In addition, the expansion ratio achieved will depend on the amount of blowing agent used to produce the foamed material.

CBAs are widely used due to the advantages that these substances show. First, their use requires little modification of the thermoplastics processing lines; second, the operating window of these materials can be very broad and finally, several CBAs produce solid decompositions products (residues) after the reaction process. These solid products act as nucleating agents for the foaming process (see section 2.4.2.2.1) and therefore, they are also known as self-nucleating particles for the cells [137]. Nevertheless, as chemical reactions and/or heat are involved, the dispersion of the blowing agent throughout the melt and the heat sensitivity of the polymer impose serious concerns that make more difficult the processing of polymeric foams [152]. Other disadvantages of using CBAs include contamination due to the unreacted blowing agent or contamination due to the solid residue from the reacted CBA.

There are two general classes of chemical blowing agents:

- **Exothermic blowing agents**: These blowing agents generate heat during their decomposition. As a consequence, once the decomposition starts, it is difficult to stop it before it reaches full decomposition, because the heat released also contributes to decompose the blowing agent [137]. **Azodicarbonamide** (ADC) is the most widely used exothermic chemical blowing agent and it has been also used in this thesis. Its decomposition temperature is about 200 ºC. The blowing gas composition is primarily N_2 and also CO, CO_2 and NH_3 are produced. About 65 % of the initial dosage remains as residue consisting of cyanuric acid, urazole, cyamelide and biuret [151]. In its most basic form ADC is a yellow fine powder with a range of particles diameters between 3 and 30 microns. Other exothermic CBAs are: 4,4'-oxybis (benzene sulfonylhydrazide) (OBSH), 5-phenyl tetrazole (5-PT), etc.
- **Endothermic blowing agents**: These blowing agents require heat to react, that is, they absorb heat during their decomposition. They decompose over wider temperature ranges than exothermic CBAs. Most commercially endothermic CBA generate $C0_2$ as the main gas. The components of endothermic CBA are essentially food additives and therefore they are generally considered as safe blowing agents as regards toxicity considerations [137]. Some examples or endothermic CBAs are: bicarbonates/carbonates, polycarboxylic acid derivates, tetrazoles, etc.

As the physical blowing agents, which are dissolved in the polymer to produce the foamed material (see section 2.4.2.1.2), the gas released by a chemical blowing agent can also be dissolved in the polymer if an appropriate pressure is applied to the blend polymer/blowing agent [153].

2.4.2.1.2 Physical blowing agents

Physical blowing agents (PBAs) provide the gas required for the expansion of the polymeric matrix by undergoing a change in its physical state. They are classified as inert gases or as volatile liquids [137,151].

- **Inert gases**: The most widely inert gases employed are N_2 and CO_2. He and Ar are other atmospheric gases that are sometimes used. To produce the foamed materials the gases should be first dissolved in the polymer. Once again, the expansion ratio (or foam density) depends on the amount of gas that is dissolved in the polymer. Gases such as N_2 and CO_2 have limited solubility in most polyolefins. The **crystallinity** of the polymeric matrix highly influences the solubility and diffusivity of the blowing agent into the polymeric matrix. In semi-crystalline polymers the gas sorption and diffusion takes place mainly in the amorphous region and therefore, when the polymer crystallinity increases a severe decrease in the solubility and diffusivity is obtained [154]. However, N_2 and CO_2 are widely used as blowing agents because they are cheap, abundant and environmentally acceptable and because they have a relative moderate critical temperature and critical pressure. For instance, CO_2, which is normally used to produce low density polyolefin based foams, is in a supercritical state, when the temperature exceeds 31 ºC and the pressure exceeds 7.38 MPa. Once the polymer is dissolved in the polymeric matrix, a thermodynamic instability

should be created to cause cell nucleation and growth, that is, to produce the cellular material [137].

- **Volatile liquids**: They evaporate at appropriate conditions to produce the gas required for foaming. There are several classes of volatile liquids. During years, chlorofluorocarbons (CFCs) were the primary physical blowing agents employed with polyolefins. The foams produced showed closed cells, low density, good mechanical properties and extremely good thermal insulation performance. Unfortunately, these gases were found to react with upper atmospheric ozone depleting the Earth's ultraviolet protection layer. As a result CFCs are no longer used (Montreal Protocol). An alternative to CFCs was hydrochlorofluorocarbons (HCFCs). However, in the same way as CFCs they are being progressively banned. Nowadays, hydrocarbons (HC) dominate the physical blowing agent category for polyolefins. Butanes, pentanes and propanes are the HC preferred for the production of commercial low-density polyolefin foams [137,151].

2.4.2.2 Principles of foam formation

Most polyolefin foams are produced by the expansion process which is based on the expansion of a gaseous phase dispersed throughout the polymer melt. As was previously seen (section 2.4.2.1) the gaseous phase is generated through the blowing agent. Regardless of the type of blowing agent the expansion process comprises several major steps: nucleation, cell growth, cell degeneration and stabilization (Figure 2.36) [155].

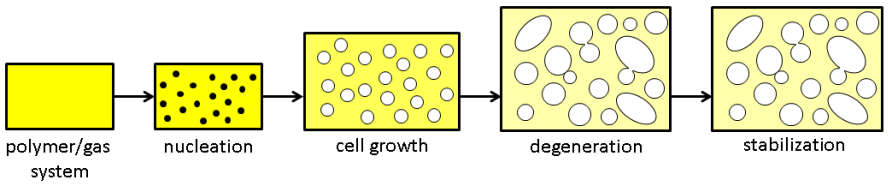

Figure 2.36. Principles of foam formation.

2.4.2.2.1 Nucleation

In general, **cell nucleation** is used to denote any process that leads to the formation of a bubble in the polymeric matrix. Nucleation starts to occur at an initiation site within a polymer melt that has been supersaturated with a blowing agent. To understand the nucleation mechanism, it should be distinguished between a situation in which the gas (generated either a CBA or a PBA) is completely dissolved in the polymer forming a homogeneous solution and a situation in which the CBA has been incorporated into the polymeric matrix but it is still in form of solid particles, because the mixture was performed at a temperature lower than decomposition temperature of the blowing agent. While in the first situation, the system becomes supersaturated when the gas solubility is reduced due to a pressure drop or a temperature increase, in the second situation the supersaturated state is achieved by heating the polymer containing the CBA [156,157]. In general there are two different kinds of nucleation mechanisms: homogeneous nucleation and heterogeneous nucleation.

The classical **homogeneous nucleation** involves nucleation in the liquid bulk of a uniform polymer-gas solution produced by a thermodynamic instability. According to the classical nucleation theory, the *homogeneous nucleation rate* (N_{HOM}) is expressed as:

$$N_{HOM} = C_0 f_0 exp\left(\frac{-\Delta G'_{HOM}}{kT}\right) \quad (2.55)$$

where C_0 is the *concentration* of gas molecules, f_0 is the *frequency factor* of the gas molecules, k is the *Boltzman's constant*, T is the *temperature* and $\Delta G'_{HOM}$ is the *activation energy*, that is, the energy required to form the nuclei, which is in turn calculated as:

$$\Delta G'_{HOM} = \frac{14\pi\sigma_{P-B}^3}{3\Delta P^2} \quad (2.56)$$

where $\sigma_{P\text{-}B}$ is the *surface free energy* of the polymer-bubble interface and ΔP is the *pressure drop*. From these equations it can be concluded that both, temperature and pressure drop highly influence the homogeneous cell nucleation rate [158,159].

On the other hand, **heterogeneous nucleation** takes place in the interface between the polymer and a new phase (particles, impurities, solid decompositions products of the CBAs, etc.). In the interface polymer-solid particle, the energy required to form the nuclei is lower and therefore solid, insoluble particles act as preferential nucleation sites [158]. These particles are often added to the polymeric matrix to provide new, heterogeneous, nucleation sites and to control the cellular density and the cell size distribution in the final foam. They are known as nucleating agents or nucleants [159]. The *heterogeneous nucleation rate* (N_{HET}) is defined as follows [98]:

$$N_{HET} = C_1 f_1 exp\left(\frac{-\Delta G'_{HET}}{kT}\right) \quad (2.57)$$

where C_1 is the *concentration* of nucleation sites, f_1 is the *frequency factor* for gas molecules joining the nucleus and $\Delta G'_{HET}$ is the *activation energy* in an heterogeneous system, that is, the free energy barrier to initiate heterogeneous cell nucleation, which is, in turn, given by:

$$\Delta G'_{HET} = \Delta G'_{HOM} S(\theta) \quad (2.58)$$

where $S(\theta)$ is a function that depends on the contact angle at the polymer/nucleating agent interface.

2.4.2.2.2 Cell growth

In order to understand and describe the **cell growth**, a cell surrounded by a liquid of molten material is considered. When the cell grows, the concentration of gas absorbed by the polymeric matrix is reduced as the gas diffuses from the gas-polymer matrix into the nucleated cell causing its growth. Cell growth continues until it stops due to the stabilization of the cellular structure by cooling (see section 2.4.2.2.4) [140,160].

One of the simplest models that allow analyzing the cell growth rate considers a single cell that grows in a Newtonian fluid with a constant viscosity [160,161]. In this model the change in the bubble radius with time (dR/dt), that is, the *cell growth rate*, is given by the following equation (Equation 2.59):

$$\frac{dR}{dt} = \frac{R}{4\eta}\left(P_i - P_o - \frac{2\gamma_{P-B}}{R}\right) \quad (2.59)$$

where R is the *bubble radius*, η is the polymeric *matrix viscosity*, P_i is the gas *pressure inside the bubble*, P_o is the *external pressure* and $\Upsilon_{P\text{-}B}$ is the *surface tension* in the polymer-bubble interface. The value of the viscosity is directly related to the bubble growth process. A high viscosity can slow down the speed of bubble growth while a low viscosity yields to a rapid and almost explosive initial bubble growth. However, constant viscosity cannot meet the requirements of controllable foaming. It is desirable that the viscosity changes during the bubble growth. The initial growth of the bubbles requires a low viscosity. Subsequently, as the polymer is stretched during the cell growth, a high extensional viscosity is required, that is, a polymeric matrix showing **strain hardening** is advantageous, so that the cell walls may withstand the deformation to which they are subjected during the last stages of bubble growth, without breaking (see section 2.5.2) [161]. If this change in viscosity does not occurs or on the other hand, it is produced but is not enough to withstand the deformation, cell ruptures may occur (see section 2.4.2.2.3) and hence, a degeneration of the cellular structure is produced [144].

2.4.2.2.3 Degeneration of the cellular structure

As it was previously mentioned, in the last stages of bubble growth, that is, when high expansions are achieved and hence, the cells are separated by thin polymer membranes, the cellular structure may degenerate if the foamed material is not stable enough. Cell degeneration can occur by the combination of three main mechanisms: coalescence, coarsening and drainage.

- **Cell coalescence**. It is the mechanism by which two growing continuous cells in a polymer melt are combined because of cell wall rupture (Figure 2.37). This usually occurs if the stretched thin cell wall separating the two cells is not strong enough to sustain the extension developed during the cell growth [156]. Moreover, cell coalescence is thermodynamically favored because the total surface area of cells is reduced by coalescence [144]. Cell coalescence increases in a significant way the cell size. Moreover, if the coalescence process is stopped in an intermediate state (by cooling the foamed material), cell opening may also occur (see Figure 2.37). Not only strain hardening reduces cell coalescence, it has been proved that maintaining a reasonably low and uniform melt temperature during processing also helps to suppress cell coalescence, as the melt strength increases by decreasing the temperature [152].

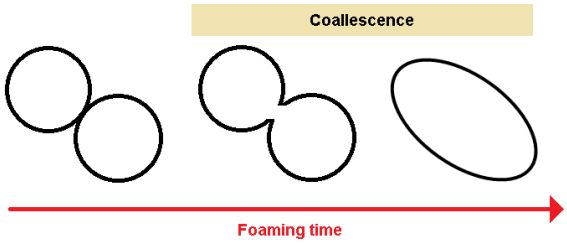

Figure 2.37. Schematic representation of the coalescence phenomenon.

- **Coarsening.** It consists on gas diffusion from the smallest cells to the largest ones (Figure 2.38). As the pressure in a small cell is higher than that in a large cell, this difference in pressure induces gas diffusion from the small bubbles to the large ones. As a result, the size of the largest cells increases and the smallest bubbles tend to get even smaller to finally disappear [140].

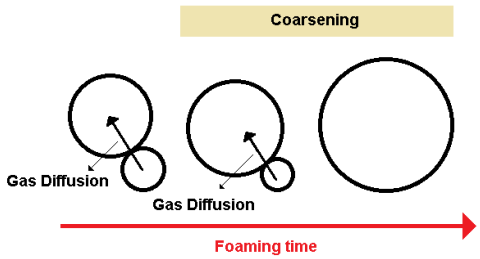

Figure 2.38. Schematic representation of the coarsening phenomenon.

- **Drainage.** It takes place during foaming as the molten polymer drains, out of equilibrium, in the fine walls separating the cells. It is caused by the action of capillary forces, which produce transport of the liquid material from the cell walls towards the edges (Figure 2.39). As a consequence the cell wall thickness is reduced and the coarsening and coalescence mechanisms are favored [158,160]. Moreover, it should be considered that this phenomenon is more pronounced when the viscosity is very low.

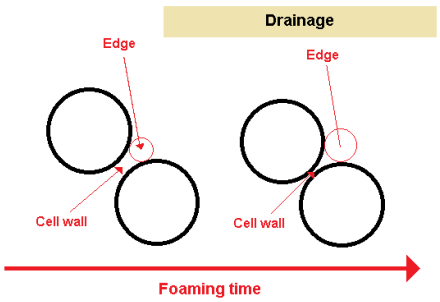

Figure 2.39. Schematic representation of the drainage phenomenon.

2.4.2.2.4 Stabilization of the cellular structure

It should be noted that the gas that has diffused into the nucleated cells eventually tends to diffuse out, to the atmosphere, because a complete separation of the two phases is thermodynamically more favorable. As the gas escapes through the thin walls, the amount of gas available for the growth of the cells decreases. As a result, if the cells do not freeze, they tend to collapse causing foam contraction. The stabilization in thermoplastic materials is performed by a rapid cooling of the sample at a temperature below the polymeric matrix crystallization temperature, to crystallize the polymer [144]. The difference between the melt temperature and the crystallization temperature ($\Delta T=Tm-Tc$) is a key parameter to analyze the stabilization of the cellular structure as the smaller this difference is, the quicker the stabilization of the cellular structure occurs, that is, the cellular structure has less time to degenerate during the cooling process due to the mechanisms previously mentioned.

2.4.2.3 Production Techniques

In this section some of the processes normally employed to produce polyolefin based cellular materials are briefly described. Moreover, a special emphasis is placed on analyzing and comparing the time scale of each foaming process.

2.4.2.3.1 Foaming at atmospheric pressure

In this process the expansion occurs at atmospheric pressure and both, physical blowing agents and chemical blowing agents can be used. Moreover, to produce the expansion, the material can be placed in a mold and therefore the expansion is restricted by the mold or a free expansion can occur when the mold is not used. Medium and high density foams are normally obtained with this technique (when the polymer is not crosslinked). In this process the foam growth rate is very slow as the time it takes the foam to reach a complete expansion is really high, in comparison with other foaming processes (the time scale is around several minutes).

Between all the foaming processes carried out at atmospheric pressure, one of the most employed processes is that known as **solid state foaming** (Figure 2.40). This method is a batch process and it was developed at the MIT in the 80s [162]. First, the polymeric sample is saturated with an inert gas in a pressure vessel. Supercritical conditions can be used to increase gas sorption, but it is not completely necessary. In this method, during saturation the sample is always in a solid state. Then, in a second step the saturated samples are removed from the pressure vessel and foamed in a temperature controlled bath at atmospheric pressure. A thermodynamic instability is created by releasing the pressure and heating the sample causing cell nucleation and growth. Finally, the foam is stabilized by cooling [163,164].

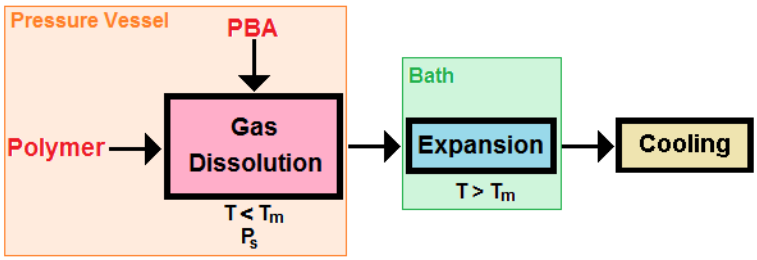

Figure 2.40. Scheme of the solid state foaming process.

Solid state foaming is one of the foaming processes employed in this thesis to produce the cellular materials. However, in this work prior to the gas dissolution process another step was performed, as the polymeric matrix was previously crosslinked using a chemical crosslinking agent. The specific foaming parameters employed in this thesis to produce the cellular materials, as well as, the details about the crosslinking step can be found in chapters 3 and 6.

As it was previously indicated, CBAs can also be used to produce polyolefin based foamed materials at atmospheric pressure. One of the best known techniques based on foaming at atmospheric pressure is **rotational molding** (Figure 2.41).

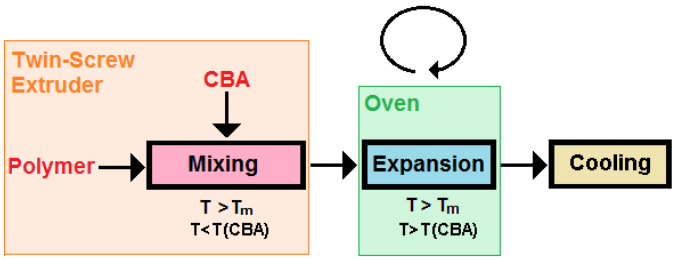

Figure 2.41. Scheme of the rotational molding foaming process.

In a first step (mixing phase), the CBA is incorporated into the polymeric matrix using a twin-screw extruder. The temperature should be higher than the polymer melting temperature (T_m) however, it is important not to subject the blend to temperatures that can activate the decomposition of the CBA. Once the blend is obtained, the material is introduced in a closed mold which is subjected to a biaxial rotation in an oven at a temperature higher than the decomposition temperature of the blowing agent. The rotation is performed to obtain a homogenous heat distribution along the whole material. When the entire polymeric matrix is melted and the blowing agent has completely released the gas, that is, when the material has completely foamed, the mold is moved to a different area for cooling [165].

Other of the foaming processes employed in this thesis is based in the rotational molding process. The main difference is that in our experiments the mold does not rotate. The mold can be maintained in a fixed position because the cellular materials produced are small in size. Furthermore, in this research, the internal structures of the polymeric foams during the expansion process inside the metallic mold, has been observed with an excellent contrast using, for the first time, **time-resolved neutron radiography**. More details of both, the process employed in this thesis and the in-situ visualization/characterization technique, which allows analyzing and understanding the mechanisms that take place during the foaming process (see section 2.4.2.2), can be found in chapters 3 and 4.

2.4.2.3.2 Extrusion process

Extrusion process is a simple process and one of the most economical processes. It is very useful to produce low-density foams. Although, in this process PBAs are normally used, CBAs can also be employed. A preferred process is a tandem extrusion system, consisting of two extruders (a primary and a secondary extruder). Figure 2.42 shows a scheme which contains all the steps that should be followed to produce non-crosslinked cellular materials by extrusion [137,140,144].

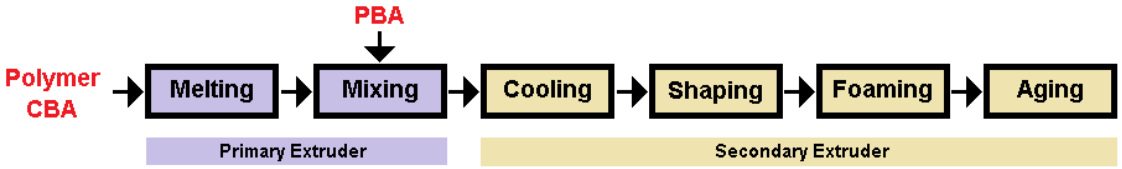

Figure 2.42. Scheme of extrusion process.

In the first extruder (primary extruder) the unit processes involved are the following:

1. *Melting*. In a first step the polymeric matrix is melted. If a CBA is used, it should be added at the same time as the polymeric matrix, to allow its decomposition.
2. *Mixing*. If a PBA is used, it should be added at this point. The goals of this mixing phase are two: to facilitate the gas dissolution in the polymeric matrix and to disperse the blowing agent homogeneously. Once the blowing agent is dissolved and dispersed, the melt viscosity is reduced, which allows reducing the process temperature.

From this point, the remaining steps are performed in the second extruder (secondary extruder):

3. *Cooling*. The melt is cooled to a temperature range that allows producing good-quality foams. If the expansion is produced at an elevated temperature, it may not be possible to stabilize the cellular structure in the last production steps.
4. *Shaping*. Once the sample is cooled enough, it is conducted through a die orifice with the required shape. In this point a pressure drop occurs (as the pressure decreases towards the die exit) and as a consequence cell nucleation is produced. However, the die is designed to prevent pre-foaming.
5. *Foaming*. On the exit from the die, the polymer expands as the growth of the cells nucleated previously occurs. It should be noted that, in this process it is said that the expansion is immediate as it is produced almost instantaneously, being the time scale of the order of a few seconds.
6. *Aging*. The cellular structure is stabilized by cooling the foamed material to a temperature below the polymer crystallization point.

2.4.2.3.3 Compression molding process

In **compression molding process** CBAs are always used. The name of this process is attributed to the fact that the shape of the foams is established by using a mold located in a hot-plate press.

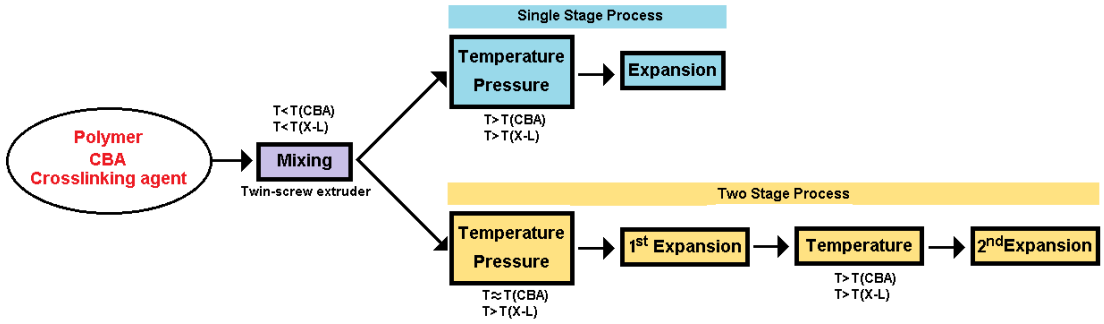

Figure 2.43. Scheme of compression molding process.

The process can be classified into two subgroups: single stage process and two stage process (Figure 2.43). In all cases a crosslinking agent is used to stabilize the growth of the cells during the material expansion [137,140].

- **Single stage process**. In a first step, the polymeric matrix is mixed with the CBA and with the crosslinking agent (X-L agent). The mixing is performed in a twin-screw extruder. The temperature should be higher than T_m but, lower than the decomposition temperatures of

both, the blowing agent and the crosslinking agent, to avoid premature crosslinking and foaming. A defined weight of compound is placed in a mold and the material is subjected to both, pressure (P_0) and temperature in a hot plate-press. In this step, the temperature should be higher than those of the CBA and the X-L agent. After a defined time (when curing is complete and the CBA is fully decomposed) the mold is opened and the expansion occurs. In this process high opening speeds of the mold (> $6x10^3$ mm/min) are required to accommodate the rapid expansion of the foam. Despite of being a rapid expansion, the foam growth rate in this process is slightly slower than the foam growth rate in the extrusion process (time scale for these foams is of the order of a few seconds). The maximum expansion ratio achieved with this process is around 10. To obtain higher expansion ratios, a two stage process should be employed.

- **Two stage process**. The first step (mixing) is common in the two processes, as Figure 2.43 indicates. Then, the material is placed in a mold and it is subjected to both, pressure and temperature. In this case the temperature should be higher than the decomposition temperature of the X-L agent and similar to the decomposition temperature of the CBA. After a certain time (when curing is complete and the blowing agent is partially decomposed), the mold is opened and the material expands between 3 and 8 times. This pre-foamed material is then placed in a mold and heated above the decomposition temperature of the CBA. In this step, the complete expansion of the material is produced. The second expansion is produced at atmospheric pressure (so that this process can be also classified as an ambient pressure foaming process) and hence, the foam growth rate is slower than in the single stage process. With this process it is possible to achieve an expansion ratio of 40. In this process two time scales should be considered. The first expansion has a short time scale of a few seconds and the second expansion has a time scale of several minutes.

However, compression molding presents two important disadvantages. On the one hand, in this process it is necessary to crosslink the polymeric matrix and therefore, the foamed materials are not recyclable (at least by conventional methods). On the other hand, it is difficult to control the final foam density, at least in the single stage process. Taking these problems into account, CellMat laboratory developed an alternative process to the conventional one known as **improved compression molding** (ICM) (Figure 2.44). The applied pressure during the foam stabilization (P_m) is the main difference of this process in comparison with the conventional single stage compression molding process. This difference is translated into several advantages [138]:

1. The density of the foamed materials is controlled by using self-expandable molds. It is possible to produce foamed materials with the same density, independently of the formulations used. These molds can apply and retain the pressure during the gas dissolution process, during the expansion process and during the foam stabilization.
2. This process allows controlling the cellular structure of a material, independently of its density, by controlling the formulation employed, the pressure, the temperature and the foaming time.
3. With this technique it is possible to achieve expansion ratios up to 10 without crosslink the polymeric matrix in different kinds of thermoplastics: pure matrices, composites, nanocomposites, etc.

4. The shape of the molds employed can be modified and hence, the geometry of the foam can be adapted to different requirements.

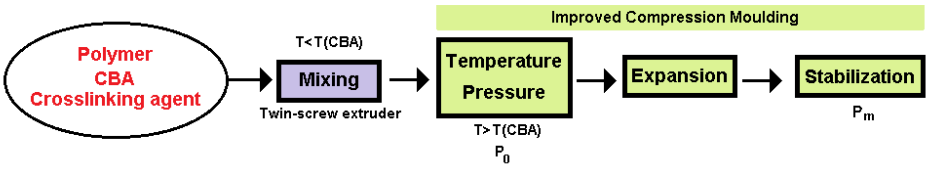

Figure 2.44. Scheme of the improved compression molding (ICM) process.

ICM is another process used in this thesis to produce the cellular materials. Different polymeric matrices have been foamed with this technique: high melt strength PP (HMS PP), linear PP, HMS PP/linear PP blends, PP/clay nanocomposites (see chapters 4 and 5). Details of the description of the ICM process can be found in chapter 3. The time scale of this process is similar to that of the single stage compression molding process.

2.4.2.3.4 Pressure quench method

In the **pressure quench method**, a PBA is required to produce the polymer expansion. It has two steps (Figure 2.45). First, a thermoplastic sample is placed in a pressure vessel and it is saturated with an inert gas (normally CO_2) under supercritical conditions. Gas saturation is performed at a temperature slightly above the polymer melting point, in order to increase gas sorption. Upon a prolonged exposure of the polymer to supercritical $C0_2$ at a high saturation pressure (P_s), a polymer/gas solution is formed. In a second step, the temperature is reduced slightly below the melting temperature, in order to have a higher polymer viscosity and hence, promote the gas retention by the polymer. Then, the pressure is rapidly released to atmospheric pressure (P_a). This rapid quench in pressure decreases the CO_2 solubility in the polymer and causes cell nucleation and growth (free expansion). The rapid depressurization of the vessel also causes the temperature in the vessel to drop which helps to stabilize the cellular structure [138,166,167]. As with the extrusion process, the foam growth rate is really high and it can be said that the expansion is almost instantaneous, being the time scale of growing of the order of a few seconds.

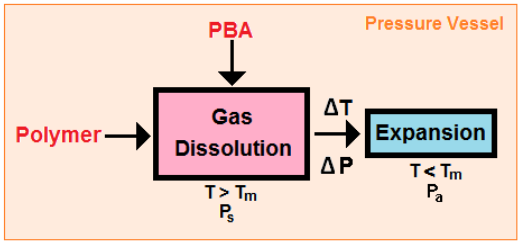

Figure 2.45. Scheme of the pressure quench method.

2.4.2.3.5 Injection molding process

Together with extrusion foaming, the **injection molding process** is another of the most popular foaming processes. This process is limited to the production of high density foams. The main advantage of this process is that allows producing cellular materials with complex forms with a high dimensional accuracy. The most habitual processes to produced polyolefin based foamed

materials by injection molding are two: low-pressure injection molding and high-pressure injection molding [138,168].

- **Low-pressure injection molding.** The first stages (melting and mixing of the polymer with a blowing agent, either CBA or PBA) are similar to those of the extrusion process (see section 2.4.2.3.2). Although, in this case, these steps take place in an extruder located in the injection unit. Then, the material (polymer + bowing agent) is injected in a mold. In this process the amount of material injected is lower than that used to produce a solid material. The pressure drop generated in the mold gate causes the cell nucleation and growth, until the material fills the mold. Due to the low temperatures of the mold, the material is cooled and ejected from the mold. As with the extrusion process and the pressure quench method the expansion is almost instantaneous due to the high pressure drop at the mold gate.
- **High-pressure injection molding.** This process differs from the previous one in the way in which the expansion occurs. In this system the mold is completely filled and the expansion is produced by displacing a part of the mold. Therefore, in this second process the foam (or cell) growth rate is slower than in the previous one.

Both processes are summarized in the following scheme (Figure 2.46):

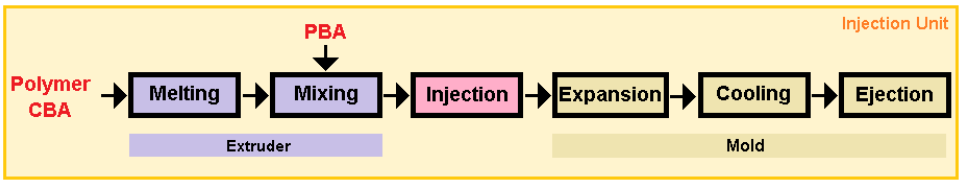

Figure 2.46. Scheme of the injection molding process.

Along section 2.4.2.3, different techniques to produce polyolefin based cellular materials have been described. As it was already shown, the foam growth rate depends on the production system employed. There are processes in which the expansion is almost instantaneous and there are also processes in which several seconds or minutes are required to obtain the maximum expansion. As it is difficult to provide a quantitative value of the foam growth rate, in Figure 2.47 a qualitative classification of the different system as high-growth rate, medium-growth rate and low-growth rate systems is given.

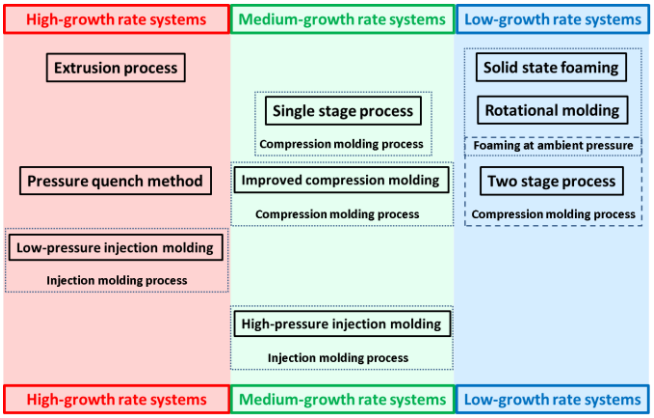

Figure 2.47. Classification of the foaming processes considering the rate at which the foam growths.

2.4.2.4 Cellular structure-mechanical properties relationships

One of the objectives of this thesis is to understand how the extensional rheological behavior of different polymeric matrices affects the cellular structure and consequently, the mechanical properties of cellular materials produced with the **same density**. While the effect of extensional rheology on the cellular structure has not been widely investigated, at least in foamed materials with the same density (see section 2.5.2), the relationships between cellular structure and mechanical properties are well known [136,167,169,170,171,172]. In this section, the influence of different structural parameters on the mechanical properties in compression tests is reviewed, because all the mechanical properties of the foamed materials presented in this thesis have been measured in compression.

First, the mechanical parameters which have been considered and analyzed in this thesis are defined. These parameters are the elastic modulus and the collapse stress. Moreover, in one of the papers (see chapter 4) the absorbed energy per unit volume has also been calculated for the different materials under study. Figure 2.48 shows the typical stress (σ)-strain (ε) curves of polyolefin based cellular materials in a compression test.

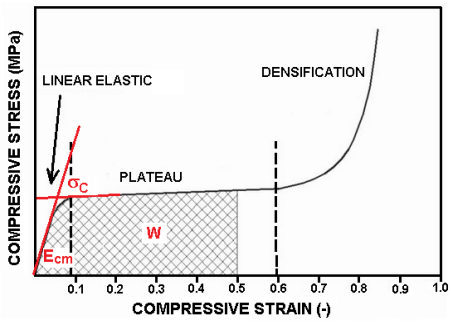

Figure 2.48. Stress-strain curve of polyolefin based cellular materials in a compression test.

Three different regions can be distinguished: the linear elastic region, the plateau region and the densification region [136]. Within the **linear elastic region** the stress grows linearly with the strain and the deformation induced in the foam is almost entirely recoverable, when the strain applied ceases. The ***elastic modulus*** (E_{cm}) is defined as the slope of the stress-strain curve in this linear elastic region. Once the strain reaches a certain level the cellular structure collapses and the foam deforms without opposing any resistance. This region, in which the stress remains constant is called **plateau region**. The limit between the linear elastic region and the plateau region is marked by the ***collapse stress*** (σ_c), which is normally defined as the intersection between a parallel line to the stress-strain response at low strains and a parallel line to the plateau region of the stress-strain curve. Finally, in the **densification region** the stress raises abruptly, because in this region the foam is so deformed that cell walls and the cell edges touch each other increasing the foam density. The area under the stress-strain curve (Equation 2.60) up to a certain deformation (ε_F) is known as ***absorbed energy per unit volume*** (W).

$$W = \int_0^{\varepsilon_F} \sigma(\varepsilon)\, d\varepsilon \tag{2.60}$$

Taking into account that cellular materials are typically used as energy absorbers, in some occasions it is desirable to determine this parameter as the best cellular material is the one that absorbs more energy for a given stress [172,173]. More details about the way in which the mechanical tests have been performed can be found in chapter 3.

Once the mechanical parameters considered in this thesis have been defined, the next step of this section consists on analyzing how these parameters are affected by the structural ones. The mechanical properties of a foamed material are conditioned on the one hand, by the mechanical properties of the solid polymeric matrix and on the other hand, by its density and cellular structure [136]. The **density of the cellular materials** is the main factor that determines their mechanical properties. In general, it is the main factor determining the physical properties of polymeric foams. In fact, any *property of a foamed material* (P_{cm}) can be expressed as a function of the same *property* but measured in the *solid matrix* (P_s) and as a function of the relative density as indicated in Equation 2.61 [136,138].

$$\frac{P_{cm}}{P_s} = C\left(\frac{\rho_{cm}}{\rho_s}\right)^n \tag{2.61}$$

where *C* is a constant with a value near to 1 and the exponent *n* is a parameter that depends on the cellular structure. For most of the cellular materials and properties *n* ranges between 1 and 2. Both parameters can be determined experimentally by fitting the experimental data to this equation. From Equation 2.61 it is possible to conclude that the properties of the foamed materials are reduced when the foam density decreases. Due to the high weight that the foam density has on the mechanical properties of the foamed materials, it is very complicated to analyze the effect of the structural parameters on the mechanical properties of foamed materials with different densities. This is the reason why in this thesis most of the cellular materials were produced with the same relative density.

Although, it is very difficult to generalize about the influence of the cellular structure on the mechanical properties, the following sub-sections aim at summarizing the general concepts that allows understanding the cellular structure/mechanical properties relationship.

2.4.2.4.1 Effect of open cell content

As it was previously indicated in section 2.4.1, foamed materials can be classified as open-cell foams, closed-cell foams and partially open-cell foams. The open cell content of a cellular material can be determined experimentally employing a gas pycnometer (see chapter 3).

When increasing the mechanical performance is the goal, open cell content is not desirable as the mechanical properties (elastic modulus and collapse stress) decrease as the open cell content increases [152]. In closed-cell foams, produced from soft polymers, gas compression is one of the terms that contributes to the mechanical properties. In open-cell foams the gas flows between the cells and its contribution to the mechanical properties is scarce, being the mechanical properties of an open cell-foam lower than those of a closed-cell foam.

2.4.2.4.2 Effect of cell anisotropy

There are some foaming processes in which the expansion is restricted to one direction, which leads to anisotropic cellular structures. These structures are characterized by being composed of cells elongated in one direction (Figure 2.49). As a consequence the mechanical properties become dependent on the compression direction.

If the compression test is performed in the direction of maximum elongation of the cells, the mechanical properties of the material (elastic modulus and collapse stress) will be higher than those of an isotropic material [136,138].

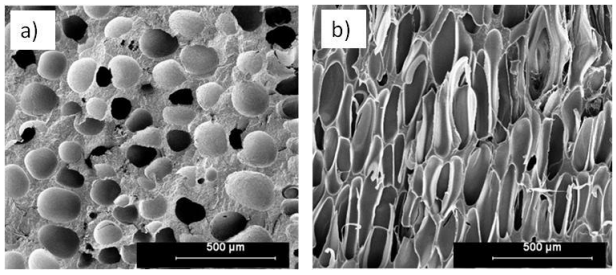

Figure 2.49. Polymeric foams with different cellular structures. a) Isotropic cellular structure. b) Anisotropic cellular structure.

2.4.2.4.3 Effect of cell size distribution

In a polymeric material the cell size distribution is a measurement of the homogeneity of the cellular structure. A narrow cell size distribution indicates that all the cells have a size close to the average value and therefore the cellular structure is very homogeneous. The mechanical properties of a foamed material are greatly affected by this parameter. In general, a heterogeneous cell size distribution leads to lower mechanical properties than a homogeneous cell size distribution, as in the first situation the proportion of solid mass is not distributed homogeneously along the foamed material and hence, the stress to which the material is subjected does not spread in an homogeneous way throughout the foamed material [136,138].

2.4.2.4.4 Effect of cell size

The cell size of a cellular material is the average cell diameter of the cells that compose the foam. To determine this parameter scanning electron microscopy (SEM) micrographs of the different foamed materials were obtained and then, they were analyzed with an image processing tool, developed in CellMat, based on the software Fiji/Image J [174]. The influence of the cell size on the mechanical properties is not clearly established. There are works in which it has been obtained that the mechanical properties increase as the cell size decreases [172,175] and there are works in which it has been found that the mechanical properties do not change with the cell size [172,176,177].

2.4.3 Polypropylene/montmorillonite foamed materials

In the previous section (section 2.4.2) a detailed analysis of polyolefin based cellular materials has been performed, including the blowing agents and production techniques employed to produce these foamed materials. A new type of foamed materials with, in general, better properties than those based on pure polyolefins can be obtained (in the same way as polyolefin based foamed materials) by the foaming of polyolefins containing nanoparticles (polyolefin based nanocomposites). Nanoparticles improve the overall properties of the foamed materials by acting at two levels. On the one hand, by improving the morphology and properties of the solid polymeric matrix, comprising the cell walls (see section 2.3.2.1), and on the other hand, by optimizing the cellular structure [141,178].

Once again the literature search has been focused on polypropylene/montmorillonite nanocomposites as it is the material employed in this thesis. The preparation of nanocomposite foams has been shown to improve the cell morphology, making the cells smaller and more isotropic. A small amount of well-dispersed nanoparticles in the polymer may serve as nucleation sites to facilitate the bubble nucleation process (heterogeneous nucleation, see section 2.4.2.2.1). Therefore, the reduction of the cell size is explained because more bubbles start to nucleate concurrently and hence, the amount of gas available for bubble growth decreases. Moreover, cell nucleation can be improved if an exfoliated structure is achieved with finer and more particles reducing the nucleation energy required for the growth of the gaseous phase [98]. Taki et al. [179] observed, in situ, the batch physical foaming of polypropylene/clay nanocomposites (with CO_2) to understand the effects of nano-sized clays on the initial stage of foaming. They found that the number of nucleated bubbles in the composite was much larger than in the unfilled polymer. They also evaluated the cell growth rate. They found that the bubble growth rate decreases as the clay content increases. The explanation to this behavior, given by the authors, was that the clay content reduced the transfer rate of CO_2 from the polymeric matrix to the bubbles by reducing on the one hand, the diffusivity of CO_2 and by reducing on the other hand, the concentration of CO_2, as when the number of nucleated bubbles is larger the amount of consumption of CO_2 (required for nucleating these bubbles) increases and hence, the amount of CO_2 remaining in the polymeric matrix is reduced. The experimental results obtained by Zheng et al. [180] and Zhai et al. [181] showed that clays have a positive impact on improving the cell morphology, the cell density and the expansion ratio of linear PP foams as the severe cell coalescence that occurs with the linear PP can be suppressed when a small amount of clay particles is added. The reduction in cell coalescence improves the cell morphology because the number of interconnected cells is reduced.

2.4.4 Microcellular foams

Microcellular foams are characterized by having average cell sizes in the order of 1 to 10 μm and cell densities higher than 10^9 cells/cm^3 [144]. The concept of microcellular foams was created in the early eighties, in response to a challenge by food and film packaging companies to reduce the amount of polymer used in their industries. As most of these applications use solid, thin-walled plastics, reducing their densities by traditional foaming processes, which produce large bubbles, was not feasible, because an excessive loss of strength was produced.

Thus was born the idea to create microcellular foams, where it is possible to have, for example, 100 cells across 1 mm thickness, and hence, it is expected to have a reasonable strength for the intended applications [137]. In general, microcellular foams exhibit higher Charpy impact strength and toughness as well as higher fatigue life and thermal stability than conventional cellular materials [144]. Microcellular foams can be produced by both, batch and continuous foaming processes using some of the methods described in section 2.4.2.3 (solid state foaming, extrusion process, pressure quench method and injection molding process). They have been produced by applying a thermodynamic instability to a polymer/gas solution in order to promote a large bubble density in the polymeric matrix. Microcellular polymers processing involves three steps: formation of the polymer/gas solution, nucleation of a large number of bubbles via a thermodynamic instability, and suppression of cell coalescence during the expansion [144]. In general, physical blowing agents are used to produce microcellular materials. The polymer/gas solution is accomplished by dissolving an inert gas into a polymeric matrix under high pressure. When a pressure vessel is used to dissolve the gas, the gas concentration available for foaming can be determined by obtaining the sorption curves as a function of time. For this purpose, the samples are periodically removed from the pressure vessel and weighted. From these curves the sorption diffusivity coefficient (D_s) can be determined as follows [182,183]:

$$\frac{M_s}{M_\infty} = 1 - \frac{8}{\pi^2}\, exp\left(\frac{-D_s \pi^2 t_s}{l^2}\right) \tag{2.62}$$

where M_s is the sorption amount at time t_s, M_∞ is the saturated sorption amount at a large sorption time and l is the specimen thickness. To produce microcellular foams it is required a high concentration of gas in order to produce a large number of cells.

The next step consists on nucleating a large number of cells changing the solubility of the gas in the polymer through a thermodynamic instability, which is accomplished by releasing the pressure and/or heating the sample. It is expected that the more rapidly the pressure drops, the greater the number of cells that will nucleate because a greater thermodynamic instability is induced. This process is very important in microcellular polymers. It governs the cellular morphology of a material and, to a large state, the properties of the material.

The next critical step in microcellular foaming consists on suppressing cell coalescence during cell growth. The fact of having a large number of nucleated cells does not guarantee the obtaining of microcellular foams, because if the cells coalesce during their growth, the initial cell density will be deteriorated. Several means have been proposed to prevent cell coalescence. One of them consists on increasing the melt strength of the polymer via temperature control [144].

2.4.4.1 HDPE based microcellular foams

As it was previously indicated (see section 2.3.3), HDPE is one of the polymers selected in this thesis due to its excellent properties. The fabrication of HDPE foamed materials, and in particular the fabrication of HDPE microcellular materials, is very complicated due to the high crystallinity and the low melt strength that HDPE shows. However, in spite of the difficulties, obtaining these materials is a topic of interest because of the potential properties of this

polymer. Due to these challenges, several ways have been followed to finally produce low-density HDPE microcellular foams. One strategy consists on introducing the gas into the polymeric matrix in a supercritical state in order to increase the amount of gas available for foaming and hence, to create a high number of nucleating points distributed homogeneously throughout the material [184]. Another strategy consists on blending the HDPE with other polymers such as PP [185,186,187] or with particles [188,189]. Thereby, it is possible to increase the bubble nucleation and also to increase the gas solubility because the polymer crystallinity decreases.

As it was previously indicated (see section 2.3.3), the solution proposed in this thesis to obtain HDPE based microcellular foams consists on crosslinking the polymeric matrix. Materials with different crosslinking degrees and hence, with different rheological behaviors, have been produced, which allows performing a systematic study of the effect of the extensional rheological behavior of the polymeric matrix on the expansion degree and cellular structure of the foamed materials (see chapter 6).

2.5 Role of extensional rheology in polymer processing

2.5.1 Introduction

The shear flow properties of polymers are frequently used to characterize polymer melts and to distinguish their processing performance. For instance, in polyolefins, the melt flow index (rate) is normally used to select a resin for a certain processing method and application. When more information about the processing performance is required a full flow curve (viscosity versus shear rate) is measured. However, there are situations in which two polymers with the same shear flow properties behave in a different way because their extensional rheological behavior is not the same [190]. Extensional rheology plays a significant role in processes in which the polymer is subjected to elongational flows, such as: fiber spinning, film blowing, thermoforming, foaming, etc. Moreover, in these processes, which are driven essentially by extensional flows, the deformations take place over a limited period of time, so the flow does not have time to get fully developed until reaching a steady-state level. For these processes transient extensional properties are more relevant than steady-state viscosities [182].

2.5.2 Role of extensional rheology in foaming

During the foaming process, bubble growth involves extensional flows. Nucleation generates a two-phase structure, where gas bubbles are surrounded by polymeric walls. As the bubbles growth, these polymeric walls are stretched. This two-phase structure implies that the polymer being stretched has lost some of the diluted blowing agent as the gas now is within the cells. Although the gas depletion process is time dependent, in general it is assumed that the gas concentration within the polymer rapidly drops to zero. Thus, the extensional deformation is only applied to the neat polymer, that is, the extensional rheology that should be considered to analyze the cell growth and the cell stabilization is that of the pure polymer [144].

To understand the role of extensional rheology in foaming a simple bubble growth model for Newtonian fluid can be illustrative. As it was shown in Equation 2.59 (section 2.4.2.2.2), the change in the bubble radius is inversely proportional to the viscosity of the polymeric matrix,

that is, a high viscosity could slow down the speed of the bubble growth. Nevertheless, a constant viscosity cannot meet the requirements of controllable foaming. It is desirable that the viscosity changes during the bubble growth. During the early stage of bubble growth a low viscosity is required. Then, it is desirable that the viscosity increases gradually as the bubbles grow further and become very high in the late state of foaming to stabilize the foam structure (Figure 2.50) [161,182,191].

In other words, to produce low density cellular materials, polymeric matrices presenting strain hardening should be used. This way, the cell walls can withstand the deformation to which they are subjected during the later stages of bubble growth without breaking [144]. In general, linear polyolefins do not possess strain hardening (see section 2.2.5.4.2). Attempts to produce low density foams with these polymers generally lead to cell coalescence and cell collapse. The fact of using a polymeric matrix with or without strain hardening is not so relevant if high density foamed materials are going to be produced, as in this case, the stretching of the polymeric matrix is not as high as that occurring during the cell growth of low density foams.

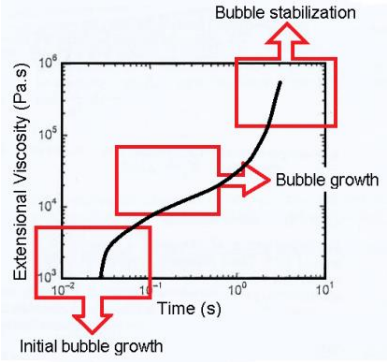

Figure 2.50. Transient extensional viscosity response of a polymer with strain hardening, with indication of the critical stages occurring during foaming.

There are several works focused on analyzing and understanding the effect of the extensional rheological behavior of the polymeric matrix on the foaming behavior. These works are mainly focused on studying how the extensional rheological properties of the polymeric matrix affect the volume expansion ratio of the foams [84,96,155,192,193,194,195,196,197,198]. Some of these works have also qualitatively analyze the cellular structure [84,199] and in several occasions the cell size and the cell density are also quantified [96,155,193,194,196,197,198,200,201]. However, it is very difficult to find systematic studies in which the effects of the rheological behavior on the cellular structure of foamed materials with the same density are analyzed. In fact, only one paper has been found [200].

The authors of these previous papers have employed different methods to relate extensional rheology and foaming behavior, which are summarized below. In several occasions only a qualitative study of the extensional rheological behavior is performed. The extensional viscosity versus time curves of different materials are compared and then they are related with the foaming behavior. Other method highly employed consists on quantifying the extensional rheological behavior by determining the ***strain hardening coefficient*** (*S*) according to Equation 2.47 (see section 2.2.5.4). This coefficient should be determined for a certain value of time (or Hencky strain) and Hencky strain rate. Now, the question is: which values of Hencky strain and

Hencky strain rate should be considered to calculate *S* in order to relate this parameter with the foaming behavior?

On the one hand, to set the appropriate Hencky strain the foam expansion ratio should be considered, this way a foaming parameter such as the expansion ratio could be related with a rheological parameter like the Hencky strain. The accurate relationship between these two parameters is very difficult to obtain and hence, this is not considered and most of the authors determine *S* for a value of the Hencky strain between 3 and 4, independently on the foam density. In his book, S. T. Lee [144] states that the total amount of deformation experienced by the polymer melt during foaming may correspond to a Hencky strain between 3 and 4, although, there is no a mathematical justification of these values. This relationship is very difficult to establish because while most of the commercial devices normally used to perform the extensional rheological tests work in uniaxial deformation, the cell deformation is biaxial, which hampers the relationship between the two types of deformations.

On the other hand, to fix the appropriate value of the Hencky strain rate the foam growth rate should be considered, which in turns depends on the foaming process employed (see section 2.4.2.3). Once again, most of the authors do not determine the appropriate value of the Hencky strain rate (taking into account the foam growth rate) and they commonly use Hencky strain rates in the range of 1 to 5 s^{-1}, independently on the foaming process employed. In the S. T. Lee's book [144] it is also said that as the bubble growth occurs over a limited period of time, typically only a few seconds, the use of strain rates in the range of 1 to 5 s^{-1} should be appropriate to quantify the rheological results.

In most of these works, the foamed materials are produced by extrusion foaming [84,155,195,196,199]. Only very few works have been found in which other foaming techniques, such as rotational molding [192], compression molding [201], injection molding [200] and foaming by gas dissolution in a pressure vessel [96,193,194,198], are used to produce the cellular materials. In this thesis (see chapter 4) the same polymeric matrices are foamed using two different foaming processes with the aim of verifying if the ranges of Hencky strain rates normally used to calculate *S* and hence, to relate the extensional behavior with the foaming behavior, are the correct ones or, by the contrary, they should be modified depending on the foaming process employed.

Finally, the amount of works that analyze the relationship between the extensional rheology of the polymeric matrix and the macroscopic mechanical properties of the foamed materials is very scarce. In fact, only two papers have been found [200,201]

Despite the fact that there are many works focused on analyzing the foaming behavior through an analysis of the extensional rheological behavior, there is still much work to be done in order to finally understand the relationship: extensional rheology/cellular structure/mechanical properties and in order to use the extensional rheology as a tool to predict the foaming behavior of an specific system. This would allow reducing costs, from a point of view of an industrial-scale production of the foamed materials. This thesis intends to complete this study by means of different research works (see chapters: 4, 5, 6 and 7).

In the following sections, a more specific literature search of the effect of extensional rheology on foaming is summarized. The different works have been classified taking into account the polymeric matrix employed on them.

2.5.2.1 Polypropylene foamed materials: Effect of extensional rheology

This section shows a brief summary of the key works found on literature dealing with similar topics to those presented in thesis. In particular, in this section, the works that employ polypropylene based polymeric matrices (linear PP, HMS PP and blends of linear and HMS PPs) to analyze the effect of the rheological behavior of the polymeric matrix on the foaming behavior are presented.

The foaming of a common linear PP is not a simple task, due to its rheological properties, especially due to its poor strain hardening and hence, due to its weak melt strength. With this polymer, it is difficult to achieve high expansion ratios during foaming because the cell walls break and the foam is not able to retain the gas during the expansion process. A way to improve the foaming of a linear PP is to incorporate long chain branches (LCB) because the PPs with LCB have a pronounced strain hardening.

Several studies have shown that foaming of long-chain branched PPs, either pure branched PP or blended with linear PP, leads to higher expansion ratios and more homogeneous cellular structures. Naguib et al. [155] analyzed the way to obtain larger volume expansion ratios. For this purpose they used a branched PP and long-chain blowing agents (pentane and butane). The fabrication route employed was extrusion foaming. They also lowered the melt temperature and optimized the process conditions. The expansion ratio achieved with the linear PP was much lower than that achieved with the branched PP, which indicates that branched PPs are more effective for the production of low-density foams. Park et al. [199] studied the cell nucleation and initial growth in linear and branched PP based cellular materials foamed by extrusion. While the degree of cell coalescence was severe in the linear PP foams and most of the cells were interconnected to each other, the branched PP gave a better foam structure. Nam et al. [198] studied the effect of modifying PP by the addition of LCB and the resulting effects on the rheological properties and performance of foams produced by extrusion. When PPs had long chain branches, the foam density became lower. It was determined that, the long-chain branching of PP was the main factor affecting the foam density. Li et al. [194] prepared and analyzed the rheological behavior of different HMS PPs. Then foamed materials were produced employing a batch foaming process by using supercritical CO_2. The HMS PPs showed the best foamability (in comparison with the linear PP) due to their optimal rheological properties. Xu et al. [193] investigated the relationships between the extensional rheological behavior and the foamability of four different polypropylenes: linear PP, linear PP with a high molecular weight component, HMS PP and crosslinked PP. Foaming was performed in a batch process using supercritical CO_2. They found that the strain hardening behavior was essential for the PP foaming process as larger expansion rations and improved cellular structures were obtained with the two PPs showing the highest strain hardening: HMS PP and crosslinked PP. Reichelt et al. [195] described the optimization of the physical foaming process by extrusion of a LCB polypropylene and the corresponding blends with a polypropylene block copolymer, by changing different process

parameters. They found a correlation between the extensional rheology and the lower limit of foam density for the blends. Blends rich in LCB PP show better foamability due to their high melt strength. Spitael et al. [196] investigated the influence of the strain hardening on foaming by extrusion of blends of linear and LCB PPs. They did not find a direct correlation between the amount of strain hardening and the foam cell density. The balance between the large nucleation of the linear PP and the reduction of the cell coalescence due to the important strain hardening of the LCB PP, led to a higher cell density in the blends of linear and branched PPs than in the neat polymers. Stange et al. [197] studied the influence of LCB on the foaming behavior of PP. Different branching contents were achieved by blending a linear PP and a LCB PP. They found an almost linear increase of the strain hardening with the amount of LCB PP. Moreover in the foaming tests, they observed a significant increase of the expansion ratio (reduction of density) by the addition of LCB PP although; this value remained constant from a concentration of the LCB PP higher than 50 %. In connection with the average cell size, they found that cell size decreased as the amount of LCB PP increased, which could be explained by a reduction of cell coalescence and cell collapse due to the increased melt strength.

2.5.2.2 Polypropylene/montmorillonite foamed materials: Effect of extensional rheology

While the effect of the rheological behavior on the foamability of pure polymeric matrices based on polypropylene has been widely investigated (see section 2.5.2.1), the number of works which analyze this effect in polypropylene based nanocomposites is scarce. There are some works in which nanoparticles are employed to improve the foaming behavior of linear PPs [180,202]. They obtained that nanoparticles have a positive impact on improving the cell morphology, the cell density and the expansion ratio. The obtained results are explained by considering that nanoparticles improve cell nucleation and reduce cell coalescence, by increasing the melt strength of the polymeric matrix. However, in these works a systematic study to analyze the effect of the rheological properties on the foaming behavior is not performed.

Below are summarized the main results obtained from different works in which a more systematic study is performed. Bhattacharya et al. [96] conducted extensional rheological measurements on different HMS PP/montmorillonites nanocomposites to analyze their effect on the foaming behavior of the mentioned nanocomposites. Foams were produced in a batch process. They obtained that the strain hardening showed by the polymer in the presence of particles played an important role in stabilizing the cellular structure. Nam et al. [198] foamed linear PP/clay nanocomposites in a batch process using supercritical CO_2. The extensional viscosity results of these materials showed that all the composites presented strain hardening. Lower cell sizes and higher cell densities were obtained with the filled polymers. Finally, Guo et al. [200] analyzed the cellular structure and properties of branched and linear PPs containing clays. In this case, foamed materials were produced by injection molding. They obtained the best and more uniform cellular structures for the nanocomposites based on the branched PP, which presented strain hardening.

2.5.2.3 Crosslinked HDPE foamed materials: Effect of extensional rheology

No works have been found in which an analysis of the effect of the rheological behavior of crosslinked HDPE polymeric matrices on the foam cellular structure is performed. Only a paper

that meets these premises has been found although, the polymeric matrix employed in this work is not HDPE, but rather a linear low density polyethylene (LLDPE). Yamaguchi et al. [75] analyzed the effect of blending crosslinked LLDPE and LLDPE on the rheological properties and foam processability. The enhanced strain hardening achieved by blending the linear polymer with the crosslinked one allowed obtaining foams with more homogeneous cellular structures, as well as, with higher expansion ratios.

2.6 References

[1] H.A. Barnes, J. F. Hutton, K. Walters. An Introduction to Rheology. Elsevier Science B. V., Amsterdam, 1989.
[2] T. G. Mezger. The Rheology Handbook for Users of Rotational and Oscillatory Rheometers (2nd Edition). Vincentz Network, Hannover, 2006.
[3] A. Y. Malkin, A. I. Isayev. Rheology: Concepts, Methods and Applications. ChemTec Publishing, Toronto, 2006.
[4] M. Reiner. Physics Today, 17, 62-62, 1964.
[5] R. I. Tanner, K. Walters. Rheology: An Historical Perspective. Elsevier Science B. V., Amsterdam, 1998.
[6] R. S. Lakes. Viscoelastic Solids. CRC Press, Boca Raton, 1999.
[7] E. Riande, R. Diaz-Calleja, M. G. Prolongo, R. M. Masegosa, C. Salom. Polymer Viscoelasticity: Stress and Strain in Practice. Marcel Dekker, Inc., New York, 2000
[8] A. J. Braihi, S. I. Salih, F. A. Hashem. International Journal of Materials Science and Applications, 4, 30-36, 2015.
[9] D. Braun, H. Cherdron, M. Rehahn, H. Ritter, B. Voit. Polymer Synthesis: Fundamentals, Methods and Practice (5th Edition). Springer, Heidelberg, 2013.
[10] J. M. Dealy, K. F. Wissbrun. Melt Rheology and its Role in Plastics Processing: Theory and Applications. Van Nostrand Reinhold, New York, 1990.
[11] R. A. L. Jones. Soft Condensed Matter, Oxford University Press, New York, 2002.
[12] N. Özkaya, M. Nordin, D. Goldsheyder, D. Leger. Fundamentals of Biomechanics: Equilibrium, Motion and Deformation (3rd Edition). Springer, New York, 2012.
[13] P. Prentice. Rheology and its Role in Plastic Processing (Report 84, Volume 7, Number 12, 1995). Rapra Technology Ltd., Shawbury, 1997.
[14] D. V. Rosato, D. V. Rosato, M. G. Rosato. Injection Molding Handbook (3rd Edition, Volume 1). Springer, New York, 2000.
[15] K. Kohlgrüber. Co-Rotating Twin-Screw Extruders: Fundamentals, Technology, and Applications. Hanser Publishers, Munich, 2007.
[16] J. Aho, S. Syrljälä. Journal of Applied Polymer Science, 117, 1076-1084, 2010.
[17] M. Chanda, S. K. Roy. Plastic Technology Handbook (4th Edition). CRC Press, Boca Raton, 2007.
[18] T A Instruments. Understanding Rheology of Thermoplastic Polymers. (http://www.tainstruments.com/pdf/literature/AAN013_V_1_U_Thermoplast.pdf)
[19] R. P. Chhabra, J. F. Richardson. Non-Newtonian Flow and Applied Rheology: Engineering Applications. Butterworth-Heinemann, Oxford, 2008.
[20] R. K. Gupta. Polymer and Composite Rheology (2nd Edition). Marcel Dekker, Inc., New York, 2000.
[21] C. W. Macosko, Rheology: Principles, Measurements and Applications. Wiley-VCH, Inc., New York, 1994.
[22] H. Münstedt, F. R. Schwarzl. Deformation and Flow of Polymeric Materials, Springer-Verlag, Berlin, 2014.
[23] C. S. Brazel, S. L. Rosen. Fundamental Principles of Polymeric Materials (3rd Edition). John Wiley & Sons, New York, 2012.
[24] J. M. Dealy, J. Wang. Melt Rheology and its Applications in the Plastic Industry (2nd Edition). Springer, Dordrecht, 2013.
[25] N. P. Cheremisinoff. Advanced Polymer Processing Operations. Noyes Publications, Westwood, 1998.
[26] J. L. White. Principles of Polymer Engineering Rheology. John Wiley and Sons, Inc., Chichester, 1990.

[27] P. M. Wood-Adams, J. M. Dealy, A. W. de Groot, O. D. Redwine. Macromolecules, 33, 7489-7499, 2000.
[28] P. M. Wood-Adams, S. Costeux. Macromolecules, 34, 6281-6290, 2001.
[29] S. Thomas, Y. Weimin. Advances in Polymer Processing: From Macro to Nano Scales. Woodhead Publishing Limited, Cambridge, 2009.
[30] M. Kontopoulou. Applied Polymer Rheology: Polymeric Fluids with Industrial Applications. John Wiley & Sons, Inc., Hoboken, 2012.
[31] R. Edam. Comprehensive Characterization of Branched Polymers. Phd Thesis, University of Amsterdam, 2013
[32] A. J. Peacock. Handbook of Polyethylene: Structures, properties and Applications. Marcel Dekker, Inc., New York, 2000.
[33] A. Santamaria. Materials Chemistry and Physics, 12, 1-28, 1985.
[34] H. M. Laun, H. Münstedt. Rheologica Acta, 15, 517-519, 1976.
[35] R. G. Larson. The structure and Rheology of Complex Fluids. Oxford University Press, Inc., Oxford, 1999.
[36] J. Aho. Rheological Characterization of Polymer Melts in Shear and Extension: Measurement Reliability Data for Practical Processing. Phd Thesis, Tampere University of Technology, 2011.
[37] J. C. García Quesada. Tema 3: Viscoelasticidad Lineal. Asignatura: Reología (Ingeniería Química), 2008. (http://rua.ua.es/dspace/bitstream/10045/3624/1/tema3RUA.pdf)
[38] W. P. Cox, E. H. Merz. Journal of Polymer Science, 28, 619-622, 1958.
[39] T. A. Instruments. The Principles and Applications of the Cox-Merz Rule. (http://www.tainstruments.com.tw/library_download.aspx?file=RN14.PDF)
[40] C. Tropea, A. Yarin, J. F. Foss. Handbook of Experimental Fluids Mechanics (Volume 1). Springer-Verlag, Berlin, 2007.
[41] J. Wiley & Sons. Properties and Behavior of Polymers (2 Volume Set). John Wiley and Sons, Inc., Hoboken, 2011.
[42] S. Goodyer. Measuring Polymers using a Rotational Rheometer in Oscillatory Mode. Anton Paar Limited, 2013.
[43] G. G. Fuller. Optical Rheometry of Complex Fluids. Oxford University Press, Inc., New York, 1995.
[44] M. T. Shaw, W. J. Macknight. Introduction to Polymer Viscoelasticity (3rd Edition). John Wiley and Sons, Inc., Hoboken, 2005.
[45] C. Oveby. Annual Transactions of the Nordic Rheology Society, 6, 129-132, 1998.
[46] M. Ansari. Rheology and Processing of High-Density Polyethylenes (HDPEs): Effects of Molecular Characteristics. Phd Thesis, University of British Columbia, 2012.
[47] A. D. Gotsis, B. L. F. Zeevenhoven, C. Tsenoglou. Journal of Rheology, 48, 895-914, 2004.
[48] D. Yan, W. J. Wang, S. Zhu. Polymer, 40, 1737-1744, 1999.
[49] F. Romani, R. Corrieri, V. Braga, F. Ciardelli. Polymer, 43, 1115-1131, 2002.
[50] D. Schulze, S. Trinkle, R. Mülhaupt, C. Friedrich. Rheologica Acta, 42, 251-258, 2003.
[51] S. Abe, M. Yamaguchi. Journal of Applied Polymer Science, 79, 2145-2155, 2001.
[52] B. Wong, W. E. Baker. Polymer, 38, 2781-2789, 1997.
[53] H. A. Barnes. A Handbook of Elementary Rheology. University of Wales Institute of Non-Newtonian Fluid Mechanics, Aberystwyth, 2000.
[54] M. Sentmanat, B. N. Wang, G. H. McKinley. Journal of Rheology, 49, 585-606, 2005.
[55] J. E. Mark. Physical Properties of Polymers Handbook (2nd Edition). Springer science, Washington, 2007.
[56] M. Sepe. Understanding the Value of Melt-volume Rate. Plastic Technology, 2014 (http://www.ptonline.com/columns/melt-flow-rate-testingpart-9)
[57] AR G2 Manual (TA Instruments)
[58] ARES User Manual (TA Instruments)

[59] J. Stange, C. Uhl, H. Münstedt. Journal of Rheology, 49, 1059-1079, 2005.
[60] A. K. Chaudhary, K. Jayaraman. Polymer Engineering and Science, 51, 1749-1756, 2011.
[61] T. C. B. McLeish, R. G. Larson. Journal of Rheology, 42, 81-110, 1997.
[62] P. Micic, S. N. Bhattacharya. Polymer Engineering and Science, 40, 1571-1580, 2000.
[63] D. Auhl, P. Chambon, T. C. B. McLeish, D. J. Read. Physical Review Letters, 103, 136001(1)-136001(4), 2009.
[64] G. Liu, H. Sun, S. Q. Wang. Journal of Rheology, 57, 89-104, 2013.
[65] A. Bach, K. Almdal, H. K. Rasmussen, O. Hassager. Macromolecules, 36, 5174-5179, 2003.
[66] J. K. Nielsen, H. K. Rasmussen, O. Hassager, G. H. McKinley. Journal of Rheology, 50, 453-476, 2006.
[67] A. Minegishi, A. Nishioka, T. Takahashi, Y. Masubuchi, J. Takimoto, K. Koyama. Rheologica Acta, 40, 329-338, 2001.
[68] H. Münstedt. Journal of Rheology, 24, 847-867, 1980.
[69] M. Sugimoto, Y. Masubuchi, J. Takimoto, K. Koyama. Macromolecules, 34, 6056-6063, 2001.
[70] J. J. Linster, J. Meissner. Polymer Bulletin, 16, 187-194, 1986.
[71] C. Gabriel, H. Münstedt. Journal of Rheology, 47, 619-630, 2003.
[72] D. Auhl, J. Stange, H. Münstedt, B. Krause, D. Voigt, A. Lederer, U. Lappan, K. Lunkwitz. Macromolecules, 37, 9465-9472, 2004.
[73] T. Takahashi, Y. Takagi, K. Minagawa, K. Iwakura, K. Koyarna. Polymer, 35, 4472-4473, 1994.
[74] P. Micic, S. N. Bhattacharya, G. Field. Polymer Engineering and Science, 38, 1685-1693, 1998.
[75] M. Yamaguchi, K. Suzuki. Journal of Polymer Science: Part B: Polymer Physics, 39, 2159-2167, 2001.
[76] M. Yamaguchi, K. Suzuki. Journal of Applied Polymer Science, 86, 79-83, 2002.
[77] N. Chen. The Effects of Crosslinking on Foaming of EVA. Phd Thesis, University of Toronto, 2012.
[78] A. Bernnat. Polymer Melt Rheology and the Rheotens Test. Institut für Kunststofftechnologie, Universität Stuttgart, 2001.
[79] S. Muke, I. Ivanov, N. Kao, S. N. Bhattacharya. Polymer International, 50, 515-523, 2001.
[80] R. P. Lagendijk, A . H. Hogt, A. Buijtenhuijs, A. D. Gotsis. Polymer, 42, 10035-10043, 2001.
[81] A. D. Gotsis, Q. Ke. SPE ANTEC, Technical Papers, 45, 1156-1161, 1999.
[82] V. V. DeMaio, D. Dong, SPE ANTEC, Technical Papers, 43, 1512-1516, 1997.
[83] A. Ghijsels, J. J. S. M. Ente, J. Raadsen. International Polymer Processing, 5, 284-286, 1990.
[84] G. J. Nam, J. H. Yoo, J. W. Lee. Journal of Applied Polymer Science, 96, 1793-1800, 2005.
[85] P. Meka, K. Imanishi, G. F. Licciardi, A. C. Gadkari. Diene Modified Polymers. Patent, US 5670595 A, 1997.
[86] W. Weng, E. J. Markel, A. H. Dekmezian, D. L. Peters. Propylene Polymers Incorporating Macromers. Patent, US 6197910 B1, 2001.
[87] W. Weng, W. Hu, A. H. Dekmezian, C. J. Ruff. Macromolecules, 35, 3838-3843, 2002.
[88] J. A. Langston, R. H. Colby, T. C. M. Chung, F. Shimizu, T. Suzuki, M. Aoki. Macromolecules, 40, 2712-2720, 2007.
[89] M. Sugimoto, Y. Suzuki, K. Hyun, K. H. Ahn, T. Ushioda, A. Nishioka, T. Taniguchi, K. Koyama. Rheologica Acta, 46, 33-44, 2006.
[90] A. J. DeNicola Jr., J. A. Smith, M. Felloni. High Melt Strength, Propylene Polymer, Process for Making it, and Use Thereof. Patent, US 5541236 A, 1996.
[91] F. Yoshii, K. Makuuchi, S. Kikukawa, T. Tanaka, J. Saitoh, K. Koyama. Journal of Applied Polymer Science, 60, 617-623, 1996.
[92] F. H. Su, H. X. Huang. Journal of Applied Polymer Science, 116, 2557-2565, 2010.
[93] D. Graebling. Macromolecules, 35, 4602-4610, 2002.

[94] B. Lu, T. C. Chung, Macromolecules, 8678-8680, 1999.
[95] Z. Zhang, H. Xing, J. Qiu, Z. Jiang, H. Yu, X. Du, Y. Wang, L. Ma, T. Tang. Polymer, 51, 1593-1598, 2010.
[96] S. Bhattacharya, R. K. Gupta, M. Jollands, S. N. Bhattacharya. Polymer Engineering and Science, 49, 2070-2084, 2009.
[97] F. H. Su, J. H. Yan, H. X. Huang. Journal of Applied Polymer Science, 119, 1230-1238, 2011.
[98] V. Mittal. Polymer Nanocomposite Foams. CRC Press, Boca Raton, 2014.
[99] E. Manias, A. Touny, L. Wu, K. Strawhecker, B. Lu, T. C. Chung. Chemistry of Materials, 13, 3516-3523, 2001.
[100] P. Svoboda, C. Zeng, H. Wang, L. J. Lee, D. L. Tomasko. Journal of Applied Polymer Science, 85, 1562-1570, 2002.
[101] H. Quin, S. Zhang, C. Zhao, M. Feng, M. Yang, Z. Shu, S. Yang. Polymer Degradation and Stability, 85, 805-813, 2004.
[102] S. Pavlidou, C. D. Papaspyrides. Progress in Polymer Science, 33, 1119-1198, 2008.
[103] P. Kiliaris, C. D. Papaspyrides. Progress in Polymer Science, 35, 902-958, 2010.
[104] M. Okamoto, P. H. Nam, P. Maiti, T. Kotaka, N. Hasegawa, A. Usuki. Nano Letters, 1, 295-298, 2001
[105] J. U. Park, J. L. Kim, D. H. Kim, K. H. Ahn, S. J. Lee, K. S. Cho. Macromolecular Research, 14, 318-323, 2006.
[106] C. M. Koo, J. H. Kim, K. H. Wang, I. J. Chung. Journal of Polymer Science, Part B: Polymer Physics, 49, 158-167, 2005.
[107] S. H. Lee, E. Cho, J. R. Youn. Journal of Applied Polymer Science, 103, 3506-3515, 2007.
[108] M. Alexandre, P. Dubois. Materials Science and Engineering, 28, 1-63, 2000.
[109] Z. Spitalsky, D. Tasis, K. Papagelis, C. Galiotis. Progress in Polymer Science, 35, 357-401, 2010.
[110] Y. Dong, D. Bhattacharyya. Composites: Part A, 39, 1177-1191, 2008.
[111] P. Singla, R. Mehta, S. N. Upadhyay. Green and Suitable Chemistry, 2, 21-25, 2012.
[112] K. N. Kim, H. Kim, J. W. Lee. Polymer Engineering and Science, 41, 1963-1969, 2001.
[113] M. Kawasumi, N. Hasegawa, M. Kato, A. Usuki, A. Okada. Macromolecules, 30, 6333-6338, 1997.
[114] W. Lertwimolnum, B. Vergnes. Polymer, 46, 3462-3471, 2005.
[115] A. B. Morgan, J. W. Gilman. Journal of Applied Polymer Science, 87, 1329-1338, 2003.
[116] Q. Zhang, Q. Fu, L. Jiang, Y. Lei. Polymer International, 49, 1561-1564, 2000.
[117] G. Galgali, C. Ramesh, A. Lele. Macromolecules, 34, 852-858, 2001.
[118] W. Lertwimolnun, B. Vergnes. Polymer, 46, 3462-3471, 2005.
[119] J. Ma, Z. Qi, Y. Hu. Journal of Applied Polymer Science, 82, 3611-3617, 2001.
[120] M. A. Treece, W. Zhang, R. D. Moffitt, J. P. Oberhauser. Polymer Engineering and Science, 47, 898-911, 2007.
[121] M. Modesti, A. Lorenzetti, D. Bon, S. Besco. Polymer, 46, 10237-10245, 2005.
[122] J. Zhao, A. B. Morgan, J. D. Harris. Polymer, 46, 8641-8660, 2005.
[123] F. J. Galindo-Rosales, P. Moldenaers, J. Vermant. Macromolecular Materials and Engineering, 296, 311-340, 2011.
[124] J. Vermant, S. Ceccia, M. K. Dolgovskij, P. L. Maffettone, C. W. Macosko. Journal of Rheology, 51, 429-450, 2007.
[125] J. C. Salamone. Polymeric Materials Encyclopedia (Twelve Volume Set). CRC Press, Boca Raton, 1999.
[126] M. Biron. Thermoplastics and Thermoplastic Composites: Technical Information for Plastics Users. Butterworth-Heinemann, Oxford, 2007.
[127] H.A. Khonakdar, J. Morshedian, U. Wagenknecht, S.H. Jafari. Polymer, 44, 4301-4309, 2003.

[128] H.A. Khonakdar, J. Morshedian, M. Mehrabzadeh, U. Wagenknecht, S.H. Jafari. European Polymer Journal, 39, 1729–1734, 2003.
[129] H. A. Khonakdar, S. H. Jafari, M. Taheri, U. Wagenknecht, D. Jehnichen, L. Haüssler. Journal of Applied Polymer Science, 100, 3264-3271, 2006.
[130] S. M. Tamboli, S. T. Mhaske, D. D. kale. Indian Journal of Chemical Technology, 11, 853-864, 2004.
[131] R. Anbarasan, O. Babot, B. Maillard. Journal of Applied Polymer Science, 93, 75-81, 2004.
[132] S. Suyama, H. Ishigaki, Y. Watanabe. Polymer Journal, 27, 371-375, 1995.
[133] W. Zhou, S. Zhu. Macromolecules, 31, 4335-4341, 1998.
[134] H. A. Khonakdar, S. H. Jafari, U. Wagenknecht, D. Jehnichen. Radiation Physics and Chemistry, 75, 78-86, 2006.
[135] D. Gheysari, A. Behjat, M. Haji-Saeid. European Polymer Journal, 37, 295-302, 2001.
[136] L. J. Gibson, M. F. Ashby. Cellular Solids: Structure and Properties (2nd Edition). Cambridge University Press, Cambridge, 1997.
[137] D. Eaves. Handbook of Polymer Foams. Rapra Technology Limited, Shawbury, 2004.
[138] C. Saiz-Arroyo. Fabricación de Materiales Celulares Mejorados Basados en Poliolefinas. Relación procesado-composición-estructura-propiedades. Phd Thesis, University of Valladolid, 2012.
[139] M. A. Rodriguez-Perez, J. I. Velasco, D. Arencon, O. Almanza, J. A. de Saja. Journal of Applied Polymer Science, 75, 156-166, 2000.
[140] D. Klempner, K. C. Frisch. Handbook of Polymer Foams and Foam Technology. Hanser Publishers, Munich, 1991.
[141] L. J. Lee, C. Zeng, X. Cao, X. Han, J. Shen, G. Xu. Polymer Nanocomposite Foams. Composites Science and Technology, 65, 2344-2363, 2005.
[142] C. A. Harper, E. M. Petrie. Plastics Materials and Processes: A Concise Encyclopedia. John Wiley & Sons Inc., New Jersey, 2003.
[143] C. Saiz-Arroyo, J. A. de Saja, M. A. Rodriguez-Perez. Polymer Engineering and Science, 52, 751-759, 2012.
[144] S. T. Lee. Foam Extrusion: Principles and Practice, CRC Press, Boca Raton, 2000.
[145] M. Lee, C. B. Park, C. Tzoganakis. Polymer Engineering and Science, 39, 99-109, 1999.
[146] C. D. Han, C. Y. Ma. Journal of Applied Polymer Science, 28, 831-850, 1983.
[147] R. Gendron, L. E. Daigneault, L. M. Caron. Journal of Cellular Plastics, 35, 221-246, 1999.
[148] R. Gendron, L. E. Daigneault. SPE ANTEC, Technical Papers, 43, 1096-1100, 1997.
[149] L. J. Gerhardt, C. W. Manke, E. Gulari. Journal of Polymer Science, Part B: Polymer Physics, 35, 523-524, 1997.
[150] C. Kwag, C. W. Manke, E. Gulari. Journal of Polymer Science, Part B: Polymer Physics, 37, 2771-2781, 1999.
[151] J. L. Throne. Thermoplastic Foam Extrusion: An Introduction. Hanser Publishers, Munich, 2004.
[152] S. T. Lee, C. B. Park, N. S. Ramesh. Polymeric Foams: Science and Technology. CRC Press, Boca Raton, 2007.
[153] G. Liu, C. B. Park, J. A. Lefas. Polymer Engineering and Science, 38, 1997-2009, 1998.
[154] S. Doroudiani, C. B. Park, M. T. Kortschot. Polymer Engineering and Science, 21, 2645-2662, 1996.
[155] H. E. Naguib, C. B. Park, U. Panzer, N. Reichelt. Polymer Engineering and Science, 42, 1481-1492, 2002.
[156] S. N. S. Leung. Mechanisms of Cell Nucleation, Growth and Coarsening in Plastic Foaming: Theory, Simulation and Experiment. PhD Thesis, University of Toronto, 2009.
[157] R. Pop-Iliev, F. Liu, G. Liu, C. B. Park. Advances in Polymer Technology, 22, 280-296, 2003.
[158] L. O. Salmazo. Cineticas de Espumacion y control de la Estructura Celular en Materiales Basados en caucho Natural y poliolefinas. Phd Thesis, University of Valladolid, 2015.

[159] R. B. McClurg. Chemical Engineering Science, 59, 5779-5786, 2004.
[160] S. Pardo. X-Ray Imaging Applied to the Characterization of Polymer Foams' Cellular Structure and its Evolution. PhD Thesis, University of Valladolid, 2014.
[161] R. Liao, W. Yu, C. Zhou. Polymer, 51, 568-580, 2010.
[162] J. E. Martini-Vvedensky, N. P. Suh, F. A. Waldman. Saturation with inert gas, depressurization, and quick-cooling. Patent, US 4473665, 1984.
[163] D. Miller, V. Kumar. Cellular Polymers, 28, 25-40, 2009
[164] V. Kumar, J. E. Weller. International Polymer Processing, 8, 73-80, 1993
[165] S. J. Liu, C. H. Tsai. Polymer Engineering and Science, 39, 1776-1786, 1999.
[166] L. Singh, V. Kumar, B. D. Ratner. Biomaterials, 25, 2611-2617, 2004.
[167] C. Saiz-Arroyo, J. A. de Saja, J. I. Velasco, M. A. Rodriguez-Perez. Journal of Materials Science, 47, 5680-5692, 2012.
[168] T.A. Osswald, L.S. Turng, P.J. Gramann. Injection Moulding Handbook. Hanser Publishers, Munich, 2002.
[169] R. E. Skochdopole, L. C. Rubens. Journal of Cellular Plastics, 1, 91-96, 1965.
[170] M. F. Ashby, R. F. Mehl-Medalist. Metallurgical Transactions A, 14, 1755-1769, 1983.
[171] A. Lopez-Gil, C. Saiz-Arroyo, J. Tirado, M. A. Rodriguez-Perez. Journal of Applied Polymer Science, In Press, DOI: 10.1002/app.42324.
[172] C. Saiz-Arroyo, M. A. Rodriguez-Perez, J. Tirado, A. Lopez-Gil, J. A. de Saja. Polymer International, 62, 1324-1333, 2013.
[173] O. Almanza, M. A. Rodriguez-Perez, J. A. de Saja. Polymer, 42, 7117-7126, 2001.
[174] J. Pinto, E. Solorzano, M. A. Rodriguez-Perez, J. A. de Saja. Journal of Cellular Plastics, 49, 555-575, 2013.
[175] E. J. Kuncir, R. W. Wirta, F. L. Golbranson. Journal of Rehabilitation Research and Development, 27, 229-238, 1990.
[176] M. A. Rodriguez-Perez, J. Lobos, C. A. Perez-Muñoz, J. A. de Saja, L. Gonzalez, B. M. A. del Carpio. Cellular Polymers, 27, 347-362, 2008.
[177] M. A. Rodriguez-Perez, J. Lobos, C. A. Perez-Muñoz, J. A. de Saja. Journal of Cellular Plastics, 45, 389-403, 2009.
[178] C. C. Ibeh, M. Bubacz. Journal of Cellular Plastics, 44, 493-515, 2008.
[179] K. Taki, T. Yanagimoto, E. Funami, M. Okamoto, M. Ohshima. Polymer Engineering and Science, 44, 1004-1011, 2004.
[180] W. G. Zheng, Y. H. Lee, C. B. Park. Journal of Applied Polymer Science, 117, 2972-2979, 2010.
[181] W. Zhai, T. Kuboki, L. Wang, C. B. Park, E. K. Lee, H. E. Naguib. Industrial and Engineering Chemistry Research, 49, 9834-9845, 2010.
[182] R. Gendron. Thermoplastic Foam Processing. Principles and Development. CRC Press, Boca Raton, 2005.
[183] M. Tang, T. B. Du, Y. P. Chen. Journal of Supercritical Fluids, 28, 207-218, 2004.
[184] S. W. Cha, N. P. Shu, D. F. Baldwin, C. B. Park. Microcellular Thermoplastic Foamed with Supercritical Fluid. Patent, US 5158986 A, 1992.
[185] S. Doroudiani, C. B. Park, M. T. Kortschot. Polymer Engineering and Science, 38, 1205-1215, 1998
[186] P. Rachtanapun, S. E. M. Selke, L. M. Matuana. Polymer Engineering and Science, 8, 1551-1560, 2004.
[187] P. Rachtanapun, S. E. M. Selke, L. M. Matuana. Journal of Applied Polymer Science, 93, 364-371, 2004.
[188] Y. H. Lee, C. B. Park, K. H. Wang, M. H. Lee. Journal of Cellular Plastics, 41, 487-502, 2005.
[189] C. Jo, H. E. Naguib. Polymer, 48, 3349-3360, 2007.
[190] D. G. Baird. Korea-Australia Rheology Journal, 11, 305-311, 1999.
[191] R. Liao, W. Yu, C. Zhou. Polymer, 51, 6334-6345, 2010.

[192] M. Emami, J. Vlachopoulos, M. R. Thomson, E. Maziers. Advances in Polymer Technology, In Press, DOI 10.1002/adv.21507, 2015.
[193] Z. Xu, Z. Zhang, Y. Guan, D. Wei, A. Zheng. Journal of Cellular Plastics, 49, 317-334, 2013.
[194] Y. Li, Z. Yao, Z. Chen, S. Qiu, C. Zeng, K. Cao. Polymer, 70, 207-214, 2015.
[195] N. Reichelt, M. Stadlbauer, R. Folland, C. B. Park, J. Wang. Cellular Polymers, 22, 315-327, 2003.
[196] P. Spitael, C. W. Macosko. Polymer Engineering and Science, 44, 2090-2100, 2004.
[197] J. Stange, H. Münstedt. Journal of Cellular Plastics, 42, 445-467, 2006.
[198] P. H. Nam, P. Maiti, M. Okamoto, T. Kotaka, T. Nakayama, M. Takada, M. Ohshima, A. Usuki, N. Hasegawa, H. Okamoto. Polymer Engineering and Science, 42, 1907-1918, 2002.
[199] C. B. Park, L. K. Cheung. Polymer Engineering and Science, 37, 1-10, 1997.
[200] M. C. Guo, M. C. Heuzey, P. J. Carreau. Polymer Engineering and Science, 47, 1070-1081, 2007.
[201] Y. Zhang, M. Kontopoulou, M. Ansari, S. Hatzikiriakos, C. B. Park. Polymer Engineering and Science, 51, 1145-1154, 2011.
[202] M. Nofar, K. Majithiya, T. Kuboki, C. B. Park. Journal of Cellular Plastics, 48, 271-287, 2012.

CHAPTER 3

MATERIALS, PRODUCTION PROCESSES AND CHARACTERIZATION TECHNIQUES

INDEX

3.1 Introduction

In this chapter the experimental aspects related to the development of this thesis are summarized. First, a detailed description of the characteristics and properties of the different raw materials employed in this thesis is given. Second, a concise description of the production processes used to produce both, the solid formulations and the foamed materials is also provided. Finally, the experimental techniques employed to characterize the raw materials, the solid formulations and the foamed materials are described.

3.2 Raw materials

The raw materials employed to perform the experimental work presented in this thesis are described in this section. The commercial names as well as some of their main characteristics are shown in the following subsections.

3.2.1 Polymeric matrices

Three different polyolefins have been selected to perform the experimental work, including two homopolymer polypropylenes (PPs) with different molecular architecture: a **linear PP** and a branched, **high melt strength, PP** (HMS PP) and a linear **high density polyethylene** (HDPE). The main characteristics of these polymers, obtained from their technical data sheets, are given in Table 3.1.

Table 3.1. Main characteristics of the polymeric matrices used (*MFR*: melt flow rate, T_m: melting point, *E*: elastic modulus and ρ: density).

LINEAR POLYPROPYLENE (linear PP)	
Commercial Name	**Characteristics**
PPH 4070 (Total Petrochemicals)	• *MFR* = 3 g/10 min (230 ºC, 2.16 kg) [*ISO 1133*] • T_m = 165 ºC [*ISO 3146*] • *E* = 1950 MPa [*ISO 527-2*] • ρ = 0.905 g/cm^3 [*ISO 1183*]

HIGH MELT STRENGTH POLYPROPYLENE (HMS PP)	
Commercial Name	**Characteristics**
Daploy™ WB135HMS (Borealis)	• *MFR* = 2.4 g/10 min (230 ºC, 2.16 kg) [*ISO 1133*] • *E* = 2000 MPa [*ISO 527-2*] • ρ = 0.905 g/cm^3 [*ISO 1183*]

HIGH DENSITY POLYETHYLENE (HDPE)	
Commercial Name	**Characteristics**
Rigidex® HD 5211EA-Y (Ineos Polyolefins)	• *MFR* = 11 g/10 min (190 ºC, 2.16 kg) [*ISO 1133*] • T_m = 131 ºC [*ASTM D2117*] • ρ = 0.951 g/cm^3 [*ISO 1872*]

These two commercial PP grades have been chosen because their melt flow rate and mechanical properties are very similar, as Table 3.1 indicates, and hence, they only differ in the type of molecular architecture. A HDPE polymer with an elevated melt flow rate has been

selected in order to make easier the crosslinking process used to modify the rheological properties of this material.

3.2.2 Nanoparticles

Two different types of montmorillonites: **natural montmorillonites** and **organomodified montmorillonites** have been used in this thesis to produce polymeric nanocomposites with the HMS PP. The characteristics of the clays employed are described in Table 3.2.

Table 3.2. Main characteristics of the nanoparticles (layered clays) employed (ρ: density and d: interlayer spacing).

NATURAL MONTMORILLONITES (Na+)	
Commercial Name	**Characteristics**
Cloisite® Na+ (Southern Clay Products)	• Natural (non-organomodified) montmorillonite • ρ = 2.86 g/cm^3 • d = 11.7 Å

ORGANOMODIFIED MONTMORILLONITES (C20A)	
Commercial Name	**Characteristics**
Cloisite® 20A (Southern Clay Products)	• Natural montmorillonite modified with a quaternary ammonium salt • ρ = 1.77 g/cm^3 • d = 24.2 Å

These particles have been selected for several reasons:

- Both types of particles have the same structure (laminated structure) as they are layered silicates.
- Both are natural montmorillonites however, while the Na+ clays have not been modified the C20A clays have been modified with a quaternary ammonium salt improving, therefore, the interaction between the clay and the polymer.
- The initial interlayer spacing of the two particles is different. This is higher in the C20A clays because of their organo-modification.

3.2.3 Compatibilizer polymer

A compatibilizer polymer has been employed with the organomodified clays (C20A) in order to improve the compatibility between the clays and the polymer.

Table 3.3. Main characteristics of the compatibilizer polymer used (*MFR*: melt flow rate, T_m: melting point, and ρ: density).

COMPATIBILIZER POLYMER (PP-MA)	
Commercial Name	**Characteristics**
Polybond 3200 (Chemtura)	• Maleic anhydride modified homopolymer PP • *MFR* = 115 g/10 min (190 ºC, 2.16 kg) [*ASTM D-1238*] • T_m = 157 ºC • ρ = 0.91 g/cm^3 [*ASTM D-792*]

As the polymeric matrix employed to produce the composites is PP, the compatibilizer agent selected is a chemically modified PP, more specifically a **maleic anhydride modified PP homopolymer**. The main characteristics of this polymer, obtained from its technical data sheet, are shown in Table 3.3.

3.2.4 Blowing agents

During this thesis two different blowing agents have been employed: a chemical and a physical blowing agent (Table 3.4). The chemical blowing agent used has been **azodicarbonamide** (ADC). It has been employed to foam all the PP based materials. **CO_2** (an inert gas) has been selected as physical blowing agent to foam the HDPE based materials.

Table 3.4. Main characteristics of the blowing agents employed.

CHEMICAL BLOWING AGENT: AZODICARBONAMIDE (ADC)	
Commercial Name	**Characteristics**
Porofor® ADC/M-C1 (Lanxess)	• Exothermic chemical blowing agent • Decomposition temperature = 210 ºC • Gas yield (volumetric at 210 ºC) = 228 ml/g • Density = 1.65 g/cm^3 • Average particle size = (3.9 ± 0.6) µm

PHYSICAL BLOWING AGENT: CO_2	
Commercial Name	**Characteristics**
CO_2 (Air Liquide)	• Liquide CO_2 • Bottle Pressure = 40 bars • Purity = 99.95 %

3.2.5 Crosslinking agent

A chemical crosslinking agent has been used to crosslink the HDPE. The main characteristics of the crosslinked agent employed in this work are described in Table 3.5.

Table 3.5. Main characteristics of the crosslinking agent employed.

CROSSLINKING AGENT	
Commercial Name	**Characteristics**
LUPEROX® 101XLS50 (Arkema)	• Organic peroxide based on 2,5-dimethyl-2,5-di-(tert-butylperoxy)hexane • The material contains: 50 % of 2,5-dimethyl-2,5-di-(tert-butylperoxy)hexane and 50 % of SiO_2 • Self-accelerating decomposition temperature: 75 ºC

The grade of crosslinking agent selected is the one typically used with the HDPE [1]. It is an **organic peroxide** that can be thermally decomposed to generate free radicals which can subsequently create an active site on a polymer backbone. The reaction between two active sites will create a strong link between the polymer chains, leading to a polymer network.

3.2.6 Antioxidants

Antioxidants have been employed in order to reduce the thermal degradation of the polymer during the production process as the polymer is subjected to high temperatures during long periods of time. The main properties of the antioxidants employed are described in Table 3.6.

Table 3.6. Main characteristics of the antioxidants employed.

ANTIOXIDANT: IRGANOX	
Commercial Name	**Characteristics**
®IRGANOX 1010 (Ciba)	• It is a sterically hindered phenolic antioxidant • Density = 1.15 g/cm^3

ANTIOXIDANT: IRGAFOS	
Commercial Name	**Characteristics**
IRGAFOS® 168 (Ciba)	• It is a trisarylphosphite processing stabilizer • Density = 1.03 g/cm^3

3.3 Production processes

In this section the production techniques employed to produce both, the solid materials and the foamed materials are described. Table 3.7 indicates in which chapters each of these techniques has been employed.

Table 3.7. Summary of the production processes employed throughout this work.

PRODUCTION OF THE SOLID MATERIALS	
Production Process	**Chapters**
Extrusion	4, 5, 6
Compression Molding	4, 5, 6
Crosslinking	6
PRODUCTION OF THE FOAMED MATERIALS	
Production Process	**Chapters**
Improved Compression Molding	4, 5
Solid State Foaming	6
Foaming at Atmospheric Pressure in a Mold	4

3.3.1 Production of solid formulations

3.3.1.1 Extrusion process

Independently on the polymeric matrices, particles, blowing agents, etc., all the solid formulations used in the different experimental works have been produced using a co-rotating twin screw extruder Collin ZK 25T with L/D of 24 [2].

The twin-screw extruder is composed of two co-rotating screws of the same diameter, which rotate inside a barrel, heated externally by five resistances (Figure 3.1).

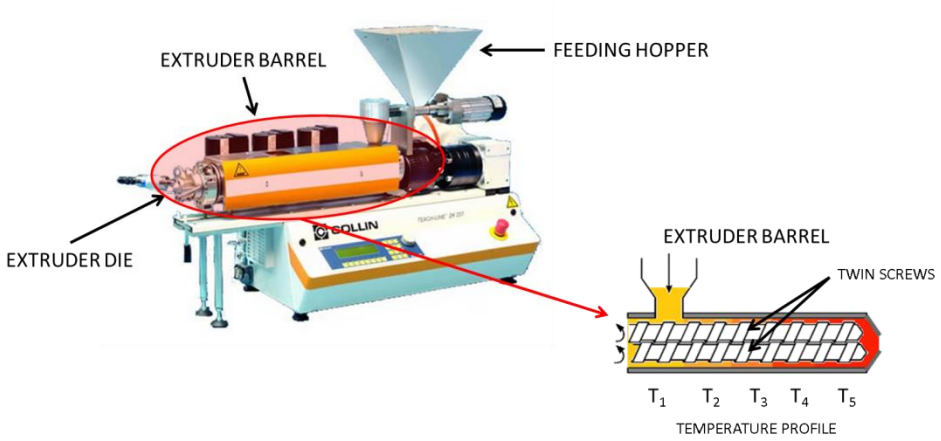

Figure 3.1. Image of a co-rotating twin-screw extruder including and scheme of the extruder barrel.

The steps followed to produce the solid formulations have always been the same (Figure 3.2):

1. All the materials required to produce the final formulation (polymers, additives, fillers, blowing agents, etc.) were first dried in a vacuum oven at a temperature of 50 ºC during approximately twelve hours.
2. Then, the raw materials were manually mixed.
3. The obtained mixture was placed in an automatic feeding hopper located at the beginning of the extruder, which introduces the material into the extruder barrel. The feeding rate, that is, the rate at which the material is introduced into the extruder barrel, can be selected by the user.
4. Once the mixture is in the extruder barrel, the polymer turns melted shortly because the extruder temperature is set higher than the melting temperature of the polymer. The temperature profile can also be defined by the user. In this thesis an ascendant temperature profile has always been established, being the temperature in the die higher than in the area near the hopper. The selection of the appropriate temperature is critical when the formulation contains additives that decompose at a certain temperature (such as chemical blowing agents and/or chemical crosslinking agents). If a decomposition of these additives during the extrusion process is not desired, the defined temperature should be higher than the polymer melting temperature and lower than decomposition temperature of the additives. The molten mixture is moved forward through the extruder barrel pushed by the co-rotating movement of the two screws. The rotational speed of the screws can also be selected by the user. It is in this step in which the additives, fillers, etc. are dispersed throughout the molten polymer due to the high temperatures and shear forces applied by the screws. Therefore, the selection of both the extruder temperature and the rotational speed of the screws are critical to achieve a good dispersion of the different components, which is fundamental, for instance, in the case of the production of solid nanocomposites.
5. The molten formulation produced, which comes out from the extruder die in the form of a circular strand, was cooled and crystallized in a water tank.
6. At the end of the water tank there is an automatic pelletizer which cuts the solid strands into cylindrical pellets. After the pelletization, the final formulations were dried in the vacuum oven, using again the conditions aforementioned.

7. In some occasions the final formulation obtained is again subjected to a new extrusion process in order to obtain a more homogeneous material with a better dispersion of the different components. This new extrusion can be performed either maintaining the previously established extrusion conditions (feeding rate, temperature profile, screws speed, etc.) or employing new ones. This thesis proves that the polymeric matrix is greatly affected by the number of extrusion cycles to which it is subjected, as changes in its rheological behavior are obtained after the extrusion process. Therefore, to compare and to relate different processes the formulations employed in each process should be produced with the same thermo-mechanical history, that is, with the same number of extrusions conducted under the same conditions.

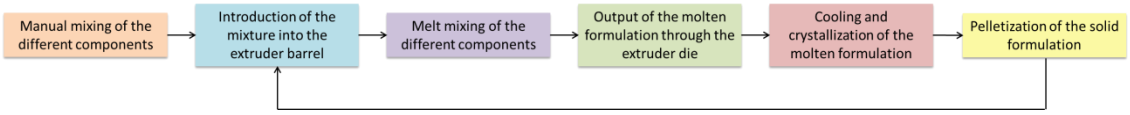

Figure 3.2. Scheme of the steps followed to produce the solid formulations using a twin-screw extruder.

A more detailed description of the extrusion parameters employed, the number of extrusion cycles to which the different formulations are subjected and the order in which the different materials are blended to produce the final formulation can be found in chapters 4, 5 and 6.

3.3.1.2 Compression molding process

Along this thesis, many of the formulations produced by extrusion have been subsequently thermoformed by compression molding in order to obtain solid precursors with a defined geometry, which are required to perform the characterization of the structure and properties of the solid materials.

For instance, to perform the shear rheology measurements cylindrical solid precursors with a thickness of 1.5 mm and a diameter of 22 mm are required. For the extensional rheological tests, the samples should be prisms with the following dimensions: 20 mm x 10 mm x 0.5 mm (length x width x thickness). The X-ray diffraction (XRD) measurements of the different solid nanocomposites have been performed in precursors with a thickness of 0.5 mm. Finally, this technique has also been employed to produce the solid precursors for the mechanical characterization, in particular for the tensile tests. In this case samples with a thickness of 4 mm have been fabricated.

The steps followed to thermoform the different materials are described below:

1. The right amount of formulation to be thermoformed was placed in a steel mold whose dimensions were selected depending on the final application of the precursor (Figure 3.3.a). The mold, in turn, was located in a hydraulic hot plate press (Figure 3.3.b).
2. The material was compression molded by applying a determined pressure (in general equal or greater than 21.8 bars) and a specific temperature (higher than the melting temperature of the polymeric matrix) during a certain period of time (Figure 3.3.c). The selection of the appropriate time and temperature depends on the type of material to be thermoformed.

3. Then, the mold containing the molten material was located in a hydraulic cold plate press (Figure 3.3.b) at ambient temperature and the materials was cooled down and crystallized under the same pressure, previously applied in the hot-plate press.

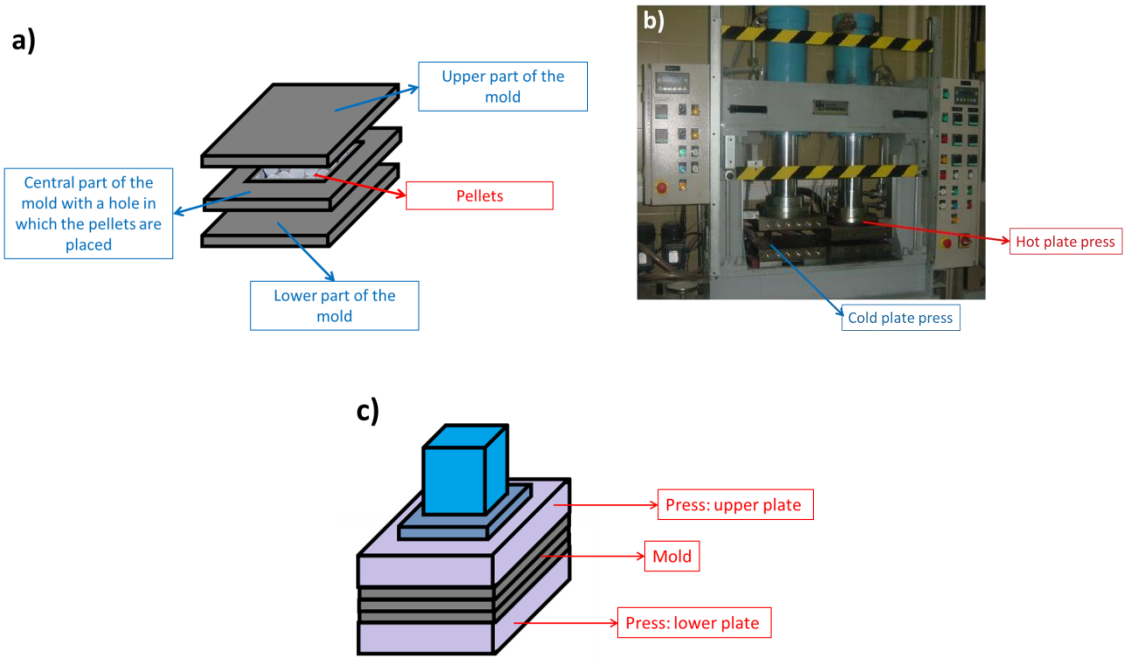

Figure 3.3. Scheme of the elements employed in the compression molding process to produce solid materials. a) Scheme of the mold. b) Image of the hydraulic hot/cold plate press used in this thesis. c) Scheme of the mold located in hot/cold plates.

This process has been optimized for each material in order to produce solid materials free of porosity.

3.3.1.3 Crosslinking process

As it was previously indicated, prior to the foaming process the HDPE materials have been crosslinked employing a chemical crosslinking agent [3].

In a first step, blends of the HDPE with different amounts of the crosslinking agent were prepared using a co-rotating twin screw extruder, as indicated in section 3.3.1.1. After this first step the materials are still not crosslinked. Then, the different formulations (pellets of HDPE + crosslinking agent) were placed in a mold with a thickness of 2 mm (Figure 3.3.a) which, in turn, was located in a hydraulic hot plate press (Figure 3.3.b). The material was compression molded by applying a pressure of 21.8 bars and a temperature of 190 ºC (higher than the melting temperature of the HDPE and higher than the decomposition temperature of the crosslinking agent) during a period of time which was varied between 15 and 60 minutes (Figure 3.3.c). During this period of time the crosslinking agent decomposes and the thermochemical crosslinking of the polymeric matrix is randomly produced. Therefore, the highest the period of time used, the highest the crosslinking degree achieved (more details can be found in chapter 6). Then, the mold containing the molten crosslinked material was located in a hydraulic cold plate press (Figure 3.3.b) at ambient temperature and the material was cooled down and crystallized under pressure (21.8 bars).

3.3.2 Production of foamed materials

Three different foaming routes have been selected to produce the foamed materials: improved compression molding (ICM), solid state foaming and foaming at atmospheric pressure in a mold. The three processes employed are described in detail in this section.

3.3.2.1 Improved compression molding (ICM)

ICM is a technique developed by the laboratory of Cellular Materials (CellMat) of the University of Valladolid and patented in the year 2013 [4]. This technique has been employed to foam all the PP based formulations: linear PP, HMS PP, blends of linear and HMS PP and PP composites (see chapters 4 and 5). One of the main advantages of this thechnique is that it allows producing cellular materials with the same density, independently on the formulation used. Moreover, the sizes of the samples produced with this technique are large enough to perform subsequently compression tests or other macroscopic characterizations. This technique is described in the following paragraphs [5,6,7,8].

Prior to the foaming process, the pellets containing the chemical blowing agent (CBA) were fabricated. For this purpose the polymeric matrix, the CBA and others additives and/or fillers were melt blended using the twin-screw extruder, as described in section 3.3.1.1. The extrusion temperature should be carefully selected. It should be higher than the melting temperature of the polymeric matrix (T_m) and lower than the decomposition temperature of the CBA, to prevent its early decomposition.

Once the formulation was fabricated, the pellets were placed in a stainless steel mold whose scheme is represented in Figure 3.4.a. Then, it was closed by screws and sealed by rubber joints which are placed between the main body and the upper and bottom parts of the mold (Figure 3.4.b).

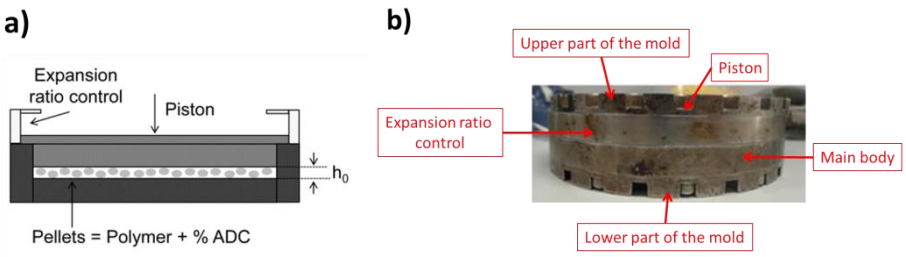

Figure 3.4. Mold employed in the ICM route. a) Scheme of the mold. b) Real image of the mold.

Once the mold was closed, it was located in a hot-plate press (Figure 3.5). An initial pressure (P_0) was applied to the system while it was heated until the foaming temperature (T_F), which, in this case, was higher than the decomposition temperature of the CBA (Figure 3.5.a). As the temperature increases, the blowing agent starts decomposing and the pressure inside the mold increases up to a certain value (P_F). After a certain time (t_F), when the blowing agent is fully decomposed and P_F reaches a stationary value, the pressure of the press is released allowing the polymer to expand until the desired ratio (Figure 3.5.b). The rate of the foam growth (depressurization rate) was maintained constant for all the foams produced in this thesis. Then, the mold was introduced in cold water to cool-down the sample and hence, to

stabilize the cellular structure as fast as possible. Finally, the mold is opened and the sample is extracted from it. As the mold remains closed during the whole process, the material is subjected to a certain pressure also during its stabilization (P_m). In this process, the growth of the cellular material is restricted by the mold and hence, the material expansion can only occur in one direction, promoting an anisotropic growth of the cells.

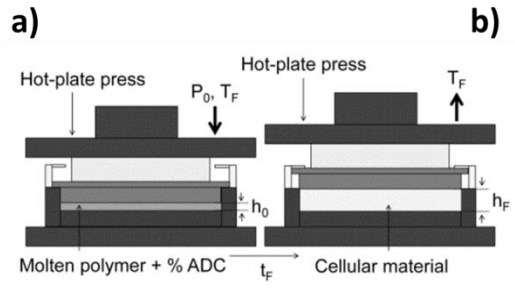

Figure 3.5. Scheme of the ICM process. a) Heating of the system until the foaming temperature (T_F) under a pressure P_0. b) Release of pressure allowing the polymer to expand from an initial height (h_0) to a final height (h_f).

The following foaming parameters have been employed in this thesis to produce all the cellular materials: an initial pressure of 41.5 bars, a foaming temperature of 200 ºC, a foaming time of approximately 15 minutes and a depressurization rate of 10 mm/min.

3.3.2.2 Solid state foaming

Solid state foaming has been the technique selected to perform the microcellular foaming of the HDPE (non crosslinked and crosslinked) based materials (see chapter 6). It was developed by Vvedensky et al. and it was patented in the year 1984 [9].

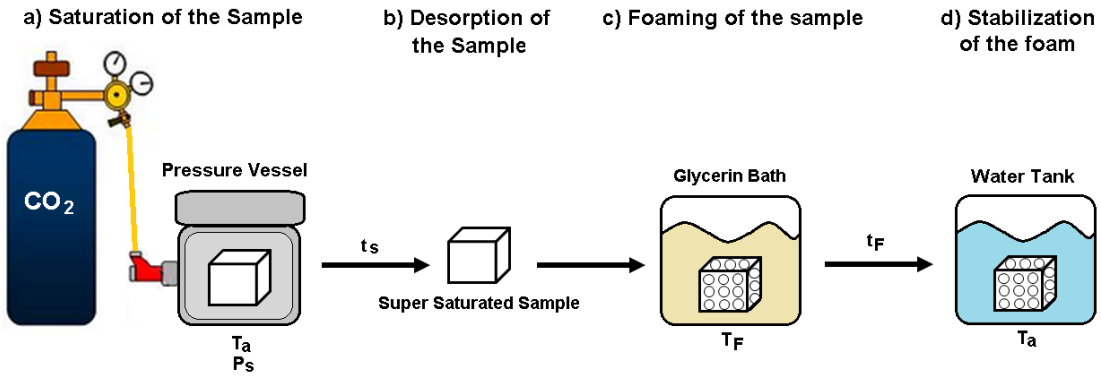

Figure 3.6. Scheme of the solid state foaming process.

The steps followed to produce the cellular materials using this technique are the following [10,11]:

1. Samples of 2 mm x 15 mm x 15 mm were obtained from the HDPE and the crosslinked HDPE (x-HDPE) sheets produced by compression molding (see section 3.3.1.3).
2. Samples were located into a small pressure vessel with a capacity of about 350 cm^3 (Figure 3.6.a). CO_2 was then delivered to the pressure vessel and samples were allowed to absorb gas at room temperature (T_a), under a determined saturation pressure (P_s) and during a

certain time (saturation time, t_s). As the saturation is performed at room temperature, the polymer always remains in a solid state (from here the name of the process: solid state foaming). In this work two saturation pressures have been used: 3 MPa and 5 MPa. These gas pressures were controlled to an accuracy of 0.1 MPa. In order to determine the appropriate saturation time, samples were removed periodically from the pressure vessel, weighted and returned to the pressure vessel. At room temperature and under a pressure of 5 MPa, 24 hours were required to reach the equilibrium gas saturation. During this stage the gas molecules diffuse into the polymer occupying the free volume between the polymer chains.

3. Once the polymer was completely saturated, the gas pressure was released. The sample enters in a supersaturated state (Figure 3.6.b) and it starts to release the excess of gas, either by diffusion to the outside or by the formation of discontinuities/voids inside the matrix. These voids will act as nuclei for the formation of the cells.
4. The next step was the foaming of the saturated sample (Figure 3.6.c). The foaming step was carried out in a temperature controlled glycerin bath at an elevated foaming temperature (T_F), higher than the melting point of the polymeric matrix. This way, the nuclei previously formed can growth into cells. In this thesis different foaming temperatures have been used, varying between 150 ºC and 190 ºC. The sample remained in the glycerin bath during a predetermined period of time (foaming time, t_F) which, in this thesis, has been varied between 15 s and 75 s.
5. After foaming, the samples were removed from the glycerin bath and cooled in water at room temperature with the aim of stabilizing the cellular structure (Figure 3.6.d).

3.3.2.3 Foaming at atmospheric pressure in a mold

The linear PP, the HMS PP and different blends of the two PPs (at different concentrations) have also been foamed by using this technique. Two different variants of this technique have been employed, which mainly differ in the type of mold used and in the heating system employed. The fact of using these two processes is because one of them was adapted to perform an in-situ characterization of the foaming process by means of time-resolved neutron radiography and the other one was employed to produce foamed materials which can be characterized by ex-situ techniques, in order to establish a correlation between the results obtained with the in-situ technique and those obtained with the ex-situ technique (see chapter 4).

One of the advantages of this system is that as the material expansion is restricted by the mold, the foam density can be easily controlled by controlling the amount of material introduced initially in the mold.

3.3.2.3.1 Foaming at atmospheric pressure in a mold for the in-situ characterization

With the in-situ visualization it is possible to analyze and to understand the mechanisms that take place during the foaming process, as it allows studying the temporal evolution of important characteristics of the cellular materials such as relative density, cell size and cell density, in other words, the material is in-situ characterized while it expands. This in-situ visualization was performed by means of time-resolved neutron radiography. To perform these experiments a mold containing the expandable material (polymer + chemical blowing

agent) was placed between a neutron source and a detector. While the mold was heated, enabling the material expansion, an image sequence of the expansion process was acquired by the detection system (see section 3.4.2.1.1). Therefore, a specific mold (whose characteristics are described below) was designed to be incorporated into the experimental set up. The employed mold is similar to the one used in the work of Solorzano et al. [12].

The mold used was a cylindrical mold fabricated in aluminum that presents a rectangular cavity where the polymer containing the chemical blowing agent was located. The internal dimensions of the cavity were: 20 mm × 20 mm × 7 mm. Two aluminum lids (4 mm in thickness) maintained the polymer into the cavity, even at high pressures, and two aluminum frames were used to keep the full system closed. A collar heater (power 250 W) was used to heat up the system under controlled conditions. A thermocouple was located in a drilled bore in the aluminum mold in a position close to the polymer. A schematic drawing of the system is provided in Figure 3.7.

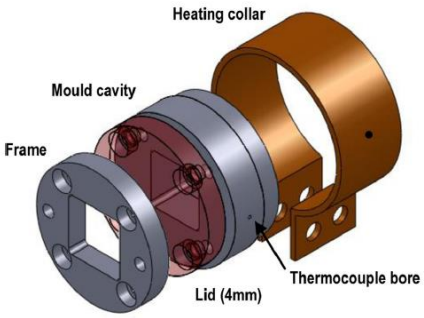

Figure 3.7. Schematic drawing of the mold used for the in-situ characterization of the foaming process.

The temperature control was carried out by means of a PID controller. All the samples were subjected to the same heating program consisting in a pre-heating of the system at a temperature of 200 ºC, during 10 minutes, followed by a heating ramp at 10 ºC/min until reaching 250 ºC. Then, the sample was kept at 250 ºC during a period of time between 1 and 2 hours, enough time to degenerate significantly the cellular structure of the foamed material.

3.3.2.3.2 Foaming at atmospheric pressure in a mold for the ex-situ characterization

Some of the materials which were in-situ foamed and characterized were also foamed at atmospheric pressure in a mold, in this case, in a traditional oven. These additional experiments were performed with the objective of correlating the results obtained after solidification with those obtained by the in-situ process.

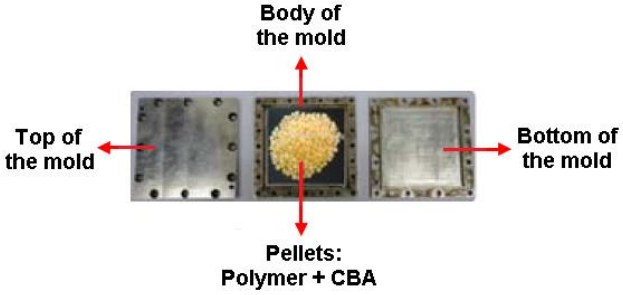

Figure 3.8. Mold used for the ex-situ foaming process.

In a first step the polymer containing the blowing agent was introduced in an aluminum mold whose internal dimensions are: 85 mm x 85 mm x 10 mm. The amount of material introduced was selected taking into account the final density required. Then, the mold was closed with several screws (Figure 3.8) and located in a pre-heated air-circulating oven at a temperature of 250 ºC (the same temperature employed in the in-situ process). The mold remained in the oven for 1350 s and subsequently, it was introduced in a tank of water at ambient temperature to cool the foam and stabilize its structure.

3.4 Characterization techniques

Different characterization techniques have been employed throughout this thesis. A detailed explanation of the experimental parameters used with each of the experimental techniques can be found in the articles in which these techniques are employed (see chapters 4, 5, and 6). Nevertheless, in this section a very brief description of the characterization techniques used, including the main characteristics measured with each one, is also included. The procedure used in the rheological characterization is explained in more detail due to the importance that this technique has in this research work. The techniques used as well as the chapters in which they are employed are listed in Table 3.8.

Table 3.8. Summary of the characterization employed throughout this work.

CHARACTERIZATION OF THE SOLID MATERIALS	
Characterization Technique	**Chapters**
Differential Scanning Calorimetry (DSC) (DSC822e from Mettler)	4, 6
Thermogravimetric Analysis (TGA) (TGA/SDTA 861 from Mettler)	4, 5, 6
Shear Rheology (AR 2000 EX from TA Instruments)	4, 5
Extensional Rheology (AR 2000 EX/SER 2 from TA Instruments/Xpansion Instruments)	4, 6
Extensional Rheology (ARES ARES-2K/EVF from TA Instruments)	4, 5
Density Determination (Gas Picnometry) (Accupyc II 1340 from Micromeritics)	4, 5, 6
X-Ray Diffraction (D8 Discover A25 from Bruker)	5
Scanning Electron Microscopy (SEM) (Quanta 200 F from FEI)	5
Tensile Tests (Universal testing Machine 5.500R6025 from Instron)	5
Gel Content Determination (Immersion in Boiling Xylene)	6
CHARACTERIZATION OF THE FOAMED MATERIALS	
Characterization Technique	**Chapters**
Time-resolved neutron radiography (Swiss Spallation Neutron Source, SINQ)	4
Scanning electron microscopy (SEM) (JSM-820 from Jeol)	4, 5, 6

Scanning Electron Microscopy (SEM) (Quanta 200 F from FEI)	5
Density Determination (Geometric Method) (Precision Balance AT 261 from Mettler)	4, 5
Density Determination (Archimedes Method) (Precision Balance AT 261 from Mettler)	6
Open Cell Content Determination (Gas Picnometry) (Accupyc II 1340 from Micromeritics)	4, 5
Compression Tests (Universal testing Machine 5.500R6025 from Instron)	4, 5
X-Ray Diffraction (D8 Discover A25 from Bruker)	5

3.4.1 Characterization of raw materials and solid formulations

3.4.1.1 Differential Scanning Calorimetry (DSC)

Thermal properties of the unfilled polymeric matrices were studied by means of a Mettler DSC822e differential scanning calorimeter. The melt temperature (T_m), the crystallization temperature (T_c) and the crystallinity (X_c) were determined from the DSC measurements.

3.4.1.2 Thermogravimetric analysis (TGA)

A thermogravimeter analyzer, TGA/SDTA 861 from Mettler was employed along this thesis to check the formulations produced in order to verify that the contents of the different raw materials comprising the formulations are the correct ones.

3.4.1.3 Rheology

3.4.1.3.1 Shear rheology

Shear rheological measurements (rotational tests and dynamic-mechanical experiments) of the HMS PP, linear PP and HMS PP-linear PP blends were performed in order to determine the zero-shear viscosity of the polymers and in order to analyze the miscibility of both PPs. Moreover the dynamical tests were also performed in the HMS PP based composites to analyze and to quantify the dispersion degree of the two types of montmorillonites used.

To perform this tests a stress controlled rheometer (AR 2000 EX from TA Instruments) was used, employing a geometry of electrically heated parallel plates with a diameter of 25 mm. Shear rheological measurements were performed under nitrogen atmosphere (to avoid polymer thermal degradation) using a gap between the two plates of 1 mm. To perform this test, cylindrical samples with a thickness of 2 mm and a diameter of 22 mm, fabricated by compression molding (see section 3.3.1.2) were produced.

Rotational tests were performed to determine the logarithmic flow curves (steady shear viscosity versus shear rate) of the unfilled polymeric matrices. To obtain the steady shear viscosity, a steady shear flow is imposed on a material for a suitable period of time until the shear stress reaches a steady state, that is, it becomes independent on time. The ratio between the measured steady state stress and the applied shear rate is the steady shear

viscosity. Different, shear rates were employed varying between 0.004 and 1 s^{-1}. From this test, it was possible to determine the zero-shear viscosity (η_0).

Dynamic-mechanical experiments were performed in both, the unfilled and the filled polymeric matrices. The protocol followed to perform these tests is explained below:

1. A strain sweep was performed at a fixed dynamic frequency (1 rad/s) to determine the linear viscoelastic regime of the different materials. In other words, this test allows selecting a strain that belongs to the linear viscoelastic regime.
2. Only, in the case of the polymeric composites a time sweep should be performed, prior to the frequency sweep, in order to recover the initial state of the particles network because when the composite is loaded, the particles network partially deforms. This time sweep was conducted at a fixed frequency of 1 rad/s and at a fixed strain, which was selected in order to be within the linear viscoelastic response of the material, during 900 s.
3. Finally, a frequency sweep over a certain angular frequency range was performed at a fixed strain (obtained in the step 1). From these measurements four parameters, as a function of the angular frequency, were analyzed: the dynamic shear viscosity (η^*), the storage modulus (G'), the loss modulus (G'') and the loss angle (δ)

The dynamic-mechanical tests of the unfilled PPs was performed at a temperature of 200 ºC and the frequency range selected was 0.1 < ω < 100 rad/s. However, in this frequency range and at this temperature, it was not possible to achieve the terminal region, where $G' \propto \omega^2$ and $G'' \propto \omega$. This regime was achieved by the application of the time-temperature superposition (TTS) principle, after performing measurements in the same range but at a temperature of 250 ºC.

In the case of the solid composites, a temperature of 250 ºC was selected to perform the dynamic characterization. Moreover, in this case, the experiments were performed over an angular frequency range of 0.01 < ω < 100 rad/s. With these conditions, it was not necessary to apply the TTS principle.

3.4.1.3.2 Extensional rheology

Two different devices have been used in this this thesis to perform the extensional rheological characterization of the solid materials. On the one hand, a stress controlled rheometer (AR 2000 EX from TA Instruments) with the accessory SER 2 (from Xpansion Instruments) in which the sample is clamped to two cylinders which rotate in opposite direction stretching the sample (see chapter 2, section 2.2.5.3). On the other hand, a strain controlled rheometer (ARES-2K from TA Instruments) with the extensional viscosity fixture (EVF). In this second device, the sample is also clamped to two cylinders. However, in this device one of these cylinders is fixed and the other one rotates. The rotating cylinder moves on a circular orbit around the fixed cylinder, while rotating around its own axis at the same time (see chapter 2, section 2.2.5.3). The solid samples (without containing the blowing agent) for the extensional rheological tests were produced by compression molding (see section 3.3.1.2). The samples fabricated are prisms with dimensions of 20 mm x 10 mm x 0.5 mm (length x width x thickness). Moreover, to evaluate the extensional viscosity measurements it is necessary to know the density at the temperature at which the experiment is going to be performed. As it

was already indicated in chapter 2, this melt density is tabulated for a high amount of polymers [13]. Furthermore, this parameter can also be experimentally determined as the ratio between the melt flow rate (MFR) which is reported as the mass per unit of time (g/10 min) and the melt volume rate (MVR) which is reported as the volume per unit of time (cm^3/10 min) [14]. Both, the tabulated and the experimentally determined values have been used in this work.

Independently on the equipment employed, the protocol followed to perform the extensional rheological tests was always the same:

1. Selection of the measurement temperature. As the main objective of this thesis consists on relating the extensional rheological behavior of the polymeric matrix with the foaming behavior, the temperature selected to perform the extensional rheological tests should be the same as the foaming temperature.
2. Pre-stretch. Once the sample has been clamped to the rotating cylinders and it has melted, a pre-stretch was performed in order to compensate the thermal expansion of the sample when it is heated up from room temperature. The pre-stretch rate was selected taking into account the values recommended for each of the two devices. Thus, a pre-stretch rate of $5x10^{-3}$ s^{-1} was used with the stress controlled rheometer and a pre-stretch rate of $7.5x\ 10^{-3}$ s^{-1} was employed with the strain controlled rheometer. The total Hencky strain applied during the pre-stretch was of approximately 0.05 (Figure 3.9).
3. Relaxation post pre-stretch. When the pre-stretch was finished the sample was kept for a certain time at a constant temperature without applying any stress. A relaxation time of 30 s was employed with the strain controlled rheometer, while this value was incremented up to 60 s with the stress controlled rheometer (Figure 3.9).
4. Test. After the relaxation step, the experiment takes place. Different Hencky strain rates ($\dot{\varepsilon}_H$) were employed to stretch the sample varying between 0.1 and 2.5 s^{-1}. Moreover, the maximum Hencky strain (ε_H) applied was varied between 2 and 3, depending on the material analyzed (Figure 3.9).

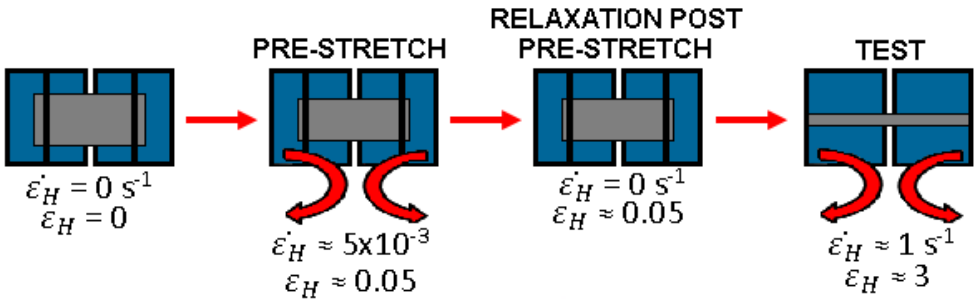

Figure 3.9. Scheme of the steps followed to perform the extensional rheological test.

3.4.1.4 Density determination

A gas pycnometer, Accupyc II 1340 from Micromeritics was used to determine the **density of the solid materials**. The pycnometer provides the volume of the solid samples with high precision as well as the density calculations. Five different measurements of each material were performed with the aim of obtaining and accurate average value of the density of the solid samples.

3.4.1.5 X-Ray Diffraction (XRD)

The solid HMS PP based composites (chapter 5) were characterized by performing XRD measurements with a Bruker D8 Discover A25 diffractometer with Cu-Kα radiation of wavelength 0.154 nm with the aim of calculating the **interlayer spacing** between the clay stacks to finally determine the structure of the layered clays (degree of intercalation/exfoliation). These measurements were performed in solid precursors produced by compression molding. Moreover, the clays as received were also characterized by XRD.

3.4.1.6 Scanning electron microscopy (SEM)

The **structure of the solid composites** containing natural clays (Na+) was analyzed using an electron scanning microscope model Quanta 200 F from FEI. A backscattered electron detector and low vacuum conditions were employed to obtain the SEM micrographs. These conditions allow distinguishing clearly the particles and the polymer, which facilitates the subsequent image analysis. The size of the particle agglomerates was quantified using the software Image J/Fifi.

3*.4.1.7 Tensile tests*

An Instron Machine (model 5.500R6025) was used to perform the **tensile tests** of the solid HMS PP based composites with the aim of analyzing how the two types of particles affect the mechanical properties of the polymeric matrix. The tensile experiments were performed according to the standards ISO 527/1 and 2. From these measurements, the tensile modulus (E_s) of the different PP composites was obtained.

3.4.1.8 Gel content determination

With the aim of determining the **crosslinking degree** achieved after the crosslinking process of the HDPE polymeric matrix (see section 3.3.1.3), the **gel content** produced in the HDPE based polymers was determined according to the ASTM standard D 2765-01. Specimens of the crosslinked ethylene polymers were immersed in xylene which was used as extracting solvent. The insoluble fraction of polymer remaining after a certain time is known as gel content.

3.4.2 Characterization of the foamed materials

3.4.2.1 In-situ characterization

3.4.2.1.1 Time-resolved neutron radiography

One of the more complex characterizations performed in this thesis is the in-situ characterization of the expansion process of the two types of PP, as well as, their corresponding blends (chapter 4). For the first time, the temporal evolution of a thermoplastic material foamed inside a mold has been characterized by time-resolved neutron radiography.

This technique has allowed visualizing the internal structure of polymeric foams inside a metallic mold, as that showed in section 3.3.2.3.1. An electrically heated aluminum mold was exposed to a neutron beam, which allows observing the foam expansion and ageing (Figure 3.10). The aluminum mold was located between a neutron source and a detection system that

allows acquiring several images of the expansion process that takes place when the mold is heated. Then, the foam stability has been analyzed by using quantitative parameters obtained by image analysis (Figure 3.10). More details about the image processing carried out can be found in chapter 4.

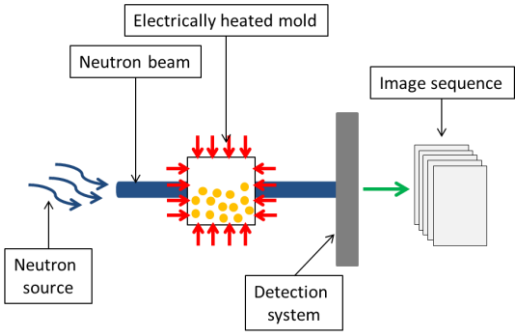

Figure 3.10. Experimental set-up employed to characterize the foam expansion by time-resolved neutron radiography.

- Neutron source: The electrically heated mold was located in the experimental hutch in the cold neutron imaging beamline ICON [15] at the Swiss Spallation Neutron Source SINQ [16] within Paul Scherrer Institute. The facility uses a pinhole geometry with variable apertures, D, at the beginning of the guide and a fixed distance between the neutron aperture and the detector of L = 7.5 m. For the experiments presented in this study a pinhole diameter of 20 mm was used, resulting into a collimation ratio L/D of 375.
- Detection system: It consists on an assembly of 6LiF/ZnS:Ag scintillator (100 microns thickness), lenses and a 16-bit cooled 2048 × 2048 pixels CCD camera (Andor Technology, model DW436). The image acquisition was conducted using a 2 × 2 binning in the CCD camera thus, yielding an effective area of 1024 × 1024 pixels and a pixel size of 27 microns. This way, the readout time from the camera was reduced and hence, the frame rate was increased. The exposure time was fixed to 5 s and the temporal resolution obtained was 10 s due to the readout delay of the camera.

3.4.2.2 Ex-situ characterization

3.4.2.2.1 Scanning electron microscopy (SEM)

A Jeol JSM-820 scanning electron microscope was used to observe the foamed samples morphology. To prepare the samples, they were first cooled using liquid nitrogen to cut them without modifying their structure and then, they were vacuum coated with a thin layer of gold to make them conductive. Different cellular parameters have been quantified: cell size distribution, average cell size (Φ), anisotropy ratio (AR), the standard deviation coefficient of the cell size distribution relative to the cell size (SDC/Φ), cell density (N_V), and coalescence ratio (CR). For this purpose, the micrographs obtained were analyzed with an image processing tool based on the software Image J/ Fiji [17].

The scanning electron microscope model Quanta 200 from FEI was also used to determine the thickness of the cell walls of the foam produced with the HMS PP based composite containing natural clays (Na+). A backscattered electron detector and low vacuum conditions were

employed to obtain the SEM micrographs. The cell wall thickness was then quantified by using the software Image J /Fiji.

3.4.2.2.2 Density determination

Throughout this thesis two different techniques have been employed to determine the density of the foamed materials. On the one hand, the geometric method consisting on dividing the weight of each specimen (measured with a high precision balance, AT 261 from Mettler) by its corresponding volume (ASTM standard D1622-08) was used with the foamed materials with a known geometry. On the other hand, the density of the foamed materials with a geometry in which it is not possible to obtain the volume by a simple measurement was determined by the Archimedes water immersion method using a high precision balance, AT 261 from Mettler (UNE-EN 1183/1).

3.4.2.2.3 Open cell content determination

The open cell content of foamed materials was determined according to the ASTM Standard D6226-10, by measuring the volume of the foamed sample with a gas pycnometer (Accupyc II 1340 from Micromeritics). If the open cell content of the samples is 0 % (the material has closed cells) the volume measured by the pycnometer matches the geometrical volume because the gas is not able to penetrate the foam. However, if the samples have a 100 % of open cell content the volume measured by the pycnometer is only the volume of the solid phase in the cellular material, because the gas, in this case, is able to penetrate the foam throughout the interconnections between cells.

3.4.2.2.4 Compression tests

Mechanical properties in compression of the whole collection of PP based foamed materials (pure PPs, PP blends and PP composites) were measured with an Instron Machine (model 5.500R6025).The compression tests were performed according to the standard ASTM D1621. From these measurements, the elastic modulus (E_{cm}), collapse stress (σ_C) and the absorbed energy per unit volume (W) were obtained.

3.4.2.2.5 X-Ray Diffraction (XRD)

Once again, XRD measurements were performed to analyze the intercalation/exfoliation degree, but in this case, of the foamed composites. The same diffractometer used to characterize the solid composites (see section 3.4.1.5) was employed with the foamed ones. In this case the foamed materials were grinded in liquid nitrogen and the XRD experiments were performed in the powder of the foam.

3.5 References

[1] F. Li, J. Ashbaugh, J. Clark. Process for Cross-Linked Polyethylene Production. Patent, US 20130216750 A1, 2013.
[2] http://www.alvestrumenti.it/files/TL_Compounder_zk-25-T_1105.pdf
[3] S. M. Tamboli, S. T. Mhaske, D. D. kale. Indian Journal of Chemical Technology, 11, 853-864, 2004.
[4] M. A. Rodriguez-Perez, J. A. de Saja, J. Escudero, A. Lopez-Gil. Procedimiento de Fabricación de Materiales Celulares de Matriz Termoplástica, Patent, WO 2014009579 A1, 2013.
[5] C. Saiz-Arroyo. Fabricación de Materiales Celulares Mejorados Basados en Poliolefinas. Relación procesado-composición-estructura-propiedades. Phd Thesis, University of Valladolid, 2012.
[6] C. Saiz-Arroyo, J. A. de Saja, J. I. Velasco, M. A. Rodriguez-Perez. Journal of Materials Science, 47, 5680-5692, 2012.
[7] C. Saiz-Arroyo, M. A. Rodriguez-Perez, J. I. Velasco, J. A. de Saja. Composites: Part B, 48, 40-50, 2013.
[8] C. Saiz-Arroyo, M. A. Rodriguez-Perez, J. Tirado, A. Lopez-Gil, J. A. de Saja. Polymer International, 62, 1324-1333, 2013.
[9] J. E. Martini-Vvedensky, N. P. Suh, F. A. Waldman. Saturation with inert gas, depressurization, and quick-cooling. Patent, US 4473665, 1984.
[10] D. Miller, V. Kumar. Cellular Polymers, 28, 25-40, 2009.
[11] J. Pinto. Fabricación y Caracterización de Materiales Poliméricos Submicrocelulares a partir de Polímeros Nanoestructurados, PhD Thesis, University of Valladolid, 2014.
[12] E. Solórzano, S. Pardo-Alonso, J.A. de Saja, M.A. Rodriguez-Perez. Colloides and Surfaces A: Physicochemical and Engineering Aspects, 438, 167–173, 2013.
[13] J. E. Mark. Physical Properties of Polymers Handbook (2nd Edition). Springer science, Washington, 2007.
[14] M. Sepe. Understanding the Value of Melt-volume Rate. Plastic Technology, 2014 (http://www.ptonline.com/columns/melt-flow-rate-testingpart-9)
[15] A. P. Kaestner, S. Hartmann, G. Kühne, G. Frei, C. Grünzweig, L. Josic, F. Schmid, E. H. Lehmann. Nuclear Instruments and Methods in Physics Research, Section A: Accelerators, Spectrometers, Detectors and Associated Equipment, 659, 387–393, 2011.
[16] B. Blau, K. N. Clausen, S. Gvasaliya, M. Janoschek, S. Janssen, L. Keller, B. Roessli, J. Schefer, P. Tregenna-Piggott, W. Wagner, O. Zaharko. Neutron News, 20, 5-8, 2009.
[17] J. Pinto, E. Solórzano, M. A. Rodriguez-Perez and J. A. de Saja. Journal of Cellular Plastics, 49, 555-575, 2013.

CHAPTER 4

POLYPROPYLENE FOAMS: EFFECT OF EXTENSIONAL RHEOLOGY ON THE FOAMING BEHAVIOR

Ester Laguna Gutiérrez

INDEX

4.1 Introduction

Due to the favorable properties of **polypropylene** (PP), high melting temperature, stiffness, capability of static load bearing, good temperature stability and high chemical resistance [1], the use of foamed materials produced with this polymer has been considered in industry, even to replace polyethylene (PE) foams or other rigid foams like polystyrene (PS) and polyurethane (PU). Nevertheless, foaming of a common linear PP is not a simple task, due to its low melt strength [2,3]. It has been proved that by the incorporation of long chain branches (LCBs) to a common linear PP the melt strength of this polymer increases [4,5]. In fact, LCB PPs are also known as high melt strength PPs (HMS PP). Nowadays, several HMS PP commercial grades are available.

The first polymeric matrix selected in this thesis has been PP due to on the one hand, the excellent properties of this polymer and on the other hand, the possibility of having commercial polypropylenes with different rheological properties. This way, by blending a common linear PP and a commercial HMS PP it is possible to obtain PP based polymeric matrices with a wide range of rheological behaviors.

In this chapter two scientific papers have been included. Both papers have a common objective: to analyze the influence of the rheological behavior on the foaming behavior of different **polypropylene blends**. However, one of the main differences between the two articles is the foaming process employed in each of them. While in the first paper the cellular materials are produced by **foaming at atmospheric pressure in a mold**, in the second paper the **improved compression molding** route is used to produce the foams. These processes differ in the rate at which the foam growth occurs (see chapter 2, section 2.4.2.3). Moreover, these papers also differ in the way in which the characterization of the foamed materials is performed. In the first one, the temporal evolution of the PP based foams is in-situ studied by using time-resolved neutron radiography, which allows visualizing the evolution of the internal structure of the foams during their production (**in-situ characterization**). In the second one, the cellular structure is first frozen, by cooling the foam and then, it is characterized by traditional methods (scanning electron microscopy), that is, an ex-situ characterization is conducted.

Taking into account the objectives of this thesis (see chapter 1, section 1.2), the results obtained from these two works would allow determining if the knowledge of the extensional behavior of the polymeric matrix is fundamental to analyze and to understand the cellular structure of the foamed materials and hence, if the extensional rheology can be used as a predictive tool with complex polymeric matrices like those showed in these studies: blends of polymers. Moreover, the fact of using two different production processes may be useful to determine on the one hand, if the relationship between extensional rheology and cellular structure is constrained by the foaming process employed and on the other hand, to determine if it is possible to relate characteristic parameters of the foaming process, like the foam/cell growth rate, with characteristic parameters of the extensional rheological test, like the Hencky strain rate (see chapter 7, section 7.4.1). Finally, due to the in-situ characterization it will be possible to visualize the mechanisms of degeneration of the cellular structure and

hence, it will be also possible to analyze how these mechanisms depend on the rheological properties of the polymeric matrix.

4.2 Foaming at ambient pressure in a mold

In this work, the extensional rheological behavior of different blends of a linear PP and a HMS PP, containing: 0, 25, 50 and 100 wt.% of the HMS PP, is characterized. From the obtained results, the strain hardening coefficient is determined (see chapter 2, section 2.2.5.4). The measurements are performed at a temperature of 200 ºC. Furthermore, a Hencky strain rate of 1 s^{-1} and a Hencky strain of 2.75 are used to quantify the strain hardening,

Then, these polymeric blends are foamed at atmospheric pressure in a mold, so that, all the cellular materials produced have the same density (225 kg/m^3). Foaming was performed at a temperature of 250 ºC. Moreover, the foaming process is in-situ characterized using time-resolved neutron radiography. With this technique, it is possible to obtain images of the foam evolution, when the foaming process is carried out inside a closed metallic mold, with a relative high spatial and temporal resolution. The experiments last typically between 1 and 2 h. Therefore, it is possible to observe not only the foam expansion but also the foam ageing, that is, the evolution of the cellular structure when the foam is subjected, for a long period of time, at high temperatures. In this work, the foam ageing is evaluated by using two different image processing techniques. With the first method the temporal evolution of the bubble coalescence is evaluated by analyzing the number of cell wall ruptures occurring during the foaming process and with the second method, the cell size evolution is studied.

Finally, these parameters (cell size and cell coalescence evolution), which allow understanding how the cellular structure degenerates, are related to the extensional rheological results in order to analyze how the extensional rheological behavior of the polymeric matrices affects their foamability.

In parallel, these polymeric matrices are also foamed at atmospheric pressure in a metallic mold but, in this case, located in a traditional air-circulating oven. The cellular structure, after solidification, is ex-situ characterized by scanning electron microscopy. This parallel study is performed in order to correlate the results obtained after solidification with those obtained in-situ.

Moreover, due to its great potential, time-resolved neutron radiography is also employed to analyze the effects that the relative density and the amount of blowing agent have on the foam stability, in this case using a single polymeric matrix. To analyze the effects obtained by varying the amount of blowing agent, three formulations containing three different contents of blowing agent (1, 2 and 7.5 wt.%) are produced.

Colloids and Surfaces A: Physicochem. Eng. Aspects 473 (2015) 46–54

Contents lists available at ScienceDirect

Colloids and Surfaces A: Physicochemical and Engineering Aspects

journal homepage: www.elsevier.com/locate/colsurfa

Polymer foam evolution characterized by time-resolved neutron radiography

E. Solórzano[a,*], E. Laguna-Gutierrez[a], S. Perez-Tamarit[a], A. Kaestner[b], M.A. Rodriguez-Perez[a]

[a] Cellular Materials Laboratory (CellMat), Condensed Matter Physics Department, University of Valladolid, Paseo de Belén, 7, 47011 Valladolid, Spain
[b] Neutron Imaging and Activation Group, Paul Scherrer Institute, 5232 Villigen, Switzerland

HIGHLIGHTS

- Dynamic neutron imaging has been used to study stability of polymer foams.
- Neutron radiography has been applied for a first time in evolving polymer foams.
- Bubble coalescence and growth have been studied by image analysis.
- Effects of density, blowing agent content and polymer rheology have been investigated.

GRAPHICAL ABSTRACT

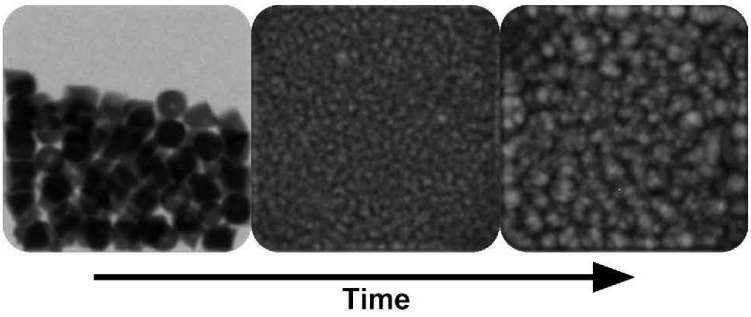

ARTICLE INFO

Article history:
Received 2 October 2014
Received in revised form 2 February 2015
Accepted 3 February 2015
Available online 10 February 2015

Keywords:
Neutron radiography
Polymer foam
Aging
Coalescence
Coarsening

ABSTRACT

For the first time, the temporal evolution of different types of polypropylene (PP) foams has been studied using time-resolved neutron radiography. This technique is advantageous since it allows visualizing the internal structure of polymeric foams inside metallic moulds during its production with excellent contrast in comparison to X-ray imaging. The experiments have been carried out in heated aluminium moulds exposed to a neutron beam (exposure time of 5 s) during a long time (1–2 h typically) thus observing the foam expansion and ageing (foam evolution at high temperature). Foam stability has been analysed as a function of different variables (liquid fraction –density–, blowing agent content and polymer rheology) by using quantitative parameters obtained by image analysis. These parameters are directly associated to cell size evolution and coalescence events. The results obtained allow determining the influence of rheological properties and process variables on the foaming behaviour of the polymer blends under study when the foaming process is carried out inside a metallic mould.

1. Introduction

The foaming process of polymeric materials is a complicated phenomenon in which several mechanisms take place simultaneously. Among others, nucleation, growth, drainage, coalescence, coarsening and solidification should be taken into account to understand and control a foaming process [1–3]. All these mechanisms

* Corresponding author. Tel.: +34 983 423572; fax: +34 983 423192.
E-mail address: esolo@fmc.uva.es (E. Solórzano).

http://dx.doi.org/10.1016/j.colsurfa.2015.02.006
0927-7757/

have a significant effect on the final cellular structure and physical properties (thermal, mechanical, etc.) of the produced foam [4]. Therefore a good understanding of these mechanisms and how they are modified by the foaming parameters and raw materials used is a key step towards the development of polymeric foams with improved properties. The study of these dynamic mechanisms is complicated and, generally, requires the use of advanced in-situ techniques in order to monitor the kinetics of these systems. A wide range of analytical techniques are used in science to analyse the evolution of processes. They are typically non-destructive methods with enough time resolution to follow a dynamic process. Some of these techniques are infrared thermography, ultrasonic imaging, X-ray imaging, X-ray diffraction, neutron imaging, infrared and Raman spectroscopy, optical testing, among others [5,6].

The application of in-situ techniques to polymeric foams has been approached by several authors from simple studies on the expansion kinetics of thermosets [7,8] and thermoplastics [9,10] that do not provide information about the evolution of the internal cellular structure to more complicated set-ups to in-situ examine the bubble nucleation in thermoplastics at high pressure conditions (30 MPa in autoclaves) by microscopy [11].

Particularly, X-ray radioscopy with time and spatial resolution has been proposed and tested on polymeric systems showing promising results [12–14]. By using this approach, it has been possible to obtain the temporal evolution of important characteristics of the cellular material such as the relative density, cell size and cell density on both thermoplastic and thermosets. Although this approach shows important advantages over previous used approaches it also has some limitations. One of the most important is that it is challenging to obtain images with high spatial and temporal resolution when the foaming process is carried out at moderate pressures (up to 4 MPa) inside a gas-tight closed metallic mould. This is due to the high X-ray absorption of metals and the low X-ray absorption of the polymeric matrix that hinders obtaining enough contrast. In fact, the previous publications using this approach have analysed the foaming process carried out at atmospheric pressure using set-ups in which the metallic lids of the mould are avoided or reduced to the maximum.

However, some of the most important technological processes to produce polymeric foams (injection moulding [15], roto-moulding [16], reactive injection moulding [17], improved compression moulding [18], etc.) are conducted at these moderate pressures inside metallic moulds (typically steel and aluminium alloys). In these processes the nucleation and growth of bubbles in the polymeric system takes place in the internal volume giving as a result foam parts with a well defined final shape and reduced density.

The mould plays a role during the process and ageing mechanisms are manifested in a different manner from those occurring in free foaming conditions. As an example macroscopic foam collapse is reduced since the foam is maintained by the mould walls. One additional advantage is that in these conditions the foam liquid fraction is fixed independently of temperature, composition, etc. The mould could additionally induced constrained growing which could result in materials with cellular structures with a significant anisotropy ratio [19,20]. In addition, temperature and surface characteristics of the walls could may induce a local densification giving as a result integral foam structures [21]. Although all these aspects are important both from scientific as well as technological perspectives, they have not been considered and studied in detail in the previous literature probably because advanced in-situ characterizing techniques are required.

Therefore, it would be very helpful to develop in-situ methods able to investigate the foam mechanisms taking place during the foaming process of polymers, at moderate pressures, and having access to their internal structure. From this point of view, the use of neutron radiography is a promising alternative. In fact, the neutron cross section for most of metals is much lower than for materials containing hydrogen (polymers). Consequently, the neutron attenuation for a metallic mould, with capacity to support high pressures, is insignificant in comparison to the absorption of the contained polymer. As a consequence neutron radiography yields optimum imaging conditions in contrast with the poor contrast obtained with X-rays in such a required configuration [22]. Therefore, it should be possible to obtain a good contrast even when the foaming process is produced in a metallic mould with significant thickness. The main limiting factor could be the spatio-temporal resolution provided by the neutron detectors which is not as high as in X-ray systems.

Bearing the previous ideas in mind in this paper we propose a methodology based on neutron radiography that allows obtaining images with enough contrast, spatial and temporal resolution to monitor the foaming process of polymeric systems taking place at moderate pressures inside metallic moulds. The methodology developed would permit observing the mechanisms taking place during the foaming processes in these conditions. Image analysis techniques will be applied on the acquired images and will allow us to quantify certain aspects related to foam ageing in the experimental conditions tested. In this research work we have tested collection of foamable systems based on thermoplastic materials (linear and high melt strength polypropylene) with different relative densities and blowing agent contents.

2. Experimental

2.1. Materials

Two different types of PP have been used in the experiments. A long-chain branched and high melt strength (HMS) PP supplied by Borealis (Daploy WB 135 HMS) and a linear PP supplied by Total Petrochemicals (PPH 4070) have been studied. The density at room temperature for both materials is 905 kg/m^3.

Different blends of these two PP materials (100, 50, 25 and 0 wt.% of HMS-PP) have been prepared with a co-rotating twin screw extruder Collin ZK 25T with L/D of 24. The rotational speed used was 80 rpm and the melt temperature was 190 °C. Two different antioxidants, Irgafos 168 and Irganox 1010 from Ciba, have also been added to the formulations. A chemical blowing agent, azodicarbonamide (ADC) Porofor M-C1 from Lanxess (d_{50} 3.9 ± 0.6 μm), has been added to these neat formulations in order to promote the foam generation at high temperatures. The previously-described extruder was used with a rotational speed of 70 rpm and a melt temperature of 180 °C. All the materials fabricated are summarized in Table 1. In this grey text denotes those neat formulations without blowing agent characterized by extensional rheology.

Table 1
Summary of the formulations produced.

Sample	HMS PP (pph)	Linear PP (pph)	ADC (pph)	Antioxidants (pph)
100–0–0	100	0	0	0.1
50–50–0	100	100	0	0.2
25–75–0	100	300	0	0.4
0–100–0	0	100	0	0.1
100–0–1	100	0	1.0	0.1
100–0–2	100	0	2.0	0.1
100–0–7	100	0	7.5	0.1
50–50–2	100	100	4.1	0.2
25–75–2	100	300	8.2	0.4
0–100–2	0	100	2.0	0.1

2.2. Extensional rheology

Measurements of extensional rheology have been carried out over neat materials (without the blowing agent) with the aim of analysing the changes in the extensional viscosity by varying the HMS-PP content. Measurements were performed using a stress-controlled rheometer (AR 2000 EX from TA Instruments) with the accessory SER-2 (Expansion Instruments). In this configuration two cylinders are used to stretch the sample, which is clamped to both cylinders rotating in opposite directions to stretch the sample [23]. Rectangular (20 mm × 10 mm) slabs of thickness 0.5 mm, fabricated by compression moulding, were used. The experiments were carried out at 200 °C.

The measurement protocol considered a pre-stretch, in order to compensate the thermal expansion of the sample when it is heated up from room temperature, and a relaxation when the pre-stretch has finished (i.e. sample is kept at the testing temperature of 200 °C with no stress during approximately 60 s). After this time the experiment takes place. Measurements have been performed at three different Hencky strain rates [24]: 0.1, 0.3 and 1 s^{-1}. The maximum Hencky strain applied has been 2.8 for all the different materials.

The evolution in the transient extensional viscosity function with time (or with strain) has been obtained for the different materials. In some polymers, a phenomenon called strain hardening takes place, which is related to a rapid increase in the extensional viscosity at high times (or strains) [25]. This phenomenon is associated to long chain branched polymers [26,27]. In general, if the polymer does not exhibit certain strain hardening it is difficult to achieve high expansion ratios during foaming because the cell walls break and the foam is not able to retain the gas during the expansion process, thus cellular structures with poor quality are obtained [28].

The Strain Hardening Coefficient (SHC), for a particular value of time (t) and Hencky strain rate ($\dot{\varepsilon}_0$), has been calculated according to Eq. (1).

$$\mathrm{SH} = \frac{\eta_E(t_r \dot{\varepsilon}_0)}{\eta^+_{E0}(t)} \quad (1)$$

where $\eta_E(t, \dot{\varepsilon}_0)$ is the extensional viscosity at a certain Hencky strain rate and $\eta^+_{E0}(t)$ is the extrapolated extensional viscosity in the linear viscoelastic regime, which can be determined using the curves for different Hencky strain rates [29,30].

2.3. In-situ foam analysis

2.3.1. Experimental set up

Pellets of the different foamable compositions were placed in an aluminium mould specially machined for this purpose. The cylindrical mould presents a rectangular cavity where the polymer containing the blowing agent is located. The internal dimensions of the cavity are 20 mm × 20 mm × 7 mm. Two aluminium lids (4 mm in thickness) maintain the polymer into the cavity even at high pressures and two frames are used to keep the full system closed. A collar heater (power 250 W) is used to heat up the system under controlled conditions. A thermocouple is located in a drilled bore in the aluminium mould in a position close to the polymer. A schematic drawing of the system is provided in Fig. 1a. Temperature control was carried out by means of a PID controller. The used system is similar to the one described by Solorzano et al. [14]. All the samples studied were subjected to the same heating program. The heating program (Fig. 1b) consisted in a pre-heating of the system at a temperature of 200 °C for 10 min in order to melt and homogenize the polymer temperature followed by a heating ramp at 10 K/min until reaching 250 °C. The sample was kept at this temperature for a time in between 1 and 2 h, sufficient to degenerate significantly the cellular structure. Different materials were studied under these conditions considering variation of relative density – i.e. amount of material introduced in the mould to reach nominal relative densities of 0.2, 0.25 and 0.3 –, blowing agent content (1, 2 and 7.5 pph of ADC) and proportions of the two studied polymers (according to Table 1).

2.3.2. Neutron imaging

The described setup was settled in the experimental hutch in the cold neutron imaging beamline ICON [31] at the Swiss Spallation Neutron Source SINQ [32] within Paul Scherrer Institute. The facility uses a pinhole geometry with variable apertures, D, at the beginning of the guide and a fixed distance between the neutron aperture and the detector of L = 7.5 m. For the experiments presented in this study a pinhole diameter of 20 mm was used, resulting into a collimation ratio L/D of 375. The detection system consisted in an assembly of 6LiF/ZnS:Ag scintillator (100 microns thickness), lenses and a 16-bit cooled 2048 × 2048 pixels CCD camera (Andor Technology, model DW436). The image acquisition was conducted using a 2 × 2 binning in the CCD camera, thus yielding an effective area of 1024 × 1024 pixels and a pixel size of 27 microns. The binning was used to reduce the readout time from the camera and thus increase the frame rate. Exposure time was fixed to 5 s and the temporal resolution obtained was 10 s due to the readout delay of the camera. Fig. 2 show a sequence of the images acquired during the experiment.

Similar experiments have been performed using X-rays in the recent years [13,14,33] although the materials, the set-ups and the methods of analysis were different. As it was mentioned in the introduction, neutron radiography offers an important additional advantage in comparison with X-ray radiography for visualizing polymers with optimum contrast [22] which is based on the enhanced neutron absorption of polymers which contain large amounts of hydrogen in their molecules [34]. In this sense, the mass attenuation coefficient of X-ray increases with increasing the atomic number, however in the case of neutrons it depends on each element [35].

2.3.3. Image processing

Foam ageing was evaluated by using two different image processing techniques. In the first method, the bubble coalescence was evaluated by means of a spatio-temporal image correlation method, i.e. by comparing consecutive images using a method similar to the one described in the work by Garcia-Moreno et al. [36]. Nevertheless, in this particular case we did not analyse the individual ruptures. Alternatively, we used the total area of the identified pixels corresponding with ruptures in every image. To this end, a binarization threshold of the detected changes in the grey level scale is previously defined. The plotted results represent the cumulative area of the identified pixels versus time. In order to eliminate statistical fluctuations due to random rupture cascades accounting for large pixel changes in comparison to local ruptures we decided to eliminate such events. A schematic description of the workflow used can be observed in Fig. 3.

The alternative technique considers a method based on FFT analysis of transmission images. The methodology is similar to the one described by Chan et al. [37]. In this methodology the pore size (Φ_{FFT}) is analysed in the Fourier space after removing the grey level fluctuations in the background (density in-homogeneities in the mesoscale). This step was done by using a high-pass filter based on large 2D median filter (15 pixels neighbourhood) and subsequently subtracting the original image from the filtered one. The output image was analysed in the reciprocal domain. The radial profile in the Fourier space is plotted and the spatial frequencies corresponding to the average pore size are identified as a broad peak. The peak position is identified by automatic methods, which permits to evaluate the peak displacement with time. Proper calibration allows

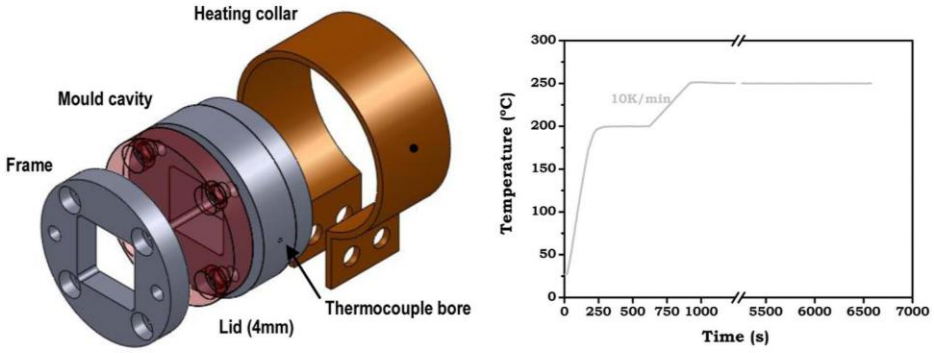

Fig. 1. (a) Schematic drawing of the experimental set up used. (b) Experimental heating curve showing the full temperature program.

correlating the spatial frequencies with the estimated average size on the identified entities (pores) in the images.

2.4. Ex-situ foam analysis

Additional experiments have been performed using an 85 mm × 85 mm × 10 mm aluminium mould with the objective of correlating the results obtained after solidification with those obtained in-situ. The final cellular structure of these materials has been evaluated and compared with the in-situ results. For this purpose the pellets containing the blowing agent are introduced in the aluminium mould which is placed in a pre-heated air-circulating oven at a temperature of 250 °C. The mould remains in the oven for 1350 s and subsequently it is introduced in cold water to stabilize the cellular structure. Materials based on the polymer blends previously described and with different relative densities have been produced for comparison.

SEM (Jeol JSM-820 scanning electron microscope) was used to perform the "ex-situ" analysis of the cellular structure. The average cell size (Φ) has been quantified using an image processing tool based on the software ImageJ/Fiji [38].

3. Results and discussion

3.1. Extensional rheology

Fig. 4a shows the transient extensional viscosity curves for the different blends under investigation, measured at three different Hencky strain rates (0.1, 0.3 and 1 s^{-1}). Curves are shifted (factor $\times 10^2$) for a better visualization of all the results. Fig. 4b shows the SHC for all materials. This value has been calculated for a Hencky strain rate of 1 s^{-1} and for a time of 2.75 s. These values will be correlated in the following sections with the stability parameters determined in the experiments. From these results, it can be concluded that HMS-PP exhibits a pronounced strain hardening while the linear PP does not exhibit this behaviour. As expected, those blends with intermediate HMS-PP content shows intermediate values for SHC. The correlation between HMS-PP content in the blends and the SCH seems to be not linear.

3.2. In-situ analysis

3.2.1. Effect of polymer type

The analysis of the foam stability for the different blends of PP at fixed blowing agent content (2 pph ADC) and fixed relative density (0.25) reveals interesting results. Foam stability has been studied both in terms of detected coalescence events and cell size evolution as explained in Section 2.3.3. Fig. 5a shows changes in the cumulative area evolution with time which provides intuitive information about the number of cell wall ruptures occurring during the foaming process. Time zero in this figure corresponds to the instant in which the cellular material has filled the mould completely and the molten cellular structure is then quasi-stable. At this moment, temperature is already constant (250 °C). From this moment, different regions in the curves can be observed. In a first region the cumulative ruptures area seems to evolve smoothly but it suffers a drastic change with a quick evolution after 700–1000 s seconds after filling the mould. In the last region, after 1600–1900 s, the foam degeneration seems to slow down probably due to the low number of pores and the rather thick cell walls. Drainage and gas pressure due to the blowing agent decomposition are the two main mechanisms causing ruptures as we will complementarily discuss in the next sections. Drainage takes some time to develop, particularly in such viscous systems, which could explain the absence of ruptures during the first seconds. Once the cell walls are sufficiently thin, ruptures triggering occurs at relatively high frequency. After

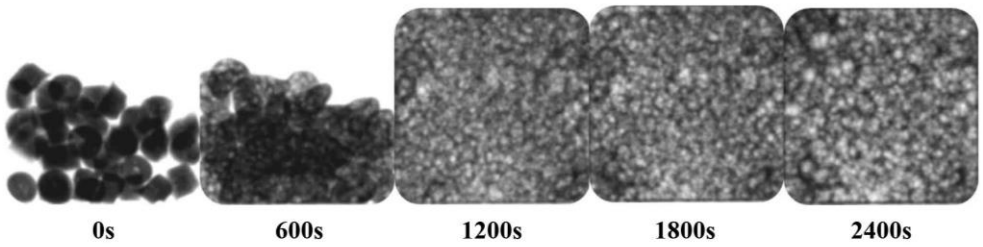

Fig. 2. Neutron radiography sequence during foam expansion and ageing (0–100–2 sample, relative density 0.2).

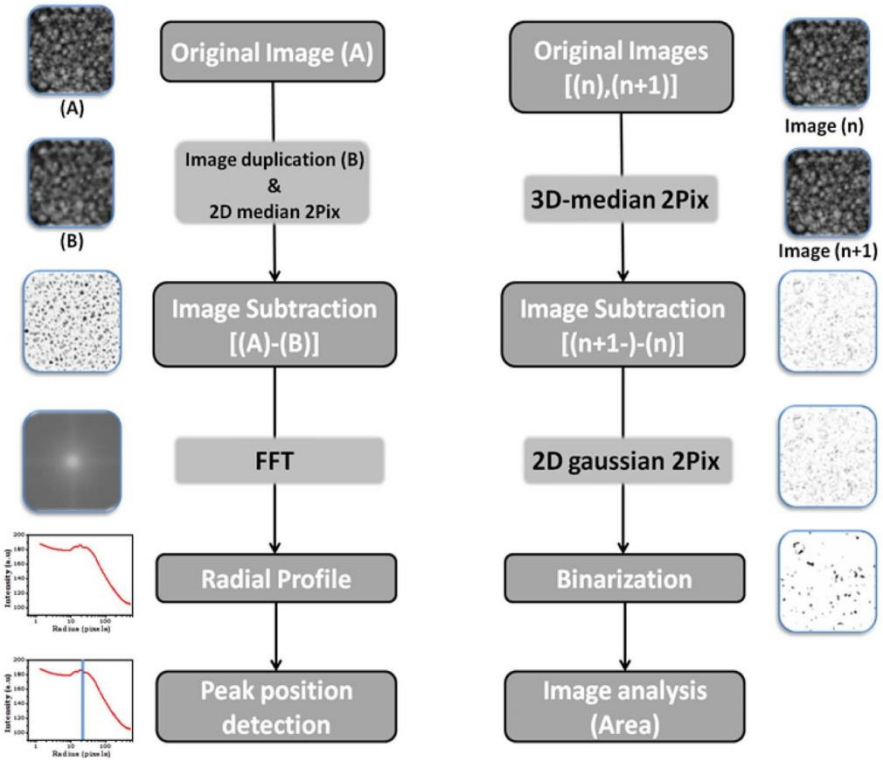

Fig. 3. Workflows for the FFT in-situ cell size analysis method in the Fourier space (left) and for the coalescence analysis by means of image correlation (right).

significant amount of ruptures had taken place the pore size increases and, as a consequence, cell walls are thicker, with again slows down the rupture phenomena. Fig. 5a, shows that the evolution of coalescence with time for the polymer blends under study is clearly different. Coalescence rate seems to depend on the amount of HMS-PP in the polymer blend. To analyse this effect in detail the slopes of the curves in the linear region (within the range 1000–2000 s) have been calculated. The results are summarized in Fig. 6 versus the SHC.

On the other hand, the cell size evolution with time for the different materials is shown in Fig. 5b. This figure shows a similar trend to the one observed for coalescence (area evolution) which points to an expected relationship between coalescence and cell size evolution. Differences for cell size evolution among polymers are more clear in comparison to Fig. 5a although the fluctuation in the cell size is high which makes more difficult to discriminate the different regions described above. These results indicate clearer differences among polymer blends in terms of cell size evolution and they also allow differentiating the initial cell sizes (when the material fills the mould) for the different polymer types. The slope of these curves in the linear region within 1000 and 2000 s has also been calculated (Fig. 6).

The rates both for cumulative area evolution and FFT cell size evolution (cell growth caused by cell wall rupture) have been

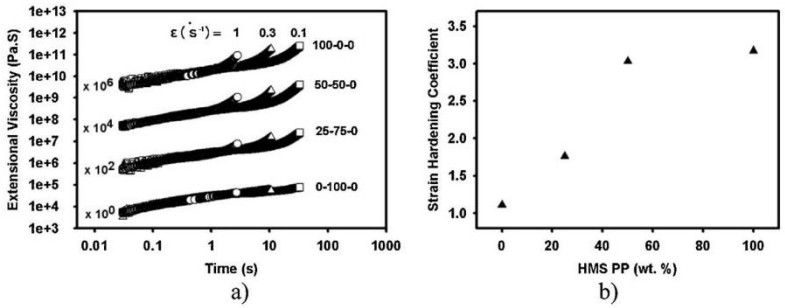

Fig. 4. Extensional rheology measurements of different PP blends. (a) Extensional viscosity of PP blends at different Hencky strain rates. (b) Strain Hardening Coefficient versus HMS PP content for a strain rate of 1 s^{-1} and a time of 2.75 s.

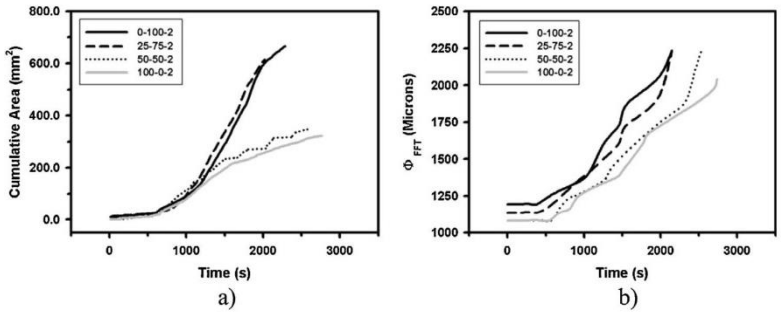

Fig. 5. Effect of polymer type on the cell coalescence and cell size evolution. (a) Changes in the cumulative area of coalescence events with time. (b) Changes in the cell size with time (2 pph ADC, relative density 0.25).

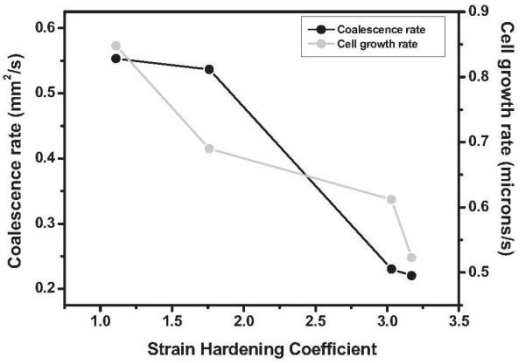

Fig. 6. SHC relationship with coalescence and cell growth rates.

represented as a function of the SHC (Fig. 6). As it can be observed both rates show a clear relationship with the SHC. The linear polymer with no strain hardening (SHC approx. 1) output the lower stability of the cell walls which gives as a result high coalescence and cell growth (degeneration) rates. When the amount of HMS PP increases the SHC is improved and the cell walls are more stable. As a result the coalescence and pore growth rates decrease. Therefore there is a reasonably correlation of the SHC with the foam stability although further studies need to be carried out.

3.2.2. *Effect of relative density*

Three different relative densities: 0.2, 0.25 and 0.3 – expansion ratios of 5, 4 and 3.3 respectively – have been studied using the same polymer blend and the same ADC content (pure linear PP, 2 pph ADC). Coalescence and cell size evolution have been studied by means of the previously explained methodologies (Section 2.3.3). Fig. 7a and b shows the obtained results. Fig. 7a shows changes in the cumulative area with time while results for cell size (Φ_{FFT}) evolution with time are shown in Fig. 7b. As explained in the previous section, the time zero corresponds to the instant in which the cellular material has filled the mould completely.

Fig. 7a reports large differences in coalescence evolution with time for the different densities. The great influence of relative density can be understood in terms of the relation between cell wall thickness and density in the case of equivalent pore sizes, i.e. the lower the relative density the thinner the cell walls. On the other hand, similarly to Fig. 5a, we can distinguish difference coalescence regimes in time although they are less evident in the case of relative density 0.2 (this experiment was stopped at shorter times). Values of the slopes in the linear regions within the range 1000–2000 s have also been calculated (Fig. 8).

Fig. 7b shows the FFT cell size evolution with time. It can be observed that initial cell size is different for the materials with different densities. As the amount of blowing agent, the polymer type and the foaming conditions are the same; the cell nucleation density should be similar in the three materials which finally yield the same number of initial pores with higher expansion, i.e. larger pores. The cell growth is also quicker in the case of the low density material considering that the wall thickness of the low density specimen is thinner so the cell walls may break easier promoting an increase in the cell size. Curiously, it can be observed that all the compared materials reach similar pore size at the end of the experiment (obviously at different times) while the coalescence analysis revealed different cumulative values at the end of each experiment. This fact could be an effect of the eliminated cascades

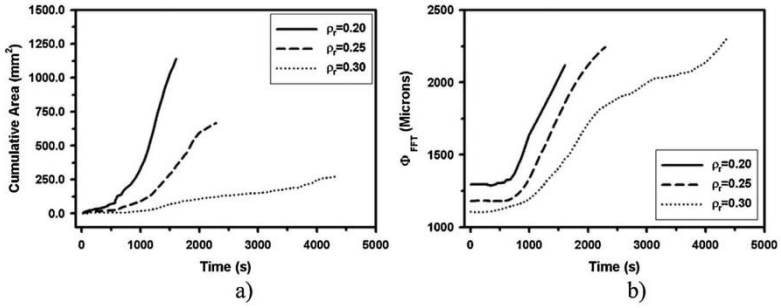

Fig. 7. Effect of the cellular material density. (a) Changes in the cumulative area with time. (b) Cell size evolution with time (pure linear PP, 2 pph ADC).

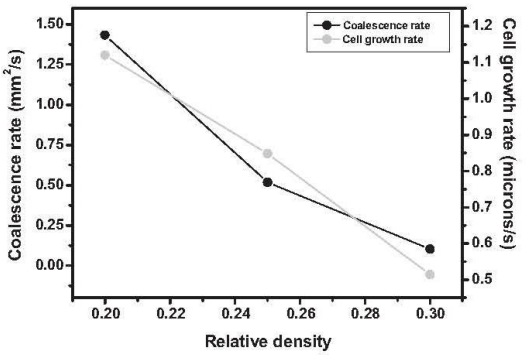

Fig. 8. Relationship of coalescence rate and cell growth rate with the relative density (pure linear PP, 2 pph ADC).

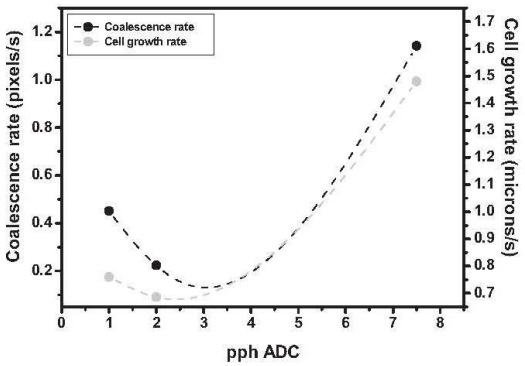

Fig. 10. Relationship of coalescence rate and cell growth rate with the blowing agent content (HMS PP, relative density 0.25).

in combination with a lower rupture detection capability of the method with density increase. The cell growth rate is higher in the low-density cellular materials in comparison to the high-density cellular materials. This result is in agreement with those obtained in Fig. 7a.

The slopes of the three curves in a linear region within the range 1000–2000 s have been calculated and correlated with the relative density in Fig. 8. The results show that both rates are completely equivalent and they correlate with density similarly to the results showed in Fig. 6.

3.2.3. *Effect of blowing agent content*

The foaming process of three different cellular materials with the same relative density (0.25) based on the same polymer (HMS PP) but with different amounts of blowing agent (1, 2 and 7.5 pph of ADC) has also been studied (Fig. 9). The evolution of the accumulative area (Fig. 9a) and the evolution of the cell size (Fig. 9b) during the foaming process have been analysed.

Both graphs show similar results, which are partially unexpected. It can be observed that the fastest degeneration in terms of coalescence and cell size evolution is obtained for the highest ADC content (7.5 pph). This can be understood in terms of excessive gas generation (cell overpressure) that causes dramatic coalescence and, as a result, cell growth. Actually 7.5 pph of blowing agent is excessive for the desired expansion (factor 4, relative density 0.25). On the other hand, the surprising result is found when comparing 1 and 2 pph ADC formulations. According to the explanation given above for the 7.5 pph ADC formulation, it would be expected to find the lowest coalescence and growth in the 1 pph ADC formulation. Nevertheless, the results are the opposite and the poorer results are found in this last case. The explanation for this phenomenon needs to consider the balance in between the gas generation and gas losses in the foam as well as the total expansion ratio. For an expansion ratio of 4 the amount of gas generated after filling the mould for the 1 pph ADC formulation might be insufficient to prevent foam collapse with time and this is observed as a higher coalescence and growth rate.

The number of experiments performed does not allow us to precisely know the optimum blowing agent content for this particular polymer type and the relative density studied but it can be approximately estimated by observing Fig. 10. The results both for coalescence and growth rates (calculated in a similar interval to previous sections) plotted versus the blowing agent content suggest that the optimum amounts in terms of these parameters would be among 2 and 3 pph of ADC.

Another interesting fact is the possibility to discriminate the different cell sizes for the different formulations at the initial time (Fig. 9b). It is observed that the lowest cell size is obtained for the material with the higher amount of blowing agent, being the largest cell size the one for the material containing the lowest amount of blowing agent. This result is related to the amount of blowing agent particles and the number of nucleated bubbles. In this sense the higher the blowing agent content the higher the nucleation and the smaller the bubbles when the foam fills the mould. This situation changes in the final foam state in the case of the material with the highest blowing agent content in which larger bubbles are obtained due to a higher coalescence.

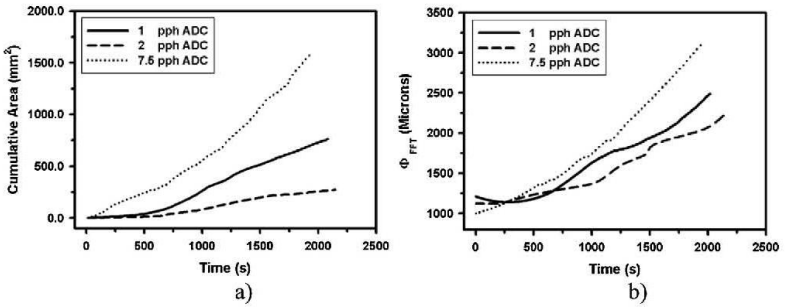

Fig. 9. Effect of the blowing agent content. (a) Changes in the cumulative area with time. (b) Cell size evolution with time (HMS PP, relative density 0.25).

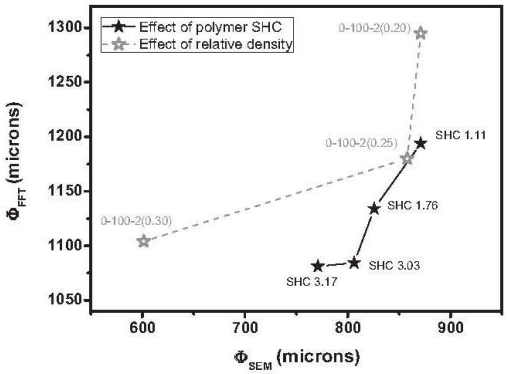

Fig. 11. Cell size comparison for in-situ and ex-situ experiments.

3.3. Comparison with ex-situ results

Different cellular materials have been complementarily manufactured according to the methodology described in Section 2.4. The cellular structure of the samples produced has been examined by scanning electron microscopy and the results, in terms of cell size, have been compared with those obtained by the in-situ methodology. To this aim, cell size at instant 1350 s – solidification time for ex-situ samples – has been taken as a reference value in the in-situ cell growth curves. Nevertheless, it is important to keep in mind that time in the in-situ curves correspond to a relative time after complete foam expansion and stabilization and therefore the time of 1350 s correspond, indeed, with the initial values plotted in these curves. It can be complementarily observed in Fig. 1 that temperature stabilization is reached at about that time. Fig. 11 shows the results of this comparison. It can be appreciated that both methods correlate reasonably well at least qualitatively showing similar trends for the effect of SCH and density. Nevertheless absolute values of the cell size are different. This could be an effect of the mould size and heating configuration, solidification and/or a low sensibility of the image analysis procedure to detect smaller pores, thus reaching higher average values.

4. Conclusions

We can state different conclusions related to methodological, rheological and processing aspects of this investigation. They can be summarized as follows:

- Neutron radiography resulted to be an ideal tool for resolving the internal structure of polymeric foamed materials in moderate pressure conditions (foaming inside thick aluminium moulds) in which X-ray imaging is not suitable. The spatial and temporal resolutions achieved are optimum for these particular experiments.
- The employed image analysis methodologies seem to correlate well with the foam stability and ageing process taking place in the different conditions explored. Both methods seem to correlate each other although the in-situ cell size determination by FFT profiling methods provides more valuable information. The validation of the in-situ results with those obtained ex-situ seems to be reasonable although the different experimental conditions used make both studies not strictly comparable. An overestimation of the cell size by the FFT method seems to be plausible although the information is still largely valuable obtaining relative tends.
- The experimental results provide important results for the interpretation of the influence of polymer rheology, foam density and blowing agent content in the foam stability. This stability is not considered in terms of the foam macroscopic collapse but in the microscale evaluating the coalescence and/or the cell size increase. Accordingly to these results the strain hardening coefficient has certain effect on foam stability although relative density seems to have a higher influence. The blowing agent also causes rapid cell degeneration when added in excessive contents. Nevertheless, all these studied variables are coupled and need to be further studied and separated in order to reveal the complete interrelationship associated to the foam stability in these materials.

Acknowledgments

This work has been supported by the Junta of Castile and Leon and the European Social Fund for the PIRTU (contract of E. Laguna-Gutierrez (EDU/289/2011)). Funding for Juan de la Cierva contract of E. Solórzano (JCI-2011-09775) and materials research project (MAT2012-34901) supported by the Ministry of Economy and Competitiveness and FEDER funds are also acknowledged. Financial assistance from the Junta of Castile and Leon (Project VA035U13) is gratefully acknowledged.

References

[1] K.C. Khemani, Polymeric foams an overview, in: K.C. Khemani (Ed.), Polymeric Foams: Science and Technology, ACS Symposium Series, Washington DC, 1997, pp. 1–7.
[2] D. Eaves, Handbook of Polymeric Foams, Rapra Technology, United Kingdom, 2004.
[3] D. Klempner, V. Sendijarevic, Handbook of Polymeric Foams and Foam Technology, second ed., Hanser Publishers, Munich, 2004.
[4] L.J. Gibson, M.F. Ashby, Cellular Solids: Structure and Properties, second ed., Cambridge University Press, Cambridge, 1997.
[5] L. Cartz, Nondestructive Testing, ASM International, Materials Park, Ohio, 1995.
[6] C. Hellier, Handbook of Nondestructive Evaluation, McGraw-Hill, New York, 2003.
[7] A. Van Thuyne, B.J. Zeegers, Kinetic study on flexible polyurethane foams formation, J. Cell. Plast. 14 (1978) 150–160.
[8] Y. Jianqiu, Z. Jianyaun, W. Dening, H. Chunpu, Y. Shengkang, C. Yiou, C. Yufu, C.X. Ziqian, S. Jin, W. Yin, A modified method for developing gel/rise profile of urethane foams, J. Cell. Plast. 26 (1990) 39–49.
[9] J.I. Velasco, M. Antunes, O. Ayyad, J.M. Lopez-Cuesta, P. Gaudon, C. Saiz, M.A. Rodriguez-Perez, J.A. de Saja, Foaming behaviour and cellular structure of LDPE/hectorite nanocomposites, Polymer 48 (2007) 2098–2108.
[10] E. Solorzano, M. Antunes, C. Saiz-Arroyo, M.A. Rodriguez-Perez, J.I. Velasco, J.A. De Saja, Optical expandometry: A technique to analyze the expansion kinetics of chemically blown thermoplastic foams, J. Appl. Polym. Sci. 125 (2012) 1059–1067.
[11] Q. Guo, J. Wang, C.B. Park, M. Ohshima, A microcellular foaming simulation system with a high-pressure drop rate, Ind. Eng. Chem. Res. 45 (2006) 6153–6161.
[12] S. Pardo-Alonso, E. Solorzano, S. Estravis, M.A. Rodriguez-Perez, J.A. De Saja, In situ evidence of the nanoparticle nucleating effect in polyurethane–nanoclay foamed systems, Soft Matter 8 (2012) 11262–11270.
[13] S. Pardo-Alonso, E. Solorzano, M.A. Rodriguez-Perez, Time-resolved X-ray imaging of nanofiller-polyurethane reactive foam systems, Colloid Surf. A 438 (2013) 119–125.
[14] E. Solórzano, S. Pardo-Alonso, J.A. de Saja, M.A. Rodriguez-Perez, X-ray radioscopy in-situ studies in thermoplastic polymer foams, Colloid Surf. A 438 (2013) 167–173.
[15] X. Xu, C.B. Park, Injection foam moulding, in: M.R. Kamal, A.I. Isayev, Avraam, S.J. Liu (Eds.), Injection Moulding Technology and Fundamentals, Hanser, Munich, 2009, pp. 273–307.
[16] D. Xu, R. Pop-Iliev, C.B. Park, Fundamental study of CBA-blown bubble growth and collapse under atmospheric pressure, J. Cell. Plast. 41 (2005) 519–538.
[17] L.J. Lee, Fundamentals of reaction injection moulding, in: G. Allen, J.C. Bevington (Eds.), Comprehensive Polymer Science, Pergamon Press, Oxford, New York, 1989.
[18] C. Saiz-Arroyo, J. Tirado, A. López-Gil, J.A. de Saja, M.A. Rodríguez-Pérez, Structure-properties relationship of medium density polypropylene foams, Polym. Int. 62 (2013) 1324–1333.
[19] B.M. Patterson, K. Henderson, R.D. Gilbertson, S. Tornga, N.L. Cordes, M.E. Cahvez, Z. Smith, Morphological and performance measures of polyurethane foams using X-ray CT and mechanical testing, Microsc. Microanal. 20 (2014) 1284–1293.

[20] A.R. Hamilton, O.T. Thomsen, L.A.O. Madaleno, L.R. Jensen, J.C.M. Rauhe, R. Pyrz, Evaluation of the anisotropic mechanical properties of reinforced polyurethane foams, Compos. Sci. Technol. 87 (2013) 210–217.
[21] E. Solorzano, M.A. Rodriguez Perez, Cellular materials, in: D. Lehmhus, M. Busse, A.S. Herrmann, K. Kayvantash (Eds.), Structural Materials and Processes in Transportation, Wiley-VCH Verlag GmbH & Co. KGaA, Weinheim, 2013.
[22] E. Solórzano, S. Pardo-Alonso, N. Kardijilov, I. Manke, F. Wieder, F. García-Moreno, M.A. Rodriguez-Perez, Comparison between neutron tomography and X-ray tomography: A study on polymer foams, Nucl. Instrum. Meth. B 324 (2014) 29–34.
[23] M. Sentmanat, B.N. Wang, G.H. McKinley., Measuring the transient extensional rheology of polyethylene melts using the SER universal testing platform, J. Rheol. 49 (2005) 585–606.
[24] H.A. Barnes, J.F. Hutton, F.R.S. K. Walters, An Introduction to Rheology, Elsevier, Amsterdam, 1989.
[25] S.T. Lee, Foam Extrusion: Principles and Practice, Technomic Publishing Company, Lancaster, 2000.
[26] R.P. Lagendijk, A.H. Hogt, A. Buijtenhuijs, A.D. Gotsis, Peroxydicarbonate modification of polypropylene and extensional flow properties, Polymer 42 (2001) 10035–10043.
[27] A.D. Gotsis, B.L.F. Zeevenhoven, A.H. Hogt, The effect of long chain branching on the processability of polypropylene in thermoforming, Polym. Eng. Sci. 44 (2004) 973–982.
[28] H.E. Naguib, C.B. Park, U. Panzer, N. Reichelt, Strategies for achieving ultra low density polypropylene foams, Polym. Eng. Sci. 42 (2002) 1481–1492.
[29] J. Stange, C. Uhl, H. Münstedt, Rheological behavior of blends from a linear and a long-chain branched polypropylene, J. Rheol. 495 (2005) 1059–1079.
[30] A.K. Chaudhary, K. Jayaraman, Extrusion of linear polypropylene–clay nanocomposite foams, Polym. Eng. Sci. 51 (2011) 1749–1756.
[31] A.P. Kaestner, S. Hartmann, G. Kühne, G. Frei, C. Grünzweig, L. Josic, F. Schmid, E.H. Lehmann, The ICON beamline – A facility for cold neutron imaging at SINQ, Nucl. Instrum. Meth. A 659 (2011) 387–393.
[32] B. Blau, K.N. Clausen, S. Gvasaliya, M. Janoschek, S. Janssen, L. Keller, B. Roessli, J. Schefer, P. Tregenna-Piggott, W. Wagner, O. Zaharko, The Swiss spallation neutron source SINQ at Paul Scherrer Institute, Neutron News 20 (2009) 5–8.
[33] E. Solórzano, F. García-Moreno, J. Pinto, S. Pardo-Alonso, M.A. Rodríguez-Pérez, Application of a microfocus X-ray imaging apparatus to the study of cellular polymers, Polym. Test. 32 (2013) 321–329.
[34] T. Imae, T. Kanaya, M. Furusaka, N. Torikai, Neutrons in Soft Matter, John Wiley and Sons, Inc., Hoboken, New Jersey, 2011.
[35] J. Banhart, A. Borbély, K. Dzieciol, F. Garcia-Moreno, I. Manke, N. Kardjilov, A.R. Kaysser-Pyzalla, M. Strobl, W. Treimer, X-ray and neutron imaging – Complementary techniques for materials science and engineering, Int. J. Mater. Res. 101 (2010) 1069–1079.
[36] F. Garcia-Moreno, E. Solórzano, J. Banhart, Kinetics of coalescence in liquid aluminium foams, Soft Matter 7 (2011) 9216–9223.
[37] C.D. Chan, M.E. Seitz, K.I. Winey, Disordered spheres with extensive overlap in projection: Image simulation and analysis, Microsc. Microanal. 17 (2011) 872–878.
[38] J. Pinto, E. Solórzano, M.A. Rodriguez-Perez, J.A. de Saja, Characterization of the cellular structure based on user-interactive image analysis procedures, J. Cell. Plast. 49 (2013) 555–575.

4.3 Foaming by improved compression molding (ICM)

In this work the rheological behavior of different blends of a linear PP and a HMS PP, containing: 0, 10, 25, 50, 75, 90 and 100 wt.% of HMS PP is analyzed. On the one hand, the rheological behavior in shear is characterized by small amplitude oscillatory tests and rotational tests in order to determine the zero shear viscosity of the different samples and the miscibility of the two PPs. Then the extensional behavior is also measured and the strain hardening coefficient is quantified. These last measurements are performed at 200 ºC and the strain hardening is quantified for a value of the Hencky strain rate of 1 s^{-1} and for a value of the Hencky strain of 3.

Then, these blends are foamed, in this case by improved compression molding (ICM), at a temperature of 200 ºC. An important difference between this technique and the employed in the previous paper is the rate at which the foam growth occurs. The foam growth rate is faster in ICM than in foaming at atmospheric pressure. This technique allows producing cellular materials with the same density (180 kg/m^3) and with a size and a shape enough for measuring mechanical properties in compression.

After cooling the foam, to stabilize its structure, the cellular structure is carefully analyzed and different structural parameters are quantified: the average cell size, the anisotropy ratio, the standard deviation coefficient of the cell size distribution relative to the cell size, the cell density and the coalescence ratio. The open cell content of the different foamed materials is also determined and finally, the mechanical properties in compression of the different cellular materials are analyzed, paying particular attention to parameters such as: the elastic modulus, the collapse stress and the absorbed energy per unit volume.

Finally, the effect of the extensional rheological behavior on the cellular structure is analyzed with the aim of establishing a relationship between extensional rheology and cellular structure. Moreover, by the fact of having cellular materials with the same density, as well as, raw polymeric matrices with similar mechanical properties, it is also possible to establish a relationship between cellular structure and mechanical properties.

Applied Polymer SCIENCE

Understanding the foamability and mechanical properties of foamed polypropylene blends by using extensional rheology

Ester Laguna-Gutierrez,[1] Rob Van Hooghten,[2] Paula Moldenaers,[2] Miguel Angel Rodriguez-Perez[1]
[1]Cellular Materials Laboratory (CellMat), Condensed Matter Physics Department, University of Valladolid, 47011 Valladolid, Spain
[2]Department of Chemical Engineering, KU Leuven, B 3001 Heverlee Leuven, Belgium
Correspondence to: E. Laguna-Gutierrez (E-mail: ester.laguna@fmc.uva.es)

ABSTRACT: In this article, the influence of the rheological behavior of miscible blends of a linear and a high melt strength, branched, polypropylene (HMS PP), on the cellular structure and mechanical properties of cellular materials, with a fixed relative density, has been investigated. The rheological properties of the PP melts were investigated in steady and oscillatory shear flow and in uniaxial elongation in order to calculate the strain hardening coefficient. While the linear PP does not exhibit strain hardening, the blends of the linear and the HMS PP show pronounced strain hardening, increasing with the concentration of HMS PP. Related to the cellular structure, in general, the amount of open cells, the cell size, and the width of the cell size distribution increase with the amount of linear PP in the blends. Also mechanical properties are conditioned by the extensional rheological behavior of PP blends. Cellular materials with the best mechanical properties are those that have been fabricated using large amounts of HMS PP. The results demonstrate the importance of the extensional rheological behavior of the base polymers for a better understanding and steering of the cellular structure and properties of the cellular materials. © 2015 Wiley Periodicals, Inc. J. Appl. Polym. Sci. **2015**, *132*, 42430.

KEYWORDS: blends; foams; mechanical properties; rheology; structure-property relationship

Received 2 January 2015; accepted 29 April 2015
DOI: 10.1002/app.42430

INTRODUCTION

A polymeric cellular material consists of a two-phase structure, in which a gaseous phase, derived from a blowing agent, has been dispersed in a solid polymeric matrix.[1,2] This structure allows these materials to be used in applications such as packaging, sports and leisure, toys, thermal insulation, automotive, military, aircraft, buoyancy, or cushioning.[3] Particularly, polyolefin-based cellular materials keep some of the properties of polyolefins such as toughness, flexibility, resistance to chemicals and abrasion, and recyclability.[4,5] Currently, polyethylene (PE)-based cellular materials dominate the market of polyolefin foams. However, owing to the favorable properties of polypropylene (PP), its use has been considered in the industry, even replacing PE foams or other rigid foams such as polystyrene or polyurethane. PP is superior to PE in several aspects. It has a high melting temperature, stiffness, and the capability of static load bearing. Moreover, PP has a cost similar to PE, good temperature stability, and a good chemical resistance.[6]

Nevertheless, foaming of common linear PP is not a simple task, owing to its rheological properties, especially owing to its weak melt strength.[7,8] It is difficult to achieve high expansion ratios (ERs) during foaming because the cell walls break and the foam is not able to retain the gas during the expansion process.[9] A way to improve the foaming of a linear PP is to incorporate long-chain branches (LCBs).[10] The PPs with LCBs have a pronounced strain hardening, which is closely related to an enhancement of the melt strength.[11] Different methods have been applied to modify PP by LCB. Most of the LCB PPs are produced by *in situ* polymerization and by post-reactor treatment. After the reactor treatment, the LCBs can be formed by reactive extrusion or by electron beam irradiation.[12,13] Nowadays, several LCB PP commercial grades are available.

Several studies have shown that foaming of LCB PPs, either pure branched PP or blended with linear PP, leads to higher ERs and more homogeneous cellular structures.[9,14–16] Naguib *et al.*[9] analyzed the way to obtain larger volume ERs. For this purpose, they used a branched PP and long-chain blowing agents (pentane and butane). The fabrication route used was extrusion foaming. They also lowered the melt temperature and optimized the process conditions. The ER obtained from the linear PP was much lower than that from the branched PP, which indicates that branched PPs are more effective for the production of low-density foams. Park and Cheung[15] studied the cell nucleation and initial growth in linear and branched PP-based cellular materials foamed by extrusion. While the degree of cell coalescence was severe in the linear PP foams and

most of the cells were interconnected to each other, the branched PP gave a better foam structure. Nam *et al.*[16] studied the effect of modifying PP by the addition of LCB and the resulting effects on the rheological properties and performance of extrusion foams. More specifically, when PPs had LCBs, the foam density became lower. It was determined that the long-chain branching of PP was the main factor affecting the foam density.

The effect of blending linear and LCB PPs on foam properties has been the subject of different studies.[17–19] Reichelt *et al.*[17] described the optimization of the physical foaming by extrusion, changing different parameters, of a LCB PP and the corresponding blends with a PP block copolymer. They found a correlation between the extensional rheology and the lower limit of foam density for the blends. Blends rich in LCB PP show better foamability owing to their higher melt strength. Spitael and Macosko[18] investigated the influence of the strain hardening on foaming by extrusion of blends of linear and LCB PPs. They did not find a direct correlation between the amount of strain hardening and the foam cell density. The balance between the large nucleation of the linear PP and the reduction of the cell coalescence due to the important strain hardening of the LCB PP can lead to a higher cell concentration in the blends of linear and branched PPs than in the neat polymers. Stange and Münstedt[19] studied the influence of LCBs on the foaming behavior of PP. Different branching contents were achieved by blending a linear PP and a LCB PP. They found an almost linear increase of the strain hardening with the amount of LCB PP. Moreover, in the foaming tests, they observed a significant increase of the ER (reduction of density) by the addition of LCB PP, although this value remained constant from a concentration of the LCB PP higher than 50%. Related with the average cell size, they found that cell size decreased with the amount of LCB PP, which can be explained by a reduction of cell coalescence and cell collapse due to the increased melt strength.

Because of the foaming method used in these papers (extrusion foaming) foam density was not constant for materials containing different amounts of LCBs. These different densities make it difficult to compare between the different foams and to analyze the structure–property relationships. Moreover, the characterization of the cellular structure was mainly based on the average cell size and cell density. A more detailed characterization of the structure was typically not reported. Finally, the size and shape of the produced materials were not sufficient to measure mechanical properties in compression tests.

Bearing these limitations in mind, one of the aims of this study is to investigate the effect of long-chain branching on the cellular structure and mechanical properties of PP-based cellular materials with the same density. For this purpose, different branching contents were achieved by blending a linear and a HMS PP. Cellular materials were fabricated by improved compression molding (ICM), a technique that allows controlling the foam density. A detailed characterization of the cellular structure has also been carried out. In addition, this investigation aims to analyze the importance of the rheological behavior in the foaming process and to find a relationship between the strain hardening, the cellular structure, and the mechanical properties of PP-based cellular materials.

EXPERIMENTAL

Materials

Two different PPs have been used. The first PP is a branched high melt strength PP (HMS PP) supplied by Borealis (PP Daploy WB 135 HMS) with a tensile modulus of 2000 MPa. The second PP is a linear PP (linear PP) supplied by Total Petrochemicals (PPH 4070) with a tensile modulus of 1950 MPa. The density at room temperature is 900 kg m^{-3} for both PPs.

Blends of the two PPs at different contents of linear PP (10, 25, 50, 75, and 90 wt %) have been prepared with a co-rotating twin screw extruder Collin ZK 25T with L/D of 24. The rotational speed used was 80 rpm and the melt temperature was 190°C. The sample code used with the different blends is the following: wt % HMS PP – wt % linear PP.

Antioxidants Irgafos 168 and Irganox 1010 (from Ciba) have also been used to reduce the thermal degradation of the polymers.

The foaming was performed using a chemical blowing agent, azodicarbonamide (ADC) Lanxess Porofor M-C1 with an average particle size of 3.9 ± 0.6 μm and a decomposition temperature of 210°C.

Foaming Process

ICM is a technique that allows controlling, regardless of the formulation, the density of cellular materials. In addition, the volumes produced by this technique are large enough to subsequently perform compression tests or other macroscopic characterizations.[20–22]

Before the foaming process, the pellets containing the blowing agent were fabricated. For this purpose, the formulations produced were mixed with 3 wt % of ADC using the same co-rotating twin screw extruder, previously described, with a rotational speed of 100 rpm and a melt temperature of 180°C. Irgafos 168 in a proportion of 0.08% and Irganox 1010 in a proportion of 0.02% by weight were added to the formulation.

Once the final formulation was fabricated, the pellets are placed in a mold [Figure 1(a)], which is located in a hot-plate press. An initial pressure (P_0) is applied to the system while it is heated until the foaming temperature (T_F), which is higher than the decomposition temperature of the blowing agent [Figure 1(b)]. As the temperature increases, the blowing agent starts decomposing and the pressure inside the mold increases up to a value (P_F). After a certain time (t_F), when the blowing agent is fully decomposed, and P_F does not continue to increase, the pressure of the press is released allowing the polymer to expand until the desired ratio [Figure 1(c)]. A scheme of the mold and of the ICM technique is shown in Figure 1.

Finally, the mold is introduced in cold water to cool down the sample and hence stabilizing the cellular structure as fast as possible.[23]

Foaming parameters t_F, P_0, and T_F can be chosen depending on the polymeric matrix type, chemical composition, blowing agent

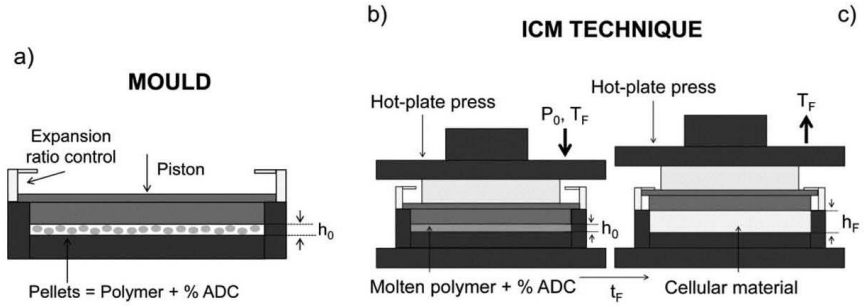

Figure 1. (a) Scheme of the mold used in the ICM technique. (b) Heating of the system until the foaming temperature (T_F) under a pressure P_0. (c) Release of pressure allowing the polymer to expand from an initial height (h_0) to a final height (h_f).

concentration, and sample geometry. In this case, t_F was 15 min, P_0 was 41.5 bars, and T_F was 200°C. These parameters were maintained for all the cellular materials fabricated.

The control of foam density is essential in this study. It is carried out by means of a self-expandable mold as can be seen in Figure 1. Owing to this, density can be fixed at a given value.[20–22] All the cellular materials have been fabricated with a density of 180 kg m^{-3} (ER 5 and relative density 0.2) independently on the chemical composition used. Foamed samples were discs with 150 mm in diameter and 10 mm in thickness.

Samples Characterization

Differential Scanning Calorimetry. Thermal properties of the pure PPs and the different PP blends were studied by means of a Mettler DSC822e differential scanning calorimeter, previously calibrated with indium, zinc, and *n*-octane. The weight of the samples was ~5.5 mg.

The melt and crystallization temperature were determined according to the following thermal protocol:

- First segment: Samples were heated from −40 to 250°C at a heating rate of 10°C min^{-1} under nitrogen atmosphere. In order to remove materials thermal history, an isothermal segment (3 min) was added at the end of this heating segment.
- Second segment: Samples were cooled from 250 to −40°C at a cooling rate of 10°C min^{-1} under nitrogen atmosphere.
- Third segment: Samples were heated a second time from −40 to 250°C at a heating rate of 10°C min^{-1} also under nitrogen atmosphere.

The melt temperature (T_m) was taken at the minimum of the heat flow–temperature curve (third segment). The crystallization temperature (T_c) was taken at the maximum of the heat flow–temperature curve (second segment), and also the difference between the melt temperature and the crystallization temperature ($\Delta T = T_m - T_c$) was calculated.

Rheological Behavior. Shear rheological measurements were performed at a temperature of 200°C under nitrogen atmosphere using a parallel plates geometry of 25 mm in diameter and a gap of 1 mm. Cylindrical samples (without blowing agent) with a thickness of 1.5 mm and a diameter of 22 mm were prepared in a hot plate press at a temperature of 220°C. A stress-controlled rheometer AR 2000 EX from TA Instruments was used to perform the tests.

Dynamic-mechanical experiments over an angular frequency range of $0.1 < \omega < 100$ rad s^{-1} were performed for all materials. A strain of 5% was used, which was in the linear viscoelastic regime for all samples. In this frequency range, the response regime, where G'' and G' and are proportional to ω and ω^2, respectively, was not reached. This regime was achieved by the application of time–temperature superposition, after performing measurements at a temperature of 250°C. Only the blends 100–0, 50–50, and 0–100 have been measured at 250°C. In addition to the oscillatory experiments, the start-up and steady-state shear viscosity were measured at different shear rates (between 0.004 and 1 s^{-1}).

Extensional rheology of the neat PPs and the different blends was measured using a strain-controlled rheometer (Ares-2K from TA Instruments) with the extensional viscosity fixture (EVF). In this geometry, two cylinders are used to wind-up the sample. One cylinder is rotating and the other measuring the force. In order to wind-up the sample equally on both sides, the rotating cylinder moves on a circular orbit around the force-measuring cylinder while rotating around its own axis at the same time. All the experiments were made at a temperature of 200°C (this is the same temperature at which the foaming process was performed). Rectangular solid samples, with dimensions of 20 mm × 10 mm × 0.5 mm ($L \times W \times T$), fabricated by compression molding, at a temperature of 200°C and a pressure of 21.8 bars, were used.

The following measurement protocol was applied:

- Pre-stretch: Once the sample is attached to the drums and it has melted a pre-stretch is performed in order to compensate the thermal expansion of the sample when it is heated up from room temperature. This pre-stretch was done at a Hencky strain rate of 7.5×10^{-3} s^{-1}.
- Relaxation post pre-stretch: When the pre-stretch is finished, the sample is kept for 30 s at a constant temperature (200°C) without applying any stress.

- Test: After this relaxation the experiment takes place. The measurements have been performed at three different Hencky strain rates: 0.1, 0.3, and 1 s^{-1}. The final Hencky strain has been 3 for all the different materials.

To evaluate the extensional viscosity measurements it is necessary to know the density at the temperature at which the experiment is being performed. For PPs this melt density is tabulated.[24] The melt density at a temperature of 200°C for PP is 750 kg m^{-3}.

Mechanical Tests. For the cellular materials, mechanical properties in compression have been measured. Stress (σ)–strain (ε) curves were obtained with an Instron Machine (model 5.500R6025) at room temperature and at a strain rate of 10 mm min^{-1}. The maximum static strain was 75% for all the experiments. The compression experiments were performed according to the standard ASTM D1621. Samples were cubes with dimensions of 20 mm × 20 mm × 10 mm ($L \times W \times T$) cut from the samples produced by ICM. The compression tests have been performed on two different samples of the same cellular material and always in a parallel direction to the foaming direction (thickness direction). Three mechanical properties were obtained from these experiments: elastic modulus (E), collapse stress (σ_C), which was measured in the intersection between a parallel line to the stress–strain response at low strains and a parallel line to the plateau region of the stress–strain curve, and absorbed energy per unit volume (W) that has been calculated as the area under the stress–strain curve up to 75% strain.

Density. Density of the cellular materials was determined by using the geometric method: dividing the weight of each specimen by its corresponding volume (ASTM standard D1622-08). Density was measured for 10 different samples from the cellular material. These samples were cubes with dimensions of 20 mm × 20 mm × 10 mm ($L \times W \times T$).

Open Cell Content. Open cell content of foamed materials was determined according to the ASTM Standard D6226-10 using a gas pycnometer Accupyc II 1340 from Micromeritics.

The following equation was used according to the ASTM standard:

$$\mathrm{OC}(\%) = 100\left(\frac{V_{\mathrm{sample}} - V_{\mathrm{pyc}}}{V_{\mathrm{sample}} \cdot p}\right), \tag{1}$$

where V_{sample} is the geometrical volume of the sample, V_{pyc} is the volume measured by the gas pycnometer, p is the sample porosity calculated by $\left(1-\frac{\rho_{\mathrm{cm}}}{\rho_s}\right)$, ρ_{cm} is the cellular material density, and ρ_s is the solid matrix density.

If the open cell content of the samples is 0% (the material has closed cells) the volume measured by the pycnometer matches the geometrical volume because the gas is not able to penetrate the foam. However, if the samples have a 100% of open cell content the volume measured by the pycnometer is only the volume of the solid phase in the cellular material, distributed between the struts and walls, because the gas in this case is able to penetrate the foam throughout the interconnections between cells.

Structural Characterization. Scanning electron microscopy (SEM) was used to analyze the cellular structure, and also to quantify the cell size distribution, the average cell size (Φ), the anisotropy ratio (AR), the standard deviation coefficient of the cell size distribution relative to the cell size (SDC/Φ), the cell density (N_V), and the coalescence ratio (CR). For this purpose, the micrographs obtained were analyzed with an image processing tool based on the software Image J.[25]

Samples were cooled using liquid nitrogen to cut them without modifying their structure; then, they were vacuum coated with a thin layer of gold to make them conductive. A Jeol JSM-820 scanning electron microscope was used to observe the samples morphology. A more detailed description of the experimental techniques can be found elsewhere.[26–28]

The average cell size (Φ) for a given material is defined as indicated in eq. (2).

$$\Phi = \sum_{i=1}^{n}\frac{\Phi^i}{n} = \sum_{i=1}^{n}\frac{\mathrm{cf}}{2n}\left(\Phi_x^i + \Phi_y^i\right), \tag{2}$$

where n is the number of counted cells, Φ^i is the three-dimensional cell size of the cell i, Φ_x^i and Φ_y^i are the chord lengths of the cell i in the x and y directions, and cf is a correction factor needed to calculate the cell size in 3D from a two-dimensional value. While the average two-dimensional cell size $\left(\frac{\Phi_x^i+\Phi_y^i}{2}\right)$ is directly measured by the software, previously mentioned, a correction factor (cf) is used to calculate the three-dimensional cell size. This correction factor was determined by Pinto *et al.*[25] Moreover, in this work, the expansion direction is the y direction. The characterization has been performed only in a plane (x–y). This is because as a consequence of the foaming process employed (ICM) it holds that ($\Phi_x^i \approx \Phi_z^i$).

The AR is defined as the ratio of the chord length in the expansion direction (Φ_y^i) to that in a perpendicular direction (Φ_x^i).[29] Taking into account this definition an isotropic cell has an AR of 1.

The SDC relative to the cell size has been calculated according to eq. (3).[21,30]

$$\frac{\mathrm{SDC}}{\Phi} = \frac{1}{\Phi}\sqrt{\sum_{i=1}^{n}\frac{\left(\Phi^i-\Phi\right)^2}{n}}. \tag{3}$$

SDC/Φ is related to the width of the cell size distribution and consequently gives information about the homogeneity of the cellular structure. A low value of SDC/Φ indicates a narrow, and therefore a homogeneous cell size distribution, where all cells have a size close to the average value.

The cell density (N_V) is the number of cells per unit volume of the solid. The following expression [eq. (4)] has been used to calculate the cell density.

$$N_V = \frac{6}{\pi\Phi^3}\left(\frac{\rho_s}{\rho_{\mathrm{cm}}} - 1\right). \tag{4}$$

In the case of no coalescence N_V measures the cell nucleation density.[25]

Table I. DSC Results of the Polypropylene Blends

Sample (HMS PP-linear PP)	T_m (°C)	T_c (°C)	ΔT (°C)
100-0	161.5	127.3	34.2
90-10	162.2	126.7	35.5
75-25	162.7	126.8	35.9
50-50	163.7	126.5	37.2
25-75	165.2	126.0	39.2
10-90	165.9	125.1	40.8
0-100	164.3	121.4	42.9

Finally, the CR has been calculated as the ratio between the potential nucleation density and the measured cell density (N_V).

$$CR = \frac{\text{Nucleants/cm}^3}{N_V}. \quad (5)$$

Chemical blowing agents such as ADC are self-nucleating particles for the cells, which means that when the blowing agent content increases, a greater number of nucleating sites are available.[2,22] The potential nucleation density can be calculated according to eq. (6).

$$\frac{\text{Nucleants}}{\text{cm}^3} = \frac{W_P \rho_C}{\rho_P V_P}, \quad (6)$$

where W_P is the weight fraction of the ADC particles used to produce the cellular materials, ρ_C is the density of the polymeric composite (PP + ADC), ρ_P is the density of particles, the ADC particles, and V_P is the volume of an individual particle. In this case it has been assumed that ADC particles are 3.9 μm side cubes. The ADC density is 1600 kg m^{-3}.

RESULTS AND DISCUSSION

Thermal Characterization

Table I shows the melting point (T_m), the crystallization temperature (T_c), and the difference between the melt temperature and the crystallization temperature (ΔT) for the different materials, obtained from the differential scanning calorimetry (DSC) curves. This difference is very important to analyze the stabilization of the cellular structure. The smaller the difference is, the quicker the stabilization of the cellular structure occurs, i.e., the cellular structure has less time to degenerate during the cooling process.

The difference between both temperatures increases significantly (nearly 9°C) if the content of linear PP increases. Therefore, from the point of view of the DSC results, it is more favorable to work with the HMS PP than with the linear PP in order to stabilize as fast as possible the cellular structure.

Rheological Behavior

The modulus of the complex shear viscosity (η^*) of the linear PP, the HMS PP, and the blend 50–50 is shown in Figure 2.

The dynamic shear viscosity of the HMS PP is somewhat lower than that of the linear PP. Blend 50–50 has a value of the viscosity between the values of the linear PP and the HMS PP. The difference between the viscosity of the linear and the HMS PP becomes more pronounced at higher frequencies. The HMS PP is the material, which exhibits the most pronounced shear thinning behavior owing to the presence of LCBs and the significant contribution of the high molecular weight parts. In this material the transition to the Newtonian plateau region occurs at lower frequencies.[31,32] In addition, it can be observed that the Newtonian plateau has been reached for the three materials at low frequencies.

To analyze the miscibility of both PPs the logarithmic additivity rule for low-molecular-weight-based blends is used.[33] This rule is expressed as follows:

$$\log(\eta^*(\omega)) = \varphi_{\text{HMS PP}} \log\left(\eta^*(\omega)_{\text{HMS PP}}\right) + (1-\varphi_{\text{HMS PP}}) \log\left(\eta^*(\omega)_{\text{linear PP}}\right), \quad (7)$$

where $\varphi_{\text{HMS PP}}$ is the HMS PP content in volume percent and $\eta^*(\omega)_{\text{HMS PP}}$ and $\eta^*(\omega)_{\text{LINEAR PP}}$ are the complex viscosities of the pure HMS PP and the pure linear PP, respectively.

Table II shows the experimentally obtained modulus of the complex shear viscosity at a frequency of 1 rad s^{-1} and the theoretical one obtained with the log additivity rule at the same frequency. It also shows the deviation of the theoretical results from the experimental results.

The maximum deviation of the theoretical value from the experimental one is only 4%, indicating that the polymeric blends obey the log additivity rule and consequently this result suggests a clear miscibility of both PPs.

The loss angle is a very sensitive indicator of the presence of LCBs in a polymer. Figure 3 shows the loss angle (δ) as a function of frequency for the materials 100–0, 50–50, and 0–100.

The linear PP demonstrates a monotonic decrease in loss angle with frequencies. The angle approaches the value of 90° at low frequencies indicating that sample is predominantly viscous. The HMS PP, however, shows an inflection in the curve with a tendency toward a plateau at high frequencies, although in this range of frequencies the plateau is not observed. Wood-Adams *et al.*[34] reported that there was a plateau in the loss angle whose magnitude and breadth depend on the degree of LCB. Finally, it

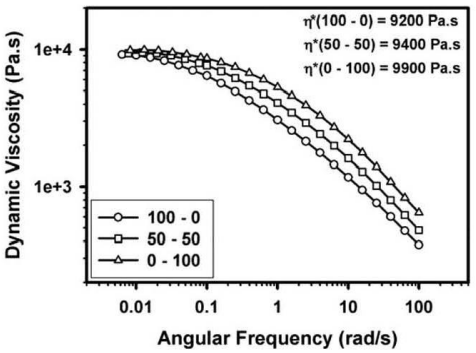

Figure 2. Dynamic shear viscosity versus angular frequency of materials: 100–0, 50–50, and 0–100.

Table II. Experimental and Theoretical Values Obtained by the Log Additivity Rule of the Complex Shear Viscosity (η^*) at a Frequency of 1 rad s^{-1} and at a Temperature of 200°C

Sample (HMS PP-linear PP)	Experimental η^* (Pa s)	Theoretical η^* (Pa s)	Deviation (%)
100-0	3065	3065	0
90-10	3198	3237	1
75-25	3420	3514	3
50-50	4088	4029	1
25-75	4792	4619	4
10-90	5050	5013	1
0-100	5295	5295	0

can be concluded that the loss angle of the HMS PP at low frequencies is somewhat lower than that of the linear PP, indicating that the HMS PP exhibits a more elastic response characteristic of solid materials.[35]

The start-up shear viscosity (η) has been measured in all the PP blends at different shear rates until the steady state was reached. Figure 4 shows the steady-state shear viscosity as a function of shear rate.

For a shear rate ($\dot{\gamma}$) of 0.01 s^{-1}, or lower, all the materials have reached a Newtonian plateau. Moreover, the shear viscosity increases with the amount of linear PP in the same way as the dynamic shear viscosity did (see Figure 2). Figure 4 also contains the values of the zero shear viscosity (η_0). Comparing the values of dynamic shear viscosity at low frequencies (at the Newtonian plateau) with the values of zero shear viscosity it can be concluded that these values are very similar and consequently these PP materials satisfy the viscoelastic limiting behavior.

$$\lim_{\omega \to 0} \eta^*(\omega) = \lim_{\dot{\gamma} \to 0} \eta\left(\dot{\gamma}\right) \tag{8}$$

Finally, extensional viscosity measurements have been performed on these PP blends. Extensional viscosity is defined as

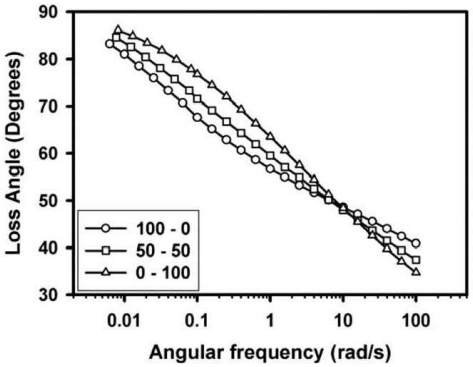

Figure 3. Loss angle versus angular frequency of materials: 100–0, 50–50, and 0–100.

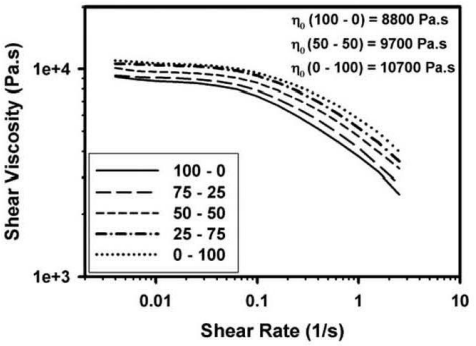

Figure 4. Shear viscosity as a function of shear rate of the pure PPs and the different blends.

the ratio between the stress and the strain rate, when a material is elongated. In some polymers, a phenomenon called strain hardening takes place, which is related to a rapid increase in extensional viscosity at high strains.[36]

The strain hardening phenomenon is associated to LCB polymers.[10,14] For polymers with the same melt flow index, an increase in the number of the long-chain branches induces strain hardening in the elongational viscosity of the melt. Because of the increase of the strain hardening behavior a strong enhancement of the melt strength appears.

Figure 5(a,b) shows the transient extensional viscosity of the seven PP blends under investigation, measured at three different Hencky strain rates. As it is indicated on the figure, the results of each blend have been multiplied by a certain value in order to compare all the materials in the same graph.

The HMS PP exhibits a pronounced strain hardening, whereas the linear PP does not display strain hardening. As the content of HMS PP increases, the slope of the curves, in the region of strain hardening, also increases.

To quantify this strain hardening behavior, the strain hardening coefficient (S), for a particular value of time and Hencky strain rate, has been determined according to eq. (9):

$$S = \frac{\eta_E^+(t, \dot{\varepsilon}_0)}{\eta_{E0}^+(t)}, \tag{9}$$

where $\eta_E^+(t, \dot{\varepsilon}_0)$ is the transient extensional viscosity as a function of time and Hencky strain rate and $\eta_{E0}^+(t)$ is the transient extensional viscosity in the linear viscoelastic regime, which can be determined in two different but equivalent ways: as three times the transient shear viscosity growth curve at very low shear rates or by extrapolating the superimposed portion of the curves for different elongation rates.[37,38] In the present work, the first option has been chosen to determine S.

Figure 6 shows the strain hardening coefficient for all materials. This value has been calculated for a Hencky strain rate of 1 s^{-1} and a time of 3 s, because during the foaming process the Hencky stain rates applied are around 1 s^{-1} and the Hencky strains are approximately between 3 and 4.[18,36]

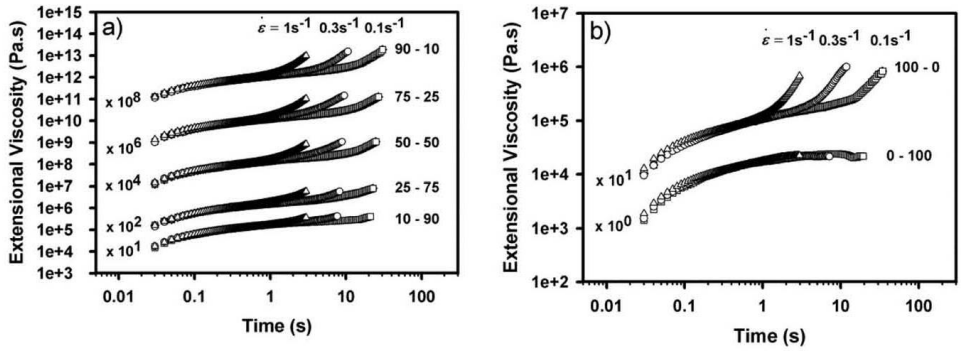

Figure 5. (a) Extensional viscosity of PP blends at different Hencky strain rates, $\dot{\varepsilon}$. (b) Extensional viscosity of pure PPs at different Hencky strain rates, $\dot{\varepsilon}$.

Essentially this coefficient increases if the amount of HMS PP increases, although this behavior is not so clear when large amounts of HMS PP are used. The linear PP has a value of S equal to 1, indicating again that this material does not present strain hardening as is also shown in Figure 5.

The shear and extensional rheological properties of the PP blends depend both on the amount of the HMS PP in the blend. However, it is clear that the extensional properties are far more sensitive to the effect of LCB. Hence, differences in the structural and mechanical properties of the resulting PP cellular materials are related to the change in the extensional properties, as the shear viscosity is only slightly decreased by the addition of the HMS PP.

Cellular Materials Density and ER

The results for the density and also for the expansion ratio (ER) of the PP cellular materials produced by the ICM route are shown in Table III. The ER is defined as the ratio between the solid density (ρ_s) and the cellular material density (ρ_{cm}).

$$ER = \frac{\rho_s}{\rho_{cm}}. \quad (10)$$

The materials with contents of HMS PP higher than 25 wt % reach the expected relative density. For the other two materials the density is slightly higher and consequently the ER is slightly lower. Under the processing conditions used, these materials are not able to achieve an ER of 5. The linear polymer is not capable of supporting the induced stretching during foaming. As a result, the cell walls are broken and the gas can escape through the open cells (see next section).

Open Cell Content

The open cell content has been measured to quantify the interconnection between the cells of the different cellular materials. High open cell content leads to poor mechanical properties, low thermal insulation, good acoustic absorption, and low dimensional stability.[39–41] In thermoplastic polymers, the open cell content is related to the expansion degree. In low-density cellular materials, the polymeric matrix is subjected to high elongational forces during the foaming. Cellular walls consequently become thinner and they can easily break. For cellular materials with very similar density the extensional rheological behavior is closely related to the open cell content as it is shown in Figure 7.

When the strain hardening coefficient is low, the open cell content of the cellular material is high. For the cellular materials fabricated with a high content of HMS PP, in which S is approximately constant, the open cell content is also constant. Moreover, it can be deduced from Figure 7 that when the polymer has a value of S lower than 4, cells are completely open for the foam densities produced. As the ER and the shear rheological properties are very similar, for all blends under investigation, it can be concluded that changes in the extensional rheological behavior lead to changes in the open cell content.

The high open cell content of the pure HMS PP (about 50%) can be explained by the high content of blowing agent used to manufacture the cellular materials (3 wt %). Subsequent studies (not published) have demonstrated that the minimum amount

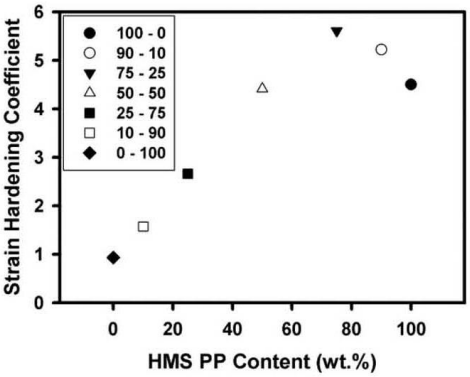

Figure 6. Strain hardening coefficient of the different blends of the HMS PP and the linear PP.

Table III. Cellular Materials Density and Expansion Ratio

Sample (HMS PP-linear PP)	Density (kg m^{-3})	SD[a] (kg m^{-3})	Expansion ratio	SD[a]
100-0	178	6	5.11	0.17
90-10	182	4	5.00	0.10
75-25	181	5	5.03	0.14
50-50	180	3	5.06	0.08
25-75	183	12	4.97	0.34
10-90	194	15	4.69	0.40
0-100	207	17	4.42	0.40

[a] Standard deviation.

of ADC required to achieve an ER of 5 with the HMS PP is almost half of that used in this study. If the amount of blowing agent is too high the open cell content can increase owing to an overpressure inside the mold during the polymer expansion process.

Cellular Structure

Figure 8 shows SEM micrographs of the different cellular materials fabricated by ICM. It is clear that the rheological properties of the blends influence the cellular structure, which in turn determines the mechanical response of PP foams.

Several conclusions can be drawn from the observation of these micrographs. First of all, SEM micrographs demonstrate, qualitatively, that the open cell content increases with the amount of linear PP, as was concluded from the quantitative pycnometry measurements (previous section). Ruptures of cell walls can be observed in the cellular materials 10–90 and 0–100. Secondly, it can be concluded that the average cell size also increases with the amount of linear PP.

Regarding the cell anisotropy, the blend 25–75 leads to a very anisotropic structure. When the amount of linear PP is reduced cells are more isotropic, although cells are never completely isotropic. The anisotropic nature of the cellular materials is mainly related to the ICM foaming process used to manufacture the cellular materials. The growth of the cellular material is restricted by the mold and the expansion can only occur in one direction, promoting this anisotropic growth.

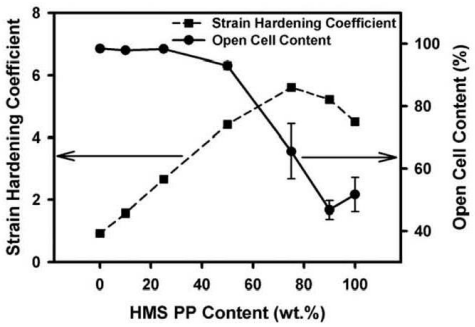

Figure 7. Correlation between the strain hardening coefficient and the open cell content.

In order to analyze the homogeneity of the cellular structure the cell size distribution of the cellular materials has been evaluated. Figure 9 shows the corresponding histograms.

All cellular materials present a wide cell size distribution. This width increases with the amount of linear PP. When the amount of HMS PP prevails the cell size distribution is narrower indicating that the cellular structure is more homogeneous. When the amount of linear PP increases the cells start to break as the polymer cannot withstand the deformation to which it is subjected and consequently larger cells begin to appear, although there are still cells that have not been broken. In fact all the histograms present a maximum for a cell size of ~250 μm; however, while the cell size of the cellular materials with a high content of HMS PP is always lower than 600 μm, in the cellular materials with a high content of linear PP there are cells with sizes up to 900 μm.

With the aim of quantifying the qualitative results previously mentioned, several characteristics of the cellular structure were measured. Figure 10 shows the results for the average cell size and AR.

The average cell size (Φ) and the AR remain almost constant for the cellular materials generated with blends with a content of the HMS PP higher than 75 wt %. In these materials also the strain hardening coefficient is almost constant. For values of the HMS PP content lower than 75 wt % and increment in the average cell size is produced when the amount of linear PP increases and therefore the strain hardening coefficient decreases. Moreover, for all these materials the open cell content is 100%, which leads to the following conclusion. PP-based open cell cellular materials with differences in the average cell size of 80 μm can be obtained by changing the proportion of linear PP and HMS PP, provided that the linear PP content is higher than 25 wt %.

Relative to the AR, the cellular material 25–75 has an AR higher than 3. This high value is a consequence of a partial rupture of the cells as well as the restricted foaming in one direction. When the amount of linear PP is higher than 75 wt % the polymer is so weak than most of the cell walls are completely broken and consequently cells lose their anisotropy.

In order to better evaluate the cell anisotropy, the average chord length in the expansion direction ($\Phi_y = \Sigma_{i=1}^{n} \frac{\Phi_y^i}{n}$) and the average chord length in a perpendicular direction to the expansion one ($\Phi_x = \Sigma_{i=1}^{n} \frac{\Phi_x^i}{n}$) have been calculated. Figure 11 shows the

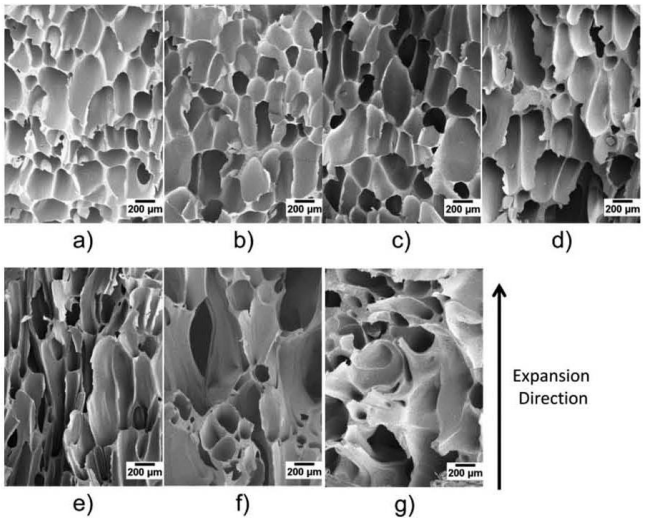

Figure 8. SEM micrographs of the cellular materials. (a) 100–0, (b) 90–10, (c) 75–25, (d) 50–50, (e) 25–75, (f) 10–90, and (g) 0–100.

average chord length in both directions as a function of the HMS PP content.

In general, the average chord length in the expansion direction (y) is higher than in the perpendicular direction (x). For cellular materials that have been fabricated with a HMS PP content higher than 75 wt % both Φ_x and Φ_y are constant. For cellular materials that have been fabricated with a HMS PP content between 25 and 75 wt %, it can be observed that while Φ_x remains almost constant Φ_y increases with the amount of linear PP. That means that in these materials some of the cellular walls, which are perpendicular to the expansion direction, are breaking and consequently cells are growing considerably in the expansion or thickness direction, making the anisotropy to increase. Finally, when the cellular materials have been fabricated with a HMS PP content lower than 25 wt %, it can be concluded that cell coalescence is produced in both directions making the cells to growth in the expansion direction and also in the perpendicular one. As a result cell loss their anisotropy, as has been already shown in Figure 10.

Another way to analyze the cell size distribution is to use the standard deviation coefficient of the cell size distribution relative to the average cell size (SDC/Φ). Owing to the large amount of samples included in this study, the use of SDC/Φ is a good and an easy way to compare the results obtained with the different blends (Figure 12).

The highest values of SDC/Φ are obtained for the cellular materials in which the amount of linear PP is predominant, as is also shown in Figure 9. This high value means that the cellular structure is very heterogeneous presenting small and large cells with a cell size far away from the average cell size. The relationship between SDC/Φ and the open cell content is shown in Figure 13.

When the amount of linear PP increases the strain hardening decreases and consequently the materials have a higher open cell content as is shown in Figure 7. Figure 13 shows that SDC/Φ increases if the open cell content increases. As the cells are breaking, new cells appear with a larger cell size resulting in a more heterogeneous cellular structure and consequently increasing SDC/Φ. Furthermore, for cellular materials with 100% open cell, SDC/Φ continues increasing as the percentage of linear PP increases.

Another parameter, related to the cellular structure, is the cell density (N_V). Results as a function of blend composition are shown in Figure 14.

It can be observed that the number of cells per cubic centimeter increases with the amount of HMS PP. This result is consistent with the average cell size results. When the amount of HMS PP is lower than 75 wt % the cell density increases with the amount of HMS PP. For these materials the average cell size decreased with the amount of HMS PP (Figure 10) indicating, as expected, that for cellular materials with the same density the cellular density increases when the average cell size decreases. Moreover, for cellular materials with a HMS PP content higher than 75 wt % the cellular density remains almost constant in the same way than the average cell size.

Finally, to conclude this study of the cellular structure, the CR has been calculated for all materials.[22] CR has been defined in eq. (5) as the ratio between the potential nucleation density of ADC–PP mixtures and the measured cell density. CR is considered as a quantitative measurement of the

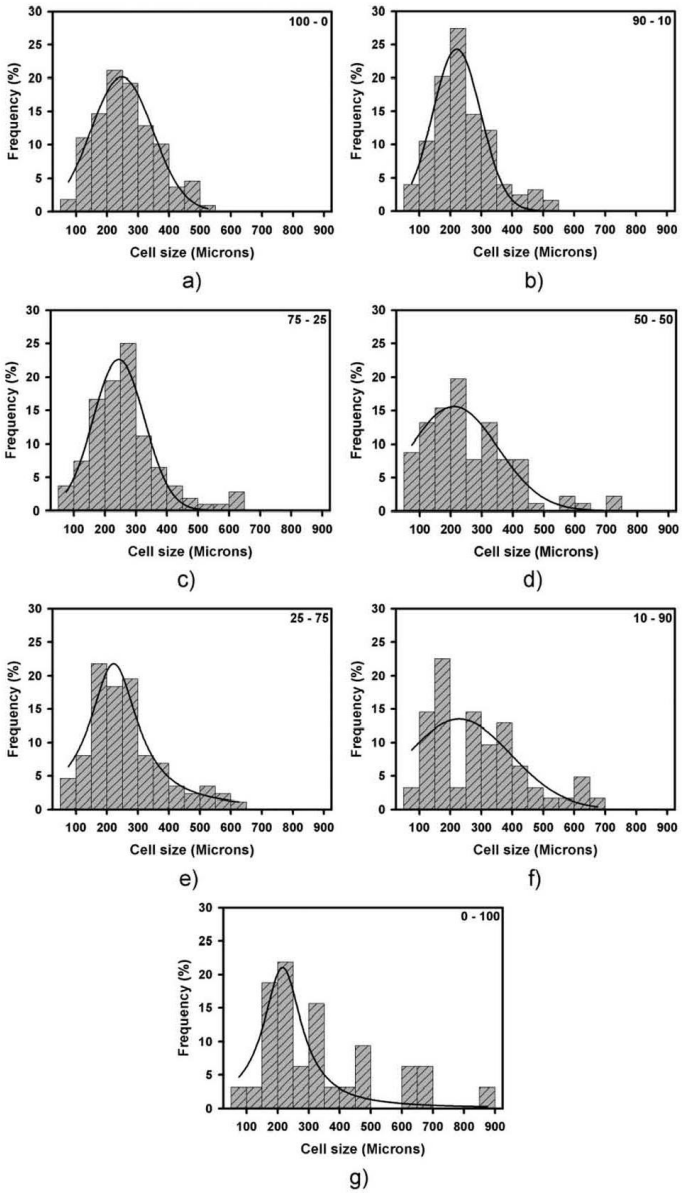

Figure 9. Cell size distribution of cellular materials. (a) 100–0, (b) 90–10, (c) 75–25, (d) 50–50, (e) 25–75, (f) 10–90, and (g) 0–100.

degeneration of the cellular structure during the foaming process. If CR is equal to 1, it means that the potential nucleation density and the cell density are the same, i.e., no degeneration of the cellular structure by coalescence or coarsening occurs. Results of CR as a function of the HMS PP content are shown in Figure 15.

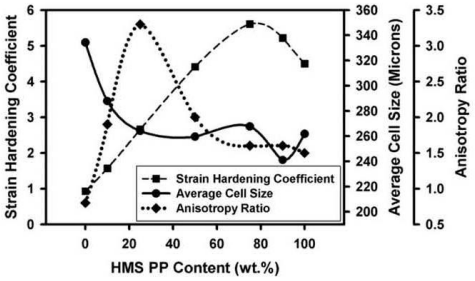

Figure 10. Effect of HMS PP content and strain hardening coefficient in the average cell size and anisotropy ratio of the cellular materials.

The CR remains constant for the cellular materials, which have been fabricated with an amount of HMS PP higher than 75 wt %. For these materials the CR is equal to 1000 which means that only 1 of every 1000 potential cells survives during the foaming process. On the other hand, when the amount of HMS PP is lower than 75 wt % the CR increases if the linear PP content also increases. For the cellular material fabricated only with the linear PP the CR is as high as 5000 indicating that in this material only 1 out of every 5000 cells survive during the foaming process. With this parameter (CR) it is easy to understand and to demonstrate how the coalescence increases if the linear PP content increases.

Mechanical Response

As with all polymer blends, the final blend properties depend on the properties of the individual components and the blend ratio. Moreover, the mechanical properties of the polymeric cellular materials also depend on the mechanical properties of the solid matrix. The tensile moduli of the different solid blend materials are the same as the tensile moduli of the HMS PP (2 GPa) and linear PP (1.95 GPa) are very similar and also the two polymers are completely miscible. As a consequence, the differences in the mechanical properties of the obtained polymeric cellular materials are mainly related to the differences in the cellular structure, open cell content, cell size, and cell AR, among others, as the density is almost the same for all cellular materials and the polymeric matrixes have very similar properties.[27]

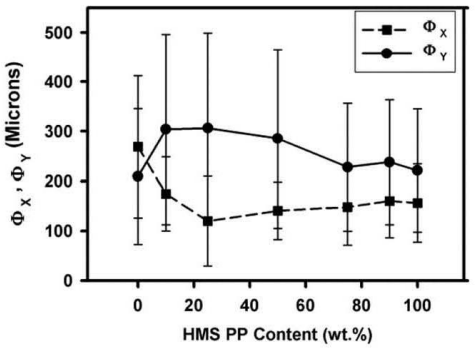

Figure 11. Average chord length in the x and y directions (Φ_x and Φ_y) as a function of the HMS PP content.

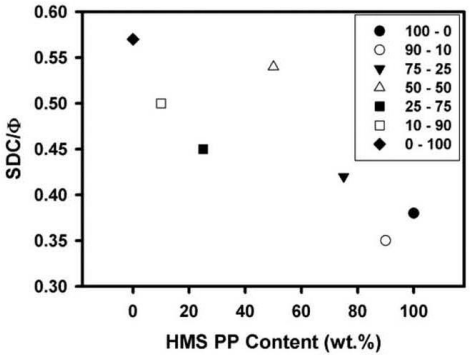

Figure 12. SDC/Φ for the complete collection of PP cellular materials.

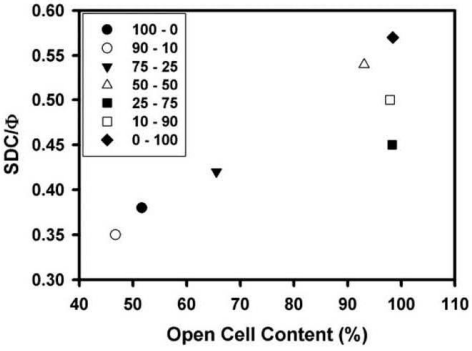

Figure 13. Relationship between SDC/Φ and the open cell content.

Foamed samples were analyzed by performing the compression test aforementioned (in the Experimental section). Experimental

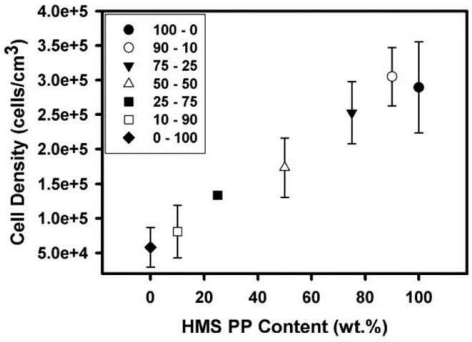

Figure 14. Variation of cell density with the HMS PP content.

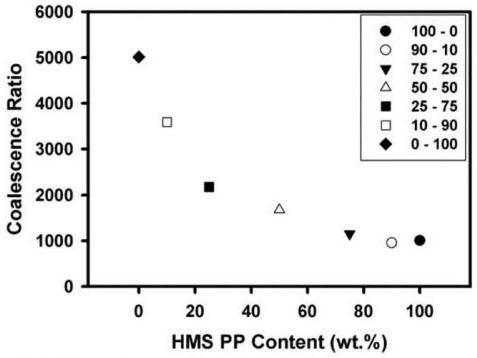

Figure 15. Coalescence ratio as a function of the HMS PP content.

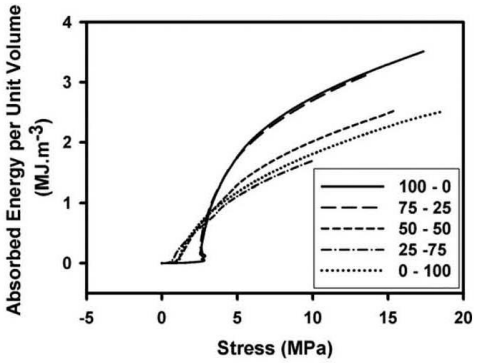

Figure 17. Energy absorption diagrams for samples with different HMS PP content.

results for elastic modulus (E) and collapse stress (σ_C) are summarized in Figure 16 together with the open cell content, to analyze the influence of this parameter on the mechanical behavior.

Comparing the results obtained for the different blends it can be observed that when the amount of HMS PP increases, the stiffness of the foamed blends improves, as the increase in the elastic modulus indicates. The elastic modulus of the cellular materials fabricated with the pure HMS PP is 10 times higher than the elastic modulus of the cellular materials fabricated with the linear PP (even if the density of these last materials is slightly higher). The same behavior is obtained for the collapse stress. There is a significant increase of the collapse stress due to the increase of the HMS PP content. In this case the collapse stress is 2.5 times higher in the cellular materials fabricated with the HMS PP than in those fabricated with the linear PP. The improvement in both mechanical properties is due to a combination of different factors: the reduction of the open cell content, the reduction of the average cell size, and the consequent increase in cell density and the reduction of the standard deviation coefficient of the cell size distribution relative to the cell size, which involves an increase of the homogeneity of the cellular structure. These aspects in turn are related to the extensional behavior of the blends.

The value of absorbed energy per unit volume (W) has also been calculated from the stress–strain curves. Taking into account that cellular materials are typically used as energy absorbers, it is desirable to comprehend how the amount of HMS PP can affect the energy absorption capability. The method used to analyze this characteristic is based on the so-called energy absorption diagrams.[22,27] An energy absorption diagram is obtaining by representing the absorbed energy, W, as a function of the stress. The absorbed energy has been calculated using eq. (11).

$$W = \int_0^{\varepsilon} \sigma(\varepsilon)\, d\varepsilon \ . \tag{11}$$

Figure 17 shows the absorbed energy per unit volume versus the stress for most of the cellular materials produced.

The best cellular material for a given stress is the one that absorbs the most energy up to this stress.[27] For stresses lower than 2.5 MPa, the cellular materials that contain an amount of HMS PP lower than 50 wt % absorb more energy than materials

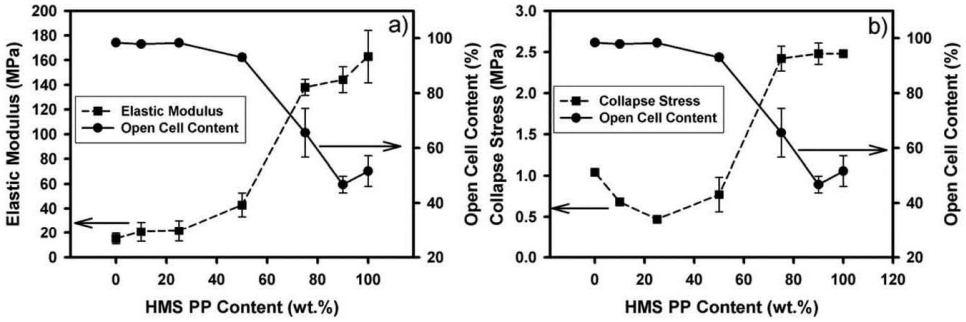

Figure 16. (a) Relationship between the elastic modulus and the open cell content for the different blends. (b) Relationship between the collapse stress and the open cell content for the different blends.

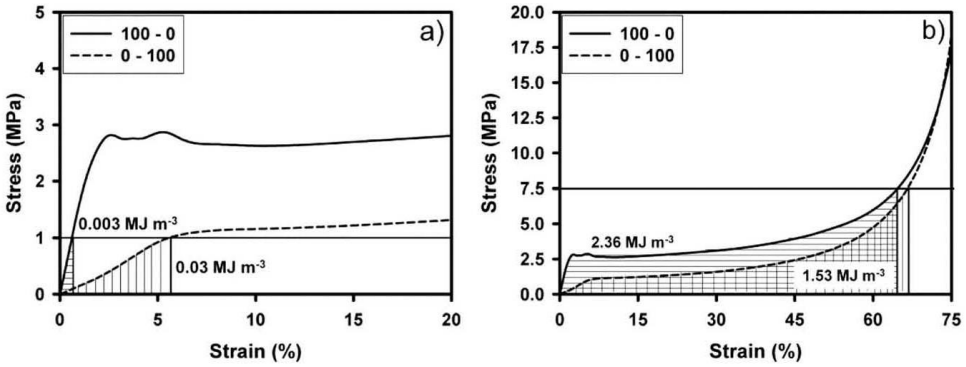

Figure 18. (a) Absorbed energy for a stress of 1 MPa. (b) Absorbed energy for a stress of 7.5 MPa.

that contain an amount of HMS PP higher than 50 wt %. For stresses higher than 2.5 MPa this behavior is completely opposite, the cellular materials that contain the highest amounts of HMS PP are the best energy absorbers. These behaviors are explained graphically in Figure 18 where the stress–strain curves for the materials 100–0 and 0–100 and the correspondent absorbed energy for a stress of 1 and 7.5 MPa are represented.

In the first figure [Figure 18(a)] the absorbed energy (area under the curve) has been calculated for a stress of 1 MPa. As the stiffness of the linear PP is lower than the stiffness of the HMS PP, the energy absorbed by the linear PP is higher than the energy absorbed by the HMS PP. However, for high stress values, the absorbed energy is higher in the HMS PP than in the linear PP as Figure 18(b) shows, indicating that depending on the required properties it is better to use one or the other cellular polymer.

CONCLUSIONS

PP-based cellular materials with very similar density have been fabricated using the ICM route. For this purpose, blends of a HMS PP and a linear PP have been used. The relationships between the extensional rheological properties of the polymeric matrix, the cellular structure, and the mechanical properties of the cellular materials have been analyzed.

The oscillatory shear viscosities satisfy the logarithmic additivity rule, which indicates that the two PPs used are miscible. The shear and extensional rheological properties of the PP blends depend on the amount of the HMS PP in the blend. However, while the extensional properties are highly sensitive to the effect of long-chain branching, the shear viscosity is only slightly decreased by the addition of the HMS PP. Consequently, the differences in the structural and mechanical properties of the resulting PP cellular materials have been related to the changes in the extensional properties.

For cellular materials fabricated with an amount of HMS PP lower than 75 wt % the following results have been obtained. The strain hardening coefficient increases with the amount of HMS PP and consequently the open cell content decreases because the cell walls are able to resist the extension to which they are submitted during the foaming process, without breaking. The cellular structure is also conditioned by the strain hardening coefficient. When the amount of HMS PP increases the cell size decreases and the cell density increases. For high linear PP contents, the cells are completely open and hence the average cell size is larger in these materials. As the cellular materials have the same density if the cell size increases, the cell density decreases. Related to the AR, it was shown that the AR increased with the amount of linear PP. Furthermore, the cell coalescence, in these materials, occurs in a plane perpendicular to the expansion direction and consequently cells are growing considerably in the expansion or thickness direction, making the anisotropy to increase. When the linear PP content is very high the cell anisotropy disappears because the coalescence in these materials is produced in all directions. Moreover, the standard deviation coefficient of the cell size distribution relative to the cell size is higher in the materials containing large amounts of linear PP, indicating that the cellular structure of these materials is more heterogeneous. Finally, the CR has been calculated to analyze the degeneration of the cellular structure during the foaming process. This ratio increases if the linear PP content increases, indicating that the amount of cells that survive during the foaming process is higher in the materials containing large amounts of HMS PP.

Relative to the mechanical properties, as the solid materials have the same properties and the density of cellular materials is the same, the mechanical properties are mainly conditioned by the cellular structure. The elastic modulus and the collapse stress increase with the amount of HMS PP because a homogeneous cellular structure with small cell sizes and also with a considerable content of closed cells leads to good mechanical properties. Moreover, both parameters remain constant for the cellular materials with cells completely open, i.e., for cellular materials fabricated with large amounts of linear PP, indicating that, in this case, the open cell content is the structural parameter which has a larger effect on the mechanical properties. Furthermore, these materials are good energy absorbers provided the stress to which they are subject is less than 2.5 MPa.

On the other hand, cellular materials fabricated with an amount of HMS PP higher than 75 wt % have a completely different

behavior. For these materials the strain hardening coefficient is almost constant and consequently the open cell content, the cell size, the cell anisotropy, the cell density, the CR, the elastic modulus, and collapse stress are also constant and do not change with the amount of HMS PP.

From this study, two main conclusions can be obtained. First, results show that the knowledge of the extensional behavior of the polymeric matrix is fundamental to analyze and understand the cellular structure and the mechanical response of cellular materials. Second, for the relative density analyzed (0.2) the same properties can be obtained with a pure HMS PP and with blends of this PP with a linear PP provided the HMS PP content is higher than 75 wt %.

ACKNOWLEDGMENTS

Financial support from PIRTU contract of E. Laguna-Gutierrez by Junta of Castilla and Leon (EDU/289/2011) and cofinanced by the European Social Fund is gratefully acknowledged. Financial support from the MICINN (MAT 2009-14001 and MAT 2012-34901), the Junta of Castilla and Leon (VA 035U13), and the EU (Nancore Project: EC project number 214148) is gratefully acknowledged.

REFERENCES

1. Frisch, K. C.; Klempner, D. In Handbook of Polymeric Foams and Foam Technology; Klempner, D., Frisch, K. C., Eds.; Hanser Publishers: Munich, Vienna, New York, Barcelona, **1991**; Chapter 1, p 1.
2. Eaves, D. In Handbook of Polymer Foams; Eaves, D., Ed.; Rapra Technology: Shrewsbury, **2004**; Chapter 1, p 1.
3. Rodriguez-Perez, M. A.; Velasco, J. I.; Arencon, D.; Almanza, O.; de Saja, J. A. *J. Appl. Polym. Sci.* **2000**, *75*, 156.
4. Saiz-Arroyo, C.; de Saja, J. A.; Rodriguez-Perez, M. A. *Polym. Eng. Sci.* **2012**, *52*, 751.
5. Saunders, J. H. In Handbook of Polymeric Foams and Foam Technology; Klempner, D., Frisch, K. C., Eds.; Hanser Publishers: Munich, Vienna, New York, Barcelona, **1991**; Chapter 2, p 5.
6. Ibeh, C. C. In Thermoplastic Materials. Properties, Manufacturing Methods and Applications; Ibeh, C. C., Ed.; CRC Press: Boca Raton, **2011**; Chapter 10, p 193.
7. Zheng, W. G.; Lee, Y. H.; Park, C. B. *J. Appl. Polym. Sci.* **2010**, *117*, 2972.
8. Naguib, H. E.; Park, C. B.; Reichelt, N. *J. Appl. Polym. Sci.* **2004**, *91*, 2661.
9. Naguib, H. E.; Park, C. B.; Panzer, U.; Reichelt, N. *Polym. Eng. Sci.* **2002**, *42*, 1481.
10. Lagendijk, R. P.; Hogt, A. H.; Buijtenhuijs, A.; Gotsis, A. D. *Polymer* **2001**, *42*, 10035.
11. Gotsis, A. D.; Zeevenhoven, B. L. F.; Tsenoglou, C. *J. Rheol.* **2004**, *48*, 895.
12. Su, F. H.; Huang, H. X. *J. Appl. Polym. Sci.* **2010**, *116*, 2557.
13. Auhl, D.; Stange, J.; Münstedt, H.; Krause, B.; Voigt, D.; Lederer, A.; Lappan, U.; Lunkwitz, K. *Macromolecules* **2004**, *37*, 9465.
14. Gotsis, A. D.; Zeevenhoven, B. L. F.; Hogt, A. H. *Polym. Eng. Sci.* **2004**, *44*, 973.
15. Park, C. B.; Cheung, L. K. *Polym. Eng. Sci.* **1997**, *37*, 1.
16. Nam, G. J.; Yoo, J. H.; Lee, J. W. *J. Appl. Polym. Sci.* **2005**, *96*, 1793.
17. Reichelt, N.; Stadlbauer, M.; Folland, R.; Park, C. B.; Wang, J. *Cell. Polym.* **2003**, *22*, 315.
18. Spitael, P.; Macosko, C. W. *Polym. Eng. Sci.* **2004**, *44*, 2090.
19. Stange, J.; Münstedt, H. *J. Cell. Plast.* **2006**, *42*, 445.
20. Saiz-Arroyo, C.; de Saja, J. A.; Velasco, J. I.; Rodriguez-Perez, M. A. *J. Mater. Sci.* **2012**, *47*, 5680.
21. Saiz-Arroyo, C.; Rodriguez-Perez, M. A.; Velasco, J. I.; de Saja, J. A. *Composites: Part B* **2013**, *48*, 40.
22. Saiz-Arroyo, C.; Rodriguez-Perez, M. A.; Tirado, J.; Lopez-Gil, A.; de Saja, J. A. *Polym. Int.* **2013**, *62*, 1324.
23. Gibson, L. J. *Mater. Sci. Eng. A* **1989**, *110*, 1.
24. Orwoll, R. A. In Physical Properties of Polymers Handbook, 2nd ed.; Mark, J. E., Ed.; Springer Science: Washington, **2007**; Chapter 37, p 611.
25. Pinto, J.; Solorzano, E.; Rodriguez-Perez, M. A.; de Saja, J. A. *J. Cell. Plast.* **2013**, *49*, 555.
26. Rodriguez-Perez, M. A.; de Saja, J. A. *Cell. Polym.* **1999**, *18*, 1.
27. Almanza, O.; Rodriguez-Perez, M. A.; de Saja, J. A. *Polymer* **2001**, *42*, 7117.
28. Rodriguez-Perez, M. A.; Diez-Gutierrez, S.; de Saja, J. A. *Polym. Eng. Sci.* **1998**, *38*, 831.
29. Gibson, L. J.; Ashby, M. F. In Cellular Solids: Structure and Properties; Gibson, L. J., Ashby, M. F., Eds.; Cambridge University Press: Cambridge, **1997**; Chapter 2, p 15.
30. Gong, W.; Gao, J.; Jiang, M.; He, L.; Yu, J.; Zhu, J. *J. Appl. Polym. Sci.* **2011**, *122*, 2907.
31. Naguib, H. E.; Park, C. B.; Hesse, A.; Panzer, U.; Reichelt, N. In Blowing Agents and Foaming Process Conference 2001. Conference Proceedings, Frankfurt, Germany, March 13–14, 2001, Rapra Technology: Shrewsbury, 2001.
32. Tabatabaei, S. H.; Carreau, P. J.; Ajji, A. *Chem. Eng. Sci.* **2009**, *64*, 4719.
33. Utracki, L. A.; Schlund, B. *Polym. Eng. Sci.* **1987**, *27*, 1512.
34. Wood-Adams, P. M.; Dealy, J. M.; de Groot, A. W.; Redwine, O. D. *Macromolecules* **2000**, *33*, 7489.
35. Liu, C.; Li, C.; Chen, P.; He, J.; Fan, Q. *Polymer* **2004**, *45*, 2803.
36. Gendron, R.; Daigneault, L. E. In Foam extrusion: Principles and Practice; Lee, S. T., Ed.; Technomic Publishing Company: Lancaster, **2000**; Chapter 3, p 35.
37. Stange, J.; Uhl, C.; Münstedt, H. *J. Rheol.* **2005**, *495*, 1059.
38. Chaudhary, A. K.; Jayaraman, K. *Polym. Eng. Sci.* **2011**, *51*, 1749.
39. Rodriguez-Perez, M. A.; Alvarez-Lainez, M.; de Saja, J. A. *J. Appl. Polym. Sci.* **2009**, *114*, 1176.
40. Lee, L. J.; Zeng, C.; Cao, X.; Han, H.; Shen, J.; Xu, G. *Compos. Sci. Technol.* **2005**, *65*, 2344.
41. Lee, S. T.; Park, C. B.; Ramesh, N. S. In Polymeric Foams: Science and Technology; Lee, S. T., Park, C. B., Ramesh, N. S., Eds.; CRC Press: Boca Raton, FL, **2007**; Chapter 5, p 93.

4.4 References

[1] G. J. Nam, J. H. Yoo, J. W. Lee. Journal of Applied Polymer Science, 96, 1793-1800, 2005.
[2] W. G. Zheng, Y. H. Lee, C. B. Park. Journal of Applied Polymer Science, 117, 2972-2979, 2010.
[3] H. E. Naguib, C. B. Park, N. Reichelt. Journal of Applied Polymer Science, 91, 2661-2668, 2004.
[4] A. D. Gotsis, B. L. F. Zeevenhoven, A. H. Hogt. Polymer Engineering and Science, 44, 973-982, 2004.
[5] A. D. Gotsis, B. L. F. Zeevenhoven, C. Tsenoglou. Journal of Rheology, 48, 895-914, 2004.

CHAPTER 5

POLYPROPYLENE NANOCOMPOSITE FOAMS: EFFECT OF EXTENSIONAL RHEOLOGY ON THE FOAMING BEHAVIOR

INDEX

5.1 Introduction

Polymer nanocomposites have been continuously developed for the last two decades because many physical properties can be improved when nanoparticles are added to a polymeric matrix [1]. Nanoparticles reinforce the polymeric matrix and therefore, they improve its mechanical properties [2,3]. Moreover, when the polymer is filled with nanoparticles there are also improvements in its thermal stability as well as in its barrier and flame retardancy properties [4,5,6]. However, not only improvements in the physical properties of the polymeric nanocomposites are obtained, the polymer morphology is also affected by nanoparticles as the changes produced in both shear and extensional rheological properties indicate [1,7,8].

In connection with the foaming process, the use of nanocomposites in the formation of foams contributes to optimize the cellular structure. On the one hand, nanoparticles are effective nucleating agents and on the other hand, it has been proved that, in some polymeric matrices (such as linear polypropylene), the presence of nanoparticles can increase the melt strength of the polymer and hence, reduce or even suppress cell coalescence [9,10,11].

Therefore, it can be said that nanoparticles could improve the overall properties of the foamed materials by acting at two levels: by improving the properties of the solid polymeric matrix (comprising the cell walls) and by optimizing the cellular structure. Nevertheless, the improvements obtained in both, the solid polymeric matrix and the cellular structure are greatly affected by the degrees of exfoliation and dispersion achieved during the mixing process, as well as, by the degree of compatibilization between the polymer and the particles.

This chapter analyzes on the one hand, the extensional rheological properties of two different high melt strength polypropylene (HMS PP) composites: the first one containing natural montmorillonites and the second one containing organomodified montmorillonites and a compatibilizer polymer. On the other hand, the effects that these particles induce on the cellular structure and mechanical properties of the foamed composites are also studied. The main objective is to analyze if it is possible to establish a relationship between extensional rheology, cellular structure and mechanical properties in these two different complex polymeric matrices. All the obtained results are presented in the paper included in the section 5.3 of this chapter. Moreover, this paper also analyzes the effect that the extrusion process has on the extensional rheological behavior of the pure HMS PP, with the aim of analyzing the importance of performing the rheological measurements in a material with the same thermo-mechanical history as the material to be foamed.

Before presenting this study and due to the importance of controlling the particles structure to obtain the desired properties, in the section 5.2 a complementary paper which analyzes the structure of these composites, that is, the degree of intercalation/exfoliation and the clay distribution in the polymeric matrix, is included. In this paper, the effects of the extrusion process (number of extrusion cycles to which the material is subjected) and type and content of clays on the clay intercalation/exfoliation and dispersion are analyzed. Moreover, this paper also analyzes the effect that the foaming process has on the structure of the particles. Through this last study, it is also possible to know the structure of the clays in the foamed materials which is very useful to understand the results obtained after the mechanical characterization of the foamed materials.

5.2 Analysis of the particles structure: degree of exfoliation and clay distribution

In this work, the effects of the extrusion process, the clay type and content and the foaming process on the clay morphology (that is, on the degree of intercalation/exfoliation and clay distribution) are studied.

This study is performed in two completely different systems. The first system comprises a material produced using non-organomodified (natural) clays and without a compatibilizer, while the second system refers to a material including both organomodified clays and a compatibilizer. Moreover, the amount of clays used in each of the systems is also modified. Composites containing three different clay contents (2.5, 5 and 7.5 wt.%) are generated. With the aim of analyzing the effect of the extrusion process, the different solid composites are subjected up to three extrusion cycles. Finally, in order to analyze the effect of the foaming process, some of these composites are foamed by the Improved Compression Molding (ICM) route.

The structure of the paper is as follows. First, the effect of the extrusion process is analyzed in the pure HMS PP by small amplitude oscillatory shear (SAOS) tests, that is, the effect that this process has on rheological functions such as the complex viscosity and the storage and loss moduli is carefully studied.

Second, the effect of the extrusion process on the clay morphology is analyzed in the two systems produced. The results included in the paper correspond to a fixed clay content (7.5 wt.%) because similar results were obtained for the composites containing other quantities of particles. Two different techniques are employed to analyze the effect of the extrusion process: X-ray diffraction (XRD) and SAOS tests.

Third, the effect of the clay content on the clay morphology is analyzed using the same experimental techniques (XRD and SAOS). In this case, the number of extrusions is maintained constant. Only the results of the materials after a total of three extrusions are shown in the paper, because similar results were obtained with the other two extrusion cycles. The experimental results allow determining parameters like the percolation threshold, for each system studied.

Finally, the effect of the foaming process on the clay morphology is also determined by using XRD. ICM is the foaming process selected because this technique subjects the material only to temperature and pressure without applying any other external forces that can contribute to exfoliate and disperse the particles (like shear). Thus, only the effects of foaming and melt stretching are observed.

Journal of Applied Polymer Science

Effects of extrusion process, type and content of clays, and foaming process on the clay exfoliation in HMS PP composites

Ester Laguna-Gutierrez,[1] Rob Van Hooghten,[2] Paula Moldenaers,[2] Miguel Angel Rodriguez-Perez[1]
[1]Cellular Materials Laboratory (CellMat), Condensed Matter Physics Department, University of Valladolid, Paseo de Belén, 47011 Valladolid, Spain
[2]Department of Chemical Engineering, KU Leuven, Celestijnenlaan 200F, B 3001 Heverlee, Belgium
Correspondence to: E. Laguna-Gutierrez (E-mail: ester.laguna@fmc.uva.es)

ABSTRACT: The use of a high melt strength polypropylene (HMS PP) matrix reinforced with layered clays could be very useful to improve the properties of materials produced with processes involving melt stretching, like foaming. The control of the particles structure, that is, the degree of exfoliation and the clay distribution in the polymeric matrix, is the key to achieve the desired properties. In this study, the effects of the extrusion process, the clay type and content, and the foaming process on the morphology of different HMS PP based composites are studied. Both, natural and organomodified clays were used. The extrusion process has a negative effect in the composites containing natural clays as their interlayer distance decreases as the number of extrusion cycles increases. On the contrary, this process improves the intercalation of the organomodified clays. However, in both composites the interlayer spacing decreases when the clay content increases. While a percolated network is formed in the composites containing organomodified clays, no network is formed with the natural clays. Finally, the effect of the foaming process has also been analyzed. The Improved Compression Moulding (ICM) route was used to produce the foamed materials. This technique subjects the materials only to a temperature and a pressure gradient without applying any other external forces that could contribute to the clay exfoliation. In this way, only the effects of foaming and melt stretching are observed. In both composites, an increase in the interlayer distance is observed when the materials are foamed. © 2015 Wiley Periodicals, Inc. J. Appl. Polym. Sci. **2015**, *132*, 42828.

KEYWORDS: clay; composites; foams; rheology; X-ray; polypropylene

Received 19 May 2015; accepted 9 August 2015
DOI: 10.1002/app.42828

INTRODUCTION

Common linear polypropylene (PP) has many desirable properties such as good temperature stability, good chemical resistance, high melting temperature, high tensile modulus, and the capability of static load bearing.[1] These beneficial properties have permitted to use polypropylene in different applications. However, its linear structure leads to poor processability in processes involving melt stretching, such as extrusion coating, film blowing, thermoforming and foaming.[2] A way to improve the polymer melt strength is to incorporate long chain branches (LCBs). The PPs with LCBs show a pronounced strain hardening and hence an improved melt strength.[3] Another way used to enhance the melt strength of linear PPs is to incorporate layered silicates. Several authors have proved that an increase in the melt strength is obtained by increasing the clay content.[4–6] Furthermore, the mechanical performance, the thermal stability and the flame retardancy of the polymeric matrix can also be improved by adding nanoparticles.[7–10] Nevertheless, all these properties are greatly affected by the degree of filler exfoliation and dispersion achieved during the mixing process. A fully dispersed and stable state will lead to optimal properties whereas the presence of particles agglomerates or a low compatibility between the particles and the polymeric matrix lead to a poor material performance, which can be even lower than that of the unfilled polymeric matrix.[11] Consequently, one of the keys to achieve the desired properties is the control of the particles structure, that is, the degree of exfoliation and the clay distribution in the polymeric matrix.

Measuring the quality of exfoliation and dispersion in a composite is not trivial. This has been traditionally characterized by X-ray diffraction (XRD) and transmission electron microscopy (TEM). Nevertheless, these traditional techniques are limited in the sense that they only prove a small volume of the sample and therefore, they should be combined with other techniques such as melt rheology. Both, linear and non-linear rheological properties are very sensitive to changes in the nanoscale and mesoscale structure and therefore, rheology can be used as a powerful tool to evaluate the dispersion of the particles in the

melt state.[12–14] Moreover, one of the main advantages of rheology is that samples of macroscopic dimensions are used and hence, rheology offers an integrated picture of the composite material.

The degree of exfoliation has been widely investigated in composites produced with a common linear PP and montmorillonites. The effects of using non-organomodified and organomodified montmorillonites have been studied together with the effects of the initial interlayer spacing and the clay content.[4,5,15–20] The effects of the amount and kind of compatibilizer employed have also been thoroughly investigated.[5,16,18–23] Finally, the production parameters have also been modified in order to analyze the effect of the production process on the clay structure.[22–26]

From these studies, it can be concluded that a better intercalation between the clay and the polymer is obtained by using organomodified montmorillonites.[15] The use of a compatibilizer improves the intercalation between the montmorillonites and the linear PP.[16,18,23] Moreover, the interlayer spacing increases as the ratio of compatibilizer increases.[23] Clay exfoliation can only be achieved when a high compatibility between polymer and clays exists.[5] There seems to be an optimum range of initial interlayer distance for obtaining an effective intercalation.[16] The aggregation of small portions of layers is produced and the level of intercalation is reduced when the clay content increases.[17] The melt processing route, that is, the way in which the different raw materials are blended, also conditions the clay structure.[26] The processing temperature is also very important. When a low processing temperature is used the shear stress is higher and therefore, the clay exfoliation is promoted.[24]

While the clay structure of linear PP/montmorillonite layered composites has been extensively investigated, as far as the author knowledge, there are no many papers that study the degree of intercalation/exfoliation of layered composites produced with a HMS PP. In fact, only one paper has been found. Bhattacharya *et al.*[27] characterized their materials by using XRD and TEM. They obtained an increase in the interlayer spacing for the polymer nanocomposites relative to the pure organomodified clay. Moreover, they found that this distance decreased as the clay content increased. TEM results revealed that the clay particles were well dispersed within the polymeric matrix. However, there is one aspect that has not been reported in this paper. HMS PP is normally produced from reactive extrusion or electron beam irradiation processes, in which LCBs are added to a common linear PP.[28,29] As a consequence, this polymer could be degraded in processes in which it is subjected to high shear forces (like in the extrusion process) and hence, changes on their rheological properties would also occur, so that the rheological study of the effect of the extrusion process on the clay morphology could be very interesting.

On the other hand, from the point of view of foaming applications, the system HMS PP/montmorillonites is very interesting due to the synergistic properties which could be achieved with the combination of this polymer and the layered silicates. However, as these properties are conditioned by the final composite morphology, the effect of the foaming process on the clay morphology should be also carefully analyzed. Up to know there are no many works focused on studying this aspect. Zheng *et al.*[30] foamed linear PP/clay nanocomposites by extrusion using CO_2 as blowing agent. They reported that supercritical CO_2 is helpful for expanding further the interlayer spacing and for promoting the partial exfoliation of nanoparticles in PP/clay nanocomposites. Zhai *et al.*[31] foamed PP/silica nanocomposites by extrusion using CO_2 as blowing agent. They found that the multisilica aggregates could be dispersed during the foaming process. They explained this result considering that the biaxial stretching action during cell growth could be transferred onto the nanoparticles.

Taking these ideas into account, the goal of this work is to analyze the effects of the extrusion process, the clay content and the foaming process on the structure of HMS PP/layered clays composites. For this purpose, two completely different composites have been studied. The first material was produced using non organomodified (natural) clays and without a compatibilizer, while in the second material both organomodified clays and a compatibilizer were used. To analyze the effect of the extrusion process, the composites have been subjected up to three extrusion cycles. The effect of the extrusion process on the dynamic rheological properties of the pure HMS PP has also been investigated to determine if the polymer is being degraded during this process. Moreover, composites containing three different clay contents (2.5, 5, and 7.5 wt %) were generated in order to analyze the effect of the clay content. Finally, cellular materials were produced by the Improved Compression Moulding (ICM) route in order to analyze the effect of the foaming process.[32–35] ICM was selected because in this foaming process the material is only subjected to temperature and pressure and hence, there are no other forces associated to the foaming process which could contribute to the clay exfoliation (such as shear forces in extrusion foaming).

EXPERIMENTAL

Materials

A branched high melt strength PP (HMS PP) supplied by Borealis (PP Daploy WB 135 HMS) with a MFI of 2.4 g/10 min (230°C/2.16 kg) was used in this study. The HMS PP density at room temperature is 0.905 g/cm^3. Two kind of commercial clays were also used. A non organomodified montmorillonite, Cloisite® Na+ supplied by Southern Clay Products with a density of 2.86 g/cm^3, from now called "Na+" and an organomodified montmorillonite with quaternary ammonium salt, Cloisite® 20A also supplied by Southern Clay Products, with a density of 1.77 g/cm^3, from now called "C20A." A maleic anhydride modified homopolymer polypropylene (PP-MA), Polybond 3200, supplied by Chemtura with a MFI of 115 g/10 min (190°C/2.16 kg), was used as a chemical compatibilizer with the organomodified clays C20A.

Antioxidants Irgafos 168 and Irganox 1010 (from Ciba) were also employed in order to reduce the thermal degradation of the polymers. The foaming was performed using a chemical blowing agent, azodicarbonamide (ADC) Lanxess Porofor M-C1 with an average particle size of 3.9 ± 0.6 μm. All the raw materials were vacuum dried at 50°C for 12 h before use.

Table I. Summary of the Formulations Produced with the Clays Na+

Sample name	HMS PP (wt %)	PP-MA (wt %)	Antioxidants (wt %)	Na+ (wt %)	ADC (wt %)	Number of extrusions
2.5Na+-1	97.4	0	0.1	2.5	0	1
2.5Na+-2	97.4	0	0.1	2.5	0	2
2.5Na+-3	97.4	0	0.1	2.5	0	3
Foam-2.5Na+-3	95.4	0	0.1	2.5	2	3
5Na+-1	94.9	0	0.1	5	0	1
5Na+-2	94.9	0	0.1	5	0	2
5Na+-3	94.9	0	0.1	5	0	3
Foam-5Na+-3	93.0	0	0.1	4.9	2	3
7.5Na+-1	92.4	0	0.1	7.5	0	1
7.5Na+-2	92.4	0	0.1	7.5	0	2
7.5Na+-2	92.1	0	0.1	7.5	0	3
Foam-7.5Na+-3	90.5	0	0.1	7.4	2	3

Composite Preparation

Composites with Na+ Clays. In the first step the natural clays (Na+), the antioxidants (a total amount of 0.1 wt % containing Irgafos 168 in a proportion of 0.08% and Irganox 1010 in a proportion of 0.02% by weight) and the HMS PP were melt-extruded using a co-rotating twin screw extruder Collin ZK 25T with L/D of 24. The rotational speed used was 50 rpm and the melt temperature was 200°C (Extrusion 1). Three composites containing three different contents of clays were produced (2.5 wt %, 5 wt %, and 7.5 wt %). Then, a second extrusion (Extrusion 2) was performed with the same twin screw extruder. In this case the rotational speed used was 120 rpm and the melt temperature was 155°C. Finally, a third extrusion (Extrusion 3) of these materials was done with the same extrusion parameters. The solid materials produced are summarized in Table I.

The pellets containing the blowing agent, for foaming, were prepared by mixing the composites obtained after the first extrusion with 2 wt % of the blowing agent (ADC). A rotational speed of 120 rpm was used and the melt temperature was 155°C. A second extrusion of the composite containing the blowing agent was performed, under the same conditions, in order to obtain a more homogenous material and in order to reach a total of three extrusions. To denote the solid composites containing the blowing agent, which were subsequently foamed, the word "Foam" has been added at the beginning of the corresponding nomenclatures (Table I).

Composites with C20A Clays. In the first step, a masterbatch containing the organomodified clays (C20A) and the compatibilizer PP-MA in the same proportion (1:1) was produced. The extruder described above was also used, with a rotational speed of 50 rpm and with a melt temperature of 200°C. Composites with the desired clay contents (2.5 wt %, 5 wt %, and 7.5 wt %) were prepared by diluting, under the same extrusion conditions, the previous masterbatch in the HMS PP. During this dilution process, the antioxidants were also added. This extrusion cycle, in which the masterbatch is diluted in the HMS PP, is called Extrusion 1 as it is the first time that the composite HMS PP/C20A is extruded. Then, the composites containing the C20A were subjected to two additional extrusion cycles under the same conditions as the Na+ composities (120 rpm, 155°C).

Using the same procedure previously described for the Na+ samples, the composites obtained after the first extrusion were also blended with the blowing agent. The solid materials produced are summarized in Table II. The material containing 7.5 wt % of C20A (for foaming) does not appear in Table II because it was not possible to produce a foamed material with the same density as the other cellular materials using this composite.

The same processing route used with the polymer containing the Na+ was also employed with the pure HMS PP, with the aim of using this last material as a reference. The solid materials produced from the pure HMS PP are summarized in Table III. No cellular materials were manufactured with this polymer.

Foaming Process

The cellular materials were prepared via the Improved Compression Moulding (ICM) route. In this process the pellets containing the blowing agent are placed in a mold. Then the mold is situated in a hot-plate press. An initial pressure is applied to the system (41.5 bars) while it is heated until the foaming temperature (200°C), which is higher than the decomposition temperature of the blowing agent. After a certain time, (approximately 15 min) when the blowing agent is fully decomposed the pressure of the press is released allowing the polymer to expand until the desired ratio. Finally, the mold is introduced in cold water to cool-down the sample and hence stabilizing the cellular structure as fast as possible.[36] The peculiarity of this foaming system is that the mold used is a self-expandable mold that allows controlling the material density by mechanical means and therefore the foam density does not depend on the formulation used. Foams with a density of 0.18 g/cm^3 were produced. These foams are discs with a diameter of 180 mm and a height of 10 mm. A more detailed description of the ICM technique can be found elsewhere.[32–35]

Table II. Summary of the Formulations Produced with the Clays C20A

Sample name	HMS PP (wt %)	PP-MA (wt %)	Antioxidants (wt %)	C20A (wt %)	ADC (wt %)	Number of extrusions
2.5C20A-1	94.9	2.5	0.1	2.5	0	1
2.5C20A-2	94.9	2.5	0.1	2.5	0	2
2.5C20A-3	94.9	2.5	0.1	2.5	0	3
Foam-2.5C20A-3	92.9	2.5	0.1	2.5	2	3
5C20A-1	89.9	5	0.1	5	0	1
5C20A-2	89.9	5	0.1	5	0	2
5C20A-3	89.9	5	0.1	5	0	3
Foam-5C20A-3	88.1	4.9	0.1	4.9	2	3
7.5C20A-1	84.9	7.5	0.1	7.5	0	1
7.5C20A-2	84.9	7.5	0.1	7.5	0	2
7.5C20A-3	84.9	7.5	0.1	7.5	0	3

SAMPLES CHARACTERIZATION

X-Ray Diffraction (XRD)

X-ray diffraction (XRD) was performed with a Bruker D8 Discover A25 diffractometer with Cu-Kα radiation of wavelength 0.154 nm to determine the structure of the layered clays. The diffraction spectrum was obtained over a 2θ range of 0–30°.

Solid precursors with a thickness of 0.5 mm produced by compression molding at a temperature of 220°C and with a pressure of 21.8 bars were used to conduct the XRD measurements of the non-foamed materials. Also the foamed materials were analyzed with this technique. These foamed materials were grinded in liquid nitrogen and the XRD experiments were performed in the powder of the foam.

Dynamic Shear Measurements

A stress controlled rheometer AR 2000 EX from TA Instruments was used to perform the tests. Dynamic shear measurements were conducted at a temperature of 250°C under a nitrogen atmosphere with 25 mm diameter parallel plates. A fixed gap of 1 mm was used to perform the rheological measurements.

Cylindrical samples with a thickness of 1.5 mm and a diameter of 22 mm were prepared in a hot-plate press at a temperature of 220°C and with a pressure of 70 bars. When the sample is loaded the particles network is partially deformed. The initial state could be recovered again waiting a certain time. In order to define a well-controlled starting point for all the rheological experiments a time sweep was previously performed at a frequency of 1 rad/s. This time sweep was conducted during 900 s.

After the initial time sweep a frequency sweep was carried out at the same strain, which was selected in order to be within the linear viscoelastic response of the material. The dynamic-mechanical experiments were performed over an angular frequency range of $0.01 < \omega < 100$ rad/s. From these measurements three parameters were analyzed, the dynamic shear viscosity (η^*), the storage modulus (G'), and the loss modulus (G'').

RESULTS

Effect of the Extrusion Process

Effect of the Extrusion Process on the Rheological Behavior of the Pure HMS PP. The effect of the extrusion process is first analyzed in the pure HMS PP. Figure 1 shows the complex viscosity (η^*), the storage modulus (G'), and the loss modulus (G'') as a function of frequency for the pure HMS PP as received and after one, two, and three extrusions.

The complex viscosity [Figure 1(a)] of the pure HMS PP at low frequency decreases as the number of extrusions increases and the transition from the Newtonian-plateau to the shear thinning regime was shifted to higher frequencies, which means that the Newtonian zone becomes broader. Moreover, the HMS PP that has not been extruded (HMS PP-0) is the material that exhibits the highest shear thinning behavior. The zero shear viscosity (η_0) in dynamic measurement has been obtained from the Eq 1 and the values are shown in Table IV.[37]

$$\eta_0 = \lim_{\omega \to 0} \frac{G''(\omega)}{\omega} \quad (1)$$

It is possible to detect a decrease in the zero shear viscosity when the number of extrusions increases. As the complex

Table III. Summary of the Formulations Produced with the Pure HMS PP

Sample name	HMS PP (wt %)	PP-MA (wt %)	Antioxidants (wt %)	Na+ (wt %)	C20A (wt %)	ADC (wt %)	Number of extrusions
HMS PP-1	99.9	0	0.1	0	0	0	1
HMS PP-2	99.9	0	0.1	0	0	0	2
HMS PP-3	99.9	0	0.1	0	0	0	3

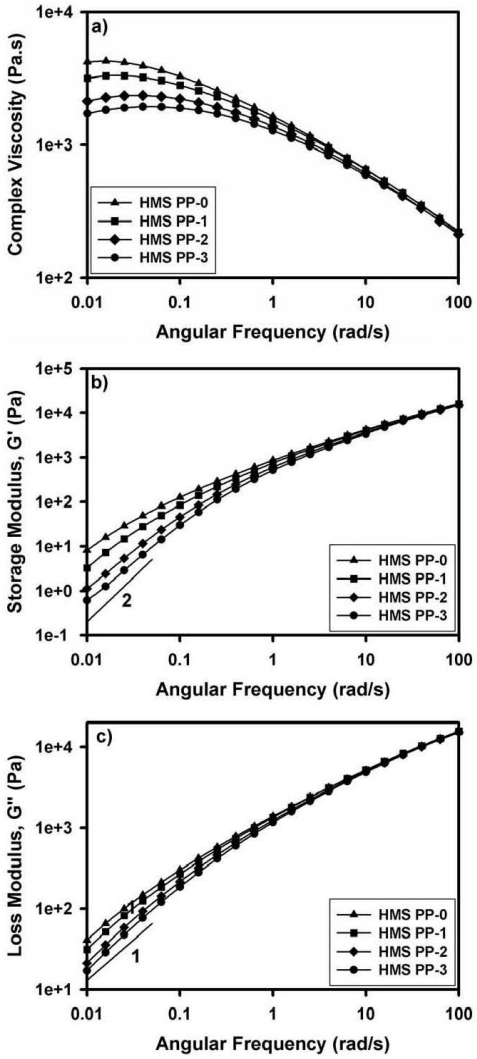

Figure 1. Linear viscoelastic properties of the pure HMS PP after being subjected to different extrusions. (a) Complex viscosity as a function of frequency. (b) Storage modulus vs. angular frequency. (c) Loss modulus vs. angular frequency. The slope of both the storage modulus and the loss modulus in the terminal region is also shown in this figure.

viscosity, the storage modulus is also affected by the extrusion process [Figure 1(b)]. Indeed, the storage modulus is very sensitive to changes in molecular structure. At low frequencies, in the terminal region where only the longest relaxation times contribute to the viscoelastic behavior, it is well known that the storage modulus is proportional to the square of the frequency, $G' \propto \omega^2$. This frequency dependency is not obtained with the HMS PP as received, since the branches add additional longer relaxations modes.[3,38] The slope of G' in the terminal region has been calculated and the values are shown in Table IV. As the number of extrusions increases, the slope of G' approaches 2. The effect of the extrusion process on the loss modulus (G'') is also shown in Figure 1(c). In the same way that $G' \propto \omega^2$ in the terminal region, the loss modulus is proportional to the frequency, $G'' \propto \omega$. The terminal slopes of G'' have also been calculated and the values are shown in Table IV. While both, the storage modulus and the complex viscosity are strongly affected by the extrusion process, no important changes are obtained in the loss modulus of the different materials. The crossover frequency (ω_x) is also shown in Table IV. This is the frequency at which G' and G'' intersect. In the materials, in which the crossover frequency is outside the measuring range, that is, ω_x is higher than 100 rad/s, this value has been calculated by extrapolating the G' and G'' curves at higher frequencies. The results show that when the number of extrusions increases the crossover point is shifted to higher frequencies.

In general, an increase in the molecular weight, molecular weight distribution or branching leads to a smaller Newtonian limit, a deviation from the terminal slopes and an increased shear thinning behavior.[38,39] Therefore, it can be concluded that some degradation of the polymer occurs during extrusion, either by a reduction in the number of branches or in the length of the chains.

Effect of the Extrusion Process on the Clay Exfoliation

XRD spectra patterns have been obtained for both, the pure clays and the polymeric composites. Clays show a characteristic diffraction peak corresponding to the (001) plane. From this peak the interlayer spacing (d) was calculated using the Bragg's equation:

$$\lambda = 2d \sin(\theta) \quad (2)$$

where λ is the wavelength and 2θ is the diffraction angle.

When this peak is shifted to lower angles means that an intercalated structure is obtained. The polymer chains penetrate the stacks of the silicate layer and swell the galleries of the silicate layers to a higher value without destroying the stacking of layers. On the other hand, it can also occur that such peak does not appear. The absence of the diffraction peak is normally attributed to an exfoliated structure. In the exfoliated or

Table IV. Linear Viscoelastic Properties of the HMS PP after Being Subjected to Different Extrusion Cycles

Sample name	Slope G' (Pa.s)	Slope G'' (Pa.s)	η_0 (Pa.s)	ω_x (rad/s)
HMS PP-0	1.38	0.97	4096	79
HMS PP-1	1.65	1.04	3140	95
HMS PP-2	1.73	1.06	2127	122
HMS PP-3	1.78	1.08	1716	134

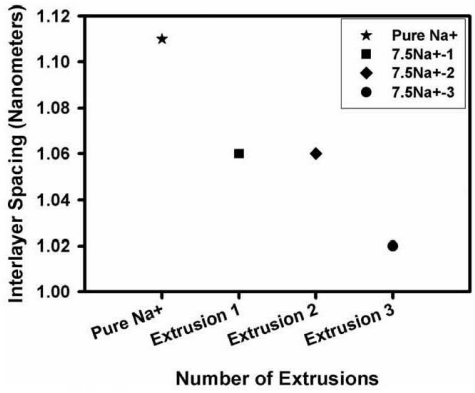

Figure 2. Interlayer spacing of the pure Na+ together with that of the Na+ composites (containing 7.5 wt % of clays) after each extrusion cycle.

delaminated system the individual silicate layers are dispersed in the polymeric matrix.

The effect that the number of extrusions has on the Na+ exfoliation is analyzed in Figure 2. Only the HMS PP composite containing 7.5 wt % of Na+ is shown in the figure because a similar behavior is obtained for the other two composites produced with 2.5 wt % and 5 wt % of Na+.

First, d of the pure natural clays Na+ as received has been measured. These particles were not organomodified and therefore the initial d is already very small (1.11 nm) which hinders the exfoliation and dispersion of the clays in the polymeric matrix. Then the effect of the extrusion process is studied. After the first extrusion a decrease in the interlayer distance occurs. Then the composite undergoes a second and a third extrusion in which again a slight decrease in d is observed. XRD results indicate that in these HMS PP/Na+ composites when the number of extrusions increases the clay platelets are closer, although the differences found in d are very small. Therefore, in this material, in which the clay exfoliation is hampered by the fact of having non organomodified clays and absence of a compatibilizer, the extrusion process has a negative effect.

The effect of the extrusion process on the complex viscosity [Figure 3(a)] is also analyzed in the polymeric composites containing the highest amount of natural clays (7.5 wt % of Na+). The same conclusions that were obtained with the pure HMS PP are obtained with the composite produced with the natural clays. When the number of extrusions increases, the viscosity decreases, the Newtonian zone becomes broader and the shear thinning behavior also decreases. Consequently, the changes obtained are mainly due to modifications in the polymeric matrix and not to the fact of adding particles. Again the zero shear viscosity is calculated using Equation 1 and the results are shown in Table V. Although no important differences are found in the complex viscosity behavior, significant changes are obtained in the absolute values of the complex viscosity by the fact of adding natural clays to the polymeric matrix. Independently on the number of extrusions, the zero shear viscosity of the polymeric composites is always 1.4 times greater than that of the pure HMS PP (Table IV). The effect of the extrusion process on the storage modulus of this composite is represented in Figure 3(b). As with the HMS PP, the main differences between the materials are found at low frequencies.

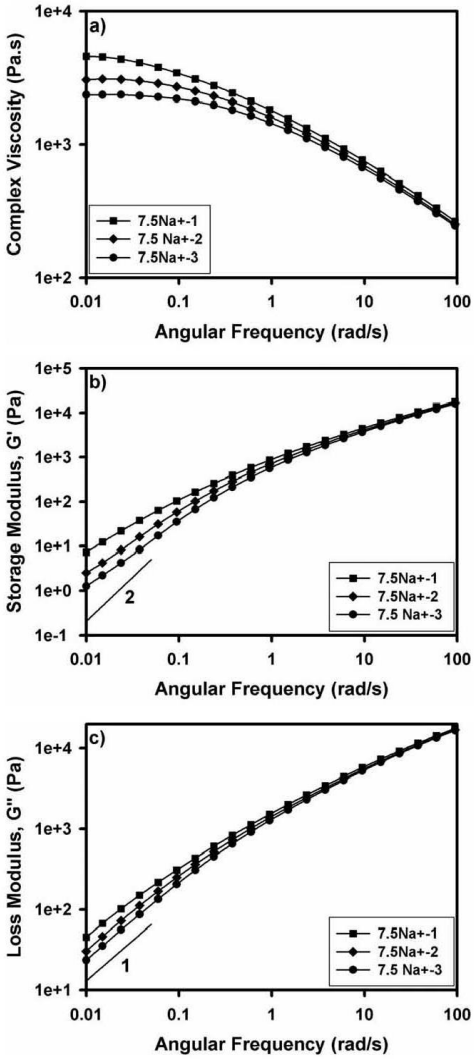

Figure 3. Linear viscoelastic properties of the composite containing 7.5 wt % of Na+ after being subjected to different extrusions. (a) Complex viscosity as a function of frequency. (b) Storage modulus vs. angular frequency. (c) Loss modulus vs. angular frequency.

Table V. Linear Viscoelastic Properties of Both the HMS PP and the Composite Containing 7.5 wt % of Na+ after Being Subjected to Different Number of Extrusions

Sample name	Slope G′ (Pa.s)	Slope G″ (Pa.s)	η_0 (Pa.s)	ω_x (rad/s)
HMS PP-3	1.78	1.08	1716	134
7.5Na+-1	1.28	0.93	4548	88
7.5Na+-2	1.35	1.00	3046	111
7.5Na+-3	1.39	0.99	2356	128

The slope of the curves in this terminal region is even lower than that of the pure HMS PP as both, Figure 3(b) and Table V indicate. Independently on the number of extrusions the slope of the PP composites is 1.2 times lower than that of the pure HMS PP. As the XRD results show that the particles are neither exfoliated nor intercalated, this decrease in the slope of the storage modulus is just a consequence of the large amount of natural clays used in this material (7.5 wt %). Finally, the loss modulus is also represented in Figure 3(c). No important changes are obtained in the loss modulus by adding the particles. As with the HMS PP the slope of G'' of the different PP composites is always 1 and the crossover frequency increases with the number of extrusions. From the analysis of the rheological results it can be concluded that when the clays are mainly agglomerated no important changes are detected in the rheological behavior of the composites in comparison with that of the unfilled polymeric matrix, apart from modifications of the absolute value of the viscosity.

The same analysis was performed with the organomodified clays, C20A. Figure 4 shows the XRD patterns of the pure C20A together with those of the composites after each extrusion. As with the HMS PP/Na+ composites only the interlayer distance of the composites containing 7.5 wt % of C20A is represented, as similar trends are obtained with the other clay contents.

XRD results show that the initial interlayer distance of the organomodified clays, C20A, as received, is 2.4 times larger than that of the natural clays, Na+. In this material the effect of the extrusion process is completely opposite to that obtained with the HMS PP/Na+ composites. The extrusion process has a positive effect and the interlayer spacing increases with the number of extrusions. Although this distance is higher, which means that the peak corresponding to the (001) plane has been shifted to lower angles, this peak still appears in the XRD results. Therefore, an intercalated structure is obtained and this intercalation is better as the number of extrusions increases, although a completely exfoliated structure is not achieved. During the melt extrusion process the clay agglomerates are under external forces from the polymer. Moreover, during this extrusion process, the polymer macromolecules are able to diffuse into the clay gaps. Both, the applied force on the clays and the diffusion of macromolecules would be affected by the extrusion conditions. During the melt extrusion process the polymer is able to separate the clay sheets due to two main reasons. First, the larger initial d that the C20A clays show favors the penetration of the polymer into the clay gallery. Second, the use of both organomodified particles and a compatibilizer (PP-MA) makes more favorable the compatibilization between the clays and the polymer and consequently, the forces that the polymer exerts on the clay agglomerates are greater.[40–43]

The effect that the number of extrusions has on the dynamic linear rheological behavior of the HMS PP composite containing the highest amount of organomodified clays (7.5 wt % of C20A+) is also analyzed. Figure 5(a) shows that the complex viscosity increases with the number of extrusions. This behavior is completely opposite to that obtained either with the pure HMS PP or with the composite containing natural clays. In this kind of composites in which organomodified clays have been used, the extrusion process has an important effect on the clay exfoliation or, as in this case, in the clay intercalation. In these materials the low frequency Newtonian viscosity is not detected. This behavior is replaced by a non-Newtonian power law behavior. Due to both, the large amount of particles used and the increase in the interlayer spacing, the presence of a space-filling network caused by attractive forces between the clay particles is favored by increasing the number of extrusions. The clay platelet network that emerges behaves as a solid-like material and therefore, the complex viscosity increases with the number of extrusions. In these materials it is not possible to determine the zero shear viscosity using Equation 1, because this equation is only valid in the terminal region, and this region has not been achieved with the C20A clays. The storage and loss modulus are shown in Figure 5(b,c), respectively. Both moduli show a plateau at low frequencies which is characteristic of solid-like materials. Moreover, when the number of extrusions increases this plateau is broader. For a constant content of clays, an important increase in both moduli is obtained by increasing the number of extrusions. This is again indicating that the particles are being intercalated and that the formation of a particle network is being favored because the intercalated particles are more likely to touch each other. Furthermore, G' and G'' do not show a crossover frequency which once again indicates a

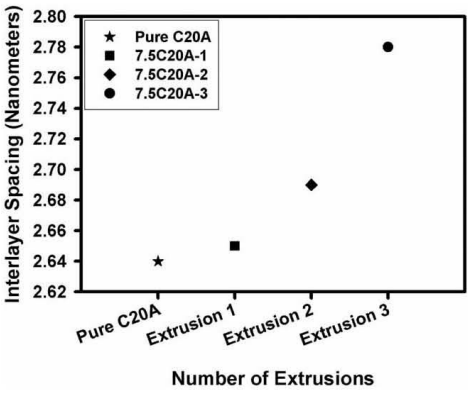

Figure 4. Interlayer spacing of the pure C20A together with that of the C20A composites (containing 7.5 wt % of clays) after each extrusion.

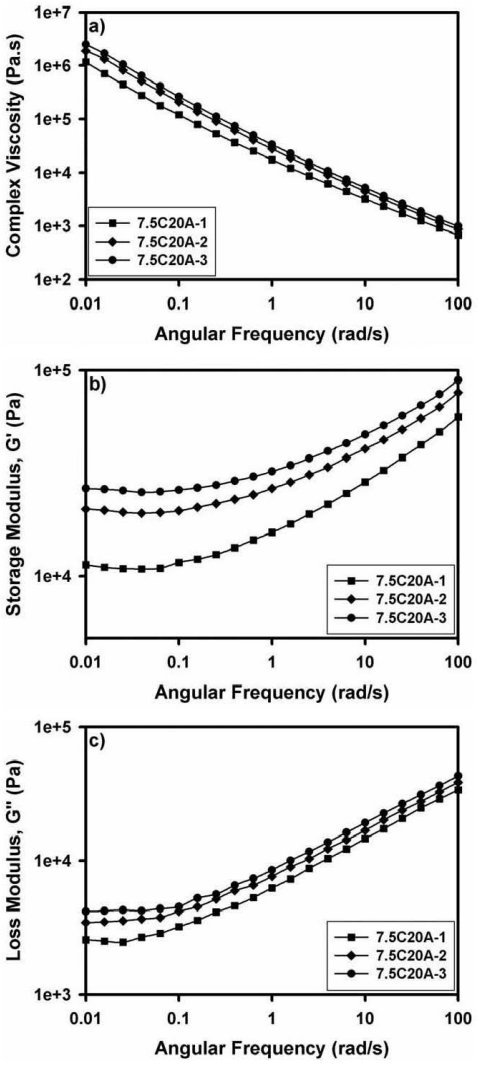

Figure 5. Linear viscoelastic properties of the composite containing 7.5 wt % of C20A after being subjected to different extrusions. (a) Complex viscosity as a function of frequency. (b) Storage modulus vs. angular frequency. (c) Loss modulus vs. angular frequency.

solid-like behavior in which the storage modulus lies well above the loss modulus in all the frequency range.

Effect of the Clay Content on the Clay Exfoliation

First, the composites containing natural clays, Na+, are studied. Figure 6 shows XRD results of the composites produced using three different clay contents, 2.5, 5, and 7.5 wt %. Now, the number of extrusions has been maintained constant. Only the results of the materials after a total of three extrusions are shown, as similar behaviors are obtained with the other two extrusion cycles.

Independently on the clay content, the interlayer distance of the natural clays as received is always higher than that of the clays when they are blended with the polymer. As it was previously shown (Figure 2) the extrusion process has a negative effect in these composites. In addition, the fact of increasing the clay content also has a negative effect in the clay intercalation as the interlayer distance decreases as the clay content increases. From the analysis of the different results it can be concluded that the extrusion process is not effective in the exfoliation of natural clays, not even for low clay contents.

The linear dynamic rheological behavior of these materials has also been analyzed. The results of the composites together with those of the pure HMS PP are shown in Figure 7. When the amount of particles increases a slight increase in the complex viscosity is also obtained [Figure 7(a)]. However, no important differences are found between the different materials, as the values of the zero shear viscosity indicate (Table VI). In connection with the storage modulus [Figure 7(b)] its slope in the terminal region decreases; although, the values of this slope are always higher than one. The fact of increasing the clay content could favor the formation of a network structure and the behavior of the system could become similar to that of a solid one. However, in this case the complex viscosity shows a Newtonian plateau in the terminal region, the slopes of both moduli in this region are close to one and both, the storage and loss modulus intersect at a certain frequency (Table VI). These results indicate that in these materials a network structure has not been formed. A solid-like behavior is obtained when $G' > G''$ throughout the whole frequency range and G', $G'' \propto \omega^0$ in the terminal region.[12] With the amount of particles used the percolation threshold is not achieved. The formation

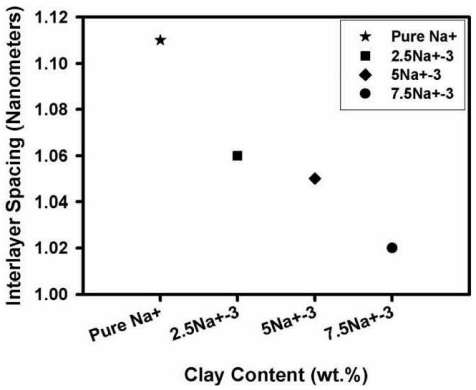

Figure 6. Interlayer spacing of the pure Na+ together with that of the Na+ composites produced with different clay contents, after three extrusions.

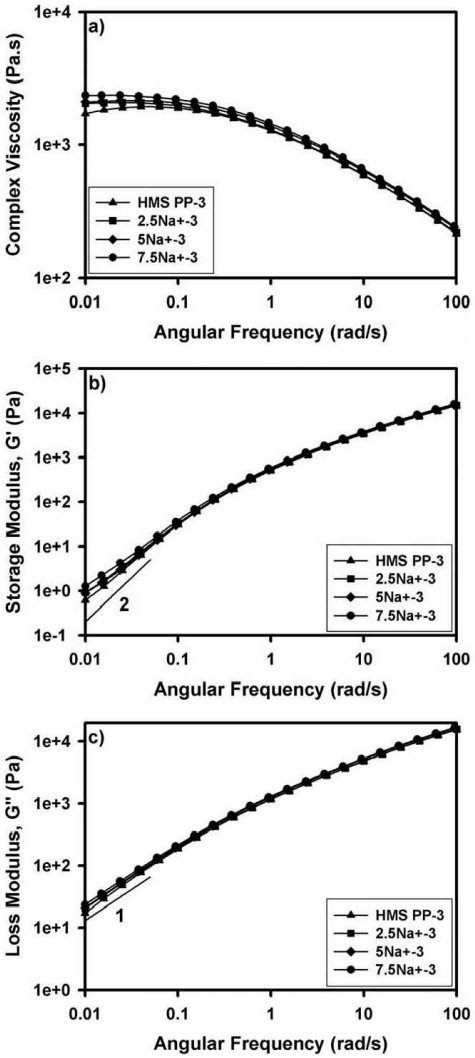

Figure 7. Linear viscoelastic properties of the pure HMS PP together with those of the composites containing different amounts of clays Na+ after being subjected to three extrusions. (a) Complex viscosity as a function of frequency. (b) Storage modulus vs. angular frequency. (c) Loss modulus vs. angular frequency.

of this percolated network is hampered by the fact of the poor intercalation achieved.

The effect of the clay content in the clay exfoliation of organomodified clays (C20A) is also analyzed in this study. The XRD

Table VI. Linear Viscoelastic Properties of Both, the HMS PP and the PP Composites Containing Different Amounts of Na+ after Being Subjected to Three Extrusions

Sample name	Slope G′ (Pa.s)	Slope G″ (Pa.s)	η_0 (Pa.s)	ω_x (rad/s)
HMS PP-3	1.78	1.08	1716	134
2.5Na+-3	1.47	1.03	2030	148
5Na+-3	1.40	1.03	2088	137
7.5Na+-3	1.39	0.99	2356	128

results for the materials after three extrusions are shown in Figure 8. Due to the positive effect that the extrusion process has on the exfoliation/intercalation of organomodified clays, the interlayer spacing of the clays in the composite is always higher than that of the clays as received, independently on the clay content used. However, as with the natural clays, Na+, d decreases when the amount of particles increases because when large amounts of particles are used it is more difficult to exfoliate them. Although the best structure is obtained with the lowest amount of particles, this structure is still an intercalated one. With the most favorable conditions used in this work, a complete clay exfoliation has not been reached.

Furthermore, the linear dynamic viscoelastic behavior of these composites is also analyzed. The results of these measurements are shown in Figure 9. The viscoelastic properties of the melts change with the variations in the clay content. Figure 9(a) shows how the low frequency Newtonian plateau is progressively replaced by a non-Newtonian power law when the clay content increases. The slope in the terminal region of the storage modulus is zero for all the composites studied [Figure 9(b) and Table VII]. However, the slope of the loss modulus decreases progressively when an increase in the clay content is produced [Figure 9(c) and Table VII]. Finally, another

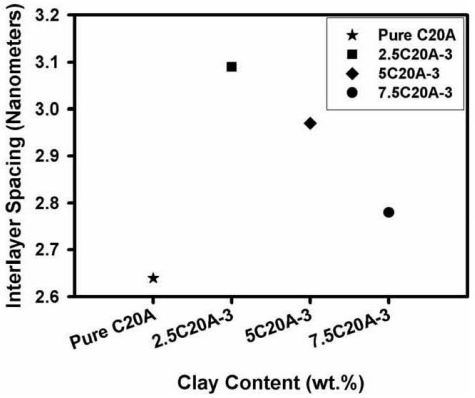

Figure 8. Interlayer spacing of the pure C20A together with that of the C20A composites produced with different clay contents after three extrusions.

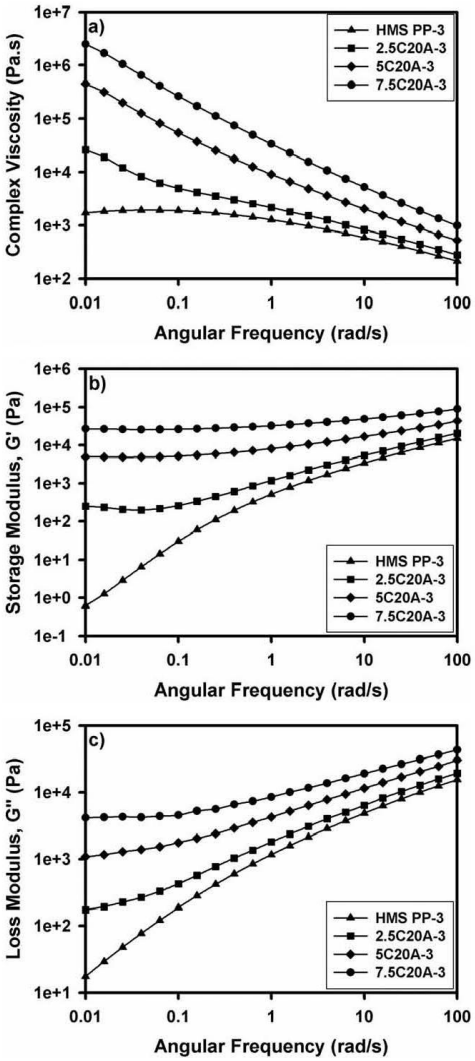

Figure 9. Linear viscoelastic properties of the pure HMS PP together with those of the composites containing different amounts of clays C20A after being subjected to three extrusions. (a) Complex viscosity as a function of frequency. (b) Storage modulus vs. angular frequency. (c) Loss modulus vs. angular frequency.

noteworthy fact is that while the composite containing 2.5 wt % of C20A shows two crossover frequencies, as Table VII indicates, for the other two higher contents G′ is greater than G″ in the whole frequency range. The rheological response of the material 2.5C20A-3 indicates that this amount of particles is close to the percolation threshold. On the other hand, the rheological response obtained with the other two materials (5C20A-3 and 7.5C20A-3), which is more a solid like behavior, indicates that this clay contents are far above the percolation threshold.[12]

The percolation threshold (Φ_{per}) has been quantified. To determine this parameter, the Equation 3 has been used.[14]

$$G' = C\left(\Phi - \Phi_{per}\right)^{n} \quad (3)$$

where C is a constant, n is a power law exponent, Φ is the clay volume fraction, Φ_{per} is the percolation threshold volume fraction and G′ is the value of the storage modulus at low frequencies. Φ_{per} is obtained by fitting to a linear regression the curve $\log G'$ versus $\log\left(\Phi - \Phi_{per}\right)$. This was done for different values of Φ_{per}. The value of Φ_{per} for which the best fit is obtained is the percolation threshold of the composite. In this system, a value of the percolation threshold of 1 wt % was obtained. This result indicates that, in the case of the organomodified clays, all the clay contents employed all above the percolation threshold.

Effect of the Foaming Process on the Clay Exfoliation

The third objective of this work is to determine the effect of the foaming process on the clay exfoliation. XRD results are shown in Figure 10 for both, the composites produced with the natural clays and the composites produced with the organomodified clays.

In the two composites, an increase in the interlayer distance is produced when the materials are foamed. Figure 10(a) shows that the interlayer distance of the foamed composites HMS PP/Na+ is even higher than that of the pure Na+. While the extrusion process had a negative effect in the clay exfoliation the foaming process helps in getting a better clay structure. In the foamed material the interlayer distance decreases when the clay content increases just as it happened in the solid composites. The interlayer distance has increased about 1.2 times compared to the solid material. The same behavior is obtained with the organomodified clays [Figure 10(b)]. Nevertheless, in this case the increase in the interlayer distance is slightly higher (1.4 times) than that obtained in the natural clays. The larger interlayer spacing of organomodified clays and the use of a compatibilizer make the foaming process to be more effective in these composites. However, the clays are not completely exfoliated, not even after the foaming process since the diffraction peak corresponding to the (001) plane still appears in the diffractograms. As there are no external forces (like shear) associated to the foaming process that help the polymer macromolecules

Table VII. Linear Viscoelastic Properties of Both, the HMS PP and the PP Composites Containing Different Amounts of C20A after Being Subjected to Three Extrusions

Sample name	Slope G′ (Pa.s)	Slope G″ (Pa.s)	ω_{x1} (rad/s)	ω_{x2} (rad/s)
HMS PP-3	1.78	1.08	-	134
2.5C20A-3	−0.17	0.29	0.02	67
5C20A-3	−0.02	0.19	-	-
7.5C20A-3	−0.03	0.03	-	-

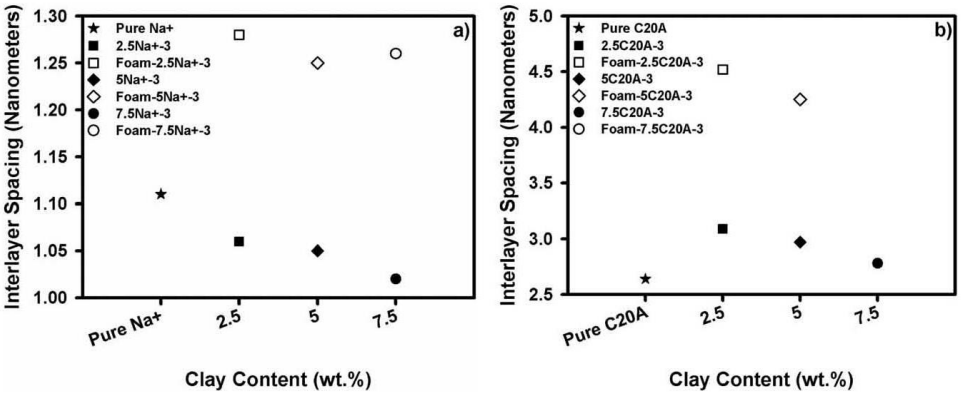

Figure 10. XRD results of the foamed materials. (a) Interlayer spacing of the pure Na+ together with that of the solid and foamed Na+ composites. (b) Interlayer spacing of the pure C20A together with that of the solid and foamed C20A composites.

to diffuse into the clay gaps, the increase in the interlayer distance is due to the expansion that the composite suffers during the foaming process. This expansion produces a physical separation of the particles and consequently their interlayer spacing increases.

CONCLUSIONS

The effects that the extrusion process, clay content and foaming process have on the morphology of two different HMS PP/clay composites have been widely analyzed in this work. For this purpose two different composites have been produced. The first composite was produced using only natural clays (Na+) and the second composite contains organomodified clays (C20A) and a compatibilizer (PP-MA).

XRD results show that while in the HMS PP/Na+ composites the extrusion process has a negative effect decreasing the clays interlayer spacing, in the HMS PP/C20A composites the extrusion process improves the clays intercalation. During this process the polymer is able to separate the clay sheets due to two reasons. First, the larger interlayer distance that the C20A clays show favors the penetration of the polymer into the clay gallery. Second, as a consequence of the greater compatibilization between the clays and the polymer, the forces that the polymer exerts on the clay agglomerates are greater, which helps to separate the clay layers. The linear dynamic rheological behavior of the pure HMS PP and the two composites was also studied. These results show that the HMS PP structure is affected by the extrusion process. During this process the polymer degrades. A reduction either in the content of branched components or in the length of the branched chain is taking place. The rheological behavior of the HMS PP/Na+ composites is affected by the extrusion process in the same way as the pure HMS PP. When the clays are not exfoliated no important changes are detected in the rheological behavior of the composites with regard to that of the unfilled polymeric matrix. Nevertheless, the rheological behavior of the HMS PP/C20A composites is completely opposite to that obtained either with the pure HMS PP or with the other composite. Results indicate that the extrusion process favors the presence of a space-filling network caused by attractive forces between the clay platelets.

The effect of the clay content on the clay exfoliation is also studied. In both composites the interlayer spacing decreases when the clay content increases. As the interaction between the particles increases due to an increase in the particle content, it is more difficult to separate them. Rheological results indicate that in the HMS PP/Na+ composites a network structure has not been formed, with the clay contents used. However, in the composites produced with the C20A clays a value of the percolation threshold of 1 wt % has been obtained indicating that all the clay contents used in this work are above the percolation threshold.

Finally, the effect of the foaming process on the clay exfoliation has also been analyzed. In the two composites, an increase in the interlayer distance is produced when the materials are foamed. The expansion that the composite suffers during the foaming process produces a physical separation of the particles and consequently their interlayer spacing increases.

ACKNOWLEDGMENTS

Financial support from PIRTU contract of E. Laguna-Gutierrez by Junta of Castilla and Leon (EDU/289/2011) and cofinanced by the European Social Fund is gratefully acknowledged. Financial support from the MICINN (MAT 2012-34901) the Junta of Castilla and Leon (VA 035U13) and the EU (Nancore Project: EC project number 214148) is gratefully acknowledged.

REFERENCES

1. Kissel, W. J.; Han, J. H.; Meyer, J. A. In Handbook of Polypropylene and Polypropylene Composites, Revised and

Expanded; Karian, H. G., Ed.; Taylor & Francis: New York, **2009**; Chapter 2, pp 10–27.
2. He, C.; Costeux, S.; Wood-Adams, P.; Dealy, J. M. *Polymer* **2003**, *44*, 7181.
3. Gotsis, A. D.; Zeevenhoven, B. L. F.; Tsenoglou, C. *J. Rheol.* **2004**, *48*, 895.
4. Koo, C. M.; Kym, J. H.; Wang, K. H.; Chung, I. J. *J. Polym. Sci. Part B: Polym. Phys.* **2005**, *43*, 158.
5. Lee, S. H.; Cho, E.; Youn, J. R. *J. Appl. Polym. Sci.* **2007**, *103*, 3506.
6. Okamoto, M.; Nam, P. H.; Maiti, P.; Kotaka, T.; Hasegawa, N.; Usuki, A. *Nano. Lett.* **2001**, *1*, 295.
7. Fu, S. Y.; Feng, X. Q.; Lauke, B.; Mai, Y. W. *Compos. Part B: Eng.* **2008**, *39*, 933.
8. Papageorgiou, G. Z.; Achilias, D. S.; Bikiaris, D. N.; Karayannidis, G. P. *Thermochim. Acta* **2005**, *427*, 117.
9. Chrissafis, K.; Bikiaris, D. *Thermochim. Acta* **2011**, *523*, 1.
10. Gilman, J. W. In Flame Retardant Polymer Nanocomposites; Morgan, A. B.; Wilkie, C. A., Eds.; Willey: Hoboken, NJ, **2007**; Chapter 3, pp 67-88.
11. Spitalsky, Z.; Tasis, D.; Papagelis, K.; Galiotis, C. *Prog. Polym. Sci.* **2010**, *35*, 357.
12. Zhao, J.; Morgan, A. B.; Harris, J. D. *Polymer* **2005**, *46*, 8641.
13. Galindo-Rosales, F. J.; Moldenaers, P.; Vermant, J. *Macromol. Mater. Eng.* **2011**, *296*, 311.
14. Vermant, J.; Ceccia, S.; Dolgovskij, M. K.; Maffettone, P. L.; Macosko, C. W. *J. Rheol.* **2007**, *51*, 429.
15. Zhang, Q.; Fu, Q.; Jiang, L.; Lei, Y. *Polym. Int.* **2000**, *49*, 1561.
16. Kim, K.; Kim, H.; Lee, J. *Polym. Eng. Sci.* **2001**, *41*, 1963.
17. Ma, J.; Qi, Z.; Hu, Y. *J. Appl. Polym. Sci.* **2001**, *82*, 3611.
18. Galgali, G.; Ramesh, C.; Lele, A. *Macromolecules* **2001**, *34*, 852.
19. Hasegawa, N.; Kawasumi, M.; Kato, M.; Usuki, A.; Okada, A. *J. Appl. Polym. Sci.* **1998**, *67*, 87.
20. Dong, Y.; Bhattacharyya, D. *Compos. Part A* **2008**, 39, 1177.
21. Kato, M.; Usuki, A.; Okada, A. *J. Appl. Polym. Sci.* **1997**, *66*, 1781.
22. Wang, Y.; Chen, F.; Wu, K. *J. Appl. Polym. Sci.* **2004**, *93*, 100.
23. Lertwimolnun, W.; Vergnes, B. *Polymer* **2005**, *46*, 3462.
24. Modesti, M.; Lorenzetti, A.; Bon, D.; Besco, S. *Polymer* **2005**, *46*, 10237.
25. Peltola, P.; Välipakka, E.; Vuorinen, J.; Syrjaälä, S.; Hanhi, K. *Polym. Eng. Sci.* **2006**, *46*, 995.
26. Treece, M. A.; Zhang, W.; Moffitt, R. D.; Oberhauser, J. P. *Polym. Eng. Sci.* **2007**, *47*, 898.
27. Bhattacharya, S.; Gupta, R. K.; Jollands, M.; Bhattacharya, S. N. *Polym. Eng. Sci.* **2009**, *49*, 2070.
28. Su, F. H.; Huang, H. X. *J. Appl. Polym. Sci.* **2010**, *116*, 2557.
29. Auhl, D.; Stange, J.; Münstedt, H.; Krause, B.; Voigt, D.; Lederer, A.; Lappan, U.; Lunkwitz, K. *Macromolecules* **2004**, *37*, 9465.
30. Zheng, W. G.; Lee, Y. H.; Park, C. B. *J. Appl. Polym. Sci.* **2010**, *117*, 2972.
31. Zhai, W.; Park, C. B.; Kontopoulou, M. *Ind. Eng. Chem. Res.* **2011**, *50*, 7282.
32. Saiz-Arroyo, C.; de Saja, J. A; Velasco, J. I.; Rodriguez-Perez, M. A. *J. Mater. Sci.* **2012**, *47*, 5680.
33. Saiz-Arroyo, C.; Rodriguez-Perez, M. A.; Velasco, J. I.; de Saja, J. A. *Compos. Part B* **2013**, *48*, 40.
34. Saiz-Arroyo, C.; Rodriguez-Perez, M. A.; Tirado, J.; Lopez-Gil, A.; de Saja, J. A. *Polym. Int.* **2013**, *62*, 1324.
35. Laguna-Gutierrez, E.; Van Hooghten, R.; Moldenaers, P.; Rodriguez-Perez, M. A. *J. Appl. Polym. Sci.* **2014**, DOI: 10.1002/app.42430.
36. Gibson, L. J. *Mat. Sci. Eng.: A* **1989**,*110*, 1.
37. Marin, G.; Montfort, J. P. In Rheology for Polymer Melt Processing; Piau, J. M.; Agassant, J. F., Eds.; Elsevier Science: Amsterdam, **1996**; Chapter 1.5, pp 95–140.
38. Wood-Adams, P. M.; Dealy, J. M.; de Groot, A. W.; Redwine, O. D. *Macromolecules* **2000**, *33*, 7489.
39. Tian, J.; Yu, W.; Zhou, C. *Polymer* **2006**, *47*, 7962.
40. Kawasumi, M.; Hasegawa, N.; Kato, M.; Usuki, A.; Okada, A. *Macromolecules* **1997**, *30*, 6333.
41. Lertwimolnum, W.; Vergnes, B. *Polymer* **2005**, *46*, 3462.
42. Velasco, J. I.; Ardanuy, M.; Realinho, V.; Antunes, M.; Fernandez, A. I.; Gonzalez-Peña, J. I.; Rodriguez-Perez, M. A.; de Saja, J. A. *J. Appl. Polym. Sci.* **2006**, *102*, 1213.
43. Reichert, P.; Nitz, H.; Klinke, S.; Brandsch, R.; Thomann, R.; Mülhaupt, R. *Macromol. Mater. Eng.* **2000**, *275*, 8.

5.3 Extensional rheology/cellular structure/mechanical behavior relationships

First of all, the effect of the extrusion process on the extensional rheological properties of the pure (unfilled) HMS PP is analyzed. For this purpose the polymer is subjected to one and three extrusion cycles. This preliminary study is conducted with the aim of analyzing and understanding the importance of comparing materials with the same thermo-mechanical history.

Subsequently, in this work the extensional rheological behavior of some of the composites analyzed in the paper included in the section 5.2 is studied. From all the composites previously produced and characterized by XRD and SAOS, only those subjected to a total of three extrusion cycles are selected to perform this second study. From the extensional rheological results the strain hardening coefficient is determined. These measurements are performed at a temperature of 200 ºC and the strain hardening is quantified for a value of the Hencky strain rate of 1 s^{-1} and for a value of the Hencky strain of 3. The mechanical properties of the solid composites are also analyzed by performing tensile tests, in order to, subsequently, explain and understand the mechanical properties of the foamed materials. Furthermore, SEM micrographs of some of the solid composites are obtained with the aim of determining the size of the particle agglomerates.

Then, these composites are foamed by ICM at a temperature of 200 ºC, so that both, the foaming temperature and the temperature employed in the rheological tests are the same. This technique allows producing cellular materials with the same density (180 kg/m^3). The cellular structure of the foamed materials is analyzed in detail. Parameters such as the open cell content, the average cell size, the standard deviation coefficient of the cell size distribution relative to the cell size, the cell wall thickness and the cell density are quantified. The mechanical properties, in compression, of the foamed materials are measured. From these measurements, the elastic modulus and the collapse stress are determined.

Finally, the effect of the extensional behavior on the cellular structure is analyzed as well as the effects that both, the cellular structure and the mechanical properties of the solid composites have on the mechanical properties of the foamed materials. The main goal of this paper is to analyze if it is possible to establish a relationship between extensional rheology, cellular structure and mechanical properties, when working with polymeric nanocomposites.

Extensional Rheology/Cellular Structure/Mechanical Behavior Relationships in HMS PP/Montmorillonite Foams with the Same Density

Ester Laguna-Gutierrez [(1)], Alberto Lopez-Gil [(2)], Cristina Saiz-Arroyo [(2)], Rob Van Hooghten [(3)], Paula Moldenaers [(3)], Miguel Angel Rodriguez-Perez [(1)]

[(1)] Cellular Materials Laboratory (CellMat), Condensed Matter Physics Department, University of Valladolid, Paseo de Belén, 7, 47011 Valladolid, Spain

[(2)] CellMat Technologies, CTTA (building), Paseo de Belén 9A, 47011 Valladolid, Spain

[(3)] Department of Chemical Engineering, KU Leuven, Celestijnenlaan 200F, B 3001 Heverlee, Leuven, Belgium

ABSTRACT

Due to its rheological properties, high melt strength polypropylenes (HMS PP) are normally employed to produce cellular materials with improved properties. However, the loss of mechanical properties produced when these polymer are foamed is still very significant. One approach to improve their mechanical properties consists on the use of nanoparticles such as montmorillonites (MMTs). The main goal of this work is to analyze the relationship between the extensional rheological behavior of the solid nanocomposite based on HMS PP and MMTs and the cellular structure and mechanical properties of foams produced from these materials. As the properties of the nanomaterials are conditioned by both dispersion and compatibilization degrees, in this study two different systems have been considered. The first system incorporates organomodified montmorillonites and a compatibilizer and the second system contains natural clays and is produced without a compatibilizer. Results indicate that the extensional rheological behavior of both materials is completely different. The strain hardening of the polymer containing organomodified clays decreases as the clay content increases. As a consequence, the open cell content of this material increases with the clay content and hence, the mechanical properties get worse. However, in the materials produced with natural clays this relationship is not so clear. While no changes are detected in the extensional rheological behavior by adding these particles, the nano-filled materials show an open cellular structure, opposite to the closed cellular structure of the pure polymer, which is caused by the fact of having particle agglomerates with a size larger than the thickness of the cell walls. This work indicates that, while in the unfilled polymers a clear relationship between extensional rheology and cellular structure is normally obtained and therefore the extensional rheology is a very useful tool to analyze and understand the cellular structure and mechanical properties of the cellular materials, in the nano-filled polymers the obtaining of this relationship is conditioned by the intercalation level of the layered clays into the polymeric matrix and the size of the particle agglomerates.

INTRODUCTION

Common linear polypropylene (PP) has many desirable properties such as good temperature stability, good chemical resistance, high melting temperature, high tensile modulus and the capability of static load bearing [1]. These beneficial properties have permitted to use polypropylene in many different applications. However, its linear structure leads to poor processability in processes involving melt stretching, such as extrusion coating, film blowing, thermoforming and foaming [2]. A way to improve the polymer melt strength is to incorporate

long chain branches (LCB) as the PPs with LCB have a pronounced strain hardening, which is closely related to an improvement of the melt strength [3]. In a previous work, different blends of a linear PP and a HMS PP were analyzed with the aim of understanding how the extensional rheological behavior of the polymeric matrix affects the cellular structure and mechanical properties of foamed materials produced with the same density [4]. Both, linear PP and blends rich in linear PP showed a low strain hardening. This low strain hardening led to a rupture of the cell walls under the extensional forces occurring during cell growth. As a result, the final foam had an elevated content of open cells, cells with large sizes and cellular structures very heterogeneous, which harmed their mechanical properties.

However, in spite of using a HMS PP to produce the foamed materials, the loss of mechanical properties when the PP is foamed at relative low densities is very strong [5]. One approach to solve this problem consists on the use of nanoparticles as they can improve the overall properties of the foam by acting at two levels. On the one hand, by improving the morphology and properties of the solid polymeric matrix comprising the cell walls and on the other hand, by optimizing the cellular structure. Among all the possible nanoparticles, those based on layered silicates, like montmorillonites, have been used in this work because they have been widely investigated, these clays are easily available and they can also be processed by employing common processing routes.

When nanoparticles are added to the polymeric matrix, many properties can be improved. Several authors have proved that montmorillonites reinforce the polymeric matrix and therefore they improve its mechanical properties [6-9]. Moreover, when the polymer is filled with nanoclays there are also improvements in the thermal stability as well as in the barrier and flame retardancy properties [10-12].

However, not only improvements in the physical properties of the polymeric nanocomposites are obtained, the polymer morphology is also affected by the nanoparticles as it is indicated by the rheological properties. Both, linear and non-linear shear rheological properties are very sensitive to changes in the particular nanoscale and mesoscale structure [13]. Furthermore, several authors have proved that the introduction of nanoparticles can also increase the melt strength of the common linear PPs or induce strain hardening to the melt [14-17]. However, while the effects of these nanoparticles on the rheological behavior of common linear PPs have been widely investigated, as far as the author knowledge, there are no many works that analyze these effects on a HMS PP. Only two papers have been found. Bhattacharya et al. [18] worked with HMS PP/organomodified clays nanocomposites containing different amounts of clays. They showed that all the polymers (pure polymer and nanocomposites) displayed strain hardening. Moreover, they obtained that the strain hardening was more pronounced in the polymeric nanocomposites than in the neat polymer. Su et al. [19] determined the melt strength and the apparent elongational viscosity from the Rheotens data. They obtained that the melt strength of nanocomposites was lower than that of the unfilled polymer. In general they found that the melt strength decreased as the clay content increased. Moreover, the same behavior was followed by the apparent elongational viscosity. The results obtained in these two papers are contradictory which might be an indicative of the need of a more thorough study of the rheological behavior of HMS PP/clays nanocomposites.

As it was previously mentioned, nanoparticles not only improve the overall properties of the foamed materials by improving the polymeric matrix properties, they also contribute to this overall improvement by optimizing the cellular structure. Several works have demonstrated that the incorporation of nanoparticles leads to foams with higher cell density, smaller cell size and more homogeneous cellular structures [17,20-22]. On the one hand, nanoparticles are highly effective cell nucleating agents and they can also increase the cell nucleation rate [17,20-22]. On the other hand, nanoparticles can also reduce or even suppress cell coalescence [17,21,22]. As it was indicated above, the presence of nanoparticles can effectively increase the melt strength of the linear PPs and hence improve their foamability. Nevertheless, this result is not so obvious in foams produced with HMS PP based nanocomposites as the effect that the nanoparticles have on the rheological behavior of this matrix is still not well understood (see previous paragraph).

The improvements obtained in both, the solid polymeric matrix and the cellular structure are greatly affected by the degree of filler intercalation/exfoliation and dispersion achieved during the mixing process as well as by the compatibilization between the particles and the polymer [23]. A fully dispersed and stable state will lead to optimal properties whereas the presence of particle agglomerates or a low compatibility between the particles and the polymeric matrix can lead to a poor material performance, in some cases, even lower than that of the virgin polymeric matrix [24]. It is for this reason that the number of works dealing with the structure of the clays in the solid composites is very high. They typically analyze the effects of using non-organomodified and organomodified montmorillonites as well as the effects of the initial interlayer spacing and the clay content [25-27]. In addition, the influence of adding or not a compatibilizer and the effects in the clay structure of the amount and type of compatibilizer have been traditionally analyzed [28-30]. Finally, the effect that the production process, required to produce the solid nanocomposites, has on the clay morphology has also been carefully studied [30,31]. All these works are mainly focused on understanding the clay structure of linear PP/montmorillonite solid nanocomposites. However, the number of papers that study the degree of intercalation/exfoliation of layered composites produced with a HMS PP is limited [18,32]. In the same way, very few works are focused on studying the structure that the particles present after the foaming process, which is also fundamental to understand the properties of the foamed materials [33,34].

Taking into account these ideas, in this work the effect of adding layered clays into a HMS PP based polymeric matrix is studied. Particularly, the effects that these particles induce on the extensional rheological behavior of the non-foamed materials as well as on the cellular structure (cell nucleation and cell coalescence) and mechanical properties of the foamed materials are deeply investigated. This study aims at establishing a relationship between extensional rheology, cellular structure and mechanical properties of HMS PP/montmorillonite based cellular materials. As it was previously shown, in the unfilled polymers the extensional rheology is a very useful tool to analyze and understand the cellular structure and mechanical properties exhibited by the cellular materials [4]; however, in the filled materials this relationship is still not well-defined. To meet these objectives, cellular materials with the same density and with different clay contents have been produced and analyzed. Moreover, due to the importance of both the exfoliation/dispersion and the compatibilization degrees, this study is performed in two completely different systems. The first system comprises a material

produced using non organomodified clays and without a compatibilizer, while the second system refers to a material including both organomodified clays and a compatibilizer. A more detailed analysis about both, the morphology (intercalation/dispersion degrees of the nanoparticles in the polymeric matrix) of all the solid composites studied in this work and the morphology of these composites after the foaming process can be found in a previous work developed by the authors of this publication [35].

EXPERIMENTAL

Materials

A branched high melt strength PP (HMS PP) supplied by Borealis (PP Daploy WB 135 HMS) with a MFI of 2.4 g/10 min (230 ºC/2.16 kg) was used in this study. The HMS PP density at room temperature is 905 kg/m^3. Two kind of commercial clays were employed as fillers for the PP composite preparation. A non-organomodified montmorillonite, Cloisite® Na+ (Na+) supplied by Southern Clay Products with a density of 2860 kg/m^3, and an organomodified montmorillonite with quaternary ammonium salt, Cloisite® 20A (C20A) also supplied by Southern Clay Products, with a density of 1770 kg/m^3. A maleic anhydride modified homopolymer polypropylene (PP-MA), Polybond 3200 supplied by Chemtura with a MFI of 115 g/10 min (190 ºC/2.16 kg), was used as a chemical compatibilizer between the polymeric matrix and the organomodified clays.

Antioxidants Irgafos 168 and Irganox 1010 (from Ciba) were also used in order to prevent the thermal degradation of the polymers.

The foaming step was performed using a chemical blowing agent, azodicarbonamide (ADC) Lanxess Porofor M-C1 with a density of 1650 kg/m^3 and an average particle size of 3.9 ± 0.6 μm.

Composite Preparation

Two kind of solid materials were produced. The first one contains the blowing agent and was used to produce the cellular materials. The second, without the blowing agent, was employed for the rheological characterization as well as for the tensile tests. Moreover, solid composites containing the two different kinds of clays were prepared. The first system, as it said, was a polymeric composite in which the clay intercalation/exfoliation and compatibilization with the polymeric matrix are not favorable. To produce this composite the polymeric matrix was blended with non-organomodified (natural) clays (Na+), without using a compatibilizer. On the other hand, in the second system, the clay intercalation/exfoliation was favored by using organomodified clays in which the initial interlayer spacing is larger and the interaction between the clay platelets and the polymer is also better. Moreover, PP-MA was also used as a compatibilizer between the polar particles and the non-polar polymeric matrix. The steps followed to produce the different polymeric composites are described below.

In a first step, all the raw materials were vacuum dried at 50 ºC for twelve hours. The two considered systems were produced in a different way.

With regards to the composites produced with the Na+, firstly the natural clays and the HMS PP were melt-compounded using a co-rotating twin screw extruder Collin ZK 25T with a L/D of 24. The rotational speed used was 50 rpm and the melt temperature was 200 ºC. Composites

containing three different contents of clays were produced (2.5, 5 and 7.5 wt.%) in this first extrusion step. Moreover, also a 0.1 wt.% of antioxidants were added to the formulation (Irgafos 168 in a proportion of 0.08 % and Irganox 1010 in a proportion of 0.02 % by weight). Secondly, these materials were blended with 2 wt.% of blowing agent (ADC). In this second extrusion step the rotational speed used was 120 rpm and the melt temperature was 155 ºC, which is well below the decomposition temperature of the blowing agent. Finally, a third extrusion of these materials was performed, under the same conditions as the second extrusion, with the aim of having the azodicarbonamide homogeneously distributed along the material. The whole process was conducted in the same extruder, previously described. The same extrusion process, which involves a total of three extrusion cycles, was used to produce the solid composites without the blowing agent. Both materials were subjected to the same extrusion process with the aim of analyzing the rheological behavior in a material having the same thermo-mechanical history as the material used for foaming.

With regards to the composites produced with the C20A, firstly a masterbatch containing the clays C20A and the compatibilizer PP-MA in the same proportion (1:1) was produced. A rotational speed of 50 rpm was employed and the melt temperature was 200 ºC. Composites with the desired clay contents (2.5, 5 and 7.5 wt.%) were then prepared by diluting, under these same extrusion conditions, the masterbatch in the HMS PP. In this point the antioxidants were also added to the different blends. Then the composites were melt-blended with the blowing agent, using the same extrusion conditions as those employed with the composites containing Na+. Again the same extrusion process was used to produce the composites without the blowing agent for the rheological characterization.

The same extrusion process used with the polymer containing the natural clays was also employed with the pure HMS PP, with the aim of using this material as reference. Moreover, the effect that the number of extrusion cycles has on the extensional rheological properties of the pure HMS PP is also studied in order to analyze the importance of comparing materials with the same thermo-mechanical histories. For this purpose, the extensional rheological behavior of the HMS PP is measured after a first extrusion cycle (HMS PP-1) and after a total of three extrusion cycles (HMS PP-3).

The produced solid materials are summarized in Table 1. The nomenclature employed includes the content and type of particles employed as well as the total amount of extrusion cycles to which the material is subjected. To denote the solid composites containing the blowing agent, which were subsequently foamed, the word “Foam” has been added at the beginning of the corresponding nomenclatures. It was not possible to produce the foamed material containing 7.5 wt.% of C20A with the same density as the other cellular materials and due to this, this material has not been included in Table 1.

Table 1. Summary of the formulations produced with the pure HMS PP and the different composites.

Sample Name	HMS PP (wt.%)	PP-MA (wt.%)	Antioxidants (wt.%)	Na+ (wt.%)	C20A (wt.%)	ADC (wt.%)	Number of Extrusion Cycles
2.5 Na+-3	97.4	0	0.1	2.5	0	0	3
5 Na+-3	94.9	0	0.1	5	0	0	3
7.5 Na+-3	92.4	0	0.1	7.5	0	0	3

2.5 C20A-3	94.9	2.5	0.1	0	2.5	0	3
5 C20A-3	89.9	5	0.1	0	5	0	3
7.5 C20A-3	84.9	7.5	0.1	0	7.5	0	3
HMS PP-1	99.9	0	0.1	0	0	0	1
HMS PP-3	99.9	0	0.1	0	0	0	3
Foam-2.5 Na+-3	95.4	0	0.1	2.5	0	2	3
Foam-5 Na+-3	93.0	0	0.1	4.9	0	2	3
Foam-7.5 Na+-3	90.5	0	0.1	7.4	0	2	3
Foam-2.5 C20A-3	92.9	2.5	0.1	0	2.5	2	3
Foam-5 C20A-3	88.1	4.9	0.1	0	4.9	2	3
Foam-HMS PP-3	97.9	0	0.1	0	0	2	3

Foaming Process

The foaming process selected to produce the cellular materials was the Improved Compression Moulding (ICM) route. In this process the pellets containing the blowing agent are placed in a mold which is afterwards positioned in a hot-plate press. An initial pressure is applied to the system (41.5 bars) while it is heated until the foaming temperature (200 ºC) which is higher than the decomposition temperature of the blowing agent. After a certain time (approximately 15 minutes) when the blowing agent is fully decomposed the pressure of the press is released allowing the polymer to expand until a desired ratio. Finally, the mold is introduced in cold water to cool-down the sample and hence stabilizing the cellular structure as fast as possible [36]. The peculiarity of this foaming system is that the mold used is a self-expandable mold that allows controlling the material density by mechanical means and therefore the foam density is independent of the chosen formulation. In this work the materials were produced with a density of 180 kg/m^3. The fact of having similar densities for all the foamed materials allows an easier comparison between materials produced with different formulations. Foamed samples were discs with 150 mm in diameter and 10 mm in thickness. A more detailed description of the ICM technique can be found elsewhere [37-39].

SAMPLES CHARACTERIZATION

X-Ray Diffraction (XRD)

X-ray diffraction (XRD) measurements were performed in order to analyze the structure of the layered clays. A Bruker D8 Discover A25 diffractometer with Cu-Kα radiation of wavelength 0.154 nm was used. The diffraction spectrum was obtained over a 2θ range of 0-30º.

Solid precursors with a thickness of 0.5 mm produced by compression molding at a temperature of 220 ºC and with a pressure of 21.8 bars were utilized to conduct the XRD measurements of the different solid polymeric composites. These measurements were also performed in the clays as received and in the foamed composites.

Extensional Rheological Behavior

The transient extensional viscosity of the pure HMS PPs, subjected to different extrusion cycles, as well as that of the composites prepared with the two types of clays was measured using a strain controlled rheometer (Ares-2K from TA Instruments) with the Extensional Viscosity Fixture (EVF). In this geometry two cylinders are used to wind-up the sample. One cylinder is rotating and the other one is measuring the force. In order to wind-up the sample equally on both sides, the rotating cylinder moves on a circular orbit around the force-

measuring cylinder while this is rotating around its own axis at the same time. All the experiments were made at a temperature of 200 ºC (this is the same temperature at which the foaming process was performed). Rectangular solid samples, with dimensions of 20 mm x 10 mm x 0.5 mm (L x W x T), fabricated by compression molding, at a temperature of 220 ºC and a pressure of 21.8 bars, were employed.

The measurement protocol used considers, firstly, a pre-stretch, in order to compensate the thermal expansion of the sample when it is heated up from room temperature. Then, when the pre-stretch was finished, the sample was kept for 30 s at a constant temperature (200 ºC) without applying any stress. After this relaxation time, the experiment took place. Measurements were performed at a Hencky strain rate of 1 s^{-1} and the maximum Hencky strain applied was 3 for all the different materials.

Density

The density of the solid materials (ρ_s) was determined using a gas pycnometer (Accupyc II 1340 from Micromeritics). The density of the cellular materials (ρ_{cm}) was determined by using the geometric method; this is by dividing the weight of each specimen by its corresponding volume (ASTM standard D1622-08). The samples used were cubes with dimensions of 20 mm x 20 mm x 10 mm (L x W x T) cut from the samples produced by ICM.

Open Cell Content

The open cell content of the foamed materials was determined according to the ASTM Standard D6226-10 using a gas pycnometer Accupyc II 1340 from Micromeritics. Once again the samples used were cubes with dimensions of 20 mm x 20 mm x 10 mm (L x W x T).

The following equation (Equation 1) was used according to the mentioned ASTM Standard:

$$OC(\%) = 100x\left(\frac{V_{sample} - V_{pyc}}{V_{sample} \cdot p}\right) \quad (1)$$

Where V_{sample} is the geometrical volume of the sample, V_{pyc} is the volume measured by the gas pycnometer and *p* is the sample porosity calculated as $\left(1 - \frac{\rho_{cm}}{\rho_s}\right)$.

Structural Characterization

Scanning Electron Microscopy (SEM) was used to analyze the cellular structure and also to quantify the cell size distribution, the average cell size (Φ), the cell density (N_V), and the standard deviation coefficient of the cell size distribution relative to the cell size (SDC/Φ). For this purpose, the obtained micrographs were analyzed using an image processing tool based on the software Image J/Fiji [40].

Samples were cooled using liquid nitrogen to cut them without modifying their structure; then, they were vacuum coated with a thin layer of gold to make them conductive. A Jeol JSM-820 scanning electron microscope was used to observe the samples morphology.

The average cell size (Φ) is the mean cell diameter in three dimensions, which is defined as indicated in Equation 2.

$$\Phi = \sum_{i=1}^{n} \frac{\Phi^i}{n} \quad (2)$$

where n is the number of counted cells and Φ^i is the three-dimensional cell size of the cell i.

The *SDC* relative to the cell size has been calculated according to Equation 3 [38,41].

$$\frac{SDC}{\Phi} = \frac{1}{\Phi}\sqrt{\sum_{\mathrm{i=1}}^{\mathrm{n}} \frac{(\Phi^i - \Phi)^2}{\mathrm{n}-1}} \tag{3}$$

SDC/Φ gives information related with the width of the cell size distribution. A low value of SDC/Φ indicates a narrow, and therefore a homogeneous cell size distribution, where all cells have a size close to the average value.

The cell density (N_V) has been defined as the number of cells per unit volume of the solid. The following expression (Equation 4) has been used to calculate the cell density.

$$N_V = \frac{6}{\pi\Phi^3}\left(\frac{\rho_s}{\rho_{cm}} - 1\right) \tag{4}$$

If any coalescence occurs during foaming, N_V measures the cell nucleation density [39].

Moreover, the solid composites containing natural clays were analyzed to measure the size of the particles agglomerates in a microscopic scale. For this purpose, an electron scanning microscope model Quanta 200 F from FEI was used. A backscattered electron detector and low vacuum conditions were employed to obtain the SEM micrographs. These conditions allow distinguishing clearly the particles and the polymer, which facilitates the subsequent image analysis. To measure the size of the agglomerates the software Image J/Fifi was employed. The micrographs were binarized and the particles assumed to be ellipses. The major axis of the ellipse was used to give an approximate value of the size of the clay agglomerates (Φ_{Na+}). These measurements have been performed in at least two micrographs of each solid material, obtained from different regions of the solid composite. The same microscope was employed to obtain high magnification micrographs from the foamed materials which were used to measure the thickness of the cell walls (δ_{CW}). The thickness of each cell wall was measured in three different zones of the wall. Moreover, approximately 10 cell walls per material were analyzed. Once again the quantitative analysis was performed employing the software Image J/Fifi.

Mechanical Tests

An Instron Machine (model 5.500R6025) was used to perform the tensile tests of five different samples of each solid composite (without containing the blowing agent). A strain rate of 50 mm/min was employed to measure the tensile modulus (E_s), which was calculated as the slope of the initial zone of the stress-strain curve. The tensile experiments were performed according to the standards ISO 527/1 and 2. The samples were conditioned under controlled atmosphere: 50 % relative humidity and 23 ºC following the standard ISO 291. The samples for the tensile test were fabricated by compression moulding at a temperature of 220 ºC and with a pressure of 21.8 bars.

The same machine was used to determine the mechanical properties in compression of the different cellular materials produced. Stress (σ)-strain (ε) curves were obtained at room temperature and at a strain rate of 10 mm/min. The maximum static strain was 75 % for all the experiments. The compression experiments were performed according to the procedure

described in the standard ASTM D1621. Samples were prisms with dimensions of 20 mm x 20 mm x 10 mm (length x width x thickness) machined from the cellular materials produced by ICM. The compression tests were performed in four different specimens of the same foamed sample and always in a direction parallel to the growing/expansion direction (thickness direction). Two parameters were obtained from these experiments: elastic modulus (E_{cm}) and collapse stress (σ_c) which was taken as the intersection between a parallel line to the stress-strain response at low strains and a parallel line to the plateau region of the stress-strain curve.

A more detailed description of the experimental techniques can be found elsewhere [42-44].

RESULTS

Polymeric Composites Morphology

As it was mentioned in the introduction, significant enhancements in the properties of a polymeric matrix can be achieved by introducing nanoparticles. However, all these potential improvements are greatly conditioned by the degree of filler exfoliation and dispersion achieved during the mixing process. The quality of exfoliation in a composite has been traditionally characterized by XRD. Clays show a characteristic diffraction peak corresponding to the (001) plane. From this peak the interlayer spacing (*d*) was calculated using the Bragg's law (Equation 5):

$$\lambda = 2dsin(\theta) \tag{5}$$

where λ is the wavelength and θ is the diffraction angle.

The interlayer spacing values obtained from the XRD results are shown in Figure 1. This distance has been calculated for both, solid and foamed composites as well as for the clays as received.

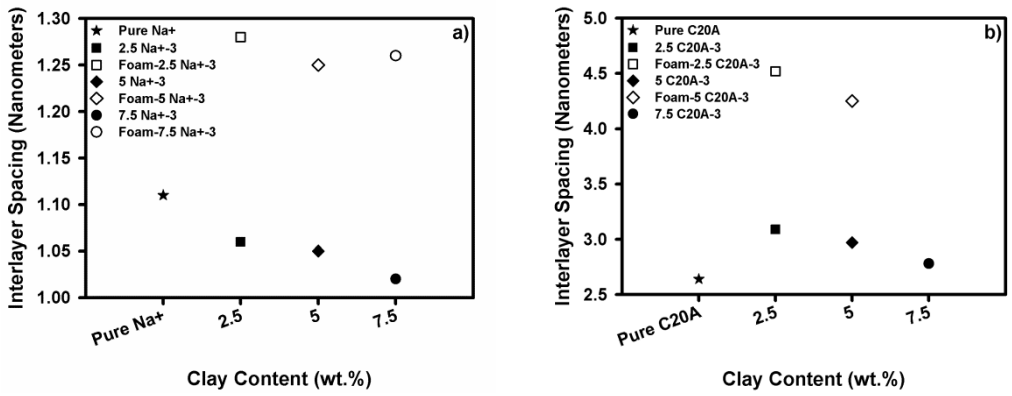

Figure 1. XRD results of the different HMS PP based composites (solid and foamed materials). a) Interlayer spacing of the pure Na+ together with that of the solid and foamed Na+ composites. b) Interlayer spacing of the pure C20A together with that of the solid and foamed C20A composites

Figure 1.a shows that independently of the clay content, the interlayer spacing of the natural clays as received is always higher than that obtained when the clays are blended with the polymer (solid composites). However, in the composites produced with the organomodified clays the interlayer distance is larger in the composites than in the clays as received (Figure 1.b). These results clearly indicate that the effect that the extrusion process has on the clay

intercalation depends on the type of particle employed. While the extrusion process has a negative effect in the natural (non-surface modified) clays, producing a further agglomeration of the particles, the same process induces a separation of the clay platelets in the organomodified particles and consequently a more intercalated structure is obtained for the second system. During the melt extrusion process the polymer is able to separate the clay platelets due to two main facts. On the one hand, the larger initial *d* that the C20A clays show favors the penetration of the polymer into the clay gallery. On the other hand, the combination of organomodified particles and a compatibilizer (PP-MA) makes more favorable the compatibilization between the clays and the polymer and consequently, the forces that the polymer exerts on the clay agglomerates are greater.

In addition, these results show that, regardless the type of particle, the interlayer spacing decreases as the clay content increases. When the clay content increases, the interaction between the clays also increases and therefore it becomes more complicated to intercalate them.

Regarding the foamed materials, in the two types of composites an increase in the interlayer distance is produced after the foaming process. In the foamed material the interlayer distance decreases as the clay content increases just as it happened in the solid composites. Figure 1 also shows that the increase in the interlayer distance obtained after the foaming process is higher in the composites containing organomodified clays (1.4 times) than in those produced with the natural clays (1.2 times). The larger interlayer spacing of organomodified clays and the use of a compatibilizer might be also facilitating a further clay intercalation during the foaming process. As there is no external forces (like shear) associated to the foaming process that could help the polymer macromolecules to diffuse into the clay gaps, the increase in the interlayer spacing could be due to the expansion that the composite suffers during the foaming process. This expansion could be inducing a physical separation of the particles and consequently an increase in the interlayer spacing.

Extensional Rheological Behavior

Before going into details with the analysis of the solid composites, it is important to present the effect that the extrusion process has on the extensional rheological behavior of the pure HMS PP. This effect has been studied in order to analyze the importance of comparing materials with the same thermo-mechanical history. Figure 2 shows the variation of the extensional rheological behavior with the number of extrusion cycles. Figure 2.a shows the transient extensional viscosity of the pure HMS PP after one (HMS PP-1) and three (HMS PP-3) extrusion cycles.

In both materials a phenomenon known as strain hardening, which is related to a rapid increase in the viscosity at high strains (or times), takes place [45]. However, when the number of extrusions increases the slope of the curves, in the region of strain hardening, decreases. From the extensional viscosity measurements the strain hardening coefficient (*S*) has been calculated according to Equation 6.

$$S = \frac{\eta_E^+(t, \dot{\varepsilon}_0)}{\eta_{E0}^+(t)} \tag{6}$$

where $\eta_E^+(t,\dot{\varepsilon}_0)$ is the transient extensional viscosity as a function of time and Hencky strain rate and $\eta_{E0}^+(t)$ is the transient extensional viscosity in the linear viscoelastic regime [46,47]. This value has been obtained for a time of 3 s and for a Hencky strain rate of 1 s^{-1}. The results obtained are shown in Figure 2.b. The strain hardening decreases approximately 2.4 times as the number of extrusion cycles increases from one to three. However, not only changes in the strain hardening coefficient are detected. The melt flow index increases from a value of 4.5 g/10 min (230 ºC/2.16 kg) for the HMS PP-1 to a value of 6.9 g/10 min (230 ºC/2.16 kg) for the HMS PP-3. These changes indicate that during the extrusion process the polymer is being somehow degraded. The viscosity reduction, which is also related to a reduction in the molecular weight, together with the decrease in the *S* could be indicating a possible reduction either in the content of branched components and/or in the length of the branched chains.

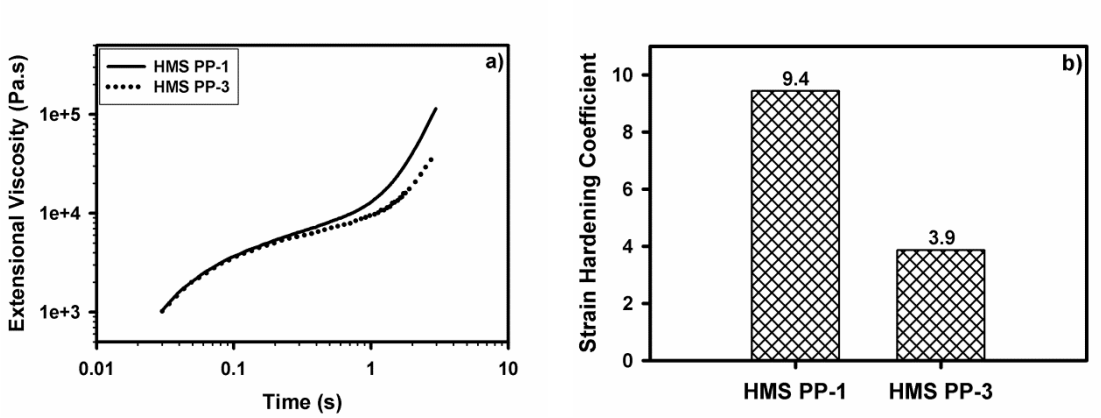

Figure 2. Extensional rheological behavior of the pure HMS PP after one and three extrusion cycles. a) Extensional viscosity vs. time measured at a Hencky strain rate of 1 s^{-1}. b) Strain Hardening Coefficient calculated for a time of 3 s and for a Hencky strain rate of 1 s^{-1}.

Due to the significant changes that the polymeric matrix suffers when it is subjected to different extrusion cycles, the extensional viscosity measurements should be performed in a material with the same thermo-mechanical history as the material or formulation that will be subsequently foamed. Thereby, the extensional rheological behavior could be related to the cellular structure and mechanical properties of the foamed materials. Moreover, to analyze the effect, in the extensional rheological properties, of adding particles to a pure polymeric matrix both, the polymeric matrix and the polymeric composite should have the same thermo-mechanical history.

The extensional viscosity of the HMS PP has been compared to that of the different composites produced with the two types of clays selected for this work. All the materials have the same thermo-mechanical extrusion (3 extrusions). Results are shown in Figure 3.

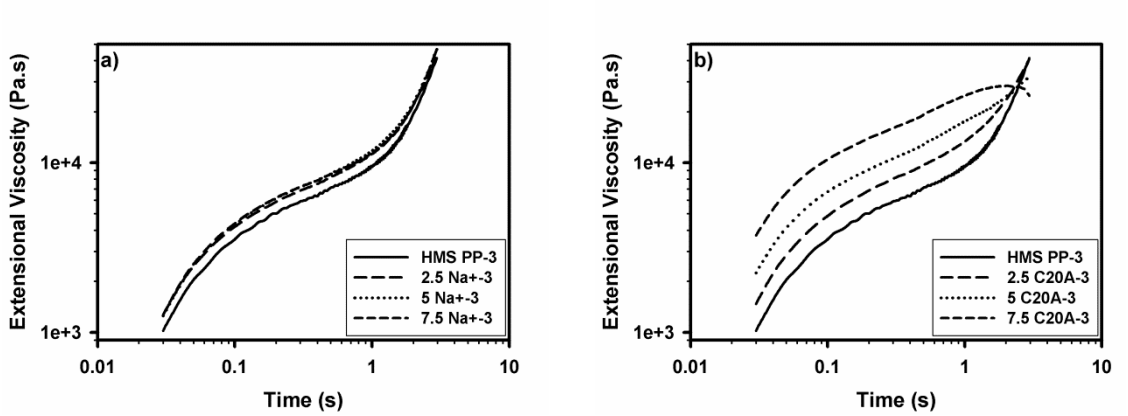

Figure 3. Extensional rheological behavior of the different polymeric composites. a) Composites produced with the natural clays (Na+). b) Composites produced with the organomodified clays (C20A).

As Figure 3.a indicates, no significant changes are produced in the extensional rheological behavior of the pure polymeric matrix by adding natural clays. Only a slight increase in the viscosity as well as a small decrease of the slope in the strain hardening region are detected. In addition, these changes are independent on the clay content. XRD results showed that these particles were completely agglomerated. Therefore, it was not possible to get a percolated network structure with the concentrations of particles used in this work [35]. When the particles are agglomerated and poorly dispersed their aspect ratios are very low and therefore they do not induce significant changes in the polymeric matrix properties. With the C20A clays the changes produced in the rheological properties are very meaningful, as it is depicted in Figure 3.b. In these composites as the clay content increases, a substantial increase in the viscosity occurs while the strain hardening decreases dramatically. In fact, the material with the highest clay content shows the so-called strain softening property since a decrease in the viscosity is detected at high Hencky strains [48]. In these composites in which the interlayer spacing of the clays was higher, an intercalated structure was achieved. In a previous work it was obtained a percolation threshold of 1 % for these composites [35]. The aspect ratio of these clays is larger than that of the natural clays and therefore the formation of a percolated network structure becomes favored. When this clay network is obtained the properties of the composite are substantially affected by the presence of the particles.

As with the pure HMS PP the strain hardening coefficient has also been calculated and the results are summarized in Table 2.

Table 2. Strain Hardening Coefficient of the different polymeric composites.

Sample Name	Strain Hardening Coefficient
HMS PP-3	3.9
2.5 Na+-3	3.8
5 Na+-3	3.6
7.5 Na+-3	3.4
2.5 C20A-3	2.8
5 C20A-3	1.7
7.5 C20A-3	0.9

While the *S* mildly decreases in the Na+ composites an abrupt reduction of this coefficient is obtained by increasing the C20A content. Two possible options have been considered to

explain this behavior. On the one hand, it has been considered the influence caused by the linear structure of the PP-MA used as compatibilizer. When a HMS PP is blended with a linear PP a reduction in the strain hardening occurs and this reduction depends on the ratio of linear PP and HMS PP employed [49]. However, the low amounts of PP-MA used in this work cannot explain the large changes produced in the *S*. Therefore, other phenomena should be considered. Several authors have found that the strain hardening can be strongly decreased by the presence of particles [50-54]. These authors have reported that particles suppress the large deformation of the matrix polymer chains around them. In other words, the region in which elongational flow exists is decreased by the existence of particles. These particles are partially converting the extensional flow in the surrounding polymer into shear flow. Consequently the particles can interfere with the occurrence of the strain hardening phenomena.

Cellular Materials Density and Expansion Ratio

The density of the different foamed materials was measured as it is indicated in the experimental section and the results are summarized in Table 3. The expansion ratio (*ER*) reached by each type of material has also been calculated according to Equation 7 and the obtained values are also included in Table 3.

$$ER = \frac{\rho_s}{\rho_{cm}} \tag{7}$$

Table 3. Cellular materials density and expansion ratio.

Sample Name	Density (kg/m^3)	Standard Deviation (kg/m^3)	Expansion Ratio	Standard Deviation
Foam-HMS PP-3	179.8	0.8	5.00	0.02
Foam-2.5 Na+-3	179.5	0.8	5.04	0.02
Foam-5 Na+-3	182.5	1.3	5.01	0.04
Foam-7.5 Na+-3	181.6	1.4	5.11	0.04
Foam-2.5 C20A-3	180.9	0.5	5.05	0.01
Foam-5 C20A-3	188.5	0.8	4.90	0.02

The employed foaming process (ICM) allows the production of cellular materials with a density and an expansion ratio very similar regardless of the formulation employed to generate them. However, the density of the cellular material containing 5 wt.% of C20A is slightly higher than that of the rest of materials and hence the expansion reached is also slightly lower. The strain hardening coefficient of this composite is very low; consequently, the polymeric composite is not capable of withstanding the induced stretching during foaming. As a result, the cell walls can easily break and the foam is not able to retain the gas during the expansion process making difficult to obtain the desired expansion ratio [55]. With the composite containing 7.5 wt.% of organomodified clays it was not possible to produce the foam with this density as this material did not show strain hardening and therefore a full collapse of the cellular structure was promoted.

Open Cell Content

The open cell content of the different cellular materials has been measured as it is an important parameter in foamed products. The influence that the amount of open cells has on the properties of different polymeric materials has been widely investigated. In general, high

open cell contents lead to poor mechanical properties, low thermal insulation, good acoustic absorption and low dimensional stability [56-58]. Figure 4 shows the open cell content results. They have been represented together with the values of the strain hardening coefficient obtained for the different composites with the aim of determining if a relationship between both parameters can be established.

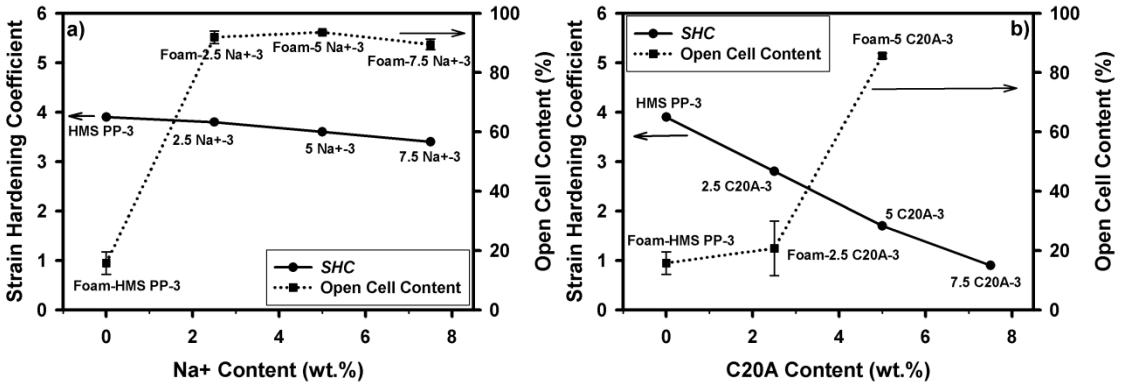

Figure 4. Correlation between strain hardening coefficient and open cell content. a) Composites produced with the natural clays (Na+). b) Composites produced with the organomodified clays (C20A).

Figure 4.a shows the open cell content of the composites containing natural clays. In these materials there is not a clear relationship between the *S* and the open cell content. While the *S* of the pure HMS PP and the different composites is the same and it remains almost unaffected by the increase in particles concentration, important changes are detected in the open cell content when the particles are added to the polymeric matrix. In addition, it is observed that the open cell content is not affected by the clay concentration. In fact, the open cell content increases from a value of 16 % to a value of 90 %, just by the fact of adding Na+. That means that by adding non-organomodified montmorillonites it is possible to switch from a closed cell structure to an open cell structure. In general, it could be said that this is not the expected behavior. When a low-density cellular material is produced, the polymeric matrix is subjected to high elongational forces during the foaming process. As a consequence, the cell walls become thinner and they can easily break. Nevertheless, if the polymeric matrix shows strain hardening, an increase in the viscosity is produced at high strains. This high viscosity hinders the rupture of the cell walls and therefore a reduction in the open cell content is normally produced. This expected behavior is observed in the composites produced with the organomodified clays (C20A) in which an increase in the open cell content is obtained when the strain hardening decreases (Figure 4.b).

The most important difference detected between the two composites is their morphology. While the Na+ clays are agglomerated, an intercalated structure was achieved with the organomodified (C20A) particles. This dissimilarity could be the reason behind the differences found in the behavior of both composites. When the particles are agglomerated, they lose their laminar shape. Therefore, it is more complicated to accommodate the particles in the cell walls, which can contribute to produce a rupture of these cell walls when the size of the clay aggregates is larger than the cell wall thickness. Therefore, if the size of the clay aggregates found in the Na+ composites is either greater or of the same order of magnitude as the cell wall thickness, these aggregates could be causing the rupture of the cell walls and thus

promoting the cell opening. To prove this, the size of these aggregates was obtained from the SEM micrographs taken from the solid composites (Figure 5.a) and in addition, the cell wall thickness of the Na+ composites was determined from the SEM micrographs, in this case, corresponding to the different foamed materials (Figure 5.b). The micrographs obtained for the intermediate content of natural clays (5 wt.%) are depicted in Figure 5. Only the results acquired for this material are shown here as similar conclusions were obtained for the other clay contents. The micrographs reveal on the one hand, the presence of large agglomerates of particles in both the solid and the foamed composites and on the other hand, that the particles are placed in both the cell edges and the cell walls. As it was previously indicated, the presence of particles or agglomerates in the cell walls could be contributing to break them, during the expansion process, if their size is similar or larger than the cell wall thickness.

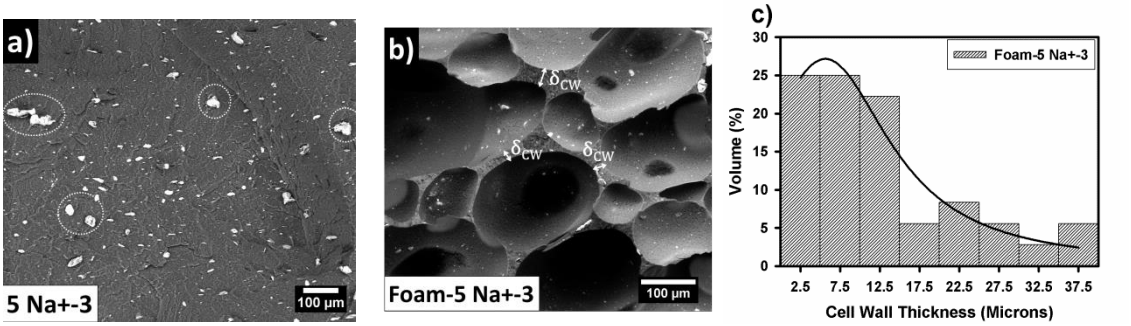

Figure 5. a) SEM micrograph of the solid composite used to measure the size of the clay aggregates (5 Na+-3). b) SEM micrograph of the foamed material employed to measure the cell wall thickness (Foam-5Na+-3). c) Cell wall thickness distribution for the Foam-5Na+-3.

A quantitative analysis of these micrographs, as well as of those of the materials produced with the other clay concentrations, was performed. The three different materials showed cell walls with and average thickness of around 15 microns. However, these wall thicknesses are very heterogeneous with values ranging from 0.5 microns to 60 microns. In addition, the cell wall thickness distribution (Figure 5.c) indicates that most of the cell walls have a thickness of approximately 5 microns. Taking into account this value, the number of agglomerates with a size higher than 5 microns has been measured in the three solid composites. In the material produced with 2.5 wt.% of Na+, 10 ± 5 % of the total amount of particles have sizes larger than 5 microns. This value becomes 12 ± 2 % in the composite produced with 5 wt.% of Na+ and 8.4 ± 0.2 % in the composite containing 7.5 wt.% of Na+. Taking all this into account, it can be concluded that the amount of particles with a size larger or similar than the cell wall thickness is really significant and therefore, they will be enough to produce an opening of the cell walls in these materials.

So, in these particular materials, the extensional rheology cannot be easily related to the open cell content because it seems that there is other phenomenon which is taking place simultaneously. In the range of Hencky strains in which the measurements were performed, no differences between the materials were found. The thickness of the sample used in the extensional rheological test is too large to notice the real effect of the particles in the cell walls.

Cellular Structure

SEM micrographs of the foams produced with both the pure HMS PP and the different polypropylene based composites can be observed in Figure 6.

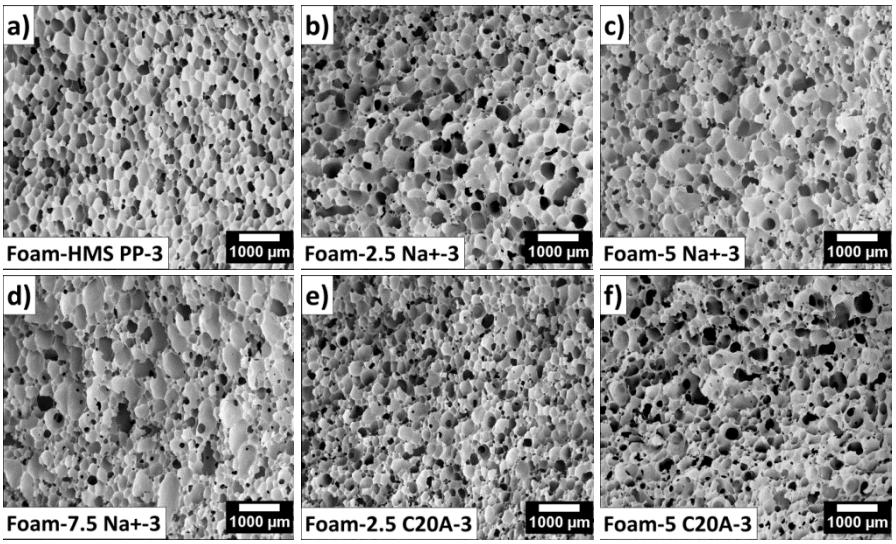

Figure 6. SEM micrographs of the different cellular materials. a) Foam-HMS PP-3. b) Foam-2.5 Na+-3. c) Foam-5 Na+-3. d) Foam-7.5 Na+-3. e) Foam-2.5 C20A-3. f) Foam-5 C20A-3.

Several conclusions can be extracted from the qualitative observation of these micrographs. The foam produced with the pure polymer is the material that shows the most homogeneous cellular structure. Nevertheless, when natural clays are added to the polymer, pores with larger sizes are detected. The same happens when organomodified clays are added, although the differences found in the cell sizes are not as significant as with the natural clays. The cell size distribution is analyzed in detail in Figure 7 where the histograms obtained from the numerical analysis of these cellular structures are represented.

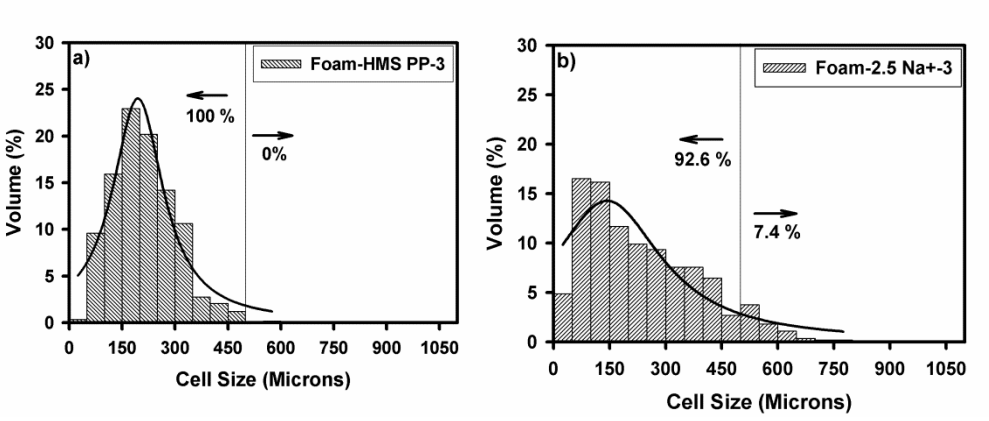

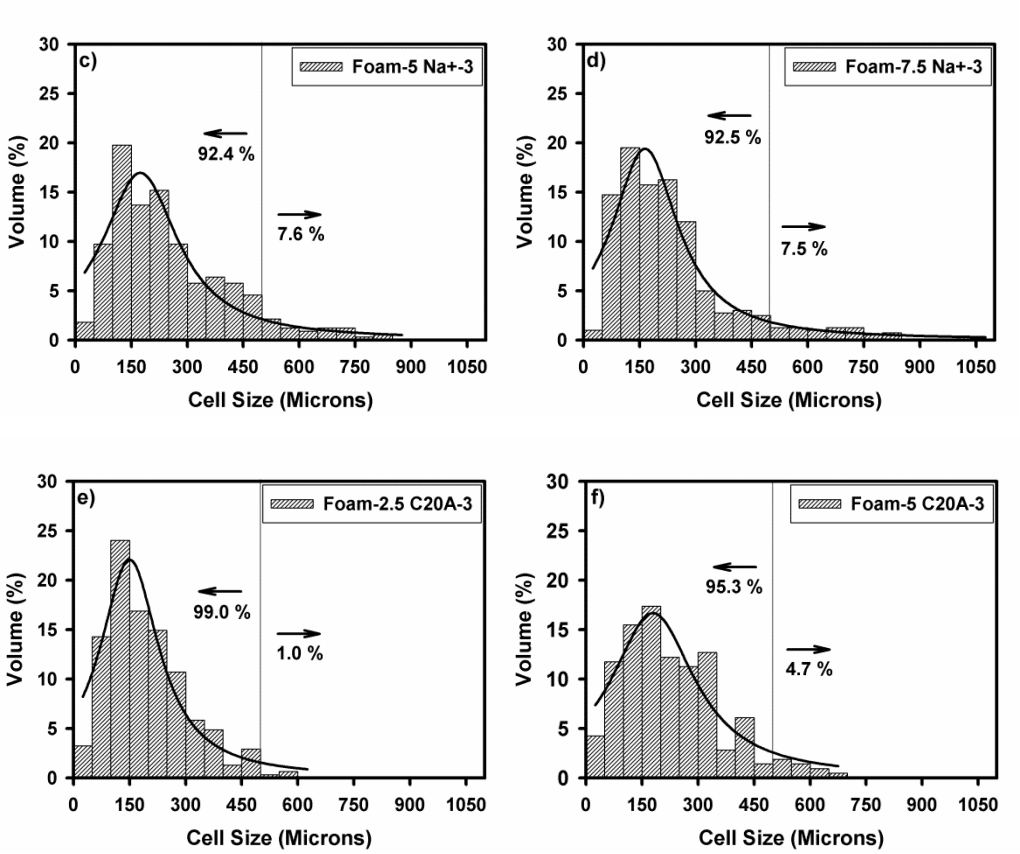

Figure 7. Cell size distribution of the cellular materials produced using the pure HMS PP and the different polypropylene based composites. a) Foam-HMS PP-3. b) Foam-2.5 Na+-3. c) Foam-5 Na+-3. d) Foam-7.5 Na+-3. e) Foam-2.5 C20A-3. f) Foam-5 C20A-3.

The narrowest cell size distribution is the one corresponding to the pure HMS PP since this is the material with the most homogenous cellular structure. All the cells of this material have sizes lower than 500 microns. Then, when clays are added to the polymeric matrix the distributions become wider since larger cells appear. Figure 7 also shows the amount of cells with sizes higher than 500 microns present in each material. These values are represented in Figure 8 as a function of the clay content.

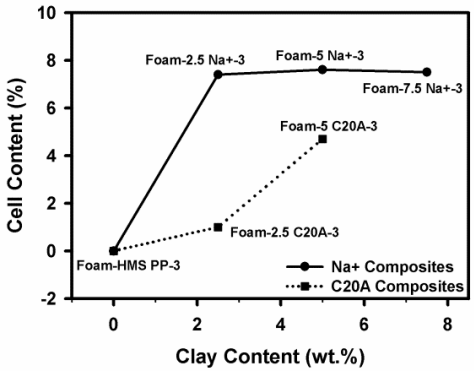

Figure 8. Cell content with a size higher than 500 microns as a function of the clay content.

In the Na+ composites, approximately 7.5 % of the analyzed cells have sizes larger than 500 microns and this value is independent on the clay content. However, in the C20A composites the amount of larger cells increases with the clay content. If this trend is compared to that

obtained with the open cell content results, it can be found that both behaviors are very similar. The presence of clay aggregates in the Na+ composites favors the rupture of the cell walls (cell coalescence) leading to higher open cell contents and to larger cell sizes. When the clays are agglomerated, neither the open cell content nor the amount of cells with a cell size higher than 500 microns depend on the clay content. This could be indicating that the Na+ contents employed are not different enough and that higher or lower clay contents should be used to detect changes in the open cell contents and in the amount of large cells. Nevertheless, when C20A clays are used, as the intercalation level of these particles is higher, lower clay concentrations are required to detect changes in both the open cell content and the cellular structure, when the clay content is changed. The same phenomena of degeneration which take place in the Na+ composites also occur in the C20A composites. However, in this case the cell wall rupture, with the consequent increase in the cell size, is favored by the reduction in the *S* promoted by the addition of organomodified clays.

In order to provide a more accurate description of the cellular structure, several parameters related to the cellular structure have been obtained from the micrographs. Two of these parameters, the average cell size and the cell density, are summarized in Table 4.

Table 4. Average cell size and cell density of the different cellular materials.

Sample Name	Cell Size (Microns)	Standard Deviation (Microns)	Cell Density (cells/cm^3)
Foam-HMS PP-3	212	88	4.9x10^5
Foam-2.5 Na+-3	237	153	2.8x10^5
Foam-5 Na+-3	255	158	1.7 x10^5
Foam-7.5 Na+-3	233	160	2.5x10^5
Foam-2.5 C20A-3	195	109	5.1 x10^5
Foam-5 C20A-3	230	135	3.0 x10^5

As it was previously indicated when particles are added to the polymeric matrix, cells with larger sizes appear and consequently an increase in the average cell size is produced for most of the analyzed foams (see the values in the Table 4). In connection with the cell density, as cellular materials with the same density are considered, when the cell size increases, this cell density decreases. Only the foamed material containing 2.5 wt.% of organomodified clays (C20A) shows a cell density higher than that of the unfilled foam. In fact, this material shows a cell size distribution similar to that of the pure material, although with a slightly smaller average cell size. As XRD results indicate (Figure 1), this is the material with the highest level of intercalation. An increase in the intercalation level translates into a large number of nucleation points per unit volume. Therefore, it seems that this kind of intercalated structures is favoring the cell nucleation causing the nucleation rate to be higher than the coalescence rate produced by the reduction in the S. Consequently, the number of cells per cubic centimeter increases and the size of the cells is reduced. In the other materials (Foam-5 C20A-3) in which the clays are less intercalated, this nucleation is not so effective and the phenomenon of degeneration of the cellular structure seems to be the predominant one, due to a clear reduction of the S.

Finally, a quantitative analysis of the homogeneity of the cellular structure has also been performed by calculating the SDC relative to the cell size (Equation 3). In Figure 9 this coefficient is represented as a function of the clay concentration.

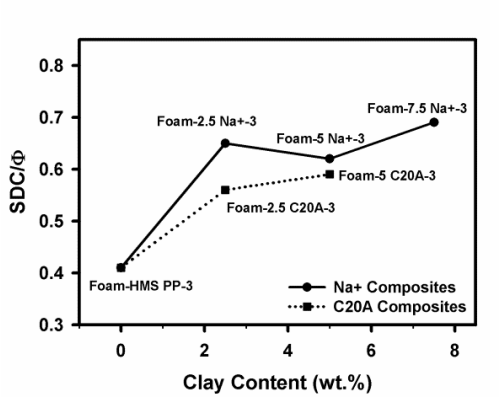

Figure 9. SDC/Φ for the complete collection of HMS PP based cellular materials.

The lowest value of SDC/Φ corresponds to the cellular material produced with the pure HMS PP. This result confirms qualitative observations as it indicates that the cellular structure of this material is the most homogeneous one. When particles are added to the polymeric matrix an increase in this coefficient is obtained. However, no significant differences are reached in this coefficient by the fact of varying the clay concentration. Figure 9 also reveals that the foams produced with the natural clays present a value of SDC/Φ slightly higher than that of the foams containing organomodified clays. This indicates that the cellular structure of these materials is more heterogeneous presenting cells with sizes far away from the average value. This indicates that the phenomenon of degeneration of the cellular structure is more intense in the foams containing natural clays (Figures 4 and 8).

Mechanical Response

Mechanical properties in compression were measured for the whole collection of cellular materials produced. As all the materials have very similar densities, the mechanical properties of the considered materials would depend on the one hand on the mechanical properties of the polymeric matrix and on the other hand on the morphology and characteristics of the cellular structure.

The solid composites were analyzed by performing tensile test and the experimental results for the tensile modulus are depicted in Figure 10.

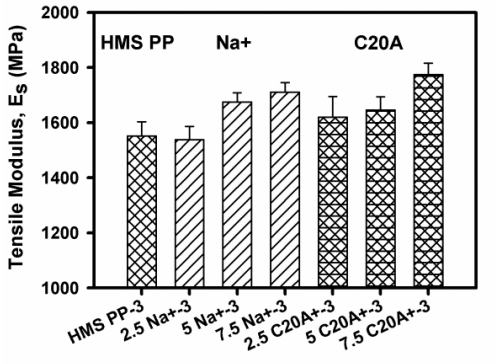

Figure 10. Experimental results from tensile tests performed in the solid composites: tensile modulus.

In general, the solid composites containing C20A clays present a tensile modulus slightly superior to that of the composites containing Na+ clays. While an increase of a 10 % with

respect to the pure polymeric matrix (HMS PP) is reached by adding 7.5 wt.% of Na+, this value increases up to 14 % in the composite containing 7.5 wt.% of C20A. The improved performance of the composites containing the organomodified clays could be expected if it is taken into account that the intercalation degree achieved for these particles is higher than that achieved for the natural clays (Figure 1). The composites containing C20A clays also contain a compatibilizer agent and hence the stress transfer is favored in this system promoting an effective increase in the tensile modulus. However, in the materials containing natural clays the degree of compatibilization between the polymer and the particles is poorer and consequently also the stress transmission.

Figure 10 also reveals that, regardless of the type of particles, the tensile modulus increases as clay concentration does, despite of the fact that when the clay content increases the interlayer spacing and therefore the intercalation degree decrease.

Experimental results of the elastic modulus (E_{cm}) and the collapse stress (σ_c), for the foamed materials, are represented in Figure 11 together with the open cell content values, in order to analyze the influence of this parameter in the mechanical behavior.

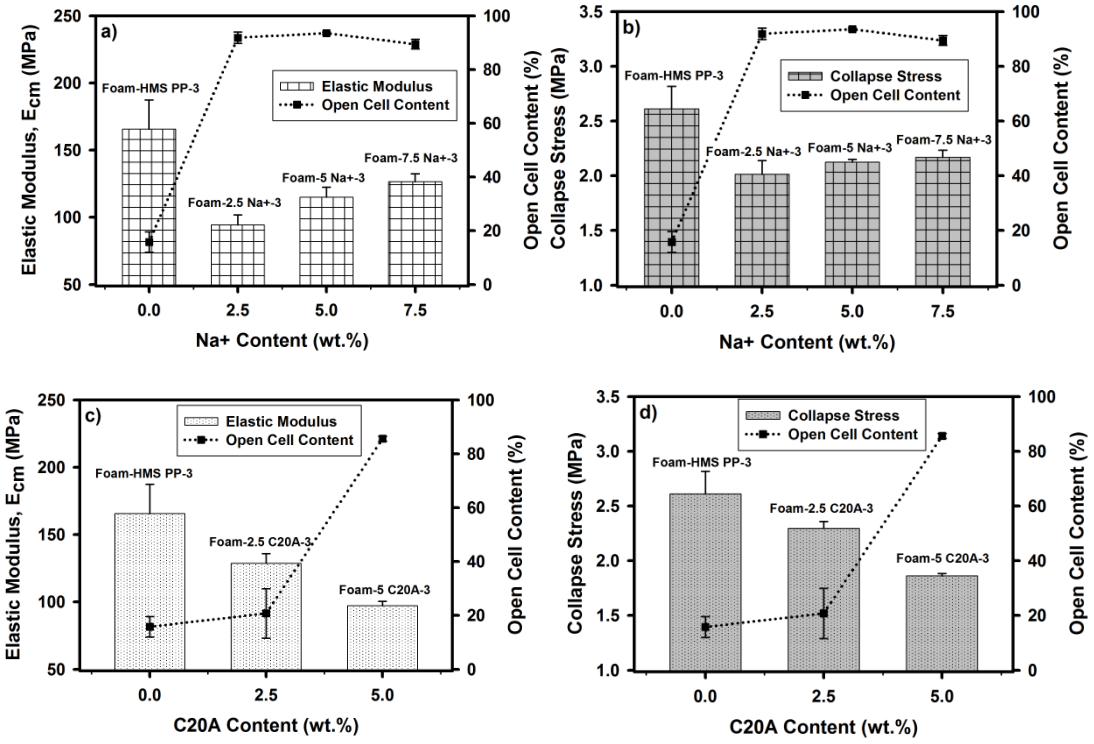

Figure 11. Experimental results from compression tests performed in the foamed composites. a) Relationship between the elastic modulus and the open cell content for the materials containing natural clays (Na+). b) Relationship between the collapse stress and the open cell content for the materials containing Na+. c) Relationship between the elastic modulus and the open cell content for the materials containing organomodified clays (C20A). d) Relationship between the collapse stress and the open cell content for the materials containing C20A.

The mechanical properties have been related to the open cell content since this is the parameter, connected with the cellular structure, in which more variations have been found by

the fact of changing both, the clay type and the clay content. Furthermore, the mechanical properties of a cellular material are highly dependent on the open cell content which means that the effects of other parameters like the cell size and the cell homogeneity can be masked by the changes in the open cell content [4]. Figure 11 shows that, for a same type of clays, both the elastic modulus and the collapse stress follow the same trend.

As the open cell content of the foamed composites containing natural clays is higher than that of the unfilled foam, their mechanical properties are always lower than those of the foam produced with the pure HMS PP (Figures 11.a and 11.b). However, when the clay content increases the mechanical properties also increases despite of the fact that the open cell content was the same for all the composites. To explain this effect, it should be considered that the mechanical properties of the solid composites increase with the clay content and hence the cell walls are stiffer when a higher amount of clays is used.

In addition, it can be pointed out that the improvements achieved in the foams are greater than those produced in the solid. While an increase of an 11 % is produced in the tensile modulus (measured in the solid composites) when the clay content increases from 2.5 wt.% to 7.5 wt.%., the elastic modulus of the foamed materials increases by 34 %. XRD results showed that a greater intercalation degree was achieved after the foaming process. As it was already proved, the fact of increasing the clay content favors the formation of a percolated network and if in addition the intercalation degree is also higher, this percolation network could be even easier to be achieved. Therefore, it can be said that despite of the high open cell contents of these materials, the intercalation degrees obtained after the foaming process promote a more effective reinforcement of the polymeric matrix comprising the cell walls, due to the presence of the particles. In these materials in which the clays are mainly agglomerated and therefore the intercaltion degrees achieved are poor, it is difficult to establish the relationship: rheology/structure/properties since, as it has been shown throughout the work, other phenomena which takes places simultaneously have to be considered.

In the foams containing C20A clays a direct relationship between the mechanical properties and the open cell content can be established (Figures 11.c and 11.d). An increase in the open cell content involves a decrease in the mechanical properties. Furthermore, the material produced with the pure HMS PP shows the most homogeneous cellular structure which also contributes to improve its mechanical properties. In these foamed materials, despite of obtaining intercalation degrees even higher than those reached with the natural clays, the fact of increasing the open cell content could be having a greater effect than the fact of improving the percolated structure, causing, finally, a deterioration of the mechanical properties. In these materials, in which an intercalated clay structure is obtained, the following relationship could be established: when the clay content increases a decrease in the strain hardening of the polymeric matrix is produced and as a consequence, the quality of the cellular structure decreases and the open cell content of the foamed materials increases, resulting in poorer mechanical properties.

CONCLUSIONS

A detailed characterization of two different types of solid composites and their corresponding foamed materials (produced with the same density) has been performed with the aim of establishing the relationship between extensional rheology, cellular structure and mechanical

properties. The first type of composite was produced using natural clays and without a compatibilizer. The second one was produced using organomodified clays and a compatibilizer (PP-MA). XRD results indicate that the production process (melt compounding), on the one hand, produces an agglomeration of the natural clays and, on the other hand, a separation of the clay platelets in the organomodified particles. The extensional rheology results indicate that the strain hardening of the composites containing natural clays is similar to that of the unfilled polymer and it is also independent on the clay content. However, a decrease in the strain hardening with the clay content was detected in the composites produced with organomodified clays. Consequently, the open cell content of the foamed materials produced with these composites increases with the clay content because the cell walls are not able to resist the extension to which they are subjected during the foaming process. Nevertheless, this expected behavior was not obtained in the foams produced with the composites containing natural clays. In this case, the composites showed an open cell structure opposite to the close cell structure of the unfilled foam. To explain this behavior both the agglomerates size and the cell wall thickness were measured. Results indicated that there is a considerable amount of agglomerates with a size higher than that of the cell walls and as a consequence they could be acting as cell openers promoting an increase in the open cell content. In general, the cell size of the cellular materials containing nanoparticles is higher than that of the unfilled cellular materials and their cellular structure is more heterogeneous, except for the material containing 2.5 wt.% of organomodified clays. For this material, the nucleation promoted by the clay particles plays a more important role than the decrease in the *S*. Finally the mechanical properties have also been analyzed in both the foamed and solid composites. Results indicate that a slight increase in the tensile modulus is detected when particles are added to the solid polymeric matrix. In the case of the foamed materials, the mechanical properties of the cellular materials containing organomodified clays decrease with the clay content due to the increase obtained in the open cell content. In the case of the cellular materials containing natural clays (with similar open cell content) an increase in the mechanical properties with the clay content is obtained indicating that the particles are effectively reinforcing the polymeric matrix.

The main conclusion of this work is that, while in the unfilled polymers the extensional rheology is a very useful tool to analyze and understand the cellular structure and mechanical properties of the cellular materials, in the filled polymers the obtaining of this relationship is conditioned by the dispersion level of the layered clays into the polymeric matrix and by the size of the particles used.

ACKNOWLEDGEMENTS

Financial support from PIRTU contract of E. Laguna-Gutierrez by Junta of Castilla and Leon (EDU/289/2011) and cofinanced by the European Social Fund is gratefully acknowledged. Cristina Saiz-Arroyo would like to acknowledge Mineco via Torres Quevedo Program (PTQ-12-05504). Finally, financial support from the MICINN and FEDER Program (MAT 2012-34901) and the Junta of Castilla and Leon (VA 035U13) is gratefully acknowledged.

REFERENCES

[1] D. Tripathi. Practical Guide to Polypropylene, Rapra Technology, Shrewsbury, 2002

[2] C. He, S. Costeux, P. Wood-Adams, J. M. Dealy. Molecular Structure of High Melt Strength Polypropylene and its Application to Polymer Design, Polymer, 44, 7181-7188, 2003
[3] A. D. Gotsis, B. L. F. Zeevenhoven, C. Tsenoglou. Effect of Long Branches on the Rheology of Polypropylene, Journal of Rheology, 48, 895-914, 2004
[4] E. Laguna-Gutierrez, R. Van Hooghten, P. Moldenaers, M. A. Rodriguez-Perez. Understanding the Foamability and Mechanical Properties of Foamed Polypropylene Blends by Using Extensional Rheology, Journal of Applied Polymer Science, In Press, DOI: 10.1002/app.42430, 2015
[5] L. J. Gibson, M. F. Ashby. Cellular Solids: Structure and Properties, Cambridge University Press, Cambridge, 1997
[6] S. Y. Fu, X. Q. Feng, B. Lauke, Y. W. Mai. Effects of Particle Size, Particle/Matrix Interface Adhesion and Particle Loading on Mechanical Properties of Particulate–Polymer Composites, Composites: Part B, 39, 933-961, 2008
[7] E. Manias, A. Touny, L. Wu, K. Strawhecker, B. Lu, T. C. Chung. Polypropylene/Montmorillonite Nanocomposites. Review of the Synthetic Routes and Materials Properties, Chemistry of Materials, 13, 3516-3523, 2001
[8] P. Svoboda, C. Zeng, H. Wang, L. J. Lee, D. L. Tomasko. Morphology and Mechanical Properties of Polypropylene/Organoclay Nanocomposites, Journal of Applied Polymer Science, 85, 1562-1570, 2002
[9] N. Hasegawa, M. Kawasumi, M. Kato, A. Usuki, A. Okada. Preparation and Mechanical Properties of Polypropylene-Clay Hybrids Using a Maleic Anhydride-Modified Polypropylene Oligomer, Journal of Applied Polymer Science, 67, 87-92, 1998
[10] S. Pavlidou, C.D. Papaspyrides. A Review on Polymer–Layered Silicate Nanocomposites, Progress in Polymer Science, 33, 1119-1198, 2008
[11] H. Krump, A.S. Luyt, I. Hudec. Effect of Different Modified Clays on the Thermal and Physical Properties of Polypropylene-Montmorillonite Nanocomposites, Materials Letters, 60, 2877-2880, 2006
[12] P. Kiliaris, C. D. Papaspyrides. Polymer/Layered Silicate (Clay) Nanocomposites: An Overview of Flame Retardancy, Progress in Polymer Science, 35, 902-958, 2010
[13] F. J. Galindo-Rosales, P. Moldenaers, J. Vermant. Assessment of the Dispersion Quality in Polymer Nanocomposites by Rheological Methods, Macromolecular Materials and Engineering, 296, 311-340, 2011
[14] C. M. Koo, J. H. Kym, K. H. Wang, I. J. Chung. Melt-Extensional Properties and Orientation Behaviors of Polypropylene-Layered Silicate Nanocomposites, Journal of Polymer Science, Part B: Polymer Physics, 43, 158-167, 2005
[15] J. U. Park, J. L. Kim, D. H. Kim, K. H. Ahn, S. J. Lee, K. S. Cho. Rheological Behavior of Polymer/Layered Silicate Nanocomposites under Uniaxial Extensional Flow, Macromolecular Research, 14, 318-323, 2006
[16] M. Okamoto, P. H. Nam, P. Maiti, T. Kotaka, N. Hasegawa, A. Usuki. A House of Cards Structure in Polypropylene/Clay Nanocomposites under Elongational Flow, Nanno Letters, 1, 295-298, 2001
[17] K. Wang, W. Zhai. Extrusion of Polypropylene/Clay Nanocomposite Foams (Chapter 3) in V. Mittal (Ed.), Polymer Nanocomposite Foams, CRC Press, Boca Raton, 2014

[18] S. Bhattacharya, R. K. Gupta, M. Jollands, S. N. Bhattacharya. Foaming Behavior of High-Melt Strength Polypropylene/Clay Nanocomposites, Polymer Engineering and Science, 49, 2070-2084, 2009

[19] F. H. Su, J. H. Yan, H. X. Huang. Structure and Melt Rheology of Long-Chain Branching Polypropylene/Clay Nanocomposites, Journal of Applied Polymer Science, 119, 1230-1238, 2011

[20] K. Taki, T. Yanagimoto, E. Funami, M. Okamoto, M. Ohshima. Visual Observation of CO_2 Foaming of Polypropylene-Clay Nanocomposites, Polymer Engineering and Science, 44, 1004-1011, 2004

[21] W. G. Zheng, Y. H. Lee, C. B. Park. Use of Nanoparticles for Improving the Foaming Behaviors of Linear PP, Journal of Applied Polymer Science, 117, 2972-2979, 2010

[22] W. Zhai, T. Kuboki, L. Wang, C. B. Park, E. K. Lee, H. E. Naguib. Cell Structure Evolution and the Crystallization Behavior of Polypropylene/Clay Nanocomposites Foams Blown in Continuous Extrusion, Industrial and Engineering Chemistry Research, 49, 9834-9845, 2010

[23] M. Alexandre, P. Dubois. Polymer-Layered Silicate Nanocomposites: Preparation, Properties and Uses of a New Class of Materials, Materials Science and Engineering, 28, 1-63, 2000

[24] Z. Spitalsky, D. Tasis, K. Papagelis, C. Galiotis. Carbon Nanotube-Polymer Composites: Chemistry, Processing, Mechanical & Electrical Properties, Progress in Polymer Science, 35, 357-401, 2010

[25] Q. Zhang, Q. Fu, L. Jiang, Y. Lei. Preparation and Properties of Polypropylene/ Montmorillonite Layered Nanocomposites, Polymer International, 49, 1561-1564, 2000

[26] K. Kim, H. Kim, J. Lee. Effect of Interlayer Structure, Matrix Viscosity and Composition of a Functionalized Polymer on the Phase Structure of Polypropylene-Montmorillonite Nanocomposites, Polymer Engineering and Science, 41, 1963-1969, 2001

[27] Y. Dong, D. Bhattacharyya. Effects of Clay Type, Clay/Compatibiliser Content and Matrix Viscosity on the Mechanical Properties of Polypropylene/Organoclay Nanocomposites, Composites: Part A, 39, 1177-1191, 2008

[28] S. H. Lee, E. Cho, J. R. Youn. Rheological Behavior of Polypropylene/Layered Silicate Nanocomposites Prepared by Melt Compounding in Shear and Elongational Flows, Journal of Applied Polymer Science, 103, 3506-3515, 2007

[29] M. Kato, A. Usuki, A. Okada. Synthesis of Polypropylene Oligomer-Clay Intercalation Compounds, Journal of Applied Polymer Science, 66, 1781-1785, 1997

[30] W. Lertwimolnun, B. Vergnes. Influence of Compatibilizer and Processing Conditions on the Dispersion of Nanoclay in a Polypropylene Matrix, Polymer, 46, 3462-3471, 2005

[31] M. Modesti, A. Lorenzetti, D. Bon, S. Besco. Effect of Processing Conditions on Morphology and Mechanical Properties of Compatibilized Polypropylene Nanocomposites, Polymer, 46, 10237-10245, 2005

[32] F. H. Su, J. H. Yan, H. X. Huang. Structure and Melt Rheology of Long-Chain Branching Polypropylene/Clay Nanocomposites, Journal of Applied Polymer Science, 119, 1230-1238, 2011

[33] W. G. Zheng, Y. H. Lee, C. B. Park. Use of Nanoparticles for Improving the Foaming Behaviors of Linear PP, Journal of Applied Polymer Science, 117, 2972-2979, 2010

[34] W. Zhai, C. B. Park, M. Kontopoulou. Nanosilica Addition Dramatically Improves the Cell Morphology and Expansion Ratio of Polypropylene Heterophasic Copolymer Foams Blown in Continuous Extrusion, Industrial and Engineering Chemistry Research, 50, 7282-7289, 2011
[35] E. Laguna-Gutierrez, R. Van Hooghten, P. Moldenaers, M. A. Rodriguez-Perez. Effects of Extrusion Process, Type and Content of Clays, and Foaming Process on the Clay Exfoliation in HMS PP Composites, Journal of Applied Polymer Science, In Press, DOI: 10.1002/app.42828, 2015
[36] L. J. Gibson. Modelling the Mechanical Behaviour of Cellular Materials, Materials Science and Engineering: A, 110, 1-36, 1989
[37] C. S. Saiz-Arroyo, J. A. de Saja, J. I. Velasco, M. A. Rodriguez-Perez. Moulded Polypropylene Foams Produced Using Chemical or Physical Blowing Agents: Structure-Properties Relationship, Journal of Materials Science, 47, 5680-5692, 2012
[38] C. Saiz-Arroyo, M. A. Rodriguez-Perez, J. I. Velasco, J. A. de Saja. Influence of Foaming Process on the Structure-Properties Relationship of Foamed LDPE/Silica Nanocomposites, Composites: Part B, 48 40-50, 2013
[39] C. Saiz-Arroyo, M. A. Rodriguez-Perez, J. Tirado, A. Lopez-Gil, J. A. de Saja. Structure-Property Relationships of Medium-Density Polypropylene Foams, Polymer International, 62, 1324-1333, 2013
[40] J. Pinto, E. Solórzano, M. A. Rodriguez-Perez, J. A. de Saja. Characterization of the Cellular Structure Based on User-Interactive Image Analysis Procedures, Journal of Cellular Plastics, 49, 555-575, 2013
[41] W. Gong, J. Gao, M. Jiang, L. He, J. Yu, J. Zhu. Influence of Cell Structure Parameters on the Mechanical Properties of Microcellular Polypropylene Materials, Journal of Applied Polymer Science, 122, 2907-2914, 2011
[42] M. A. Rodriguez-Perez, J. A. de Saja. The effect of Blending on the Physical Properties of Crosslinked Closed Cell Polyethylene Foams, Cellular Polymers, 18, 1-20, 1999
[43] O. Almanza, M. A. Rodriguez-Perez, J. A. de Saja. The Microstructure of Polyethylene Foams Produced by a Nitrogen Solution Process, Polymer, 42, 7117-7126, 2001
[44] M. A. Rodriguez-Perez, S. Diez-Gutierrez, J. A. de Saja. The Recovery Behavior of Crosslinked Closed Cell Polyolefin Foams, Polymer Engineering and Science, 38, 831-837, 1998
[45] S. T. Lee. Foam Extrusion: Principles and Practice, Technomic Publishing Company, Lancaster-Pennsylvania, 2000
[46] J. Stange, C. Uhl, H. Münstedt. Rheological Behavior of Blends from a Linear and a Long-Chain Branched Polypropylene, Journal of Rheology, 495, 1059-1079, 2005
[47] A. K. Chaudhary, K. Jayaraman. Extrusion of Linear Polypropylene–Clay Nanocomposite Foams, Polymer Engineering and Science, 51, 1749-1756, 2011
[48] J. M. Dealy, J. Wang. Melt Rheology and its Applications in the Plastic Industry (2nd Edition), Springer Science+Business Media, Dordrecht, 2013
[49] J. Stange, H. Münstedt. Effect of Long-Chain Branching on the Foaming of Polypropylene with Azodicarbonamide, Journal of Cellular Plastics, 42, 445-467, 2006
[50] T. Takahashi, H. Nakajima, Y. Masubuchi, J. Takimoto, K. Koyama. Strain hardening Property and Internal Deformation of Polymer Composite Melts under Uniaxial Elongation, 54, 538-543, 1998

[51] T. Takahashi, W. Wu, H. Toda, J. Takimoto, T. Akatsuka, K. Koyama. Elongational Viscosity of ABS Polymer Melts with Soft or Hard Butadiene Particles, Journal of Non-Newtonian Fluid Mechanics, 68, 259-269, 1997

[52] M. Kobayashi, T. Takahashi, J. Takimoto, K. Koyama. Influence of Glass Beads on the Elongational Viscosity of Polyethylene with Anomalous Strain rate Dependence of the Strain-Hardening, Polymer, 37, 3745-3747, 1996

[53] M. Kobayashi, T. Takahashi, J. Takimoto, K. Koyama. Flow-Induced Whisker Orientation and Viscosity for Molten Composite Systems in a Uniaxial Elongational Flow Field, Polymer, 36, 3927-3933, 1995

[54] J. F. Le Meins, P. Moldenaers, J. Mewis. Suspensions of Monodisperse Spheres in Polymer Melts: Particle Size Effects in Extensional Flow, Rheologica Acta, 42, 184-190, 2003

[55] H. E. Naguib, C. B. Park, U. Panzer, N. Reichelt. Strategies for Achieving Ultra Low-Density Polypropylene Foams, Polymer Engineering and Science, 42, 1481-1492, 2002

[56] M. A. Rodriguez-Perez, M. Alvarez-Lainez, J. A. de Saja. Microstructure and Physical Properties of Open-Cell Polyolefin Foams, Journal of Applied Polymer Science, 114, 1176-1186, 2009

[57] L. J. Lee, C. Zeng, X. Cao, H. Han, J. Shen, G. Xu. Polymer Nanocomposite Foams, Composites Science and Technology, 65, 2344-2363, 2005

[58] S. T. Lee, C. B. Park, N. S. Ramesh. Polymeric Foams: Science and Technology, CRC Press, Boca Raton-Florida, 2007

5.4 References

[1] V. Mittal. Polymer Nanocomposite Foams. CRC Press, Boca Raton, 2014.
[2] S. Y. Fu, X. Q. Feng, B. Lauke, Y. W. Mai. Composites: Part B, 39, 933-961, 2008.
[3] E. Manias, A. Touny, L. Wu, K. Strawhecker, B. Lu, T. C. Chung. Chemistry of Materials, 13, 3516-3523, 2001.
[4] S. Pavlidou, C.D. Papaspyrides. Progress in Polymer Science, 33, 1119-1198, 2008.
[5] H. Krump, A.S. Luyt, I. Hudec. Materials Letters, 60, 2877-2880, 2006.
[6] P. Kiliaris, C. D. Papaspyrides. Progress in Polymer Science, 35, 902-958, 2010.
[7] F. J. Galindo-Rosales, P. Moldenaers, J. Vermant. Macromolecular Materials and Engineering, 296, 311-340, 2011.
[8] J. U. Park, J. L. Kim, D. H. Kim, K. H. Ahn, S. J. Lee, K. S. Cho. Macromolecular Research, 14, 318-323, 2006.
[9] K. Taki, T. Yanagimoto, E. Funami, M. Okamoto, M. Ohshima. Polymer Engineering and Science, 44, 1004-1011, 2004.
[10] W. G. Zheng, Y. H. Lee, C. B. Park. Journal of Applied Polymer Science, 117, 2972-2979, 2010.
[11] W. Zhai, T. Kuboki, L. Wang, C. B. Park, E. K. Lee, H. E. Naguib. , Industrial and Engineering Chemistry Research, 49, 9834-9845, 2010.

CHAPTER 6

MICROCELLULAR FOAMS BASED ON HIGH DENSITY POLYETHYLENE

INDEX

6.1 Introduction

High density polyethylene (HDPE) is the third material selected to perform the experimental work of this thesis. HDPE is a polymer with excellent properties. HDPE is tough, stiff, chemical and abrasion resistant and presents a low absorption and permeability to water and moisture. Moreover, HDPE can withstand higher temperatures than other polymers such as low density polyethylene (LDPE) or ethylene vinyl acetate (EVA), which is an essential requirement for some applications [1,2]. The foamed materials produced with the HDPE keep its properties, making the foams produced with this polymer to be very interesting for applications where a high impact protection is needed (automotive, military applications, etc.) [3].

However, as polypropylene (PP), HDPE is a linear polymer and hence, its low melt strength hinders its use for the production of low density foams [4]. Moreover, its high crystallinity makes difficult the dissolution of the gas into the polymeric matrix which once again, hinders the use of this polymer for foaming applications [5,6]. Nevertheless, one of the main advantages of HDPE is that it can be easily crosslinked by using, for instance, organic peroxides which allows modifying on the one hand, its rheological properties and on the other hand, its crystallinity [7,8].

In the work presented in this chapter crosslinked HDPEs (x-HDPEs) are produced with different crosslinking degrees. The main objective of this work consists on analyzing the effect of the rheological behavior of these polymers on the foaming behavior. In this case, microcellular materials are produced by solid state foaming so that the expansion is performed in a glycerin bath and hence, the cellular materials are not produced with the same density.

Besides the type of polymeric matrix employed, this work differs from those presented in the chapter 1 (HMS PP-linear PP blends) in several aspects:

- The viscosity of the polymeric matrix changes abruptly by changing the crosslinking degree.
- The crystallinity and consequently, the amount of gas available for foaming are also modified when the crosslinking degree is changed.
- The cellular materials do not have the same density.

Therefore, taking into account the main objective of this thesis: understanding the foaming behavior of polymeric systems by analyzing their extensional rheological properties, it could be said that the polymeric system selected in this work is really complex because, in addition to the extensional rheological properties, all these aspects should be also considered to understand the structure of the different cellular materials produced.

Furthermore, this work goes a step further because the effects of foaming parameters like the foaming time and the foaming temperature on the expansion ratio and cellular structure are also analyzed, with the aim of understanding the mechanisms that take place in the production of these microcellular foams. This analysis is performed in the material with the lowest crosslinking degree and in the material with the highest crosslinking degree, which allows also determining in which way the foaming mechanisms are conditioned by the crosslinking degree, and hence, by the rheological properties of the polymeric matrices.

6.2 Analysis of the effect of the rheological behavior and the foaming parameters on the foamability of x-HDPEs

First, a HDPE polymeric matrix is crosslinked by using an organic peroxide. Different x-HDPEs are produced, which differ in their crosslinking degree. Then, an extensive characterization of the different solid materials is carried out. The gel content produced in the HDPE polymers by crosslinking, the thermal properties of these materials, their density and the extensional rheological properties of the different x-HDPEs are carefully determined and analyzed. As in the other works presented in this thesis, from the extensional rheological measurements the strain hardening coefficient is obtained; in this case, it is calculated for a Hencky strain rate of 1 s^{-1} and for a Hencky strain of 2.

The amount of gas available for foaming depends on the crystallinity of the polymeric matrix and hence, on the crosslinking degree. To determine this parameter the sorption curve (gas concentration as a function of the saturation time) of the different materials is determined.

Once the solid matrices are characterized, they are foamed by the solid state foaming process. As the expansion is carried out in a glycerin bath it is not possible to control the foam density. The expansion achieved depends on the one hand, on the properties of the polymer and on the other hand, on the foaming parameters (foaming time and foaming temperature). Different foaming times are employed to produce the cellular materials, varying from 15 to 45 s. Also the foaming temperature is modified. The temperature range selected from foaming varies between 150 and 190 ºC. Moreover, another parameter which is also modified to analyze its effect on the foam behavior is the saturation pressure. Before expanding the different materials they are saturated with CO_2 at two different saturation pressures (3 and 5 MPa).

The density of the cellular materials is characterized and parameters related to the cellular structure such as the average cell size and the cell density are also quantified. All the results, obtained after the experimental characterization, are then interrelated, which allows analyzing the following effects:

- Effect of the saturation pressure on the foam behavior (foam density and cellular structure).
- Effect of the foaming time on the foam behavior.
- Effect of the foaming temperature on the foam behavior.

All these effects are analyzed in both, the cellular materials produced with the HDPE with the highest crosslinking degree and the cellular materials produced with the HDPE with the lowest crosslinking degree, that is, the one produced with the uncrosslinked HDPE.

Then, to finish this study, the effect of the crosslinking content on the foam behavior is analyzed in cellular materials produced with a fixed saturation pressure, foaming time and foaming temperature.

ANALYZING AND UNDERSTANDING THE MECHANISMS WHICH TAKE PLACE IN THE PRODUCTION OF CROSSLINKED HDPE-BASED MICROCELLULAR FOAMS

Ester Laguna-Gutierrez[1], Javier Pinto[2], Vipin Kumar[3], Miguel A. Rodriguez-Perez[1]

[1] Cellular Materials Laboratory (CellMat), Condensed Matter Physics Department, University of Valladolid, Paseo de Belén, 7, 47011 Valladolid, Spain

[2] Nanophysics‑Smart Materials Group, Istituto Italiano di Tecnologia (IIT), Via Morego, 30, 16163 Genova, Italy

[3] Department of Mechanical Engineering, University of Washington, Seattle, WA 98195, USA

ABSTRACT

Obtaining high density polyethylene (HDPE) based microcellular foams is a topic of interest due to the synergistic properties that can be obtained by the fact of achieving a microcellular structure using a polymer with a high number of interesting properties. However, due to the high crystallinity of this polymer the production of low density microcellular foams, by a physical foaming process, is not a simple task. In this work, the solution proposed to manufacture these materials consists on using crosslinked HDPEs, with different crosslinking degrees. In addition, the foaming conditions, i.e. the foaming time and the foaming temperature, have also been modified with the aim of analyzing and understanding the mechanisms taking place during the foaming process to control this process and therefore, to obtain cellular materials with low density and improved cellular structures. Results indicate that there is a time and a foaming temperature optima for which the nucleation rate and the cell growth rate prevails over other phenomena like cell coalescence and gas diffusion out the material. Therefore, with these foaming conditions the lowest densities and the best cellular structures are obtained. Moreover, when the gel content increases the amount of gas available for foaming increases and the rheological properties improve, as the polymers show strain hardening. As a consequence, the relative density decreases and the cell nucleation density increases. After this detailed study, it was concluded that cellular materials with relative densities of 0.37 and with cell sizes of approximately 2 microns can be produced using a saturation pressure of 5 MPa, a foaming time of 30 s, a foaming temperature of 160 ºC and a crosslinked HDPE with a gel content of 50 %.

INTRODUCTION

Microcellular foams are characterized by having average cell sizes in the order of 10 µm and cell densities higher than 10^9 cells/cm^3 [1]. The concept of microcellular materials was created in the earlier 80s, in response to food and packaging companies to reduce materials cost without compromising mechanical properties [2,3]. These microcellular foams exhibit higher Charpy impact strength and toughness as well as higher fatigue life and thermal stability than conventional cellular materials [1].

One of the most common methods used to produce microcellular foams is a batch process known as “solid state method”. This method was developed in the MIT in the 80s [4]. It consists of a two-steps method. In the first stage the polymeric sample is saturated with a non-reactive gas in a pressure vessel. Then, the saturated samples are removed from the pressure vessel and foamed in a temperature controlled glycerin bath. Finally, the foam is stabilized by cooling.

The area of microcellular foams has been widely investigated in the last years although this research has been primarily focused on the foaming of amorphous polymers [5]. The number of investigations in which the microcellular foaming of semi-crystalline polymers is analyzed, by using the solid state foaming technology, is lower due to the difficulties found to manufacture microcellular materials with this kind of polymers. The main problems are related to the influence that crystallinity has on the solubility and diffusivity of the blowing agent into the polymeric matrix, particularly a severe decrease in the solubility and diffusivity is obtained by increasing the crystallinity [5,6,7]. As a consequence, obtaining microcellular foams of semi-crystalline polymers is not a simple task. More specifically, the fabrication of HDPE microcellular materials, by solid state foaming, with low densities is still more complicated due to the quite high crystallinity (around 60 to 70 %) that this polymer shows. However, in spite of the difficulties, obtaining HDPE microcellular foams is a topic of interest because of the interesting properties of this polymer. HDPE foams are tough, stiff, chemical and abrasion resistant and present a low absorption and permeability to water and moisture [8,9]. Moreover, HDPE foams can withstand higher temperatures than low density polyethylene (LDPE) or ethylene vinyl acetate (EVA), which is an essential requirement for some applications [10].

Due to the challenges previously mentioned to foam a pure HDPE most of the authors have mixed the HDPE with other polymers such as polypropylene (PP) [5,6,11,12] or particles [13,14] with two purposes. On the one hand, improving the bubble nucleation and on the other hand, reducing the foams density by decreasing the polymer crystallinity and consequently increasing the gas solubility. As far as we know, there are only two works in which a pure HDPE has been successfully foamed with a microcellular structure employing the "solid state method" previously described [7,15]. Doroudiani et al. [7] investigated the effect of the crystallinity and morphology of different semicrystalline polymers, among them HDPE, on the microcellular processing. They varied the crystallization and morphology of the different polymers by subjecting the samples to a compression molding process (at a temperature of 280 ºC) in which the cooling rate was modified. They obtained the best cellular structures with the samples cooled at the highest rate, in which the lowest crystallinities were achieved. Miller et al. [15] modified the processing conditions (saturation pressure, foaming time and foaming temperature) with the aim of producing low density HDPE foams with a microcellular structure. They found a processing window effective to produce low density cellular materials (relative densities of 0.36) with the polymers saturated at a pressure of 3 MPa and foamed at temperatures higher than the melting point.

In this work, blends of HDPE with different amounts of a crosslinking agent have been produced. It is well known that crosslinking has a direct effect on the crystallization process; in general an increase in the crosslinking degree is related to a decrease in the polymer crystallinity [16,17,18]. Moreover, as a consequence of the polymeric matrix crosslinking, changes in the extensional rheological properties of this polymeric matrix, in the molten state, could be also obtained, helping to suppress cell coalescence and therefore to increase the expansion ratio keeping, at the same time, very small cell sizes [19,20,21,22].

The main objective of this work is to perform a thorough study to analyze and understand the foaming mechanisms (nucleation and coalescence) which take place in this particular system with the aim of controlling the foaming process and obtaining cellular materials with low

density and improved cellular structures. For this purpose, the saturation pressure, the foaming time and the foaming temperature have been modified. The effects that each of these parameters have on the materials density, cell size and cell nucleation density have been extensively analyzed. The main difference of this work with that performed by Miller et al. [15] is that these analyses are conducted in different types of crosslinked HDPEs with different crystallinities and with different rheological behaviors, which also allows analyzing the effect of the crosslinking degree on the foaming behavior.

EXPERIMENTAL

Materials

The HDPE used in this study is a commercially available grade, Rigidex HD 5211 EA-Y supplied by Ineos Polyolefins with a density of 0.95 g/cm^3 and a melt flow rate of 11 g/10 min (190 ºC, 2.16 kg). An organic peroxide, Luperox 101XLS50 supplied by Arkema was used as crosslinking agent. This peroxide is composed by 50 % in weight of Luperox 101 and 50 % in weight of SiO_2. A commercial grade carbon dioxide (CO_2) was used as blowing agent.

Sample Preparation

Different blends of HDPE with the crosslinking agent have been prepared by extrusion using a co-rotating twin screw extruder Collin ZK 25T with L/D of 24. The rotational speed was 50 rpm and the melt temperature was 135 ºC. Three blends of HDPE with different amounts of crosslinking agent (1 phr, 2.4 phr and 4 phr) were produced.

Then, both the materials containing the crosslinking agent and the neat HDPE were compression molded in a hot plate press. Both, pressure and temperature were maintained constant for the different blends, 21.8 bars and 190 ºC, respectively. However, time was changed in order to achieve different crosslinking degrees. Times of 30 minutes were used for the samples with 1 phr, 2.4 phr and 4 phr of crosslinking agent. Moreover times of 15 minutes and 60 minutes were also used for the samples with 2.4 phr of organic peroxide. Sheets of 2 mm and 0.5 mm in thickness were produced and these samples were used to manufacture the cellular materials (2 mm in thickness) as well as to perform the extensional viscosity measurements (0.5 mm in thickness). The nomenclature used to designate the solid crosslinked HDPE (x-HDPE) materials is the following: C_c-t_c where C_c is the crosslinking agent content and t_c is the crosslinking time.

Gas Sorption

HDPE sheets (2 mm in thickness) were cut into 15 mm x 15 mm squares and placed in a pressure vessel. CO_2 gas was introduced at room temperature and samples were allowed to absorb the gas. Most of the HDPE samples were saturated at a pressure of 5 MPa. Nevertheless, some samples were also saturated at a pressure of 3 MPa in order to analyze the effect of the saturation pressure on the cellular materials density and structure.

Samples were periodically removed from the pressure vessel, weighed and returned to the pressure vessel. Therefore, with these measurements it was possible to obtain the gas concentration, i.e. the weight percentage of CO_2 dissolved in the polymer, as a function of the saturation time. Results show that at room temperature (T_a) and under a pressure of 5 MPa,

24 hours are necessary to reach the equilibrium gas concentration. The sorption diffusivity coefficient (D_s) was obtained from these measurements using Equation 1 [23,24]:

$$\frac{M_s}{M_\infty} = 1 - \frac{8}{\pi^2}\, exp\left(\frac{-D_s \pi^2 t_s}{l^2}\right) \quad (1)$$

where M_s is the sorption amount at time t_s, M_∞ is the saturated sorption amount at a large sorption time and *l* is the specimen thickness.

Foaming Process

The procedure to produce the microcellular foams was the "solid state method" [4,15,25]. First, the samples were saturated with CO_2 as was described in the previous section using a saturation pressure of 5 MPa at room temperature. During this saturation process the polymer was always in a solid state. Then, the samples were removed from the pressure vessel and introduced in a temperature controlled glycerin bath. A thermodynamic instability was created by releasing the pressure and heating the sample causing cell nucleation and growth. Different foaming temperatures and times were selected to manufacture the cellular materials. After foaming, samples were removed from the bath and cooled in water at room temperature. All the cellular materials fabricated are summarized in Table 1.

Table 1. Summary of the cellular materials produced using a saturation pressure of 5 MPa.

Name (C_c-t_c-T_F-t_F)	Crosslinking Content - C_c (phr)	Crosslinking Time - t_c (min)	Foaming Temperature - T_F (ºC)	Foaming Time - t_F (s)
0-0-T_F-t_F	0	0	150, 160, 170, 180, 190	15, 30, 45, 75
1-30-T_F-t_F	1	30	150, 160, 170, 180, 190	15, 30, 45, 75
2.4-30-T_F-t_F	2.4	30	150, 160, 170, 180, 190	15, 30, 45, 75
4-30-T_F-t_F	4	30	150, 160, 170, 180, 190	15, 30, 45, 75

The nomenclature employed to designate the foamed materials is as follows: C_c-t_c-T_F-t_F where C_c is the crosslinking content, t_c is the crosslinking time, T_F is the foaming temperature and t_F is the foaming time.

In order to analyze the effect of the saturation pressure on the foams density both the uncrosslinked HDPE and x-HDPE fabricated with the maximum amount of peroxide were also saturated at a pressure of 3 MPa. These materials were subsequently foamed. Table 2 shows the cellular materials fabricated with this new saturation pressure. These materials are designated by including a number three at the beginning of their nomenclature.

Table 2. Summary of the cellular materials produced using a saturation pressure of 3 MPa.

Name (C_c-t_c-T_F-t_F)	Crosslinking Content - C_c (phr)	Crosslinking Time - t_c (min)	Foaming Temperature - T_F (ºC)	Foaming Time - t_F (s)
(3)0-0-T_F-t_F	0	0	170	15, 20, 30, 45
(3)4-30-T_F-t_F	4	30	180	15, 20, 30, 45

Samples Characterization

Extensional Rheological Behavior

The transient extensional viscosity of the uncrosslinked HDPE as well as that of the x-HDPEs produced with the minimum and the maximum amounts of peroxide (1 phr and 4 phr) was measured using a stress controlled rheometer (AR 2000 EX from TA Instruments) with an extensional rheology test fixture (SER 2 from Xpansion Instruments). In this geometry two clamps hold the sample to two drums, which rotate in opposite direction, stretching the sample, at a certain Hencky strain rate [26].

All the experiments were made at a temperature of 170 ºC. Rectangular solid samples with dimensions of 20 mm x 10 mm x 0.5 mm fabricated by compression molding, as was previously described, were used to perform the extensional viscosity measurements.

The measurement protocol considered a pre-stretch, in order to compensate the thermal expansion of the sample when it is heated up from room temperature and then a relaxation when the pre-stretch has finished (i.e. sample is kept at the testing temperature of 170 ºC with no stress during approximately 60 s). After this relaxation time the experiment takes place. Measurements were performed at three different Hencky strain rates: 0.5, 1 and 2.5 s^{-1}. The maximum Hencky strain applied was 2 for all the different materials.

Gel Content

The gel content (*GC*) produced in the HDPE based polymers by crosslinking was determining according to the ASTM standard D 2765-01. Specimens of the crosslinked ethylene polymers were first weighed and then immersed in xylene which was used as extracting solvent. Samples were kept in boiling xylene during 1.5 hours, which is the minimum time necessary to completely dissolve the uncrosslinked HDPE. After this time the samples were removed from xylene and dried in a vacuum oven pre-heated at 150 ºC. Finally the specimens were reweighed to determine the insoluble fraction of polymer and therefore, the gel content according to Equation 2.

$$GC\ (\%) = 100 - \left[100\left(\frac{w_0 - w_f}{w_0}\right)\right] \qquad (2)$$

where w_f is the weight of the specimen after extraction and drying and w_0 is the weight of the original specimen. Three samples were used to determine the average gel content for each material.

Differential Scanning Calorimetry

The thermal properties of the neat HDPE and the different x-HDPE materials were studied by means of a Mettler DSC822e differential scanning calorimeter, previously calibrated with indium, zinc, and *n*-octane. The weight of the samples was approximately 6 mg and all the experiments were performed under nitrogen atmosphere. On the one hand, to obtain the crystallization temperature (T_c) the experiments were performed between 200 and -40 ºC at 20 ºC/min. On the other hand, to obtain the crystallinity (X_c) and the melting temperature (T_m) the experiments were performed between -40 and 200 ºC at 10ºC/min. The crystallinity was calculated dividing the heat of fusion in the DSC curve by the heat of fusion of a 100 % crystalline material (288 J/g for a 100% crystalline polyethylene) [27,28]. Before performing

these two experiments the samples were heated from -40 ºC to 200 ºC at a heating rate of 10 ºC/min and maintained at 200 ºC during three minutes in order to remove the materials thermal history.

Density

Density of the non-foamed (solid) polymeric matrixes was determined for both, the HDPE and the x-HDPEs. For this purpose a gas pycnometer was employed (AccuPyc II 1340 from Micromeritics). The pycnometer provides the volume of the solid samples with high precision as well as the density calculations. Five different measurements of each material were performed with the aim of obtaining and accurate average value of the solid samples density.

On the other hand, cellular materials density was determined by the Archimedes water immersion method using a high precision balance (Mettler AT 261). Moreover the relative density of the cellular materials was determined according to Equation 3.

$$\rho_R = \frac{\rho_{cm}}{\rho_s} \tag{3}$$

where ρ_{cm} is the cellular material density and ρ_s is the solid matrix density.

Structural Characterization

Scanning Electron Microscopy (SEM) was used to analyze the cellular structure, and also to quantify the average cell size (Φ), the standard deviation of the cell size and the cell nucleation density (N_V). For this purpose, the micrographs obtained were analyzed with an image processing tool based on the software Fiji/Image J [29].

Samples were cooled using liquid nitrogen to cut them without modifying their structure; then they were vacuum coated with a thin layer of gold to make them conductive. A Jeol JSM-820 scanning electron microscope was used to observe the samples morphology.

The average cell size (Φ), which is the mean cell diameter in three dimensions, was calculated using Equation 4.

$$\Phi = \sum_{i=1}^{n} \frac{\Phi^i}{n} \tag{4}$$

where n is the number of counted cells and Φ^i is the three-dimensional cell size of the cell i.

The standard deviation of the cell size (*SDC*), parameter that measures the dispersion of the cell sizes, was calculated according Equation 5.

$$SDC = \sqrt{\sum_{i=1}^{n} \frac{(\Phi^i - \Phi)^2}{n-1}} \tag{5}$$

The cell nucleation density (N_V) is the number of cells per unit volume of the solid material [29]. The following expression (Equation 6) was used to calculate this parameter.

$$N_V = \frac{N_{V-CM}\rho_s}{\rho_{cm}} = \frac{N_{V-CM}}{\rho_R} \tag{6}$$

where $N_{V\text{-}cm}$ is the number of cells per unit volume of the cellular material. To calculate $N_{V\text{-}CM}$, the following equation (Equation 7) was used:

$$N_{V-cm} = \left[\frac{nM^2}{A}\right]^{\frac{3}{2}} \quad (7)$$

where *M* is the magnification factor of the micrograph and *A* is the micrograph area.

RESULTS AND DISCUSSION

Analysis of Solid Samples

Extensional Rheological Behavior

During the foaming process the bubble growth involves extensional or elongational flow, as the cell walls are stretched. The extensional viscosity is defined as the ratio between the stress and the strain rate, when a material is elongated. Figure 1.a shows the transient extensional viscosity of the uncrosslinked HDPE (0-0) as well as the x-HDPEs 1-30 and 4-30, measured at three different Hencky strain rates (0.5, 1 and 2.5 s^{-1}).

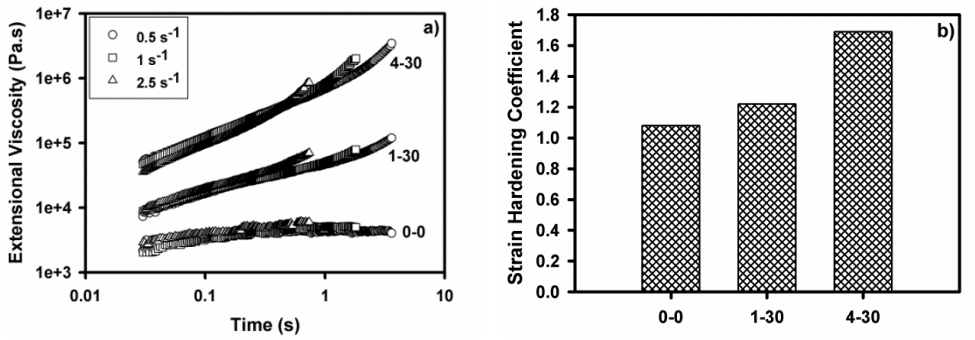

Figure 1. Extensional rheological behavior of the uncrosslinked HDPE (0-0) and the x- HDPEs produced with the minimum (1 phr) and maximum (4 phr) contents of organic peroxide. a) Extensional viscosity vs. time measured at different Hencky strain rates (0.5; 1 and 2.5 s^{-1}) b) Strain hardening coefficient calculated for a time of 2 s and for a Hencky strain rate of 1 s^{-1}.

When the amount of crosslinking agent increases, an increase in the viscosity of the materials is also obtained. Furthermore, while the x-HDPEs show a rapid increase of the extensional viscosity with time and this behavior become more intense as the amount of crosslinking agent increases, the linear HDPE does not show this behavior. This phenomenon is called strain hardening [30]. In general, if the polymer does not exhibit strain hardening it is difficult to achieve high expansion ratios during foaming because the cell walls break, i.e. cell coalescence is produced and the foam is not able to retain the gas during the expansion process [31]. This strain hardening results from the molecular entanglements in the melt state which can be produced by the introduction of branching or crosslinking [32,33]. With the aim of quantifying this behavior, the strain hardening coefficient (*S*) has been calculated from the extensional viscosity measurements, according to Equation 8.

$$S = \frac{\eta_E^+(t, \dot{\varepsilon}_0)}{\eta_{E0}^+(t)} \quad (8)$$

where $\eta_E^+(t,\dot{\varepsilon}_0)$ is the transient extensional viscosity as a function of time and Hencky strain rate and $\eta_{E0}^+(t)$ is the transient extensional viscosity in the linear viscoelastic regime [34,35]. This value has been obtained for a time of 2 s and for a Hencky strain rate of 1 s^{-1}. Results are shown in Figure 1.b. An increase in the *S* is obtained by increasing the amount of crosslinking agent. In fact, the *S* of the material containing the highest amount of organic peroxide is 1.6 times higher than that of the uncrosslinked HDPE.

Gel Content

HDPE was chemically crosslinked, firstly by incorporating organic peroxide and then by activating the peroxide, using for this purpose a fixed temperature and different crosslinking times. The crosslinking is randomly produced in the molten state where the polymer has only amorphous structure. In this state, the peroxide links the molecules into a three-dimensional network [18,36].

Figure 2 shows the gel content which is defined as the fraction of polymer that is insoluble under the test conditions (see Experimental Section).

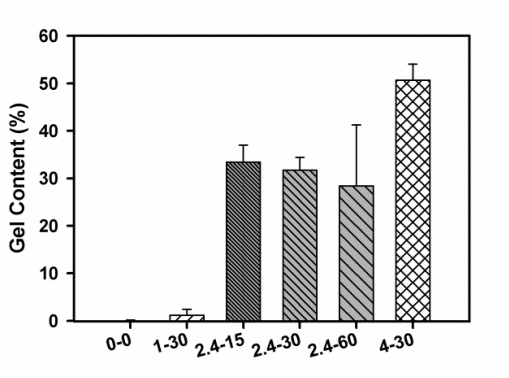

Figure 2. Gel content of the uncrosslinked HDPE and the different x-HDPE.

An increase in the gel content is observed when the amount of crosslinking agent increases while the crosslinking time is kept constant. Furthermore, from Figure 2 it can be derived that the gel content of the crosslinked materials fabricated employing the same content of peroxide is very similar, independently of the time used to crosslink such materials (i.e. for the lowest time used, 15 minutes, the maximum gel content has already been achieved).

Thermal Characterization

Table 3 shows the melting point (T_m), the crystallization temperature (T_c) and the crystallinity (X_c), determined from the DSC measurements, of the uncrosslinked HDPE and the different x-HDPEs.

It is well known that crosslinking has a direct effect on the crystallization process. Formation of crosslink junctions when the polymer is in a molten state modifies the reorganization and chain folding during the crystallization process. The crosslinks act as defect centers, hindering both, the crystal growth as well as the formation of crystals. As a result imperfect crystallite with smaller sizes and also less in content are formed [16,17,18].

Table 3. Melting temperature (T_m), crystallization temperature (T_c) and crystallinity (X_c) of the neat HDPE and the different crosslinked materials.

Name (C_c-t_c)	T_m (ºC)	T_c (ºC)	X_c (%)
0-0	129.7	114.2	67.7
1-30	130.0	107.9	62.9
2.4-15	128.9	106.7	60.2
2.4-30	130.1	106.0	57.1
2.4-60	130.5	106.4	58.9
4-30	127.9	107.1	55.8

Results show that the crystallization temperature (T_c) is lower in the x-HDPEs although no changes in the crystallization temperature are caused by changing the content of the crosslinking agent. Moreover the melting temperature (T_m) remains almost constant and only a reduction of this temperature is observed in the material with the highest crosslinking content. However, the crystallinity decreases significantly with the amount of crosslinking agent. The slight modifications obtained in the thermal properties could be due to the low crosslinking degrees achieved in this work, as the maximum gel content achieved has been 50 %.

Diffusivity and Gas Concentration

Figure 3 shows the CO_2 concentration as a function of time of the neat, uncrosslinked, HDPE together with the same curves obtained for the different x-HDPEs. The sorption curves as a function of time have been obtained at room temperature and under a pressure of 5 MPa using samples with a thickness of 2 mm.

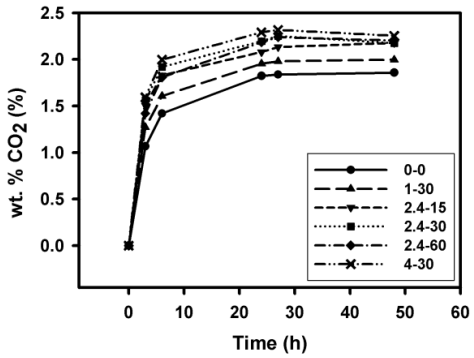

Figure 3. Sorption curve of HDPE and x-HDPE obtained at 5 MPa and room temperature.

From Figure 3 it can be concluded that the equilibrium gas concentration increases with the amount of crosslinking agent (see also Table 4). Moreover, no significant differences are observed between samples with the same amount of crosslinking agent and different crosslinking times, in which the crystallinity was the same (Table 3) as well as the gel content (Figure 2). Both, solubility and diffusivity of CO_2 in a semi-crystalline sample are functions of crystallinity. When crystallinity decreases an increment in the free space available for the gas molecules to diffuse into the polymer is produced and due to this the solubility increases. In other words, the presence of crystalline regions makes difficult the gas diffusivity into the polymeric matrix and therefore the equilibrium CO_2 concentration decreases [7,37,38]. The

values of the sorption diffusivity coefficient (D_s) as well as the values of the gas concentration at equilibrium are shown in Table 4 for the different materials.

Table 4. Comparison of sorption diffusivity and gas concentration at equilibrium for the neat HDPE and the different x-HDPE materials.

Name (C_c-t_c)	D_s (10^{-11} m^2/s)	Gas Concentration (wt. %)
0-0	2.71	1.86
1-30	3.06	1.99
2.4-15	3.44	2.18
2.4-30	3.50	2.18
2.4-60	3.23	2.20
4-30	3.65	2.25

Moreover, it can be seen in Figure 3 that at 5 MPa, the material with the maximum crosslinking content (4-60) absorbs approximately 2.3 wt.% of gas, being as well the polymer that absorbs more gas. This low value is indicating that CO_2 has a very low solubility in polyethylene at subcritical pressures and room temperature compared to other polymers like PVC (7.5 wt.% at 4.8 MPa and T_a) [25], PC (9 wt.% at 4.8 MPa and T_a) [39], ABS (12 wt.% at 5 MPa and T_a) [40].

Furthermore, the experimental value of the gas concentration achieved for the neat HDPE (1.8 wt.% at 5 MPa and T_a) is in agreement with that reported in the literature [15].

Due to the similar characteristics that the three solid crosslinked materials fabricated with the same content of peroxide (2.4 phr) but changing the crosslinking time show, only one of these three materials (that fabricated with a crosslinking time of 30 minutes) has been finally foamed.

Analysis of Foamed Samples

Effect of the Saturation Pressure

The effect of the saturation pressure on both, the cellular materials density and the cellular structure is analyzed in this section. Figure 4.a shows the relative density versus time of the uncrosslinked HDPE saturated at two different pressures, 3 and 5 MPa. The foaming was performed at 170 ºC. In the same way the x-HDPE 4-30 has been analyzed, in this second case the foaming was performed at 180 ºC. Results are shown in Figure 4.b.

Results show that no significant differences were found between the two pressures. For short foaming times (less than 30 s), lower densities are achieved when the material is saturated at the highest pressure (5 MPa). This is the expected behavior. Normally, an increase in the saturation pressure is connected with an increase in the amount of gas available for foaming and therefore with a reduction in the material density [41]. However, when the foaming time increases up to 45 s the lowest saturation pressure (3 MPa) leads to lower densities. Nevertheless, for this foaming time foam collapse is observed and therefore the results obtained at this time are not representative. Moreover, Figure 4 also shows that the curve relative density versus foaming time presents a minimum at a foaming time of 30 s. This behavior is explained in detail in the following section.

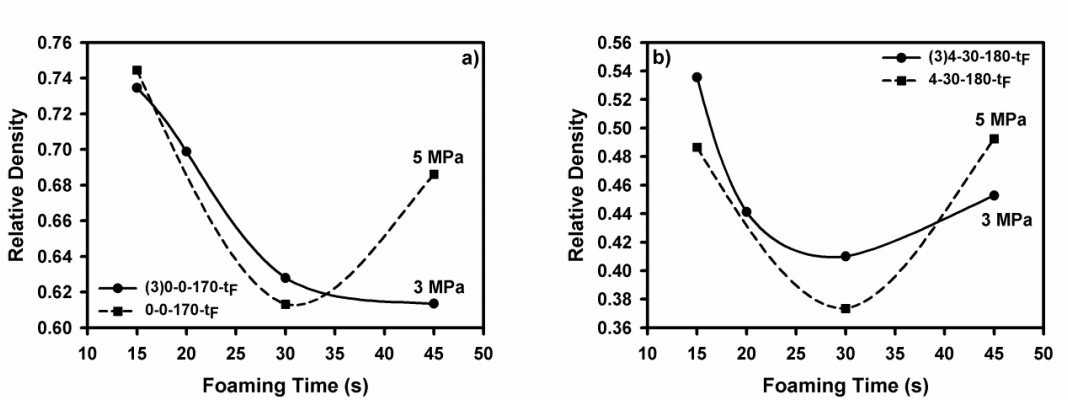

Figure 4. Relative density as a function of the foaming time. a) Uncrosslinked HDPE saturated at two pressures: 3 and 5 MPa. b) x-HDPE, containing 4 phr of organic peroxide, saturated at two pressures: 3 and 5 MPa.

The cellular structure of these foamed materials was also analyzed (Figure 5). A foaming time of 30 s was selected to compare the different materials.

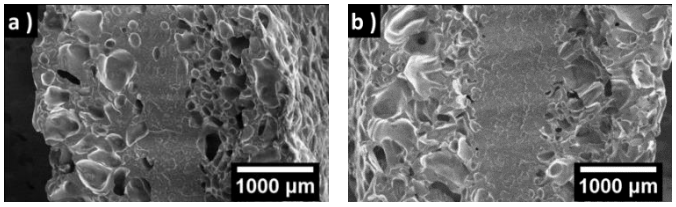

Figure 5. SEM micrographs of the cellular materials fabricated with the uncrosslinked HDPE using two different saturation pressures. a) 3 MPa. b) 5 MPa.

The cellular structure of both materials is very similar. In these materials it is possible to see a non-homogeneous foaming. While the surface is foamed, the center of both materials is solid. This heterogeneous structure could be explained taking into account several factors. First of all, the amount of gas available for foaming is very low in both experiments. Secondly, the external region is the first to be heated and therefore the foaming is produced earlier in this section. Once the external region is foamed, this surface acts as a thermal insulator hindering the expansion of the internal region. Moreover, it is also possible to see that this surface structure shows cells with a very large size. As the polymer used to produce the cellular materials does not show strain hardening, the cell walls are not able to resist the extension to which they are subjected during the foaming process and consequently cell coalescence occurs. Moreover, there is another reason which also explains the large cells found in the material surface. The gas from the surface is the first to diffuse out of the material and therefore the amount of gas available for foaming is less in the surface. Consequently, cell nucleation is also lower. As the average bubble size is strongly influenced by the number of bubbles that are nucleated, a drop in the nucleation density leads to larger cells [42].

To analyze in more detail the effect of the saturation pressure in the foam behavior, a quantitative analysis of these structures has been performed and the average cell size and the cell nucleation density have been determined. Results are shown in Table 5. In this table the standard deviation of the cell size is also shown. This value is measuring the dispersion of the cell sizes.

Table 5. Average cell size and cell nucleation density of the foamed materials fabricated with the uncrosslinked HDPE using different saturation pressures. These cellular materials were produced using a foaming temperature of 170 ºC and a foaming time of 30 s.

Name (C_c-t_c-T_F-t_F)	Cell Size (Microns)	Standard Deviation (Microns)	Cell Nucleation Density (Cells/cm^3)
(3)0-0-170-30	162.9	121.5	$8.3x10^4$
0-0-170-30	157.9	123.6	$7.2\ x10^4$

The quantitative analysis confirms that there are no differences between the two materials. Both the cell size and the cell nucleation density are very similar which indicates that, for these saturation pressures, the fact of using one or another pressure does not have an important effect on the cellular structure. Moreover, the standard deviation values are very high which indicates that the cellular structures are very heterogeneous presenting cells with large and small sizes.

In the same way, the effect of the saturation pressure in the cellular structure of the foamed materials produced with the x-HDPE containing the highest amount of peroxide is also analyzed. Figure 6 shows the SEM micrographs of these cellular materials.

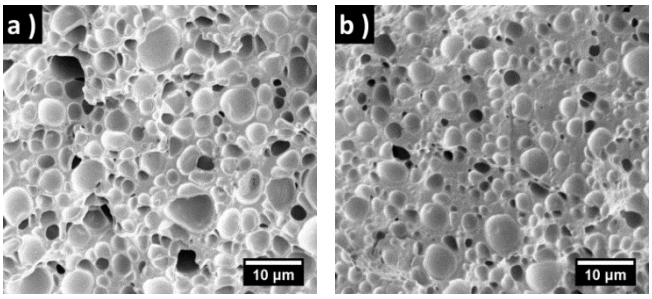

Figure 6. SEM micrographs of the cellular materials fabricated with the x-HDPE containing the highest amount of peroxide (4 phr) using two different saturation pressures. a) 3 MPa. b) 5 MPa.

The cellular structure of these materials is more homogeneous than that of the uncrosslinked HDPEs. In this case, the amount of gas available for foaming is large enough to produce a complete expansion of the material, i.e. both the center and the surface are completely foamed. Again, the average cell size and the cell nucleation density have been obtained from the previous micrographs. Results are shown in Table 6.

Table 6. Average cell size and cell nucleation density of the foamed materials produced with the x-HDPE containing 4 phr of organic peroxide and using different saturation pressures. A foaming temperature of 180 ºC and a foaming time of 30 s were used to manufacture these cellular materials.

Name (C_c-t_c-T_F-t_F)	Cell Size (Microns)	Standard Deviation (Microns)	Cell Nucleation Density (Cells/cm^3)
(3)4-30-180-30	2.6	1.5	$6.4x10^{10}$
4-30-180-30	1.9	1.1	$6.7x10^{10}$

As with the materials produced with the uncrosslinked HDPE, there are small changes in the cellular structure by the fact of changing the saturation pressure from 3 MPa to 5 MPa. A slight reduction of cell size was found in the material produced at 5 MPa.

Taking into account the obtained results, all the other cellular materials produced in this study were saturated with the highest saturation pressure (5 MPa) as, in general, the lowest densities were obtained with this pressure.

Effect of the foaming time

Once the saturation pressure has been selected, the effect of the foaming time on the materials density and cellular structure is analyzed in this section. Firstly, the relative density is represented versus the foaming time for the different materials as well as for the following temperatures: 150 ºC, 160 ºC, 170 ºC and 190 ºC (Figure 7). In this section the temperature is also considered with the aim of determining if the behaviors obtained when the density is represented as a function of time are also dependent on the foaming temperature.

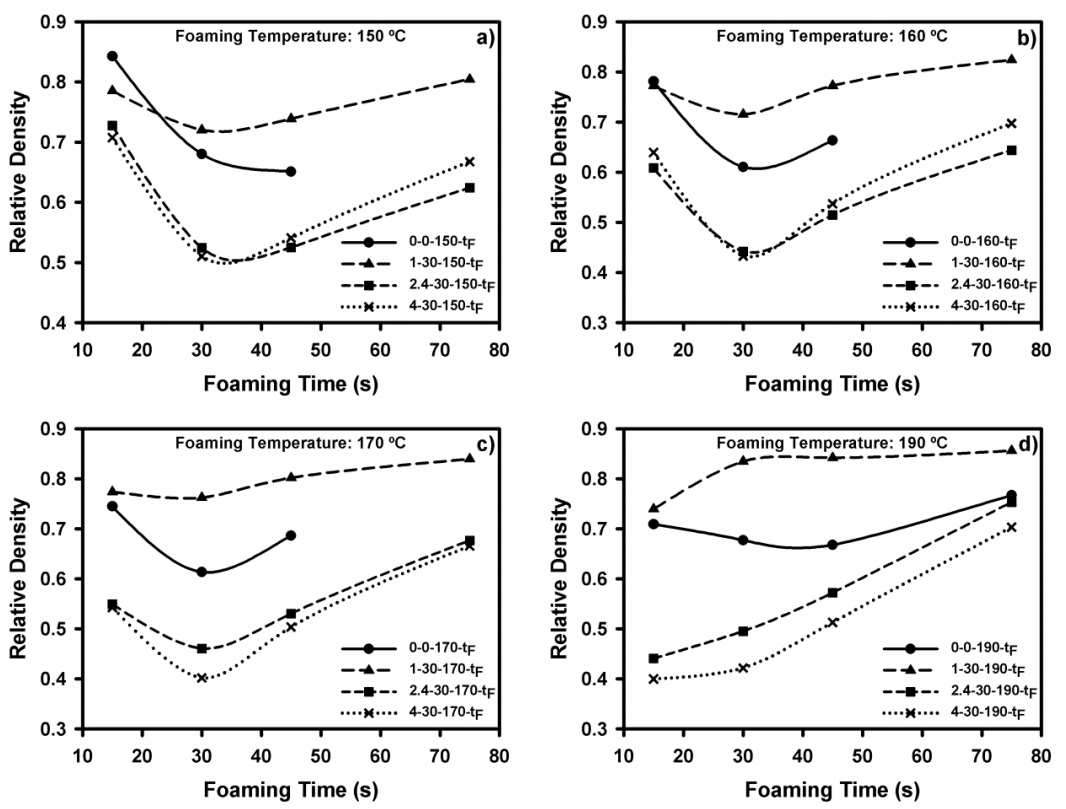

Figure 7. Relative density of the different materials as a function of the foaming time for the different foaming temperatures. a) 150 ºC. b) 160 ºC. c) 170 ºC. d) 190 ºC.

With the exception of the cellular materials fabricated with the highest foaming temperature in which the relative density increases with time, for the rest of materials the relative density shows a minimum for a foaming time of approximately 30 s. The minimum density (0.37) has been achieved using the polymer containing the highest amount of peroxide (4 phr) and with the following foaming conditions: a foaming time of 30 s and foaming temperature of 160 ºC. If the foaming time is not high enough, the materials do not foam completely and only the surface is expanded, consequently only a small reduction in density, relative to that of the solid material, is obtained. As the foaming time increases from 15 to 30 s a reduction in density is obtained. This time allows producing a large expansion of the material. Then, when the foaming time increases again, an increase in the the cellular materials density is produced. The gas is continuously diffusing out of the material and therefore if the structure is not frozen in

an optimum time the cells begin to collapse causing foam contraction. Moreover, when the foaming time increases cell coalescence also occurs. These two phenomena make the density to increase if the foaming time is too high. In general, the materials manufactured with the highest temperature do not follow this behavior. In this case the foaming temperature employed is really high and therefore the gas diffusion is faster in these materials than in the previously described foams. The minimum in density is not observed because this minimum could be appearing at lower times than those studied in this work, i.e. a similar behavior than that obtained with the other temperatures could be obtained if lower foaming times were considered.

Taking into account the previous results, the effect of the foaming time on the cellular structure has been studied considering only a representative temperature (160 ºC). Moreover, this study has been performed in the two most extreme materials: the uncrosslinked HDPE and the material produced with the x-HDPE containing the highest amount of peroxide.

The cellular structure of the materials fabricated with the uncrosslinked HDPE (0-0) at different foaming times is shown in Figure 8.

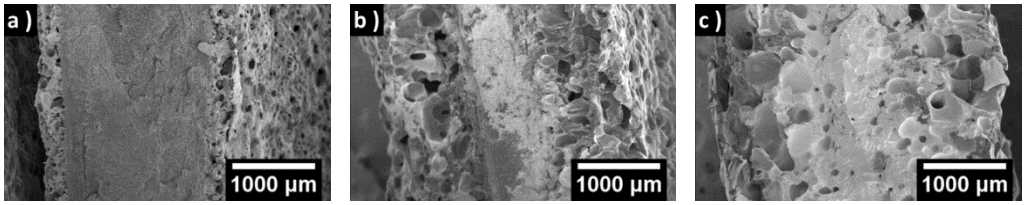

Figure 8. SEM micrographs of the cellular materials fabricated with the uncrosslinked HDPE, with a foaming temperature of 160 ºC and with different foaming times. a) 15 s. b) 30 s. c) 45 s.

Only the surface of these materials is foamed. The differences obtained in density could be perfectly related to the cellular structures of the different foamed materials. In the material foamed with the lowest time (15 s) almost all the material is still solid and only a very narrow band of the surface has been foamed. Therefore the reduction of density obtained in this material is very low. For a higher foaming time (30 s) a significant reduction in density is obtained. SEM micrograph of this material shows that the foamed band is wider than in the previous material. Finally for the highest foaming time (45 s) an increase in the density is again produced. The width of the foamed band is similar to that of the previous material but larger cells appear on the surface which indicates that cell coalescence and therefore foam collapse have been produced making the overall density to increase.

In the same way, the cellular structure of the foamed materials fabricated with the x-HDPE containing 4 phr of crosslinking agent has been analyzed. The SEM micrographs are shown in Figure 9. In this case most of the samples are completely foamed and therefore the micrographs have been taken from the center of the sample in order to compare the cellular structure under the same conditions. Figure 9 shows the most representative structures of each material.

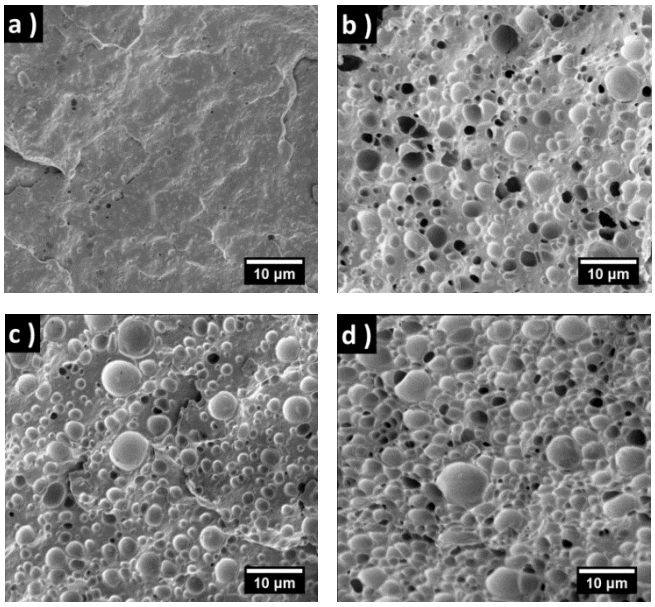

Figure 9. SEM micrographs of the cellular materials fabricated with the x-HDPE, containing 4 phr of organic peroxide, with a foaming temperature of 160 ºC and with different foaming times. a) 15 s. b) 30 s. c) 45 s d) 75 s.

Excepting the material manufactured with the lowest foaming time (15 s) the rest of materials are completely foamed, i.e. both the surface and the center are expanded.

In order to analyze more accurately the cellular structure of the foamed materials both the cell size and the cell nucleation density have been quantified. The results obtained, for the two materials, are shown in Figure 10.

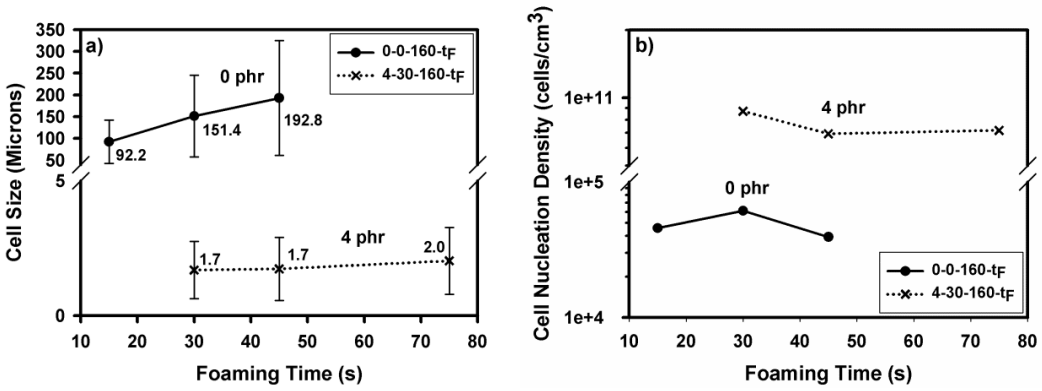

Figure 10. Effect of the foaming time on the cellular structure in both the foamed uncrosslinked HDPE and the foamed x-HDPE containing 4 phr of crosslinking agent. a) Cell size as a function of the foaming time. b) Cell nucleation density vs. foaming time.

The average cell size (Figure 10.a) of the foamed materials produced with the x-HDPE (4 phr) does not change with the foaming time; however, an increase of this parameter is produced when the material foamed is the uncrosslinked HDPE. The cell size is doubled by going from 15 to 45 s. Another important fact is that the average cell size of the foamed uncrosslinked HDPE materials is two orders of magnitude higher than that of the cellular materials produced with the x-HDPE. The gas available for foaming is higher in the crosslinked material; consequently the number of nucleation sites is also greater in this material. As the average cell size is

strongly influenced by the number of bubbles that nucleate, an increase in the nucleation density leads to smaller cell sizes [42]. Moreover, coalescence is also less intense for the crosslinked material, due to its strong strain hardening (see Figure 1), which also conducts to cells with smaller sizes. In both types of materials, the standard deviation of the cell size is really high which indicates that the cellular structures are very heterogeneous. Figure 10.b shows the cell nucleation density versus the foaming time. This parameter allows comparing materials with different densities, as this parameter takes into account the relative density of the foamed materials (see Equation 5). Therefore, with this parameter it is possible to analyze both the nucleation and coalescence mechanisms. In general, when the foaming times are low, the nucleation is the predominant phenomena. Then, when the foaming time increases cell coalescence also takes place. In the material produced with the uncrosslinked HDPE, an increase in the cell nucleation density is produced when the foaming time increases from 15 to 30 s. This indicates that new cells have appeared. Although cell coalescence could be also happening, in these foaming times, the nucleation phenomenon prevails over the coalescence one. Then, when the foaming time increases from 30 to 45 s, cell coalescence is the predominant phenomenon making the cell nucleation density to decrease. In the cellular materials based on the x-HDPE, N_V remains practically constant. This behavior can be explained taking into account the rheological results represented in Figure 1. The strain hardening that the x-HDPE exhibits helps to stabilize the cellular structure.

Effect of the foaming temperature

In this section the effect of the foaming temperature on the materials relative density and cellular structure is studied. To perform this analysis a foaming time of 30 s has been selected as, in general, with this foaming time the lowest densities are achieved (see Figure 7). In Figure 11 the relative density of the different foamed materials is represented versus the foaming temperature.

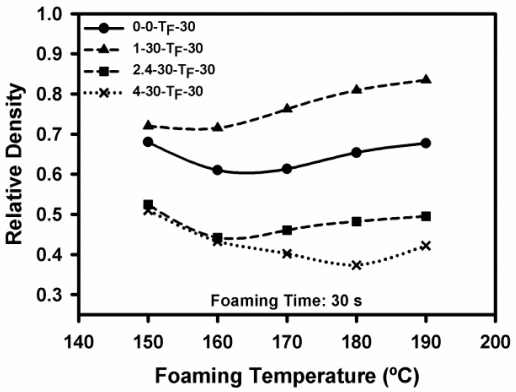

Figure 11. Relative density of the different materials produced using a foaming time of 30 s, as a function of the foaming temperature.

When the foaming temperature increases the viscosity of the polymeric materials decreases and therefore the initial growth of the cells is favored. This greater growth could be related to a reduction in the materials density. Moreover, the classical nucleation theory (Equation 9) says that the homogeneous nucleation rate (N_{HOM}) also increases with temperature, which can also contribute to reduce the foams density [43].

$$N_{HOM} = C_0 f_0 exp\left(\frac{-\Delta G'_{HOM}}{kT}\right) \quad (9)$$

where, C_0 is the concentration of gas molecules, f_0 is the frequency factor of the gas molecules, $\Delta G'_{HOM}$ is the activation energy, k is the Boltzman's constant and T is the temperature.

However, the fact of increasing the foaming temperature has also disadvantages. When the temperature increases the chain mobility increases and therefore the diffusion rate also increases [44]. The blowing agent that has diffused into the nucleated cells eventually tends to diffuse out of the material. As the gas escape through the cell walls, the amount of gas available for the cell growth decreases. As a result, if the cells do not freeze they tend to collapse causing foam contraction and therefore increasing the materials density [45]. Moreover, an increase in the foaming temperature is also related to an increase in the cell coalescence, as the polymer melt strength decreases when the temperature increases [46]. As a consequence, the overall density of the material increases.

Figure 11 indicates that the behavior followed by all materials is the same. When the temperature increases first, the relative density decreases and then, this parameter increases. When the foaming temperatures are low, the polymer withstands the extension without breaking and therefore a reduction in density is produce by increasing the temperature. However, when the temperatures are higher, the gas escapes more easily and also the cell coalescence prevails over the cell nucleation and the cell growth and therefore an increase in the foam density is obtained.

Changes in the cellular structure by varying the foaming temperature are analyzed again in the two extreme materials: the uncrosslinked HDPE (0-0) and the x-HDPE containing the highest amount of organic peroxide. To perform this analysis the foaming time considered for both materials is once more 30 s. Figure 12 shows the complete area of the cellular materials fabricated with the uncrosslinked HDPE, for the different foaming temperatures analyzed.

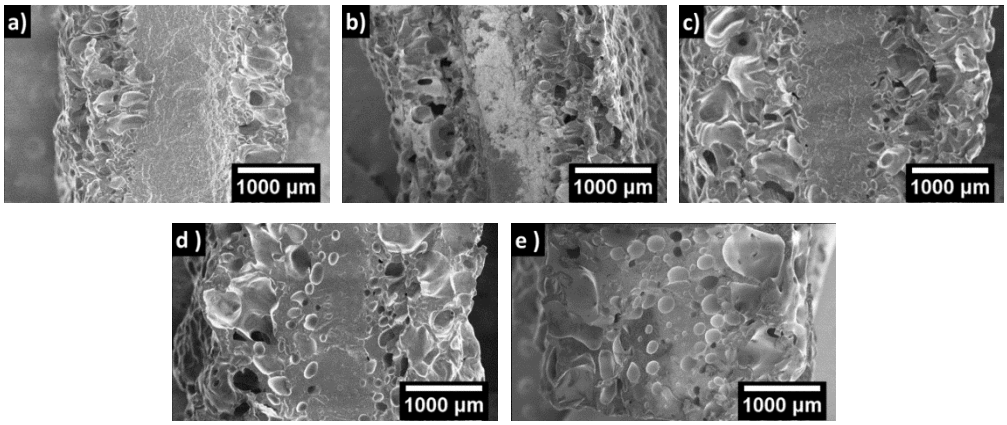

Figure 12. SEM micrographs of the cellular materials fabricated with the uncrosslinked HDPE, with a foaming time of 30 s and with different foaming temperatures. a) 150 ºC. b) 160 ºC. c) 170 ºC. d) 180 ºC. e) 190 ºC.

In general, the center of these foamed materials is mostly solid while the surface is foamed. Nevertheless, it can be seen that when the temperature increases some isolated pores begin to appear in the center. Moreover, it can also be appreciated that larger surface cells are obtained by increasing the foaming temperature. The surface cells are the first to be formed,

therefore if the foaming temperature is very high cell coalescence is produced and consequently an increase in the foams density occurs.

In the same way the cellular structure of the foamed x-HDPEs containing 4 phr of crosslinking agent, fabricated employing different foaming temperatures, has been carefully analyzed. Figure 13 shows the SEM micrographs of the different materials. In this case most of the samples are completely foamed and therefore the micrographs have been taken from the center of the sample in order to compare the cellular structure under the same conditions.

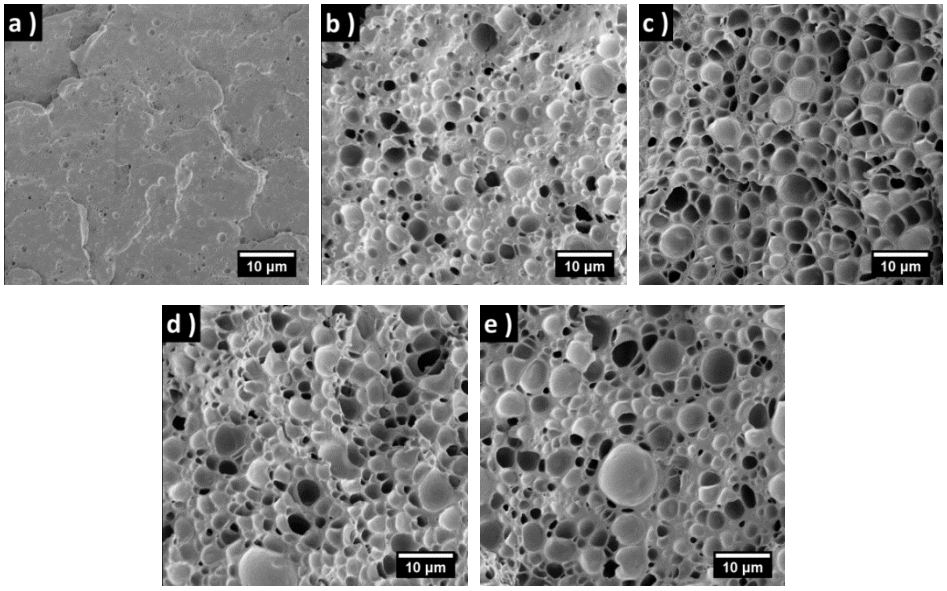

Figure 13. SEM micrographs of the cellular materials fabricated with the x-HDPE, containing the highest amount of organic peroxide (4 phr), with a foaming time of 30 s and different foaming temperatures. a) 150 ºC. b) 160 ºC. c) 170 ºC. d) 180 ºC. e) 190 ºC.

The center of the material produced employing the lowest foaming temperature (150 ºC) is not foamed and consequently the global density of this material is the highest.

In order to analyze more accurately the cellular structure of the foamed materials, the average cell size and the cell nucleation density have been quantified. Both parameters are represented as a function of temperature in Figure 14.

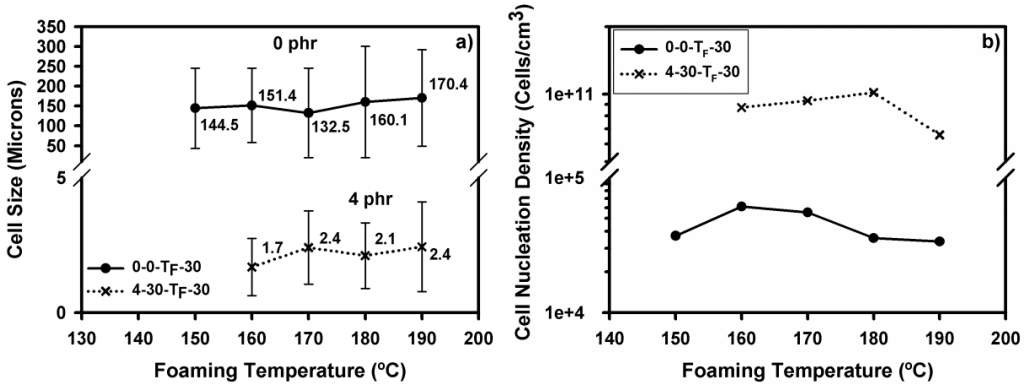

Figure 14. Effect of the foaming temperature on the cellular structure in both the foamed uncrosslinked HDPE and the foamed x-HDPE containing 4 phr of crosslinking agent. a) Cell size as a function of the foaming time. b) Cell nucleation density vs. foaming time.

In general, a slight increase in the cell size is detected by changing the foaming temperature. Furthermore, the cell size standard deviation is again really high, independently on the foaming temperature, which gives an idea of the heterogeneity of the cellular structures. To analyze the mechanisms which take place during the foaming process, the behavior of the cell nucleation density is analyzed. In the cellular materials produced with the uncrosslinked HDPE, N_V increases when the temperature goes from 150 to 160 ºC. Moreover in this range of temperature also a reduction of the relative density was detected (Figure 11). This indicates that, in this temperature range, cell coalescence has not yet occurred, as it was previously concluded. Therefore, the increase on the temperature favors the nucleation rate and consequently the cell nucleation density increases. Then, when the temperature raises again the cell nucleation density decreases indicating that cell coalescence is now the prevailing mechanism. In the foamed x-HDPE a similar behavior is detected. However, the coalescence phenomenon begins to occur at higher temperatures (180 ºC). The large strain hardening of this materials helps to stabilize their cellular structure. Therefore, higher temperatures are required to produce a degeneration of the mentioned structure.

Effect of the Crosslinking Content

Throughout the previous sections, important differences have been found between the two extreme materials: the uncrosslinked HDPE and the x-HDPE with the highest content of peroxide. These different behaviors indicate that the effect of the crosslinking degree on the foam density and cellular structure should be analyzed in detail. For this purpose, the relative density is represented as a function of the gel content (Figure 15). Both, the foaming time and the foaming temperature have been kept constant. A foaming time of 30 s and a foaming temperature of 160 ºC have been considered.

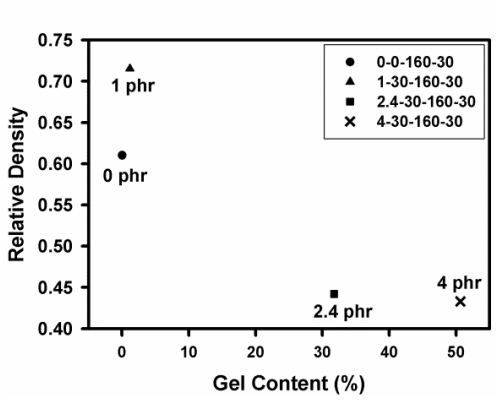

Figure 15. Relative density as a function of the gel content for the cellular materials fabricated with a foaming time of 30 s and a foaming temperature of 160 ºC.

In general, when the crosslinking degree and therefore the gas concentration increases the relative density decreases. As a result of this increase in the gas available for foaming, cellular materials with higher expansion ratios and therefore with lower relative densities can be produced by changing the content of the crosslinking agent employed. Moreover, as the strain hardening also increases with the amount of crosslinking agent, higher expansion ratios can be also achieved due to the ability of the foam to retain the gas during the foaming process.

On the other hand, the microcellular material fabricated with a content of peroxide of 1 phr does not follow this trend. The gas concentration in this material is higher than in the

uncrosslinked HDPE but its relative density is also higher. When a polymer is crosslinked its viscosity is enhanced to a very high value as was indicated in Figure 1. Therefore, the viscosity of the polymer 1-30 is higher than that of the uncrosslinked HDPE. Moreover, the gas concentration of this material is lower than the gas concentration of the other x-HDPEs. This increment in the viscosity together with a not very high amount of gas available for foaming hinders the cells growth. As a consequence, the cellular materials fabricated with this polymer exhibit the highest densities.

SEM micrographs of the four cellular materials studied in this section are shown in Figure 16.

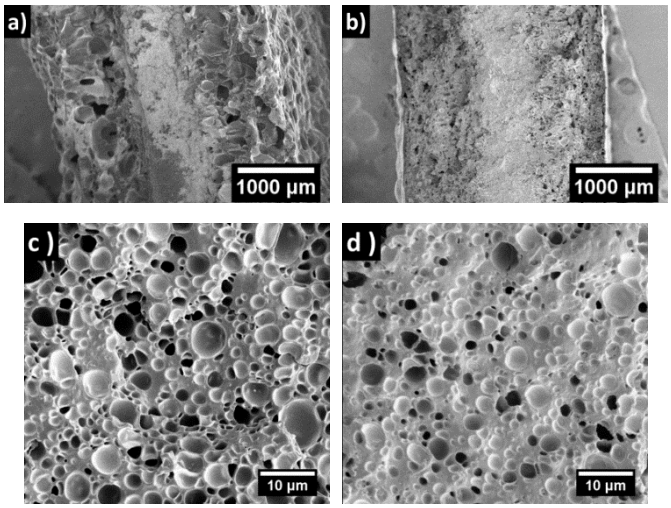

Figure 16. SEM micrographs of the cellular materials fabricated employing different x-HDPE. a) 0-0-160-30. b) 1-30-160-30. c) 2.4-30-160-30. d) 4-30-160-30.

Figures 16.a and 16.b show the complete area of the cellular materials produced with the polymers containing the lowest amounts of crosslinking agent (0 phr and 1 phr). In these micrographs it is possible to see a non-homogenous foaming. The surface of both materials is completely foamed however, while the center of the material containing the lowest amount of peroxide is completely solid, a small number of pores appear on the material containing 1 phr of organic peroxide. Nevertheless, with the x-HDPEs containing higher contents of peroxide (2.4 phr and 4 phr) a complete expansion is obtained. The amount of gas available, in these second materials, is large enough so that the whole material is foamed. As both the center and the surface are completely foamed, greater reductions in density are obtained in these materials. In this case, to illustrate the cellular structure in more detail, the micrographs show a central region of the foamed materials (Figures 16.c and 16.d).

To have further details of how the cellular structure is affected by increasing the amount of crosslinking content, the average cell size and cell density have been quantified. The results obtained are represented as a function of the gel content in Figure 17.

In general, when the gel content increases a reduction in the cell size and an increase in the cell nucleation density is observed. In this case the cellular materials are produced using the same foaming parameters and therefore the changes obtained in the cellular structure can be explained taking into account on the one hand, the amount of gas available for foaming and on the other hand, the rheological properties of the polymeric matrices. When the gel content increases the gas available for foaming also increases. Therefore, an increase in the number of

nucleation sites is also produced. Consequently, both the surface and the center expand and therefore the cell nucleation density increases. Furthermore, an increase in the number of nucleation sites also leads to a reduction in the cell size. On the other hand, when the gel content increases the strain hardening also increases. Consequently, the cell walls are more resistant to the extension and the cell coalescence decreases. As a result, cellular structures with lower cell sizes and higher cell nucleation densities are obtained. Another fact that could be affecting this behavior is the composition of the crosslinking agent as it is composed by 50 % of a organic peroxide and 50 % of SiO_2, which could be acting as a nucleating agent and hence, producing a higher reduction in the cell size when the amount of crosslinking agent increases.

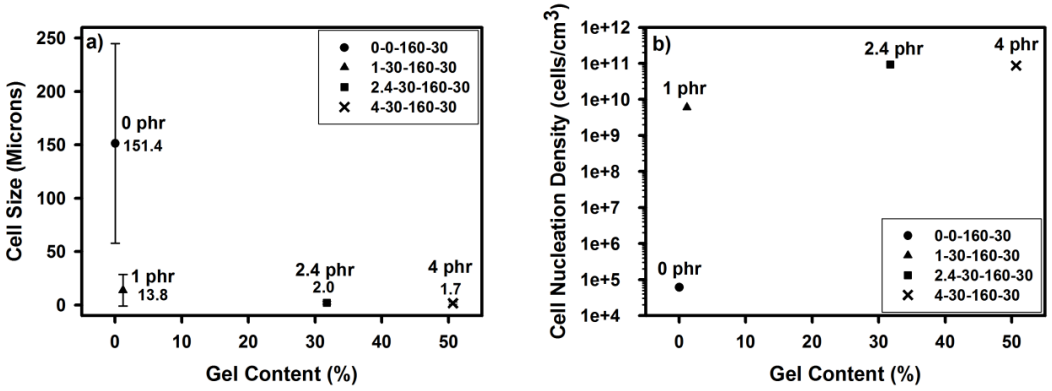

Figure 17. Effect of the crosslinking content on the cellular structure a) Cell size as a function of the gel content. b) Cell nucleation density vs. gel content.

CONCLUSIONS

In this work, the effect that the foaming time, the foaming temperature and the crosslinking content have on the density and microcellular structure of the foamed materials has been analyzed with the aim of understanding the mechanisms taking place during the foaming process. First, the solid materials were studied. When the amount of crosslinking agent increases both, the strain hardening coefficient and the gel content increase. Moreover, a reduction in the crystallinity is also observed with the consequent increase in the amount of gas available for foaming. Then, a thorough study of the foamed materials was performed. In the first place, the effect of the saturation pressure has been analyzed, without finding significant differences between the two pressures studied: 3 and 5 MPa. Then, the effect of the foaming time is examined. A minimum in density has been obtained by changing the foaming time. In connection with the cellular structure, the effect of the foaming time is analyzed on both, the uncrosslinked HDPE and the x-HDPE containing the highest amount of peroxide (4 phr). The structure of the foams produced with the x-HDPE is very stable. No changes are detected neither in the cell size nor in the cell nucleation density because of the high strain hardening that this material shows. In the foams produced with the uncrosslinked HDPE, at low foaming times the nucleation phenomenon is the predominant one and therefore the cell nucleation density increases with the foaming time however, as of 30 s the coalescence phenomena prevails over the nucleation one making the cell nucleation to decrease. The effect of the foaming temperature has also been carefully analyzed. As with the foaming time, a minimum in the relative density was obtained by changing the foaming temperature. In this case, the cell nucleation density shows a maximum independently on the

material used to produce the cellular materials. At low foaming temperatures cell coalescence has not yet occurred and therefore the increase in temperature favors the cell nucleation rate. However, when these temperatures are very high, the coalescence phenomenon prevails over other phenomena, making the cell nucleation density to decrease. Moreover, due to the favorable rheological properties of the x-HDPE, the maximum in the cell nucleation density is produced at higher temperatures than that of the uncrosslinked HDPE. Finally, the effect of the crosslinking content has also been analyzed. While the relative density and the cell size decrease with the gel content, an increase in the cell nucleation content is obtained. This behavior has been explained considering on the one hand, the increase in the amount of gas available for foaming and on the other hand, the improvements achieved in the rheological behavior by the fact of increasing the gel content. To conclude, the results indicate that cellular materials with relative densities as low as 0.37 and with cell sizes of approximately 2 microns can be produced using a saturation pressure of 5 MPa, a foaming time of 30 s, a foaming temperature of 160 ºC and a crosslinked HDPE with a gel content of 50 %.

ACKNOWLEDGEMENTS

Financial support from PIRTU contract of E. Laguna-Gutierrez by Junta of Castilla and Leon (EDU/289/2011) and cofinanced by the European Social Fund is gratefully acknowledged. Financial support from the MICINN (MAT 2012-34901) and the Junta of Castilla and Leon (VA 035U13) is gratefully acknowledged.

REFERENCES

[1] C. B. Park. Continuous Production of High-Density and Low-Density Microcellular Plastics in Extrusion. In Foam Extrusion: Principles and Practice, S. T. Lee (Ed.), Technomic Publishing Company Inc, Lancaster, 2000.

[2] J. Martini, F. A. Waldman, N. P. Suh. Proceedings of SPE Antec 82, San Francisco, 1982

[3] J. Martini, F. A. Waldman, N. P. Suh. Pat. US 4473665 A, 1982

[4] J. E. Martini-Vvedensky, N. P. Suh, F. A. Waldman. Saturation with Inert Gas, Depressurization, and Quick-Cooling, Pat. US 4473665, 1984

[5] P. Rachtanapun, S. E. M. Selke, L. M. Matuana. Microcellular Foam of Polymer Blends of HDPE/PP and Their Composites with Wood Fiber, Journal of Applied Polymer Science, 88, 2842-2850, 2003

[6] S. Doroudiani, C. B. Park, M. T. Kortschot. Processing and Characterization of Microcellular Foamed High-Density Polyethylene/Isotactic Polypropylene Blends, Polymer Engineering and Science, 38, 1205-1215, 1998

[7] S. Doroudiani, C. B. Park, M. T. Kortschot. Effect of the Crystallinity and Morphology on the Microcellular Foam Structure of Semicrystalline Polymers, Polymer Engineering and Science, 21, 2645-2662, 1996

[8] J. C. Salamone. Polymeric materials encyclopedia, Twelve Volume Set, CRC Press, Boca Raton, Florida, 1999

[9] M. Biron. Thermoplastics and Thermoplastic Composites. Technical Information for Plastics Users. Butterworth-Heinemann, Oxford, 2007

[10] D. E. Eaves. New Foams from the Nitrogen Autoclave Process. Cellular Polymers, 2º International Conference, Paper 3. Rapra Technology Limited, Shrewsbury, 1993

[11] P. Rachtanapun, S. E. M. Selke, L. M. Matuana. Relationship between Cell Morphology and Impact Strength of Microcellular Foamed High-Density Polyethylene/Polypropylene Blends, Polymer Engineering and Science, 8, 1551-1560, 2004
[12] P. Rachtanapun, S. E. M. Selke, L. M. Matuana. Effect of the High-Density Polyethylene Melt Index on the Microcellular Foaming of High-Density Polyethylene/Polypropylene Blends, Journal of Applied Polymer Science, 93, 364-371, 2004
[13] Y. H. Lee, C. B. Park, K. H. Wang and M. H. Lee. HDPE-Clay Nanocomposite Foams Blown with Supercritical CO2, Journal of Cellular Plastics, 41, 487-502, 2005
[14] C. Jo, H. E. Naguib. Constitutive modeling of HDPE polymer/clay nanocomposite foams, Polymer, 48, 3349-3360, 2007
[15] D. Miller, V. Kumar. Fabrication of Microcellular HDPE Foams in a Sub-Critical CO_2 Process, Cellular Polymers, 28, 25-40, 2009
[16] H. A. Khonakdar, J. Morshedian, U. Wagenknecht, S. H. Jafari. An Investigation of Chemical Crosslinking Effect on Properties of High-Density Polyethylene, Polymer, 44, 4301-4309, 2003
[17] H. A. Khonakdar, J. Morshedian, M. Mehrabzadeh, U. Wagenknecht, S. H. Jafari. Thermal and Shrinkage Behaviour of Stretched Peroxide-Crosslinked High-Density Polyethylene, European Polymer Journal, 39, 1729–1734, 2003
[18] H. A. Khonakdar, S. H. Jafari, M. Taheri, U. Wagenknecht, D. Jehnichen, L. Haüssler. Thermal and Wide Angle X-ray Analysis of Chemically and Radiation-Crosslinked Low and High Density Polyethylenes, Journal of Applied Polymer Science, 100, 3264-3271, 2006
[19] G. J. Nam, J. H. Yoo and J. W. Lee. Effect of Long-Chain Branches of Polypropylene on Rheological Properties and Foam-Extrusion Performances. Journal of Applied Polymer Science, 96, 1793-1800, 2005
[20] P. Spitael, C. W. Macoko. Strain Hardening in Polypropylenes and Its Role in Extrusion Foaming. Polymer Engineering and Science, 44, 2090-2100, 2004
[21] J. Stange, H. Münstedt. Effect of Long-chain Branching on the Foaming of Polypropylene with Azodicarbonamide. Journal of Cellular Plastics, 42, 445-467, 2006
[22] M. Yamaguchi, K. Suzuki. Rheological Properties and Foam Processability for Blends of Linear and Crosslinked Polyethylenes, Journal of Polymer Science: Part B: Polymer Physics, 39, 2159–2167, 2001
[23] M. Tang, T. B. Du, Y. P. Chen. Sorption and Diffusion of Supercritical Carbon Dioxide in Polycarbonate, Journal of Supercritical Fluids, 28, 207-218, 2004
[24] R. Gendron. Thermoplastic Foam Processing. Principles and Development, CRC Press, Boca Raton, Florida, 2004
[25] V. Kumar, J. E. Weller. A Process to Produce Microcellular PVC, International Polymer Processing, 8, 73-80, 1993
[26] M. Sentmanat, G. H. McKinley. Measuring the transient extensional rheology of polyethylene melts using the SER universal testing platform, Journal of Rheology, 49, 585-606, 2005
[27] T. R. Crompton. Polymer Reference Book, Rapra Technology Limited, Shrewsbury, 2006
[28] A. J. Peacock. Handbook of Polyethylene: Structure, Properties and Applications, Marcel Dekker, Inc., New York, 2000
[29] J. Pinto, E. Solórzano, M. A. Rodriguez-Perez and J. A. de Saja. Characterization of the Cellular Structure Based on User-Interactive Image Analysis Procedures, Journal of Cellular Plastics, 49, 555-575, 2013

[30] R. Gendron, L. E. Daigneault. Rheology of Thermoplastic Foam Extrusion Process. In Foam Extrusion: Principles and Practice, S. T. Lee (Ed.), Technomic Publishing Company Inc, Lancaster, 2000.
[31] H. E. Naguib, C. B. Park, U. Panzer, N. Reichelt. Strategies for Achieving Ultra Low Density Polypropylene Foams, Polymer Engineering and Science, 42, 1481-1492, 2002
[32] A. B. Lugao, B. W. H. Artel, A. Yoshiga, L. F. C. P. Lima, D. F. Parra, J. R. Bueno, S. Liberman, M. Farrah, W. R. Tercariol, H. Otaguro. Production of High Melt Strength Polypropylene by Gamma Irradiation, Radiation Physics and Chemistry, 76, 1691–1695, 2007
[33] M. Sugimoto, T. Tanaka, Y. Masabuchi, J. Takimoto, K. Koyama. Effect of Chain Structure on the Melt Rheology of Modified Polypropylene, Journal of Applied Polymer Science, 73, 1493–1500, 1999
[34] J. Stange, C. Uhl and H. Münstedt. Rheological Behavior of Blends from a Linear and a Long-Chain Branched Polypropylene. Journal of Rheology, 495, 1059-1079 (2005)
[35] A. K. Chaudhary, K. Jayaraman. Extrusion of Linear Polypropylene–Clay Nanocomposite Foams. Polymer Engineering and Science, 51, 1749-1756 (2011)
[36] S. M. Tamboli, S. T. Mhaske, D. D. Kale. Crosslinked Polyethylene, Indian Journal of Chemical Technology, 11, 853-864, 2004
[37] A. S. Michaels, H. J. Bixler. Solubility of Gases in Polyethylene. Journal of Polymer Science, 50, 393-412, 1961
[38] S. Kanehashi, A. Kusakabe, S. Sato, K. Nagai. Analysis of Permeability; Solubility and Diffusivity of Carbon Dioxide; Oxygen; and Nitrogen in Crystalline and Liquid Crystalline Polymers, Journal of Membrane Science, 365, 40-51, 2010
[39] V. Kumar, J. Weller. Production of Microcellular Polycarbonate Using Carbon Dioxide for Bubble Nucleation, Journal of Engineering for Industry, 116, 413-420, 1994
[40] R. E. Murray, J. E. Weller, V. Kumar. Solid-State Microcellular Acrylonitrile-Butadiene-Styrene Foams, Cellular Polymers, 16, 413-425, 2000
[41] S. K. Goel, E. J. Beckman. Generation of Microcellular Polymeric Foams Using Supercritical Carbon Dioxide. I: Effect of Pressure and Temperature on Nucleation. Polymer Engineering and Science, 34, 1137-1147, 1994
[42] V. Kumar, J. E. Weller. A Model for the Unfoamed Skin on Microcellular Foams, Polymer Engineering and Science, 34, 169-173, 1994
[43] J. Colton, N. P. Shu. Nucleation of Microcellular Foam: Theory and Practice, Polymer Engineering and Science, 27, 500-503, 1987
[44] S. C. George, S. Thomas. Transport Phenomena through Polymeric Systems, Progress in Polymer Science, 26, 985-1017, 2001
[45] C. B. Park, A. H. Behravesh, R. D. Venter. Low Density Microcellular Foam Processing in Extrusion Using CO_2, Polymer Engineering and Science, 38, 1812-1823, 1998
[46] M. H. Wagner. Elongational Viscosity and its Meaning for the Praxis, pp 198-205. In Polypropylene an A-Z Reference, J. Karger-Kocsis, Polymer Science and Technology Series, Vol 2, Springer Science+Bussines Media, 1999

6.3 References

[1] J. C. Salamone. Polymeric Materials Encyclopedia (Twelve Volume Set). CRC Press, Boca Raton, 1999.
[2] M. Biron. Thermoplastics and Thermoplastic Composites: Technical Information for Plastics Users. Butterworth-Heinemann, Oxford, 2007.
[3] D. Eaves. Handbook of Polymer Foams. Rapra Technology Limited, Shawbury, 2004.
[4] S. T. Lee. Foam Extrusion: Principles and Practice, CRC Press, Boca Raton, 2000.
[5] S. Doroudiani, C. B. Park, M. T. Kortschot. Polymer Engineering and Science, 38, 1205-1215, 1998.
[6] S. Doroudiani, C. B. Park, M. T. Kortschot. Polymer Engineering and Science, 21, 2645-2662, 1996.
[7] H. A. Khonakdar, J. Morshedian, U. Wagenknecht, S. H. Jafari. Polymer, 44, 4301-4309, 2003.
[8] M. Yamaguchi, K. Suzuki. Journal of Polymer Science: Part B: Polymer Physics, 39, 2159-2167, 2001.

CHAPTER 7

DEVELOPMENT OF A METHODOLOGY TO USE THE EXTENSIONAL RHEOLOGY AS A TOOL TO PREDICT THE FOAMABILITY OF COMPLEX POLYMERIC SYSTEMS

INDEX

7.1 Introduction

In this chapter a methodology of work is developed taking into account the results obtained in the previous chapters (chapters 4, 5 and 6). The main objective of this methodology is to establish a set of guidelines that allow performing and interpreting the extensional rheological tests so that they can be finally related to the foaming process. In this way, anyone who follows these steps could be able to use the extensional rheology as a predictive tool that allows selecting, from a group of polymeric matrices, the most suitable for foaming applications without the necessity of foaming and characterizing the different polymers.

Prior to the development of the methodology of work, different sections are included in this chapter in which the following topics are covered:

1. To analyze in which types of polymeric matrices this methodology can be applied.
2. To analyze the importance of performing the extensional rheological measurements in a material with the same thermo-mechanical history as that of the material employed for foaming.
3. To analyze the importance of performing the extensional rheological measurements at the same temperature as that used for foaming.
4. To determine if it is possible to relate the Hencky strain rate (characteristic parameter of the extensional rheological test) with the foam growth rate, as both parameters give an account of the rate at which the polymer is elongated.
5. To determine if it is possible to relate a characteristic parameter of the extensional rheological test, like the stretching ratio, with a characteristic parameter of the foaming process, like the expansion ratio, as both parameters give an account of the expansion suffered by the polymer.

Some of these topics are related to the performance of the extensional rheological measurements (topics 2 and 3) and others, with the interpretation of the extensional rheological results (topics 4 and 5), always taking into account the final objective of this thesis: to establish a relationship between the extensional rheological behavior and the foaming one.

The conclusions obtained from the studies developed in each of these sub-sections allow establishing the methodology of work.

7.2 Polymeric matrices appropriate for this methodology

In this thesis four different complex polymeric matrices have been employed to perform all the experimental work: pure polyolefins, polyolefin blends, polyolefin based composites and crosslinked polyolefins.

The results obtained previously indicate that it is possible to use the extensional rheology as a predictive tool in the following systems:

- **Pure polymeric matrices:** In this thesis three different pure polymeric matrices have been analyzed: a linear polypropylene (linear PP), a high melt strength polypropylene (HMS PP) and a high density polyethylene (HDPE). All the polymers studied belong to the group of polyolefins. However, as it was already indicated in chapter 1 (section 1.3), different

research projects have emerged from the investigation performed in this thesis. Through this additional works, it has been also possible to demonstrate that other pure polymeric matrices, among others, polystyrene (PS), low density polyethylene (LDPE) and ethylene vinyl acetate (EVA) are also appropriate for this methodology as their extensional rheological behavior can be related perfectly with their foaming behavior [1].

- **Blends of miscible polymers:** One of the works included in this thesis demonstrates that extensional rheology can also be used as a tool to predict the foamability of blends of miscible polymers. In particular, this conclusion has been obtained after performing a systematic study with different blends of a linear PP and a HMS PP (see chapter 4). As in the case of the pure polymeric matrices, this behavior has also been tested in other different blends of polymers (which are not included in this thesis), in this case blends of immiscible polymers, such as linear PP with LDPE and linear PP with EVA [1]. Although, for these non-miscible blends, in particular, the experimental results also indicated a good relationship between the extensional rheological behavior and the foaming behavior, a more complete study, including a greater number of immiscible polymers, should be performed to finally assert if it is possible to apply the methodology developed in this thesis to any mixture of polymers or, by the contrary, this methodology should be restricted to blends of miscible polymers.
- **Crosslinked polymers:** The third complex system, in which it has been proved that the extensional rheology can be used as a predictive tool and consequently, it is an appropriate system for this methodology, is the one formed by crosslinked polymers containing different degrees of crosslinking. In particular, the relationships between the extensional rheological behavior and the foaming behavior of different crosslinked HDPEs (x-HDPEs) have been carefully analyzed in this thesis.

In connection with the **polymeric composites**, it can be said that, in general, it is not possible to use the extensional rheology as a tool to predict the foamability of all the possible types of polymeric composites. In this thesis, two different types of polymeric composites have been tested (see chapter 5). The first system contains a HMS PP and natural layered clays. In this system the particles are completely agglomerated. The second system contains a HMS PP, organomodified layered clays and a compatibilizer polymer. In this second system the clays are intercalated and a percolated network structure is obtained. Results indicate that the extensional rheological behavior and the foaming one can only be related in the composites in which an **intercalated and dispersed structure** is obtained. When the particles are agglomerated their size could be higher than the thickness of the cell walls causing cell rupture. Consequently, from the works presented in chapter 5, it can be concluded that in composites containing layered clays, the obtaining of a relationship between the extensional rheological and the foaming behavior is conditioned by the dispersion level of the layered clays into the polymeric matrix.

Due to the huge amount of polymeric composites that can be produced by using, for instance, particles with different sizes, particles with different shapes, different contents of particles, etc., it could be very interesting to perform a complementary study to verify if the conclusion obtained in this work can be generalized to other polymeric composites. The main objective of this complementary study could be to determine if it is possible to obtain, for each foam

density, the minimum size that the particles or particle agglomerates should have in order to be able to use the extensional rheology as a predictive tool.

7.3 Parameters to be considered to perform the extensional rheological measurements

This section is related to the way in which the extensional rheological measurements of a certain polymeric matrix should be performed to finally establish a relationship between these measurements and the foaming behavior of this polymer. Therefore, this section deals with analyzing on the one hand, the thermo-mechanical history that the polymeric matrix should have and on the other hand, the appropriate temperature to perform the rheological tests.

7.3.1 Analysis of the importance of performing the extensional rheological tests and the foaming process in polymers with the same thermo-mechanical history

This section aims at analyzing the importance of performing the extensional rheological tests in a polymer with the same thermo-mechanical history as that presented by the polymer to be foamed. In other words, this section analyzes the importance of using formulations produced with the same number of extrusion cycles and with the same extrusion conditions to perform on the one hand, the extensional rheological measurements and on the other hand, to produce the cellular materials.

As it has been seen throughout this thesis, to produce a cellular material by using a chemical blowing agent (CBA), in most of the foaming processes, a previous step (to the foaming step) is required in which the polymeric matrix is melt blended with the CBA. This process is normally performed in a twin-screw extruder because the blowing agent should be effectively dispersed in the polymeric matrix. Moreover, the extrusion should be performed at a temperature higher than the melting point of the polymer but lower than the decomposition temperature of the CBA. In many instances, the mixture polymeric matrix/blowing agent issubjected to a second or even a third extrusion cycle in order to obtain an even more homogeneous dispersion of the CBA.

Nevertheless, the polymeric material used to perform the extensional rheological characterization cannot contain the blowing agent because this characterization would become invalid if the material tested expands during its characterization. Therefore, this characterization is normally performed in the same formulation as that used for foaming but, without containing the blowing agent. Consequently, in most of the experimental works, the number of extrusion cycles to which both, the formulation used in extensional rheology and the formulation used for foaming are subjected, is different.

Taking these ideas into account, the question now is the following: to what extent the extrusion process affects the extensional rheological behavior of the polymeric matrix? In order to answer this question, Figure 7.1 shows three examples that analyze the effects of the number of extrusion cycles on the extensional rheological behavior of different polymeric matrices: high melt strength polypropylene (HMS PP), ethylene vinyl acetate (EVA) and low density polyethylene (LDPE). These analyses were performed by subjecting the polymeric matrices to different extrusion cycles maintaining, for each material, the extrusion conditions (that is, maintaining the temperature profile, the feeding rate and the speed of the screws).

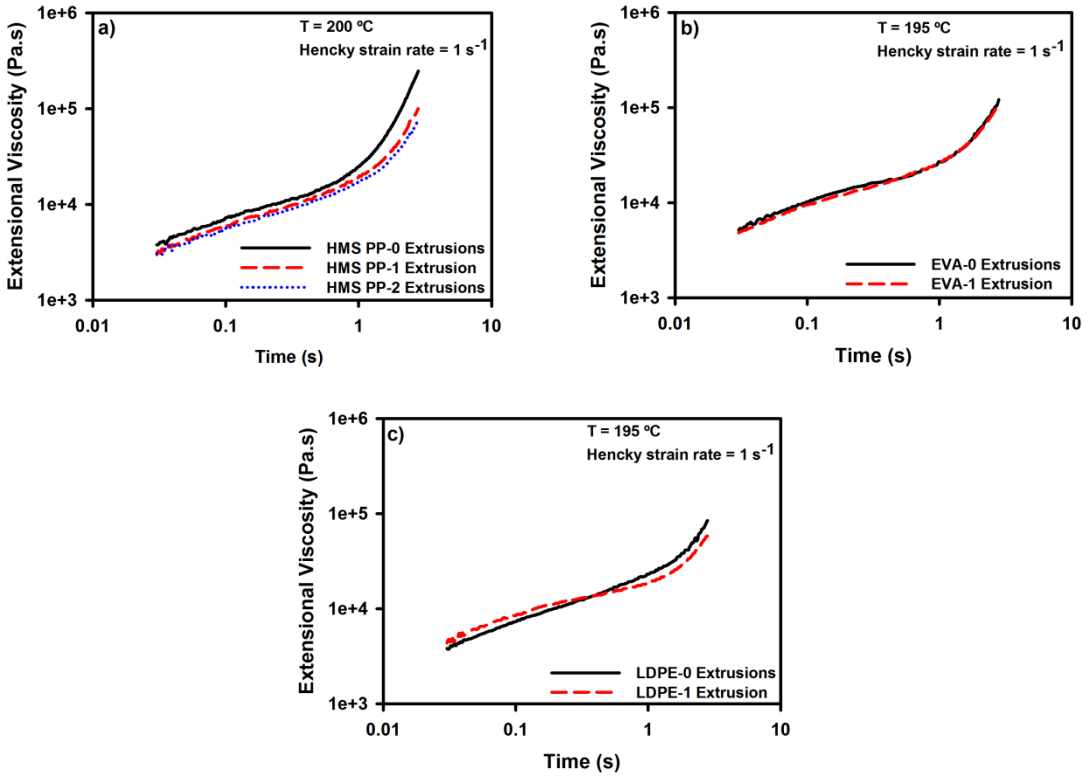

Figure 7.1. Effect of the number of extrusion cycles on the extensional rheological behavior of different polymeric matrices. a) High melt strength polypropylene (HMS PP). b) Ethylene vinyl acetate (EVA). c) Low density polyethylene (LDPE).

Figure 7.1 indicates that the extrusion process does not affect in the same way to all the polymeric matrices. However, from these examples, it can be concluded that, in general, the extensional rheological behavior of the polymeric matrix is affected by the extrusion process.

In order to analyze in more detail the effect of the extrusion process, Figure 7.2 shows the strain hardening coefficient (calculated for a Hencky strain of 2.8 and for a Hencky strain rate of 1 s^{-1}) of these materials. A decrease in the strain hardening coefficient is produced by increasing the number of extrusion cycles. During the extrusion process the molecular structure of the polymer can be modified, either by the time that the polymer is in a molten state or by the shear forces to which the polymer is subjected.

From this section, it can be concluded that, in order to relate the extensional rheological behavior and the foaming behavior, the complete thermo-mechanical history to which a polymeric matrix is subjected, prior to be foamed, should be considered to finally perform the extensional rheological measurements in a polymer processed under the same conditions.

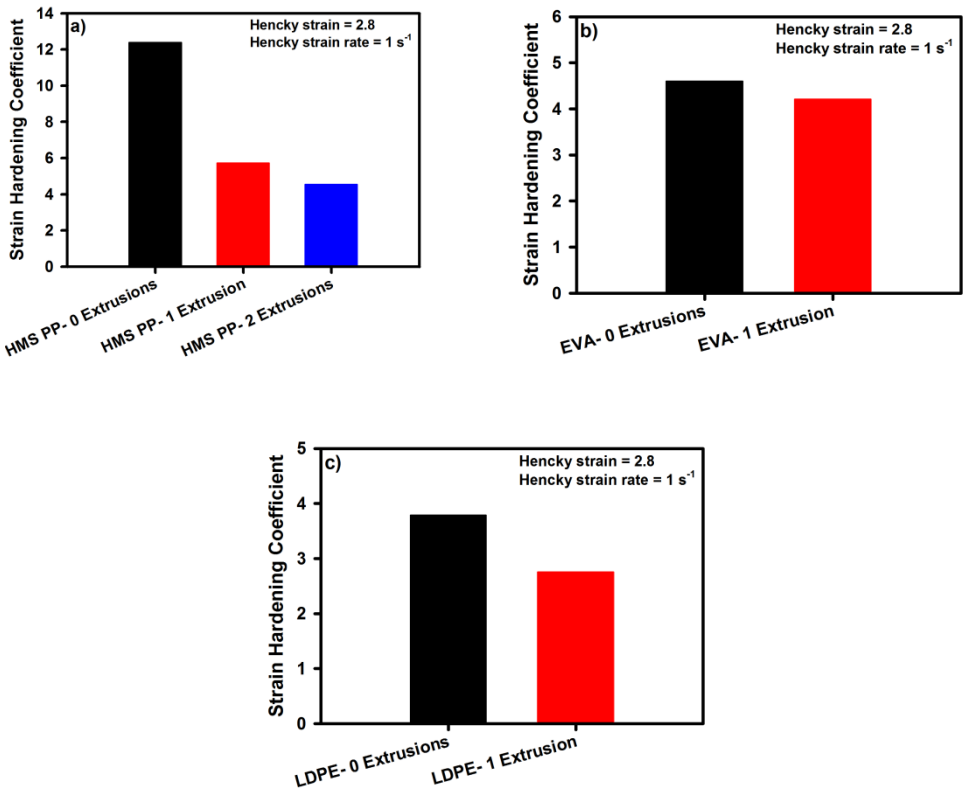

Figure 7.2. Effect of the number of extrusion cycles on the strain hardening coefficient of different polymeric matrices. a) High melt strength polypropylene (HMS PP). b) Ethylene vinyl acetate (EVA). c) Low density polyethylene (LDPE).

7.3.2 Analysis of the importance of performing the extensional rheological tests and the foaming process at the same temperature

Temperature is a parameter which is present in both, the rheological measurements and the foaming process. Common sense indicates that the same temperature should be used in both processes in order to establish a relationship between them. However, in some cases it may happen that it is not possible to perform the rheological test at the same temperature as that used for foaming. For instance, the temperature employed to produce polystyrene foams by a gas dissolution process normally varies between 100 ºC and 120 ºC [2]. These temperatures are close to the glass transition temperature of polystyrene (approximately 100 ºC) [3]. Due to the high viscosity that polystyrene shows at this temperature, it is not possible to perform the extensional rheological test at the same temperature as that used in the foaming test.

Taking these ideas into account, this section aims at analyzing how the changes in the temperature of measurement affect the extensional rheological properties. This way, it will be possible to determine the importance of performing the extensional rheological tests and the foaming process at the same temperature.

For this purpose, Figure 7.3 shows four examples which analyze the effect of the temperature on the rheological behavior of different polymeric matrices: the three polymers previously analyzed (HMS PP, EVA, LDPE) and also a polystyrene (PS). Figure 7.3 shows the curves of extensional viscosity versus time obtained at two different temperatures.

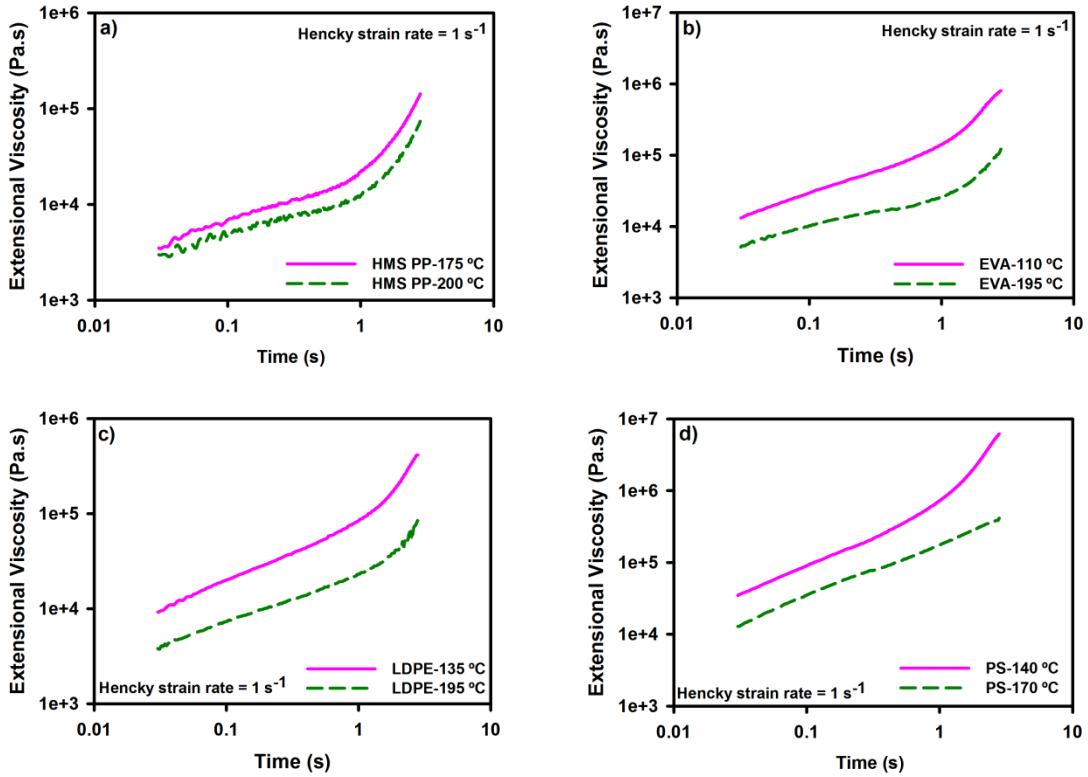

Figure 7.3. Effect of the temperature of measurement on the extensional rheological behavior of different polymeric matrices. a) High melt strength polypropylene (HMS PP). b) Ethylene vinyl acetate (EVA). c) Low density polyethylene (LDPE). d) Polystyrene (PS).

From these figures it is possible to conclude that when the temperature increases on the one hand, the viscosity decreases due to the high mobility of the polymeric chains and on the other hand, the strain hardening is reduced (as Figure 7.4 also indicates).

An interesting fact that can be detected in these figures, in particular in Figures 7.3.d and Figures 7.4.d, is that the polystyrene does not show strain hardening if the temperature of measurement is very high. This particular example indicates the great importance of performing the extensional viscosity measurements at the same temperature as that used for foaming, because the results could be misinterpreted when different temperatures are used. In the situations in which it is not possible to use the same temperature in both tests, it is recommended to perform the extensional rheological measurements at a temperature as close as possible to the foaming temperature.

However, the trends observed in these examples (decrease in the strain hardening by increasing the temperature) cannot be generalized to all the polymeric matrices. In Chapter 2, section 2.2.5.4.3, a literature search of the works which analyzed the effect of the temperature on the strain hardening coefficient was performed. This chapter indicated that the way in which the temperature influences the strain hardening is still unclear as there are polymeric matrices in which the strain hardening increases by increasing the temperature and other polymeric matrices (like those showed in this section) in which an opposite behavior is obtained.

Anyway, what is clear is that in one way or another, the extensional rheological behavior of a certain polymeric matrix is highly influenced by temperature and hence, this parameter should be considered when the extensional rheological tests are performed with the aim of understanding the foamability of the polymeric matrix.

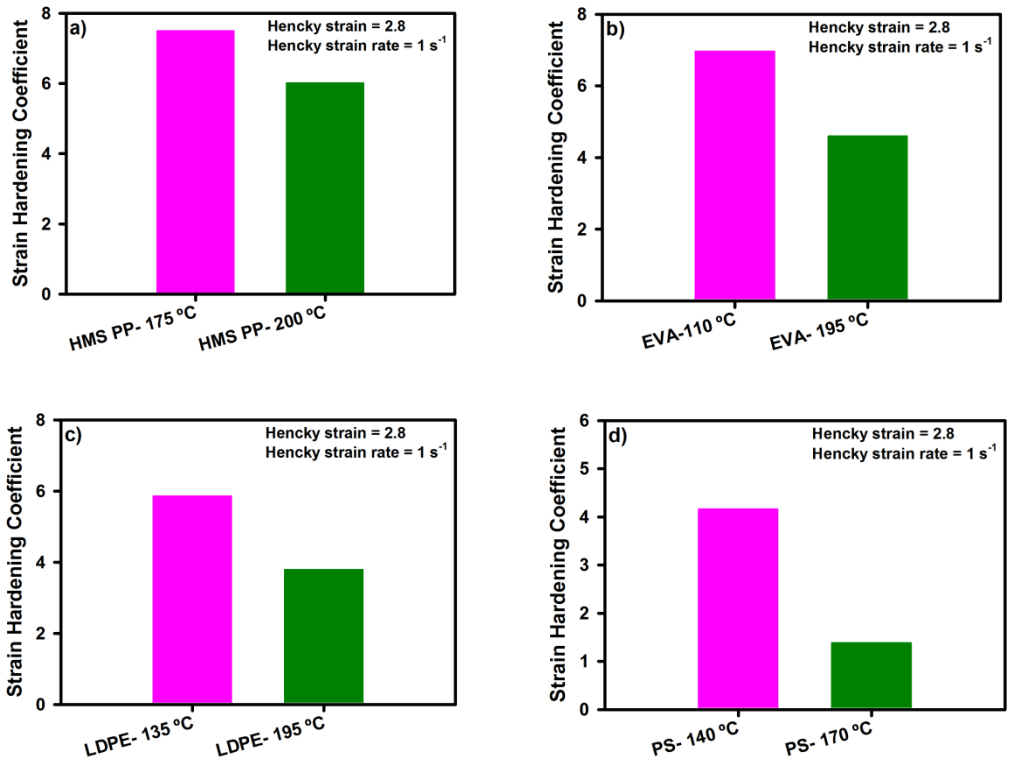

Figure 7.4. Effect of the temperature of measurement on the strain hardening coefficient of different polymeric matrices. a) High melt strength polypropylene (HMS PP). b) Ethylene vinyl acetate (EVA). c) Low density polyethylene (LDPE). d) Polystyrene (PS).

7.4 Parameters to be considered to interpret the extensional rheological measurements

The classical way, which has also been employed in the papers included in this thesis, in which the extensional rheological results are normally displayed in order to be related with the foaming process, is the following: the extensional viscosity, obtained at different Hencky strain rates, is represented as a function of the measurement time. With the same objective in mind, it has also been observed that in several occasions the strain hardening is quantified by calculating the strain hardening coefficient (at a fixed Hencky strain and Hencky strain rate), Nevertheless, the experience acquired in this thesis suggests that this classical way of displaying the rheological results may not be the most appropriate one.

In this section, a new way of displaying the data obtained after the extensional rheological characterization is proposed. This new way of presenting the results is intended to facilitate the establishment of a relationship between the extensional rheological behavior of the polymeric matrix and characteristic aspects of the foaming process such as the foam resistance to be stretched, the expansion ratio or the foam growth rate.

The new way proposed to display the extensional rheological results consists on representing the strain hardening as a function of the stretching ratio for different Hencky strain rates. Thereby, it could be possible to establish, in a more direct way, a relationship between characteristic parameters of the extensional rheological test and characteristic parameters of the foaming process, such as the strain hardening and the polymer resistance to be stretched, the Hencky strain rate and the foam or cell growth rate (which depends on the foaming process employed) and finally,the stretching ratio and the expansion ratio (or foam density). These relationships between the different parameters are summarized in Figure 7.5.

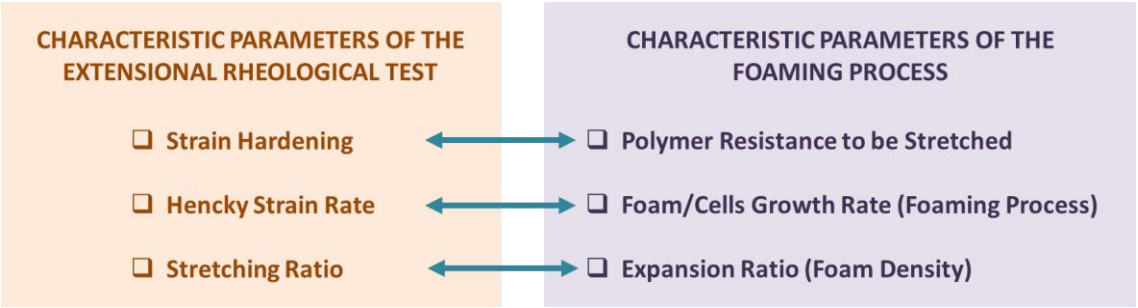

Figure 7.5. Relationships between characteristic parameters of the extensional rheological test and characteristic parameters of the foaming process, proposed by the new methodology developed in this thesis.

The steps taken to depict the strain hardening as a function of the linear expansion ratio are listed below:

1. The strain hardening as a function of time and Hencky strain rate is calculated from the extensional viscosity measurements (Equation 7.1). The classical way of representing these measurements is shown in Figure 7.6.a, for a HMS PP.

$$SH(t,\dot{\varepsilon_H}) = \frac{\eta_E(t,\dot{\varepsilon_H})}{\eta_{E0}(t)} \tag{7.1}$$

   where $\eta_E(t,\dot{\varepsilon_H})$ is the transient extensional viscosity as a function of time and Hencky strain rate and $\eta_{E0}(t)$ is the transient extensional viscosity in the linear viscoelastic regime, which can be determined in two different but equivalent ways: as three times the transient shear viscosity curve at very low strain rates or by extrapolating the superimposed portion of the extensional curves, measured at different Hencky strain rates [4,5]. The same equation has been used along this thesis to determine the strain hardening coefficient (*S*). However, while the strain hardening coefficient (S) is a numerical value (that is, *S*, as its name indicates, is a coefficient) because it is calculated for a certain value of time and Hencky strain rate, the strain hardening proposed in this section (*SH*) is a function, which depends on both, time and Hencky strain rate. Figure 7.6.b shows an example of the rheological behavior of a HMS PP where the strain hardening is represented as a function of time for different Hencky strain rates.

2. In this second step, the strain hardening is obtained as a function of Hencky strain (instead of time) and Hencky strain rate, using for this purpose Equation 7.2 [6].

$$\varepsilon_H = \dot{\varepsilon_H} t \tag{7.2}$$

Figure 7.6.c shows the strain hardening of the HMS PP as a function of the Hencky strain, for different Hencky strain rates.

3. Finally, the strain hardening is obtained as a function of the stretching ratio for each Hencky strain rate, considering the relationship that exists between the Hencky strain and the stretching ratio (Equation 7.3) [6].

$$\varepsilon_H = \ln(\lambda) = \ln(l/l_0) \tag{7.3}$$

where $\lambda = l/l_0$ is the stretching ration, that is, the ratio between the final length of the sample (l) and the initial length of the sample (l_0). Figure 7.6.d shows, once again for the HMS PP, the final representation of the extensional rheological results, in which the strain hardening is represented as a function of the stretching ratio for different Hencky strain rates.

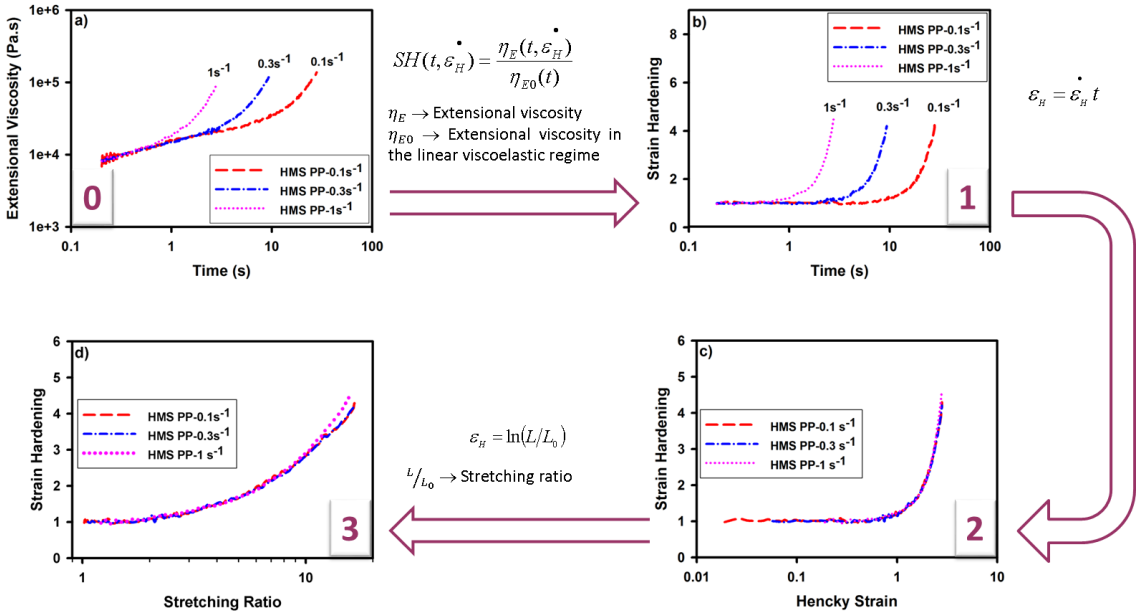

Figure 7.6 Steps followed to obtain the strain hardening as a function of the linear expansion ratio. The curves are for a HMS PP. a) Extensional viscosity behavior. b) Strain hardening vs time for different Hencky strain rates. c) Strain hardening vs Hencky strain for different Hencky strain rates. d) Strain hardening vs stretching ratio for different Hencky strain rates.

Once the new way of displaying the extensional rheological results is designed, the following steps consist on the one hand, on analyzing in which way the Hencky strain rate can be related with the foam growth rate and hence, with the foaming process and on the other hand, on analyzing in which way the stretching ratio can be related with the foam density (or expansion ratio).

7.4.1 Analysis of the relationships between the Hencky strain rate and the foam growth rate

This section aims at analyzing if it is possible to establish a relationship between the Hencky strain rate and the foam growth rate, which in turns depends on the foaming process, in order to determine the appropriate Hencky strain rate at which the strain hardening coefficient

should be determined to interpret the rheological results taking into account the foaming process employed.

The first concept that should be considered to relate the two parameters is the type of extension employed in each process. As it has been indicated along this thesis, in general, the polymeric matrices are characterized by performing uniaxial extensional measurements. In this thesis, the experimental devices used to perform the extensional rheological characterization also subject the material to a uniaxial extension. Biaxial and planar extensional experiments are less common due to several factors [6]:

- The demanding experimental conditions.
- The small number of experimental equipment available to perform planar and biaxial tests.
- The ranges of total elongation and elongational rates which can be experimentally achieved are not so broad compared to those achieved in uniaxial elongation.

However, the type of extension experienced by the polymer comprising the cell walls when the cell growth is produced, is a biaxial extension [7].

It can be concluded that two completely different processes are being compared. Therefore, the establishment of a mathematical relationship between them is not possible. In other words, as the main mode of deformation during bubble growth and hence, during foam growth is biaxial extension and the extensional rheological behavior of the polymeric matrix is normally determined under a uniaxial flow, it is not possible to relate numerically neither the Hencky strain rate with the foam growth rate nor the expansion ratio with the stretching ratio (see also section 7.4.2).

Despite the fact that all these parameters cannot be related through a numerical value, the uniaxial extensional rheology can still be used as an effective tool to predict the foaming behavior, as the strain hardening is present in both, biaxial and uniaxial extension although, it is more pronounced in the latter. The relationships between the two behaviors have already been investigated [8,9]. A qualitative correlation between the strain hardening in uniaxial and biaxial elongation has been found, which allows understanding the foaming process, with predominantly biaxial deformation, by using the results obtained after a rheological characterization in uniaxial flow.

As it was already indicated in chapter 2 (section 2.5.2), the strain hardening coefficient is normally calculated for a value of the Hencky strain rate between 1 and 5 s^{-1}, independently on the foaming process employed. Moreover, in spite of not considering the type of foaming process used to produce the cellular materials, to analyze the extensional rheological behavior of the polymeric matrices, it has been possible to understand two of the principal mechanisms of the foaming process: cell growth and cell degeneration, through an analysis of the extensional rheological properties of the polymeric matrix employed to produce the cellular materials. Without going too far, in the works presented in this thesis, in which different complex polymeric matrices have been employed to understand their foamability by using extensional rheology, the same value of the Hencky strain rate has been used to determine the strain hardening coefficient despite the fact that the foams have been produced by using different foaming processes.

Taking these ideas into account, when comparing different types of polymeric matrices with the aim of selecting the most suitable one for foaming applications, the following question must be answered: is it always possible to compare the different polymeric materials using the same Hencky strain rate, independently on the foaming process? In order to give an answer to this question, Figure 7.7 shows examples of different polymeric matrices whose rheological behavior (strain hardening) depends on the Hencky strain rate in different ways. The range of Hencky strain rates proposed to compare the strain hardening of the different materials varies between 0.5 and 5 s^{-1}. This range has been selected taking into account the knowledge acquired during the development of this thesis, as well as, the knowledge acquired through the works found in bibliography (see chapter 2, section 2.5.2). The range of appropriate Hencky strain rates proposed by S.T. Lee in its book "*Foam Extrusion: Principles and Practice*" [10] varied between 1 and 5 s^{-1}. In this thesis, it has been decided to extend this range up to Hencky strain rates of 0.5 s^{-1}, with the aim of taking into account other foaming processes slower than the extrusion process (see chapter 2, section 2.4.2.3).

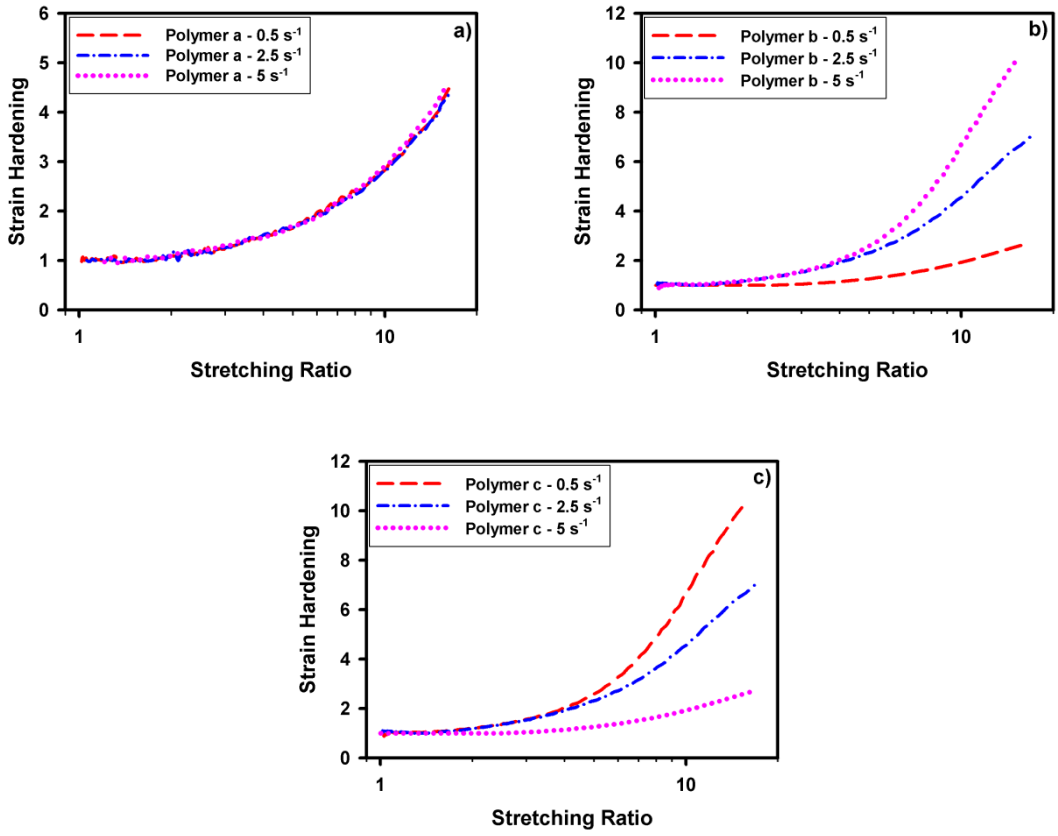

Figure 7.7. Analysis of the dependence of the strain hardening with the Hencky strain rate. a) Polymeric matrix whose strain hardening is independent on the Hencky strain rate. b) Polymeric matrix whose strain hardening decreases as the Hencky strain rate decreases. c) Polymeric matrix whose strain hardening increases as the Hencky strain rate decreases.

From the examples depicted in Figure 7.7, it can be observed that the way in which the strain hardening depends on the Hencky strain rate varies from one to another material. Therefore, when the extensional rheological properties of different polymeric matrices are going to be compared, with the aim of using the extensional rheology as a predictive tool to select the

most appropriate polymer for foaming applications, it is necessary to know, for each material, the way in which its strain hardening depends on the Hencky strain rate. The following paragraphs describe possible situations in which it is not possible to use the extensional rheology as a predictive tool due to the different trends followed by the different materials.

- Between *Polymer a* and *Polymer b*, which is the most appropriate polymer for foaming applications? The strain hardening of *Polymer b* is higher than that of *Polymer a* at Hencky strain rates equal to or greater than 2.5 s^{-1}. Nevertheless, this trend is completely opposite when Hencky strain rates lower than 2.5 s^{-1} are considered. In this case, the selection of the most suitable material will depend on the rate of the foaming process. However, as it is not possible to determine mathematically the Hencky strain rate that should be considered for each foaming process, it is not possible to determine which polymer is the most suitable one for foaming applications without producing the cellular materials.
- Between *Polymer b* and *Polymer c*, which is the most appropriate for foaming applications? These two polymeric matrices present opposite behaviors. *Polymer b* should be more suitable for fast foaming process and by the contrary, *Polymer c* should be more appropriate for slow foaming processes. Once again, with these types of polymers the extensional rheology cannot be used as a predictive tool.

From these two examples, it can be concluded that the extensional rheology could be only used as a predictive tool when comparing polymeric matrices whose strain hardening depends on the Hencky strain rate in the same way.

As the polymeric matrices employed in each of the papers presented in this work derived from the same type of polymer, their rheological behaviors followed the same trends. This is the reason why in each of these papers, it was possible to compare the different materials by calculating the strain hardening coefficient for a fixed value of the Hencky strain rate. Moreover, this value was fixed without taken into account the foaming process employed.

Nevertheless, these conclusions cannot be generalized to all the situations that can be found, as the examples showed in Figure 7.8 indicate.

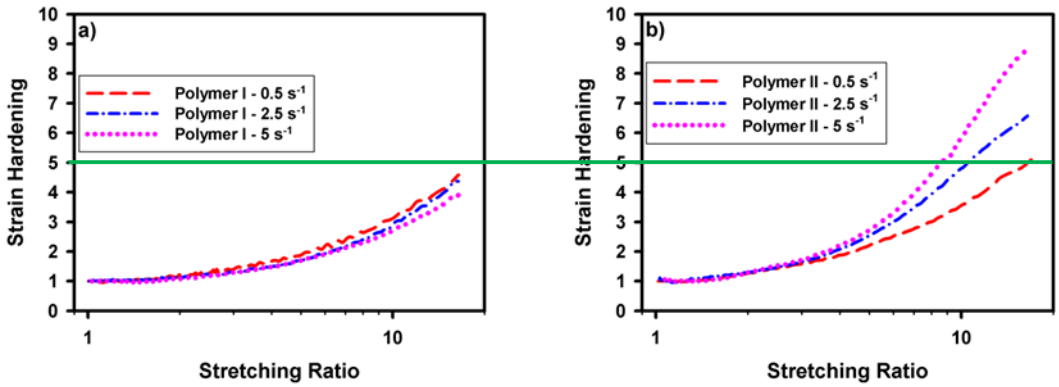

Figure 7.8. Example of two polymeric matrices which opposite behaviors in which the extensional rheology can be used as a predictive tool.

The example depicted in Figure 7.8 shows two polymeric matrices with a completely opposite behavior; while the strain hardening of *Polymer I* decreases as the Hencky strain rate increases, the strain hardening of *Polymer II* increases with the Hencky strain rate. However, it is also possible to observe that the strain hardening of *Polymer I* is lower than that of *Polymer II* for all the Hencky strain rates considered, which indicates that, independently on the foaming process employed, *Polymer II* is more appropriate for foaming applications than *Polymer I*. Summarizing, in this particular system it is also possible to use extensional rheology as a predictive tool.

The main conclusion that can be obtained in this section, which analyzes the different ways in which the strain hardening depends on the Hencky strain rate, is the following: the extensional rheology cannot be used as a predictive tool if the strain hardening of the polymeric matrices under study does not depend on the Hencky strain rate in the same way, with the exception of those materials whose strain hardening is either higher or lower than that of the other materials under study, for all the Hencky strain rates considered. When the rheological properties of the different materials follow the same trend any value of the Hencky strain rate can be fixed to perform a comparison between the different materials.

Throughout this section, it has been mentioned that, for instance, polymers presenting a behavior as that depicted in Figure 7.8.b should be more suitable to produce foams by using fast foaming process (like extrusion) because, their strain hardening increases as the Hencky strain rate increases. The question now is the following: is it possible to prove experimentally this fact? When the foam growth rate is modified, changes in several parameters affecting the cellular structure are also produced. Cell nucleation rate is one of the parameters most affected by the foam growth rate [11,12]. Therefore, in an experimental test, it is very difficult to determine if the changes produced in the cellular structure by modifying the foam growth rate result from the changes produced in the extensional rheological behavior of the polymeric matrix or on the other hand, these changes are a consequence of the modifications produced in, for instance, the cell nucleation rate.

7.4.2 Analysis of the relationships between the stretching ratio and the foam density (or expansion ratio)

This section aims at analyzing if it is possible to establish a mathematical relationship between the stretching ratio and the foam density, in order to determine the appropriate value of the stretching ratio that should be considered to compare different polymeric matrices, taking into account the final densities of the foamed materials produced with them.

As it was indicated in the previous section (section 7.4.1), the establishment of a mathematical relationship between the stretching ratio and the foam expansion ratio is not possible. That means that for a known value of the density of the foamed materials, it is not possible to determine the appropriate value of the stretching ratio that should be considered to calculate the strain hardening coefficient, with the aim of establishing a relationship between the extensional rheological process and the foaming one.

Although, it is not possible to relate quantitatively the stretching ratio and the expansion ratio, the new way of representing the results obtained after performing the extensional rheological

characterization is very useful to select directly the most appropriate material for foaming applications, from a group of different polymeric matrices. Figure 7.9 shows an example of the rheological behavior of different polymeric matrices obtained for the same value of the Hencky strain rate. From this figure several assertions can be obtained:

- At low stretching ratios, all the materials exhibit the same strain hardening. That means that when the polymer is subjected to low extensions, for instance, during the production of high density foamed materials, the strain hardening is independent on the polymeric matrix employed. In other words, it is the same to use one or another polymeric matrix to produce high density foamed materials.
- The polymeric matrix presenting the highest increase in the strain hardening (in the example the sample called *Polymer 4*) is the most appropriate material to produce low density cellular materials because, it is the material presenting the highest resistance and hence, it is the material that will withstand the highest deformations.
- By the contrary, the polymer called *Polymer 1* is not suitable to produce low density cellular materials because the strain hardening of this polymer remains constant with the stretching ratio (its value is always one). Therefore, as the strain hardening does not increase as the cells grow, the cells do not resist the extension and they break.
- For a fixed stretching ratio, that is, for a fixed foam density, if all the polymeric materials have expanded successfully to the desired density, their cellular structure will be conditioned by the extensional rheological behavior of the polymeric matrix. In general, the materials presenting high values of the strain hardening show a homogeneous cellular structure with low cell sizes, high cell densities and low open cell contents.
- A polymeric matrix with a rheological behavior as that presented by *Polymer 3* is not the most suitable one for foaming applications. The drop in the strain hardening indicates a premature rupture of the polymer before the end of the rheological test. This often leads to a lack of control over the foaming process because, in general, the foamed samples obtained with these types of polymers are not reproducible. For instance, if we had to choose between *Polymer 2* and *Polymer 3*, *Polymer 2* would be more suitable than *Polymer 3*, in spite of having a slightly lower strain hardening.

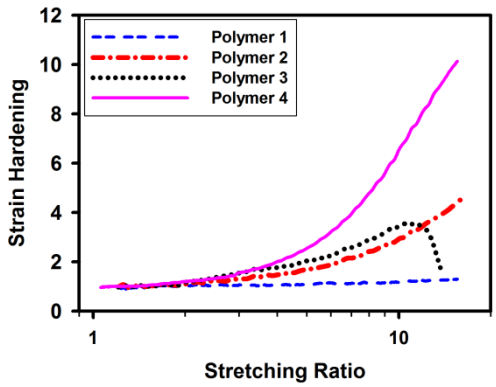

Figure 7.9. Strain hardening vs. stretching ratio of different polymeric matrices.

Figure 7.9 also shows that, in general, if a certain polymer presents a strain hardening higher than that presented by any other polymer, this trend is satisfied in all the stretching ratio range. That means that, the value of the stretching ratio (or Hencky strain) selected to

calculate the strain hardening coefficient is not conditioned by the foam expansion ratio (or foam density). Consequently, any value of the stretching ratio used to quantify the extensional rheological behavior is usually appropriate to finally relate this behavior with the foaming one. This also explains why the traditional way of interpreting and quantifying the rheological results, in which the strain hardening coefficient is normally determined for a Hencky strain value between 3 and 4 (see chapter 2, section 2.5.2), has allowed understanding the foaming behavior. Nevertheless, this new way of displaying the rheological results is useful to analyze, for each group of polymeric matrices, if there is any polymer that does not fulfil this trend (like *Polymer 3* in Figure 7.9) and hence, a more careful analysis of the rheological results should be performed.

7.5 Guidelines that should be followed in order to use the extensional rheology as a tool to predict the foamability of different polymeric matrices

Basically, this section aims at putting together all the knowledge acquired during the thesis to finally establish a methodology of work, by establishing a set of guidelines that should be followed in order to be able to use the extensional rheology as tool to determine, from a group of different types of polymeric matrices, the most suitable one for foaming applications. These steps are described below:

1. Determine if the polymeric matrices under studio belong to any of the polymeric systems defined in section 7.2, for which it has been demonstrated that it is possible to understand their foamability by using extensional rheology.
2. Perform the extensional rheological measurements in a material subjected to the same thermo-mechanical history as that employed with the material used to produce the foams.
3. Select the temperature of the extensional rheology test. This temperature should be the same (or very similar) as that used during the foaming process.
4. Perform the extensional rheological tests at different Hencky strain rates, varying between 0.5 and 5 s^{-1}, and up to a Hencky strain of approximately 3.
5. Depict the results obtained after the extensional rheological characterization as indicated in section 7.4, where the strain hardening is represented as a function of the stretching ratio.
6. Analyze the dependence of the strain hardening with the Hencky strain rate to determine if the extensional properties of these polymers can be compared independently on the foaming process employed and hence, it is possible to use the extensional rheology as a predictive tool (see section 7.4.1).
7. For a defined value of the Hencky strain rate, determine the most appropriated polymeric matrix for foaming applications by comparing the curves strain hardening vs. stretching ratio, for the different materials, as indicated in section 7.4.2.

7.6 References

[1] E. Laguna-Gutierrez, A. Lopez-Gil, C. Saiz-Arroyo, M. A. Rodriguez-Perez. Extensional Rheology: a Tool to Predict the Foamability of Complex Systems such as Polymer Blends and Recycled Polymers. Study presented in: 12th International Conference on Foams Materials & Technology, Iselin, NJ, USA, September 2014.
[2] S. Doroudiani, M. T. Kortschot. Journal of Applied Polymer Science, 90, 1412-1420, 2003.
[3] http://www.polymerprocessing.com/
[4] J. Stange, C. Uhl, H. Münstedt, Journal of Rheology, 49, 1059-1079, 2005.
[5] A. K. Chaudhary, K. Jayaraman, Polymer Engineering and Science, 51, 1749-1756, 2011.
[6] H. Münstedt, F. R. Schwarzl. Deformation and Flow of Polymeric Materials, Springer-Verlag, Berlin, 2014.
[7] P. Spitael, C. W. Macosko. Polymer Engineering and Science, 44, 2090-2100, 2004.
[8] P. Hachmann, J. Meissner. Journal of Rheology, 47, 989-1010, 2003.
[9] J. Stange, H. Münstedt, Journal of Rheology, 42, 445-467, 2006.
[10] S. T. Lee. Foam Extrusion: Principles and Practice, CRC Press, Boca Raton, 2000.
[11] L. O. Salmazo. Cineticas de Espumacion y control de la Estructura Celular en Materiales Basados en caucho Natural y poliolefinas. Phd Thesis, University of Valladolid, 2015.
[12] R. B. McClurg. Chemical Engineering Science, 59, 5779-5786, 2004.

CHAPTER 8

CONCLUSIONS AND FUTURE WORK

INDEX

8.1 Conclusions

This final section summarizes all the main conclusions and remarkable achievements of this research work. The section is written according to the scope and objectives of this thesis.

The **first objective** of this thesis was:

To analyze and understand in which situations the extensional rheology can be used as a tool to predict the foamability of complex polymeric systems.

To fulfil this objective a **systematic study** has been performed in which the effects that the extensional rheological behavior of different polymeric matrix have on the foaming behavior have been analyzed under different conditions.

1. In this systematic study, on the one hand, the effects of the extensional rheological properties of **different types of polymeric matrices** on the cellular structure of the foamed materials produced with the **same foaming process** have been analyzed in detail. The main conclusions obtained after this study are summarized below:

- The extensional rheological properties of three different types of polymeric matrices (pure polypropylenes, miscible polypropylene blends, and polypropylene based composites) were measured and analyzed.
- In the case of the solid polymeric composites, a detailed analysis of their structure was performed in which the level of particle dispersion and their intercalation/exfoliation degrees were quantified.
- The effects of the extrusion process, the clay type and content and the foaming process on the structure of the different composites were also analyzed.
- All the polymeric matrices (pure polypropylenes, miscible polypropylene blends, and polypropylene based composites) where then foamed, with **similar densities**, by improved compression molding (ICM) and its cellular structure and mechanical properties were characterized in detail.
- When working either with pure polypropylene matrices or with miscible polypropylene blends, it was demonstrated that it is possible to understand the cellular structure of the foamed materials by analyzing the extensional rheological properties of the polymeric matrix. In these systems a relationship between extensional rheology, cellular structure and mechanical properties was established.
- When working with polypropylene composites the extensional rheology cannot be always related with the cellular structure of the foamed materials. The obtaining of a relationship between extensional rheology and cellular structure is conditioned by the size and by the dispersion level of the particles into the polymeric matrix.
- Extensional rheology is not the most suitable tool to understand the structure of the foamed composites when the particles, comprising the composite, are agglomerated and the size of these agglomerates is higher than the thickness of the cell walls. In this type of systems while no changes are detected in the extensional rheological behavior of the polymeric matrix, important variations are detected in the cellular structure.

- When the particles are not agglomerated, that is, they are dispersed, a relationship between extensional rheology, cellular structure and mechanical properties can be obtained.

2. On the other hand, the influence of the **process** selected to produce the foamed materials on the establishment of a relationship between extensional rheology and cellular structure has also been studied. For this purpose the **same polymeric matrices** were foamed by using **different foaming processes**. The main conclusions obtained after this study are summarized below:

- The extensional rheological properties of two different types of polymeric matrices (pure polypropylenes and miscible polypropylene blends) were measured and analyzed.
- These two types of polymeric matrices were then foamed by using two different foaming processes: ICM and foaming at atmospheric pressure in a mold. With these two processes, it was possible to control the density of the foamed materials.
- While the structure of the cellular materials produced by ICM was characterized through an ex-situ analysis, an in situ-analysis of the evolution of the cellular structure during the foaming process was performed in the materials foamed at atmospheric pressure in a mold.
- Through this in-situ characterization, it has been possible to visualize and quantify the effects that the extensional rheological properties of the different polymeric matrices have on the cell growth and on the cell degeneration.
- The results obtained after both, the in-situ and the ex-situ characterization are in agreement: the way in which the foam ages, which, in turns, determines the final structure of the foamed materials, is conditioned by the extensional rheological properties of the polymeric matrix.
- The in-situ analysis also demonstrates that besides the rheological properties, the foam stability also depends on the final density of the foamed materials and on the amount of blowing agent used to produce the foams.
- If the extensional rheological properties, in particular the strain hardening, of the polymeric matrices to be compared depend in the same way on the Hencky strain rate, it is possible to establish a relationship between extensional rheology and cellular structure, independently on the foaming process employed.

3. To conclude this systematic study, the way in which both, the rheological properties of the polymeric matrices and the foaming parameters (foaming time and foaming temperature), affect the ability of these polymers to achieve **high expansion ratios** and hence, low densities, has also been analyzed. The main conclusions obtained after this study are summarized below:

- The rheological properties of different types of polymeric matrices, obtained from a high density polyethylene (HDPE) which has been crosslinked by using different amounts of an organic crosslinking agent, were measured and analyzed.
- The different crosslinked HDPEs (x-HDPEs) were foamed by the solid state foaming process. With this process it is very difficult to control the foam density. Different foaming times and foaming temperatures were used to produce the foams.

- When the crosslinking content increases on the one hand, the amount of gas available for foaming increases and on the other hand, the extensional rheological behavior of the polymeric matrix improves. As a consequence, cellular materials with higher expansion ratios, lower cell sizes and higher cell densities are obtained.
- After analyzing the effect of the foaming time, it can be concluded that the cellular structure of the material with the highest crosslinking degree is the most stable with time, due to the high strain hardening that this material presents.
- Cell coalescence occurs at higher temperature in the HDPE with the highest crosslinking degree than in the uncrosslinked HDPE, due to the favorable extensional rheological properties of the x-HDPE.

Therefore, a general conclusion from this systematic study can be obtained, taking into account the specific conclusions summarized in the previous paragraphs.

For the following groups of polymeric matrices: pure polymers, blends of miscible polymers and crosslinked polymers, extensional rheology is the tool that allows understanding on the one hand, the cellular structure of the foams produced with the same density and on the other hand, the cellular structure and the ability of the polymers to achieve high expansion ratios, if the process selected to produce the foams does not allow controlling the density of the cellular materials. Therefore, in these polymeric systems, the extensional rheology could be used as a tool to predict the foamability of the polymeric matrices, without the need of producing and characterizing the foams.

Moreover, the relationships between extensional rheology and cellular structure can be established independently on the foaming process selected to produce the cellular materials, provided that the strain hardening of the materials to be compared depends in the same way on the Hencky strain rate.

Once, the first objective of this thesis has been fulfilled and hence, it is possible to know in which polymeric systems the extensional rheology can be used as a predictive tool, the **second objective** of this work was:

To develop a methodology to perform the extensional rheological measurements and to analyze the obtained results in conditions which are useful to understand the foaming tests; a possible application of this methodology to the selection of the appropriate formulations without the need to produce the foams will be taken into account.

To fulfil this objective different studies were performed which allow determining on the one hand, the most appropriate way to perform the extensional rheological measurements and on the other hand, the most appropriate way to display and interpret the extensional rheological results so that, the extensional rheology can be used as a tool to determine from a group of polymeric matrices the most suitable one for foaming applications. The following conclusions were obtained:

- The extensional rheological measurements should be performed in a polymer with the same thermo-mechanical history as that of the polymer used for foaming because, the rheological behavior of a polymer is highly influenced by its thermo-mechanical history.
- The extensional rheological behavior of a certain polymeric matrix is highly influenced by temperature and hence, this parameter should be considered when the extensional rheological tests are performed with the aim of understanding the foamability of the polymeric matrix. In other words, it is advisable to perform the extensional rheological test at the same temperature as that used for foaming.
- A new way of displaying the extensional rheological results has been designed, which consists on representing the strain hardening as a function of the stretching ratio for different Hencky strain rates.
- This new way of representing the extensional rheological results allows analyzing the dependence of the strain hardening with the Hencky strain rate, for the different polymers under study. It has been proved that the type of dependence followed by the different polymeric matrices is fundamental to determine if the extensional rheology can be used as a predictive tool without taking into account the foaming process employed to produce the cellular materials.
- With this new way of displaying the results, it was demonstrated that at low stretching ratios, all materials exhibit the same strain hardening and hence, it is the same to use one or another polymeric matrix to produce high density foamed materials.
- For higher stretching ratios, in general, if a certain polymer presents a strain hardening higher than that presented by any other polymer, this trend is satisfied in all the stretching ratio range. That means that, the value of the stretching ratio (or Hencky strain) selected to determine the strain hardening coefficient is not conditioned by the foam expansion ratio (or foam density).
- It is not possible to establish a mathematical relationship between the Hencky strain rate and the foam growth rate (or foaming process) and between the stretching ratio and the foam expansion ratio (or foam density) because the extensional rheological measurements subject the sample to an uniaxial extension and by the contrary, the type of extension experienced by the polymer comprising the cell walls, when the cell growth is produced, is a biaxial extension.

From these studies, it was possible to develop a methodology of work by establishing a set of guidelines that should be followed in order to be able to use the extensional rheology as tool to determine from a group of different types of polymeric matrices the most suitable one for foaming applications.

The methodology developed in this thesis is a powerful tool from an industrial point of view. By following the guidelines established in this methodology, a large amount of polymeric matrices can be compared in order to select the most suitable one for foaming applications without the need to produce and characterize the foams, which leads to a significant costs reduction.

8.2 Future work

This is the first thesis developed in CellMat which deals with the relationships between extensional rheology and cellular structure. As the extensional rheology has been proved to be a powerful tool to understand the foamability of different polymeric matrices, making this tool to be very interesting from an industrial point of view, we expect that the knowledge acquired during this research could be a starting point for new research works, some of which could be focused on the following topics.

- **Research on other types of pure polymeric matrices.** The investigation performed during this thesis has been focused in a single type of polymeric matrices, polyolefins. This research could be extended to other types of polymers like **elastomers** (natural rubbers, styrene-butadiene rubbers, styrene ethylene butylene styrene copolymers, etc.), **amorphous thermoplastics** (polystyrenes, polycarbonates, poly(methyl methacrylates), polyvinyl chlorides) or other types of semi-crystalline thermoplastics (polyamides, polyoxymethylenes, etc.).
- **Research on blends of immiscible polymers**. In this thesis, it has been demonstrated that it is possible to establish a relationship between extensional rheology and foaming behavior when working with blends of miscible polymers. This study should be also performed in blends of immiscible polymers, such as: polystyrene and polyethylene or polyethylene and polypropylene, to analyze if in these systems it is also possible to establish the aforementioned relationship.
- **Research on other types of micro/nano composites**. In this thesis, two different types of composites have been analyzed; those produced with natural clays and those produced with organomodified clays. It was demonstrated that the size of the particle agglomerates is a key aspect that determines if the extensional rheology and the foaming behavior can be related. Due to the huge amount of polymeric composites that can be produced by using, for instance, particles with different sizes, particles with different shapes, different contents of particles, etc., it would be very interesting to perform a new study to verify if the conclusion obtained in this work can be generalized to other polymeric composites. The main objective of this new study could be to determine if it is possible to obtain, for each foam density, the minimum size that the particles or particle agglomerates should have in order to be able to use the extensional rheology as a predictive tool.
- **Analysis of the mechanisms which cause the strain hardening to change when particles are added to a polymeric matrix.** In this thesis, it was observed that the strain hardening of the composites containing a high melt strength polypropylene (HMS PP) and intercalated and dispersed particles was lower than that of the unfilled polymers. However, in the works presented in chapter 2 (section 2.5.2.2), it is obtained that the strain hardening of the composites produced with a common linear PP increases when it is filled with nanoparticles. Therefore, it would be very interesting to perform an experimental work that allows understanding why when nanoparticles are added to a polymer, the strain hardening increases in some polymers and in other polymers this parameter decreases.
- **Analysis of the relationships between biaxial extensional rheology and foaming behavior.** In this thesis a relationship between uniaxial extensional rheology and foaming

behavior has been established for different complex polymeric matrices. As during the growth of the cells, the polymer is biaxially stretched it would be very interesting to carry out a similar study to that presented in this thesis but, performing the extensional rheological measurements in a biaxial mode. With these rheological results it could be also possible to analyze if a mathematical relationship between Hencky strain rate and foam growth rate and between stretching ratio and foam expansion ratio can be established.

- **To perform the extensional rheological measurements using a universal testing machine (INSTRON).** In chapter 7 (section 7.3.2), it was indicated that in some cases the viscosity of the polymeric matrix is so high that, it is not possible to analyze its extensional rheological behavior by using a conventional rheometer. Therefore, it would be very interesting to have an alternative technique to perform these measurements when it is not possible to use a rheometer. A possibility could be the use of a universal testing machine that allows performing the tensile tests in an oven. A future work could be the tuning of this technique to be finally used as an alternative technique to rheology.